“Investigating the Applicability of Single-Channel Electroencephalography in Cochlear Implant Patients”

by

Alejandro Lopez Valdes, B.S., M.Sc.

A dissertation submitted to the

University of Dublin, Trinity College Dublin

for the degree of

Doctor of Philosophy

in the

Department of Mechanical and Manufacturing Engineering

Trinity College Dublin

Dublin, Ireland.

Supervised by:

Professor Richard B. Reilly

June 2017

Declaration

I, Alejandro Lopez Valdes, confirm that this thesis has not been submitted as an exercise for a degree at this or any other university and is entirely my own work.

I agree to deposit this thesis in the University's open access institutional repository or allow the Library to do so on my behalf, subject to Irish Copyright Legislation and Trinity College Library conditions of use and acknowledgement.

Signed,

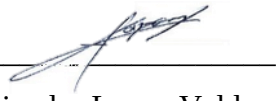

Alejandro Lopez Valdes

June 23rd , 2017

Summary

Hearing impairment affects over 5% of the population worldwide. Namely, about a quarter of a million adults in Ireland are estimated to have permanent hearing impairment due mainly to ageing and/or noise exposure. Cochlear implants (CI) can partially restore hearing in severely deafened patients by electrically stimulating the auditory nerve. Effective clinical assessment and adequate device programing is crucial for the rehabilitation of hearing after implantation. Current behavioural gold standards for assessing CI performance may fall short when assessing younger patient populations or difficult to test individuals. This thesis presents the results of investigating the applicability of objective electrophysiological metrics for assessing CI performance, introducing a new approach to reduce the effect of electrical artefact in CI electroencephalography recordings (EEG), deriving new neural based correlates of CI performance and evaluating them in a clinical environment.

Chapter 3 presents the development of a three-stage CI artefact attenuation methodology. The aim of the chapter is to characterise the CI related artefact as seen in high resolution, single-channel, EEG recordings. The full representation of the artefact allowed for the development of an attenuation framework that succeeds in the extraction of the desired neural signal from the contaminated EEG data. The chapter details the origins of the CI artefact and discusses the application of single-channel EEG recordings in CI populations.

Chapter 4 presents the development of an objective metric of spectral ripple discrimination based on single-channel EEG recordings and a mismatch paradigm. It is shown that neural estimates of spectral ripple discrimination correlate with traditional, behaviourally acquired, spectral ripple discrimination thresholds in a CI population. Due to the established relationship between spectral ripple discrimination and speech

perception performance in CI users, the findings from this chapter suggest that CI performance could be objectively assessed via single-channel EEG.

Chapter 5 investigates an alternative approach to objectively estimate spectral ripple discrimination in CI users. Exploring different EEG paradigms, this chapter provides a comparison of neural spectral ripple discrimination estimates as derived with a mismatch paradigm and an acoustic change (ACC) paradigm. The findings reported in this chapter suggest that, while it is possible to acquire neural spectral ripple discrimination thresholds via an ACC paradigm, the mismatch paradigm proved to be a more robust approach when estimating objective thresholds.

Chapter 6 integrates the methods and tools introduced in the previous chapters for a longitudinal and clinical evaluation of spectral ripple discrimination and speech perception performance in newly implanted CI users. The aim of this chapter is to characterise the dynamics of the objective spectral ripple discrimination metric and its relationship with the dynamics of speech perception performance. This chapter presents advantages, challenges and limitations of the implementation of single-channel EEG recordings in a clinical environment. The results reported in this chapter provide supporting evidence that spectral ripple discrimination is a potential acute predictor of speech perception performance. Furthermore, EEG results suggest that neural estimates of spectral ripple discrimination may require longer maturation time when assessing CI performance.

Chapter 7 investigates the development of an objective metric of temporal processing, specifically fine structure processing, in a CI population based on a mismatch paradigm and Schroeder-phase harmonic complexes. It is shown that the artefact attenuation methodology presented in Chapter 3 is suitable for use with temporal stimuli like the Schroeder-phase harmonic complexes. However, the adequate evaluation of an objective neural metric for temporal fine structure discrimination seemed to be hindered by the poor performance of this CI population.

The single-channel EEG approach implemented in this thesis suffers from limited data dimensionality. However, its high temporal resolution allows for a complete characterisation of CI artefact. It has been shown that artefact free EEG responses can be retrieved from CI users under three different paradigms. The results presented in this thesis provide a valuable insight into the application of single-channel EEG for the clinical assessment of CI performance. Further research should be directed to the optimisation of the paradigms to be utilised in the clinic.

Acknowledgements

This thesis would have not been possible without an invaluable support network.

Special thanks to:

Prof. Richard Reilly for his incredible support and trust throughout these past four years. Thank you for taking me under your wing and being such a positive influence on my PhD. I could not have wished for a better role model!

Dr. Myles Mc Laughlin and Ms. Laura Viani for introducing me to the world of cochlear implants and supporting my research efforts through the entirety of the process. Their dedication to the field and their patient oriented attitude made my experience a journey of personal growth. Their enthusiasm for our work really kept me going!

The people of the National Cochlear Implant Programme, the Neural Engineering group and Trinity Centre for Bioengineering, for all their support both academically and personally. Their help coordinating my research and providing a place for scientific discussion and academic growth was crucial to me. It has been an honour to be a member of these wonderful groups that strive for excellence.

To all the CI patients who generously volunteered their time, often more than once, to the purpose of this research. I know that sometimes a ‘sambo’ and a drink were not enough to put up with my poor choice of films!

To my housemates, Susan, Giovanni, Kate, Helena and Eleonora for making 42 Percy Place my home! To Alessandro, Erin, Mick and Ciara for adopting me as member of their families in the most crucial of times! To the DOPs for all the memories and mischief!

To my friends and family for their continuous encouragement and for being there for me even if I was absent. It has been a hard journey and at times I was not the best travel buddy, thank you for not letting go of me!

A special mention to Martin, Niamh, Saskia and Giovanni for going through the details of this document providing constructive feedback and keeping me on track, but most importantly, for keeping me sane!

This research was kindly supported by the Programme for Research in Third-Level Institutions and co-funded under the European Regional Development fund and by Cochlear Ltd.

ALEJANDRO LOPEZ VALDES

Trinity College Dublin
June 2017

Publications Arising from this Thesis

Journal Articles

- M. Mc Laughlin, **A. Lopez Valdes**, R. B. Reilly, and F.-G. Zeng. Cochlear Implant Artifact Attenuation in Late Auditory Evoked Potentials: A Single Channel Approach. Hearing Research, 302:84-95. August 2013
- **A. Lopez Valdes**, M. Mc Laughlin, L. Viani, J. Smith, P. Walshe, F.-G. Zeng and R. B. Reilly. Objective assessment of spectral ripple discrimination in cochlear implant listeners using cortical evoked responses to an oddball paradigm. PLoS One, 9(3):e90044. March 2014

Articles In Preparation

- **A. Lopez Valdes**, M. Mc Laughlin, L. Flood, J. Smith, C. Simoes-Franklin, P. Walshe, L. Viani and R. B. Reilly. Dynamics of cochlear implant patient progression over one year from device switch-on as assessed in clinic by electrophysiology and non-linguistic metrics. (*in prep*).

Conference Papers

- **A. Lopez Valdes**, J. Smith, L. Viani, P. Walshe, M. Mc Laughlin, F.-G. Zeng and R. B. Reilly. Auditory Mismatch Negativity in Cochlear Implant Users: A Window to Spectral Discrimination, In Engineering in Medicine and Biology Society, Proceedings of the 35th International Conference of the IEEE Engineering in Medicine and Biology Society, 2013:3555-8. 2013
- **A. Lopez Valdes**, J. Smith, L. Viani, P. Walshe, M. Mc Laughlin, F.-G. Zeng and R. B. Reilly. Electrophysiological Correlates of Spectral Discrimination for

Cochlear Implant Users, In Engineering in Medicine and Biology Society, Proceedings of the 7th International IEEE EMBS Neural Engineering Conference, 2015:671-4. 2015

- A. M. Leijsen, **A. Lopez Valdes**, J. Smith, L. Viani, P. Walshe, M. Mc Laughlin and R. B. Reilly. An Approach to Develop an Objective Measure of Temporal Processing in Cochlear Implant Users Based on Schroeder-phase Harmonic Complexes, In Engineering in Medicine and Biology Society, Proceedings of the 7th International IEEE EMBS Neural Engineering Conference, 2015:699-702. 2015

Poster Presentations

- **A. Lopez Valdes**, M. Mc Laughlin, L. Viani, J. Smith, F. Zeng, and R. B Reilly, Using Cortical Evoked Potentials to Estimate Speech Perception in Cochlear Implant Users, in 7th International Symposium on Objective Measures in Auditory Implants, Amsterdam, September 2012.
- M. Mc Laughlin, **A. Lopez Valdes**, L. Viani, P. Walshe, J. Smith, R. B. Reilly and F.-G. Zeng, A Spectrally Rippled Noise Mismatch Negativity Paradigm for Objectively Assessing Speech Perception in Cochlear Implant Users, MidWinter Meeting - Association for Research in Otolaryngology. Baltimore, February 2013.
- M. Mc Laughlin, **A. Lopez Valdes**, R. B. Reilly, F.-G. Zeng. Expanding Cochlear Implant Neural Response Measurement Capabilities to Cortical Potentials. Conference on Implantable Auditory Prostheses. Lake Tahoe, July 2013.
- **A. Lopez Valdes**, M. Mc Laughlin, L. Viani, J. Smith, P. Walshe, F.-G. Zeng and R. B. Reilly. A longitudinal assessment of spectral ripple discrimination and speech perception in new cochlear implant users. 8th International Symposium on Objective Measures in Auditory Implants, Toronto. October 2014
- A. M. Leijsen, **A. Lopez Valdes**, M. Mc Laughlin, L. Viani, J. Smith, P. Walshe, F.-G. Zeng and R. B. Reilly. Using Schroeder-phase Harmonic Complexes to Develop an Objective Measure of Temporal Processing in Cochlear Implant Listeners. 8th International Symposium on Objective Measures in Auditory Implants, Toronto. October 2014
- **A. Lopez Valdes**, M. Mc Laughlin, L. Flood, J. Smith, C. Simoes-Franklin, P. Walshe, L. Viani and R. B. Reilly, Longitudinal Assessment of Spectral Ripple

Discrimination and Speech Perception Evolution in Cochlear Implant Users. 8th Speech in Noise Workshop, Groningen, January 2016.

- **A. Lopez Valdes**, M. Mc Laughlin, L. Flood, J. Smith, C. Simoes-Franklin, P. Walshe, L. Viani and R. B. Reilly. Longitudinal Assessment of Spectral Ripple Discrimination and Speech Perception Evolution in Cochlear Implant Users. MidWinter Meeting – Association for Research in Otolaryngology, San Diego, February 2016.

Table of Contents

List of Figures

List of Tables

Glossary of Acronyms

3AFC	Three Alternative Forced Choice
ABR	Auditory Brainstem Response
AC	Auditory Cortex
ACC	Acoustic Change Complex
ACE	Advance Combinational Encoder
AD	Analogue to Digital
AEP	Auditory Evoked Potential
AP	Action Potential
ASSR	Auditory Steady State Response
CAEP	Cortical Auditory Evoked Potential
CAP	Compound Action Potential
CI	Cochlear Implant
CIAC	Cochlear Implant Artefact Correction
CN	Cochlear Nucleus
CWT	Continuous Wavelet Transform
Cz	Central Midline
DA	Digital to Analogue
DCA	Low-Frequency Artefact
DCN	Dorsal Cochlear Nucleus
EABR	Electrical Auditory Brainstem Response
ECAP	Electrical Compound Action Potential
ECochG	Electrocochleography
EEG	Electroencephalography
EPSP	Excitatory Post-Synaptic Potentials
ERP	Event Related Potential

f0	Fundamental Frequency
FDA	Food and Drug Administration
HFA	High-Frequency Artefact
IC	Inferior Colliculus
ICA	Independent Component Analysis
IPSP	Inhibitory Post-Synaptic Potentials
ISI	Inter Stimulus Interval
MCL	Most Comfortable Level
MGN	Medial Geniculate Nucleus
MLR	Mid-latency Response
MMN	Mismatch Negativity
MMW	Mismatch Waveform
NCIP	National Cochlear Implant Programme
NMT	Nucleus MATLAB Toolbox
NR	Neural Response
PA	Pulse Amplitude
PA	Psychoacoustic
pBP	Partial Bipolar
pTP	Partial Tripolar
RF	Radio Frequency
RPO	Ripples Per Octave
SC	Superior Colliculus
SE	Stimulus Envelope
SIG	Signal
SOC	Superior Olivary Complex
SPS	Sound Processing Strategy
SSD	Sum of Squared Differences
TP	Tripolar
VCN	Ventral Cochlear Nucleus

Chapter 1 Introduction

Hearing plays a major role in human development and social performance. Apart from being a crucial cue for attention and awareness, most aspects of learning and development take place by integrating information received through the ears. Information perceived through the ears is fundamental for language development and our ability to speak. Deprivation of hearing during early stages of development will have an impact on speech and language development (Moeller et al., 2010), and in adults, hearing impairment can commonly lead to social isolation, depression and premature cognitive decline (Davis et al., 2016; Tseng et al., 2016).

The introduction of cochlear implant (CI) technology as a standard treatment for severe to profound sensorineural hearing loss has resulted in tremendous benefits for hearing impaired populations of all ages (Zeng, 2004; Waltzman and Roland, 2005; Mosnier et al., 2015). Up until the start of 2016, the Food and Drug Administration (FDA) in the United States of America estimated that approximately 324,200 people worldwide have received a CI (NICDC, 2016). Despite their success, hearing restoration outcomes in CI users remains largely variable, thus, creating the need for constant evaluation of CI outcome performance.

To date, behavioural testing such as sound discrimination tasks, word and speech recognition tests and pure tone audiograms are the gold standard for evaluating CI outcomes. However, the widening of the candidacy criteria for implantation has allowed for infants under 12 months of age (Waltzman and Roland, 2005) and very elderly adults (Wong et al., 2016) to be able to receive a CI. This situation limits the applicability of behavioural testing, mainly because of the high subjectivity of the tests and the low reliability of the CI respondents (e.g. pre-lingual infants or difficult to test adults).

A number of objective electrophysiological metrics have been proposed to evaluate outcomes in CI users. These metrics include electrocochleography (ECochG) (Shepherd

and Javel, 1997), auditory brainstem responses (ABR) (Abbas and Brown, 1988) and cortical auditory evoked potentials (CAEP) (Martin, 2007; Sandmann et al., 2010; Torppa et al., 2012; Visram et al., 2015). The first two of these are bound to the peripheral auditory pathway and can provide good insights into the integrity of the signal pathways, the perception of sound, and are typically utilised for objectively estimating loudness thresholds for CI users. However, they are limited when it comes to evaluating higher-order processes like speech perception. Per contra, CAEPs have been shown to provide better information of higher-order processing of speech and complex sounds (Martin et al., 2008). Although widely employed in research, traditionally CAEPs are acquired via multi-channel electroencephalography (EEG) which represents a shortcoming for their application in routine clinical practice due to the lengthy set-up times, expense of the equipment and the discomfort to the patient.

Owing to the potential benefit of CAEPs, acquired via EEG, for assessing different aspects of CI outcomes, including higher-order processing of speech (Groenen et al., 2001; Small and Werker, 2012) and musical sounds (Torppa et al., 2012), the aim of this thesis is to reduce the dimensionality of CI EEG acquisition and investigate the applicability of single-channel EEG in the clinical assessment of CI outcomes.

1.1 Hearing and Sensorineural Hearing Loss

Under normal conditions, the human ear is capable of processing sound in great detail. In particular, it can detect and process sounds in the frequency range of 20 Hz to 20 kHz, and within a sound pressure range of 20 to 200,000,000 µPascal or 0 to 140 dB(SPL).

Figure 1.1 depicts an anatomical sketch of the normal human ear. Sound waves arriving at the outer ear (1) will travel through the ossicular chain in the middle ear (2) before reaching the cochlea in the inner ear (3) undergoing a number of modulations that will extract information about the source of the sound and pre-emphasise the frequencies in the range of 2-5 kHz which are directly related to speech perception. At the cochlea, the organ of corti is responsible for the final transformation of sound from wave into electrical information that will ascend to the auditory neural pathway through the auditory nerve (4).

The organ of corti runs along the entire length of the cochlea, from the base to the apex, and is comprised of a tectorial membrane, basilar membrane and four rows of

specialised epithelial cells denominated hair cells (see Figure 1.2). Auditory nerve fibres along the basilar membrane are tuned to a preferred frequency. Low frequency sounds will stimulate the apex of the cochlea whereas high frequency sounds will stimulate the base of the cochlea. This feature is known as tonotopy, and it is the underpinning principle for place coding, one of two important sound frequency discrimination mechanisms which help human beings to hear and differentiate pitch. When sound reaches the cochlea, vibrations at specific locations along the basilar membrane generate a shear force between the apical processes of the hair cells and the tectorial membrane. The displacement of the hair cells triggers a reaction that will result in the depolarisation of the spiral ganglion neurons from the auditory nerve and the transmission of sound information through the neural pathway up to the auditory cortex.

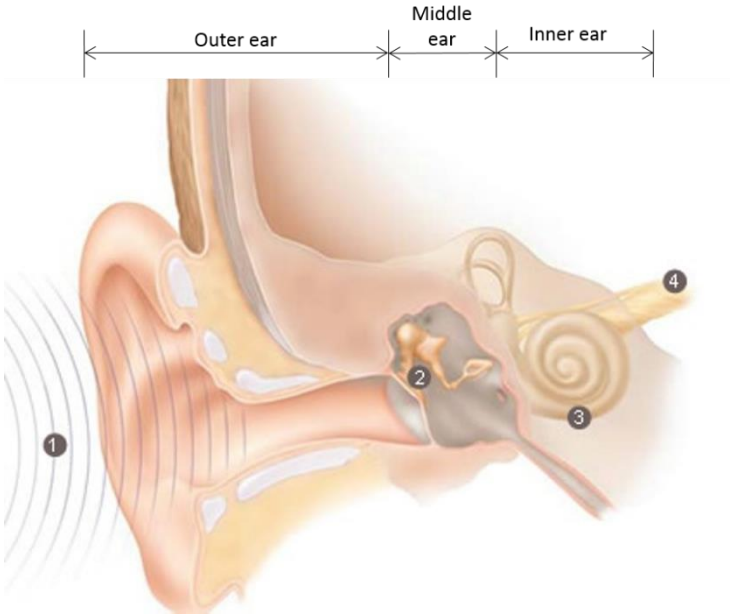

Figure 1.1 Anatomical sketch of the normal human ear.
Sound waves arrive at the outer ear (1) travel through the ossicular chain (2) into the cochlea (3) to be converted into electrical impulses that travel through the auditory nerve (4) to the central auditory system (Courtesy of Cochlear Ltd.).

The auditory system can fail at any of the stages depicted in Figure 1.1, resulting in hearing loss. Hearing loss can be described by three parameters: type (i.e. conductive, sensorineural, mixed, or neural), depending on the location of the problem; degree (i.e. mild to profound), depending on the severity of the impairment; and laterality (i.e. unilateral or bilateral), depending on the affected ear. If the hearing loss is caused by blockage of the outer ear (e.g. excessive wax in the ear canal) or trauma to the middle ear (e.g. rupture of the tympanic membrane or breakage of the ossicles) the hearing loss is considered conductive. Damage of the inner ear (e.g. hair cell degeneration) is considered

sensorineural hearing loss while damage to the neural structures of the auditory system is denominated neural hearing loss.

According to the World Health Organisation, 360 million people, globally, suffer from disabling hearing impairment, and one in every three adults over 65 years of age are affected by disabling hearing loss (WHO, 2015). Hearing impairment can expose individuals and families to social and economic burdens. In children, it may delay or interrupt development of language and cognitive skills which in turn leads to a deficit in academic progress (Conti et al., 2016), while in adults, it leads to social isolation, depression and premature cognitive decline (Davis et al., 2016; Tseng et al., 2016).

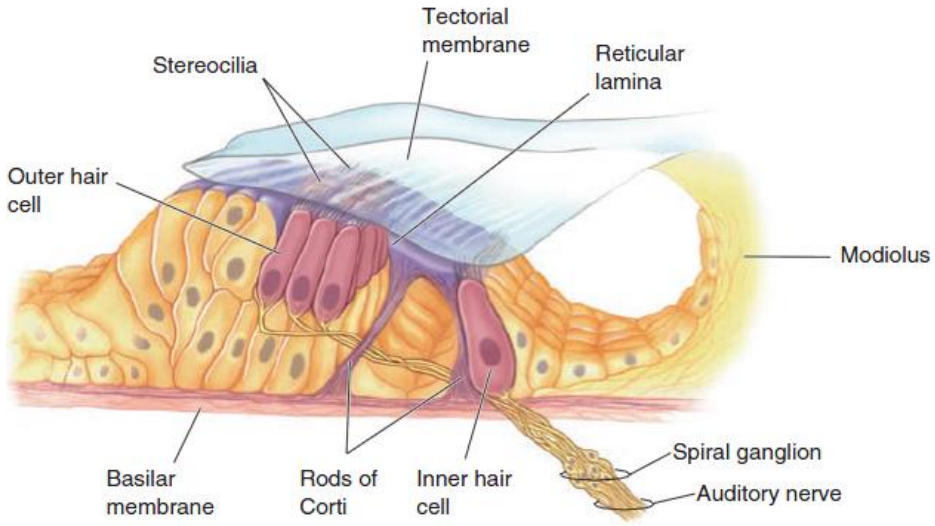

Figure 1.2 Anatomical sketch of the organ of corti.
The organ of corti runs along the entire length of the cochlea and it houses the specialised hair cells that are responsible for the transduction of sound into electrical impulses. Reprinted from (Bear et al., 2007).

Figure 1.3 shows a comparison of a healthy cochlea (left) with no hair cell degeneration versus a profoundly damaged cochlea (right) where the distribution of surviving hair cells is scarce leading to sensorineural hearing loss. Hair cell degeneration, or death, is permanent in humans and other mammals. Depending on the degree of degeneration, or death, sensorineural hearing loss could range from mild to profound.

In Ireland, it is estimated that some 3,000 to 4,500 preschool and school age children have a permanent hearing impairment. Similarly, 8% of the adult population is affected by permanent acquired hearing loss of a significant degree, rising to 50% in the population above 75 years of age. Namely, about a quarter of a million adults in Ireland are estimated to have permanent hearing impairment due mainly to ageing and/or noise exposure (HSE, 2011).

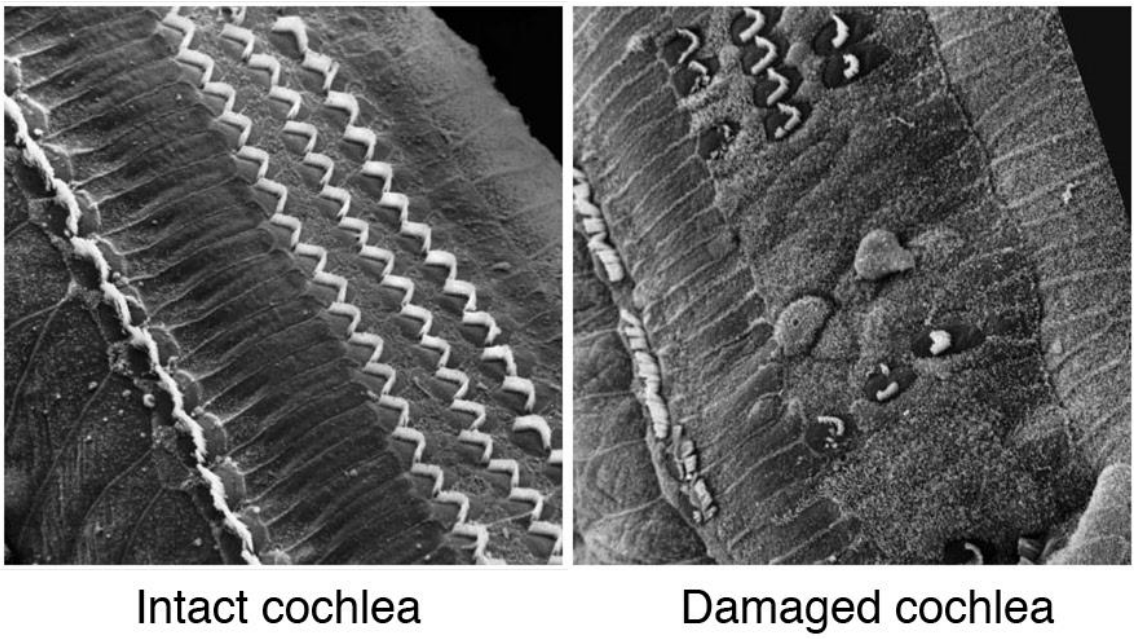

Figure 1.3 Microscopic view of healthy and damaged cochleas.
This microscopic view of a healthy and a damaged cochleas shows clearly the effect of hair cell degeneration. The four rows of hair cells identified in the healthy cochlea are no longer distinguishable on its damaged counterpart underpinning a sensorineural hearing loss (Courtesy of the House Ear Institute).

1.2 Hearing Restoration with Cochlear Implants

In the case of sensorineural hearing loss, permanent rehabilitation is required through assistive listening devices such as hearing aids. Progressive hearing loss will lead to a stage of severe to profound impairment in which hearing aids can no longer elicit sound perception. At this stage, direct electrical stimulation devices such as CI can be surgically implanted to partially restore hearing capabilities.

The CI is an active implantable device that makes possible the partial restoration of hearing by electrical stimulation of the auditory nerve. The device has been in constant development and clinical use since 1985. With more than approximately 324,200 implanted devices globally (NICDC, 2016), it is currently one of the most successful neural implants. The Irish population has been able to benefit from the success of CI technology since the foundation of the National Cochlear Implant Programme (NCIP) in 1995. To date, over 900 people have been implanted by the NCIP, of which 14% were adults over 60 years of age and 40% were children under 5 years of age.

The CI device is comprised of three components, two externally worn and one internally implanted as depicted in Figure 1.4. The external components include a sound processor with a microphone array (1) and a radio frequency (RF) transmitter coil (2).

The sound processor translates the sound picked up by the microphone array into a set of stimulation parameters and encodes for the transmission to the internally implanted component (3) via transcutaneous RF.

The internally implanted component includes an RF receiver coil, a decoding/stimulating chip, a reference ball electrode (usually placed on the mastoid bone) and an electrode array of 12 to 24 electrodes placed inside the cochlea. The implanted RF coil receives the encoded stimulation parameters and power from the external components. The decoding chip decodes the stimulation parameters and implements them to biphasic pulsatile stimulation that is then conveyed to the corresponding electrode of the electrode array inside the cochlea. The electrode array directly stimulates the spiral ganglion neurons of the auditory nerve (4), from where information is relayed through the neural auditory pathways to the auditory cortex.

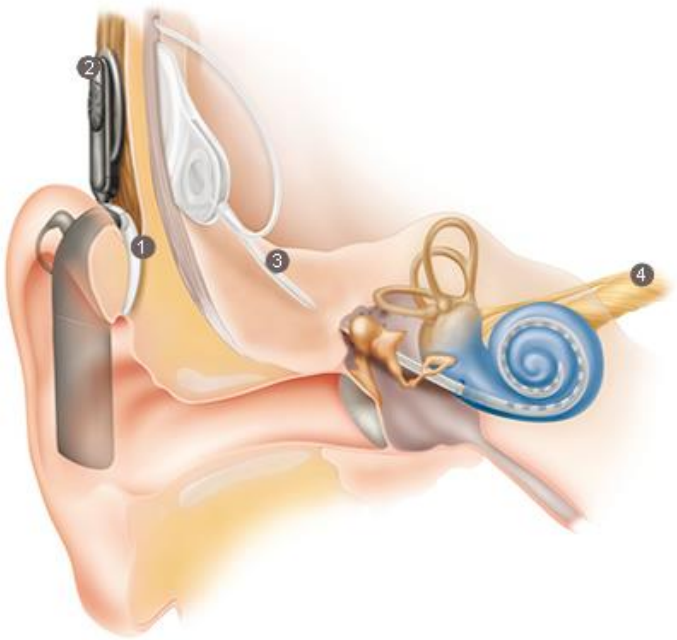

Figure 1.4 Anatomical sketch of the CI components in placement.
Sounds are recorded by an external microphone (1), processed and then transmitted through an RF coil (2) to the internal part of the implant. After decoding, electrical pulses are sent via an electrode array in the cochlea (3) to directly stimulate the auditory nerve (4) (Courtesy of Cochlear Ltd.).

The mechanism by which the CI device translates the sound information picked up by the microphones into the appropriate stimulation parameters is determined by the speech processing strategy (SPS). Different CI manufacturers would have a proprietary SPS, however, most modern strategies are a variation of the envelope based processing strategy depicted in Figure 1.5. Briefly, incoming sound is decomposed into a number of

processing channels by a bank of band-pass filters. Each processing channel includes an envelope extraction stage, a compression stage and a modulation stage. In the compression stage the dynamic range of the acoustic signal is mapped onto the much smaller electrical dynamic range of the stimulation. The compressed envelope then modulates a train of biphasic pulses that will be delivered to each one of the electrodes in the cochlea in a non-simultaneous manner. Information deriving from the low frequency bands is sent to the apical (deeper) electrodes whilst the high frequency information is sent to the basal (shallower) electrodes. Taking advantage of the frequency map or tonotopy of the auditory nerve fibres.

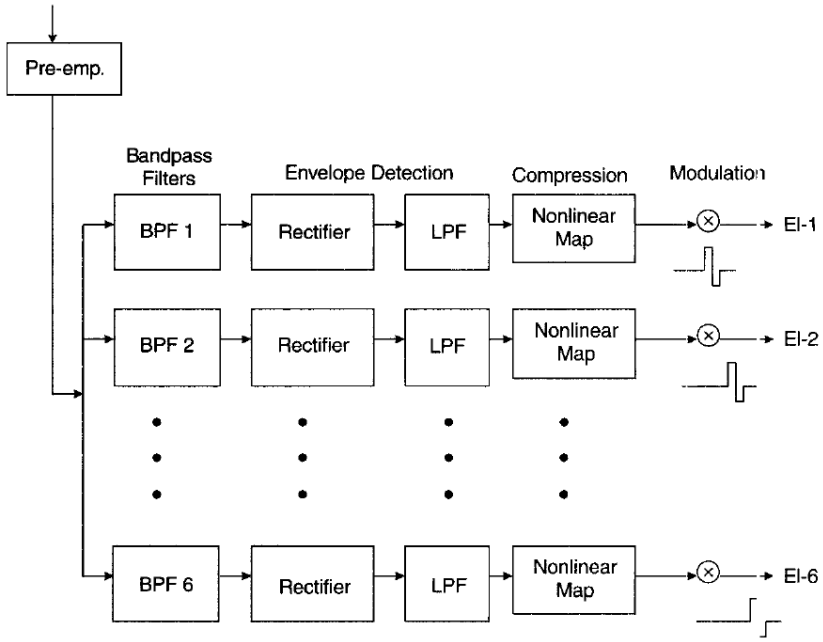

Figure 1.5 Block diagram of envelope based speech processing strategies.
Treated input sound is decomposed in a number of frequency bands by a bank of band pass filters. The envelope of each frequency band is extracted and non-linearly compressed in order to modulate a train of biphasic pulses that will be delivered to each electrode inside the cochlea in a non-simultaneous manner (Loizou, 1999).

Due to its coarse nature, envelope based processing strategies may not be optimal when conveying fine structure information (i.e. frequency variations within one processing channel). In order to address this issue, a number of variations the SPS have been implemented. The use of bell-shaped and overlapping band-pass filters, higher stimulation pulse-rates, current steering between adjacent electrodes and the inclusion of short groups of pulses at the apical electrodes, are some of the commercially available implementations that aim to enhance the quality of the acoustic information represented in the electrical stimulation for both speech and musical sounds. For a more in depth review of the SPS strategies commercially available refer to Zeng et al. (2008).

A large variability in speech performance outcomes can be found among CI users. Implantees with the same implant, speech processor and speech processing strategy can span in speech perception performance from below 10% to 90% score in speech performance tests (Niparko, 2009). This variability is attributed to a number of factors: age of implantation, duration of hearing deprivation, use or no use of hearing aids, whether the CI was pre-lingually or post-lingually implanted, aetiology, and the rehabilitation process among others (Cooper and Craddock, 2005).

Hearing restoration with CIs imposes significant challenges in the impaired listener when compared to normal hearing individuals. The degradation of the auditory system has consequences beyond audibility, impacting the ability of the hearing-impaired listeners to fine tune their hearing to a particular listening scenario in terms of temporal structure, spatial location, pitch resolution among others (Niparko, 2009). For CI users, dynamic range of sound intensity is greatly reduced, from 120 dB in acoustic hearing to 50-60 dB in electric hearing (Niparko, 2009) which in turn needs to be adjusted effectively to capture the desired speech range for rehabilitation (Zeng et al., 2002). Frequency resolution is also affected in CI implantation, the rate and place theories explained in Section 1.1 is reduced to a mere carrier stimulation pulse rate and placement of the electrode array (Zeng, 2004). Accounting for insertion depth of the electrode array and electric field overlap a typical 22 electrode CI has effectively 6 to 8 independent stimulation sites (Zeng, 2004; Niparko, 2009). Some deficits of spectral and temporal processing can be compensated with adequate speech processing strategies. However, the loss of efferent or descending top-bottom interactions remain absent resulting in degraded speech intelligibly in complex situations such as multi-talker scenarios (Niparko, 2009).

The programming or fitting of the CI as well as the hearing rehabilitation process play a major role in improving the odds for a real hearing benefit with the device. Nonetheless, both rely heavily on subjective feedback from the patient which is far from ideal in populations where reliable feedback is not possible as is the case in very young children under the age of 12 months (Cosetti and Roland, 2010). The current gold standards for speech perception evaluation are behavioural protocols like words and speech recognition tests or consonant and vowel recognition tests. Such behavioural tests may lead to a subjective assessment of speech perception due to the required patient engagement, cognitive load, and test anxiety, among other factors. A recent study by Huinck and Mylanus (2016) evaluating the effect of age at implantation in 95 elderly implanted patients identified that speech perception outcomes are mediated by the level

of education of the study participants. This suggests that the behavioural assessment of speech perception may have unidentified biases when evaluating the real benefit of the CI itself, prompting for the need of objective metrics of speech perception performance.

The introduction of objective electrophysiological metrics such as the compound action potential (CAP) the auditory brainstem response (ABR) or the auditory steady state response (ASSR) has shown potential benefit for fitting of the CI stimulation threshold parameters (Swanepoel and Hugo, 2004; Botros and Psarros, 2010; Hofmann and Wouters, 2010). Despite the fact that the correlation between behaviourally fitted implant maps and objectively fitted maps shows large cross-subject variability, objective means of cochlear implant fitting provide a good base creating initial maps until the patients are capable of providing reliable feedback (Cosetti and Roland, 2010).

However, the objective metrics currently available relate mainly to low levels of neural sound processing as occurs in the auditory nerve and the brainstem nuclei and have little or no correlation with speech perception outcomes (Firszt et al., 2002a). In contrast, neural biomarkers of higher-order sound processing could provide a better indication of CI speech perception outcomes. Multi-channel EEG studies have investigated brain plasticity in CI users (Sharma et al., 2002; Bauer et al., 2006; Pantev et al., 2006; Gilley et al., 2008; Sharma et al., 2009; Campbell and Sharma, 2016; Sharma et al., 2016) as well as cortical processing of speech and sounds (Martin and Boothroyd, 2000; Groenen et al., 2001; Dimitrijevic et al., 2004; Sandmann et al., 2010; Torppa et al., 2012; Han and Dimitrijevic, 2015). This provides a strong indication that it may be possible to identify a neural biomarker that can be implemented in the clinic to provide an objective indication of the performance level of a given CI user.

1.3 Research Goal and Collaborations

The principal goal of this thesis was to investigate the applicability of single-channel EEG for the clinical assessment of CI speech perception outcomes. A novel approach for the acquisition of single-channel EEG in CI users was developed. Based on the existing literature, potential neural biomarkers of sound discrimination were examined. Studies to derive objective metrics of sound discrimination and their applicability in a clinical setting were conducted as part of this thesis.

This research involved a close collaboration with the National Cochlear Implant Programme in Beaumont Hospital, Dublin, Ireland and the Hearing and Speech

Laboratory at the University of California at Irvine, United States of America. These collaborations enabled patient-oriented research, striving for translational results. Beaumont Hospital ensured that the studies were performed in line with current ethical guidelines and that all electronic data were kept confidential and secured at all times.

1.4 Thesis Outline

This thesis is organised into a series of Chapters. In Chapter 2, a background of the concepts of EEG, with focus on the electrophysiology of the auditory system, is provided together with a review of the challenges associated with the acquisition of EEG in CI users and the different approaches to attenuate CI induced signal contamination. A specific review on the relationship between electrophysiology and speech perception outcomes in CI users, including behavioural non-linguistic tests is also presented in this chapter.

Chapter 3 begins with the characterisation of the CI induced artefact in EEG data, as recorded with a customised single-channel EEG acquisition system. The CI artefact characterisation is followed by the development and validation of a novel three-stage CI artefact attenuation method that allows an appropriate extraction of neural responses from CI contaminated EEG recordings.

Having presented a new methodology for recording single-channel EEG form CI users, Chapter 4 presents the development of a neural metric for sound discrimination. Neural estimates of spectral discrimination were derived taking advantage of a discrimination indexing EEG paradigm such as the mismatch negativity (MMN) (Naatanen et al., 2007) and complex spectrally rippled noise stimuli (Henry and Turner, 2003).

Chapter 5 presents the evaluation of an additional EEG paradigm aiming to expand the number of objective neural tools available to audiologists for the assessment of sound discrimination. In addition to the MMN approach described in Chapter 4, an alternative paradigm, the acoustic change complex (ACC), was evaluated as a potential candidate to estimate neural thresholds of spectral ripple discrimination in CI users.

In Chapter 6, the objective methods and metrics presented in Chapter 3 and Chapter 4 were evaluated longitudinally in the clinic. Behavioural and objective measures of sound discrimination and speech perception were gathered from a cohort of newly

implanted CI users over the period of one year post-implantation. The applicability of these metrics was evaluated in terms of their ability to predict CI outcome performance.

Chapter 7 examines the possibility of objectively evaluating temporal sound-feature discrimination via single-channel EEG. Mismatch responses were recorded from CI users when presented with Schroeder phase harmonic complexes (Schroeder, 1970) and contrasted with behavioural perception as reported by the participants.

Finally, Chapter 8 presents a discussion of the main findings of the research carried out in this thesis and outlines limitations, recommendations and future work that would build-up on the foundations of this research.

Chapter 2 Auditory Electrophysiology: EEG and its Application in Cochlear Implant Research

This chapter provides an overview of the literature relevant to this thesis and is divided into four sections. The first section provides an introduction to the neural pathways of the auditory system, starting from the auditory nerve and ascending to the auditory cortex. The second section describes EEG as a brain imaging technique, focusing on its applications for understanding sound processing in humans from an evoked potential perspective. The third section discusses the challenges and opportunities of recording EEG data from CI users. After reviewing studies investigating cortical sound processing in CI users employing EEG, this chapter discusses the challenges faced due to the electrical interference caused by the CI stimulation. Lastly, the fourth section presents the main hypothesis and research questions that drive the content of this thesis.

2.1 Neural Pathways of the Auditory System

Auditory processing of sound is carried out by a whole system of interacting neural nuclei. Specific patterns of information are extracted as soon as the signal reaches the nuclei located in the brainstem and are refined in complexity as they approach the auditory cortex. The complexity of the auditory neural pathway and its different processing stations is depicted in Figure 2.1. The spiral ganglion neurons that innervate the organ of corti, as explained in Section 1.1, form the auditory branch of the vestibulocochlear nerve relaying information to the first nuclei of the central auditory system, the cochlear nucleus (CN).

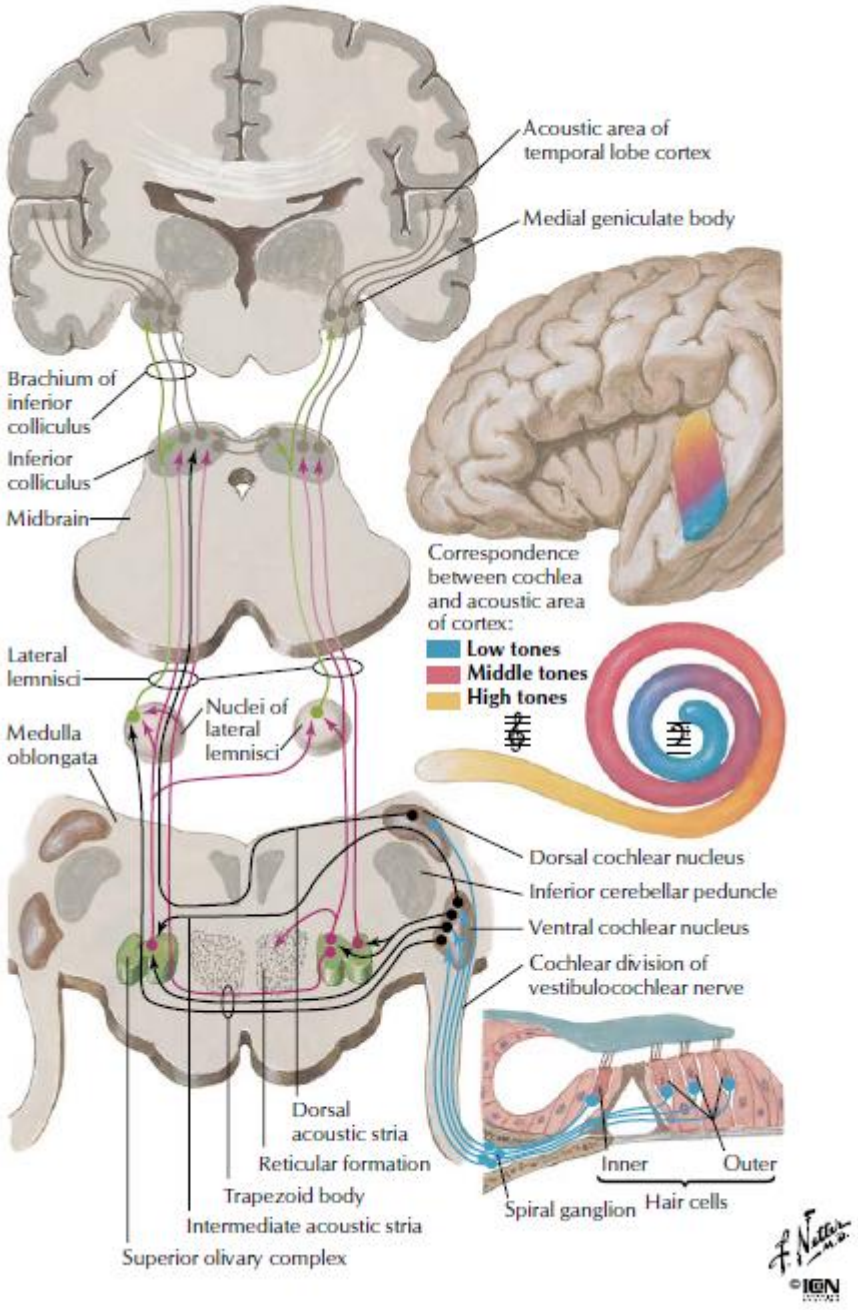

Figure 2.1 Schematic of the neural pathways of the auditory system.
Spiral ganglion neurons from the auditory nerve convey electrical signals to the dorsal and ventral cochlear nuclei. The ascending pathway projects ipsi- and contra- laterally to the superior olivary complex, continuing on to the inferior colliculus and the medial geniculate body of the thalamus for a final projection to the auditory cortex on the superior temporal gyri of both cerebral hemispheres (Hansen et al., 2002).

The CN preserves the tonotopical organization of the cochlea and can be subdivided into the dorsal and ventral cochlear nuclei (DCN and VCN respectively). The different type of cells present at each nuclei may account for the differentiation of processes carried out at each. The DCN may play a particular role in detecting spectral contrast while the VCN may be specialized for processing the temporal structure of sounds (Schnupp et al., 2011).

Axons from the DCN travel directly to the inferior colliculus (IC) while axons from the VCN take an indirect route with an additional relay at the superior olivary complex (SOC). It is to be noted that the majority of the afferent projections from the CN are relayed contra-laterally to the higher nuclei, thus, neurons in the midbrain and cortex are most strongly excited by sounds arriving at the opposite ear (Purves, 2012). The first bilateral, or stereophonic representation of sound is processed at the SOC. Information from both ears converges at the SOC, where the anatomical arrangement of cells allows the fine integration of excitation and inhibition from either side that underpins the basis for sound localization in the form of inter-aural time and intensity differences (Clark, 2006).

Afferent projections from the SOC and the DCN converge at the inferior colliculus (IC). The IC is believed to be responsible for the spatial representation of sounds and the capacity to process components of biologically relevant sounds such as those made by a predator or used for communication (Purves, 2012). Some fibres from the IC interact with the superior colliculus (SC) to enable eye and head movements towards unexpected sounds (Schnupp et al., 2011). The final relay nucleus before arriving at the auditory cortex is the medial geniculate nucleus of the thalamus (MGN). Here some output axons are connected to the limbic structures of the brain and are thought to coordinate certain types of emotional responses and conditioned reflexes to sound. However, the majority of the outputs form the MGN end at the auditory cortex (AC) in the temporal lobes (Schnupp et al., 2011). For a more in-depth description of the auditory nuclei mentioned above, their cellular composition, their influence on the processing of sound, as well as their influence on the development of auditory prostheses refer to the books by Schnupp et al. (2011) and by Clark (2006).

The AC is divided into three regions: core, belt and parabelt. The core is a tonotopical representation of the cochlea in the brain and is mostly involved in the conscious perception of sound and higher-order processing of sound such as sensory memory. The belt area has less tonotopical organization and participates in the processing

of complex sounds, whereas the parabelt projects to several regions in the frontal lobe as well as portions of the parietal and temporal lobes to auditory association areas involved in speech understanding and speech production (Purves, 2012).

The neural mechanisms of sound processing do not only occur from the bottom-up along the auditory pathway, but information is also relayed in a top-down direction from the AC to the innervation of the hair cells in the cochlea. This anatomical arrangement highlights tune-ability of the system in face of different auditory environments (Schnupp et al., 2011).

2.2 Electrophysiology of Sounds

When sound reaches the cochlea, it generates a vibration along the basilar membrane which displaces the apical processes of the auditory hair cells within the organ of corti. As outlined in Section 1.1, the displacement of the hair cells triggers a reaction that will result in the depolarization of the spiral ganglion neurons from the auditory nerve. At this point, sound is no longer represented in the form of a mechanical wave, but instead it is transmitted through the auditory pathway in the form of electrical pulses denominated action potentials (AP).

APs are generated as a result of depolarizing voltage changes in the membrane of a target neuron, generated by the total sum of excitatory (EPSP) and inhibitory (IPSP) signals converging at the dendrites or cell body of the neuron. These excitatory and inhibitory signals are known as post-synaptic potentials (PSPs). If the total sum of PSPs converging at the target neuron is excitatory, and the depolarizing voltage reaches a threshold (i.e. from -65 mV to -50 mV), an AP is generated. However, if the total sum of PSPs is inhibitory, the neuron hyperpolarizes preventing an AP from being generated. APs are conducted along the axon of the neuron until they reach the synaptic endings where they will trigger a signalling cascade to generate either excitatory or inhibitory PSPs on their target neurons (Clark, 2006).

Due to the electrical nature of information transfer in the auditory pathway, it is possible to record the electrophysiological processes within the auditory system either invasively with intracellular recordings, as in Figure 2.2, or non-invasively, as in Figure 2.3, with electrodes located on the skin. The study of the electrophysiology of the auditory pathway has been a crucial element for understanding the mechanism underlying sound processing in both animal models and humans.

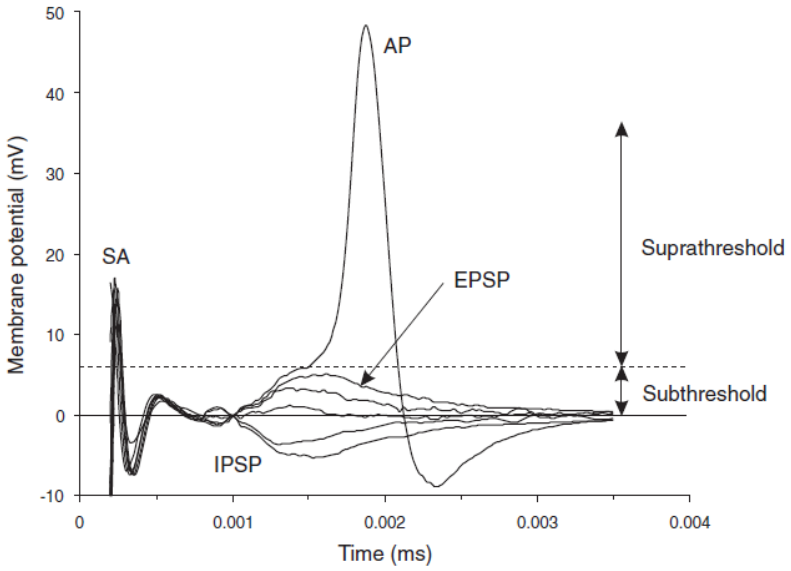

Figure 2.2 Membrane voltages in the cochlear nucleus of a rat.
Intracellular recording of excitatory and inhibitory post-synaptic potentials in a globular bushy cell in the cochlear nucleus of a rat. An action potential is generated as a result of a total excitatory sum of post-synaptic potentials exceeding the depolarization threshold (Clark, 2006).

Owing to the fact that the use of invasive measurements of neuronal activity is not sustainable in humans, non-invasive, scalp-based recordings of electrical fields derived from synchronous activity of large populations of neurons are preferred when investigating the electrophysiology of auditory processes. Berger (1929) demonstrated that it was possible to record electrical responses from the brain using electrodes placed on the scalp. These responses were the origin of the electroencephalogram (EEG) which reflects the summation of excitatory and inhibitory PSPs from large populations of neurons (e.g. pyramidal neurons in the cerebral cortex) oriented parallel to each other as seen in Figure 2.3. Compared to other brain imaging techniques, EEG offers almost instantaneous temporal resolution. Nonetheless, due to the distance between electrodes and brain activity source, and the effect of volume conduction, EEG lags behind in terms of spatial resolution, which can be somewhat compensated with a high number of recording electrodes (i.e. 128, 256 or 512 electrodes), and smaller signal amplitude (Poeppel et al., 2012).

Building on the possibility of studying the cerebral electrophysiological signals measured via EEG, Davis (1939) demonstrated the possibility of recording time-locked changes in the ongoing EEG to various sounds. This marked the introduction of event related potentials (ERPs) as a technique to investigate the reaction of the brain to specific stimuli. ERPs provide a direct, instantaneous, millisecond-resolution of neural activity

triggered by a sensory input (Luck, 2014). The extraction of ERPs from EEG recordings commonly consists of averaging epochs of brain waves that are time-locked to an external sensory stimulus such as a tone burst or a speech sound. There are three basic assumptions underpinning ERP recordings: 1) the neural activity related to the external stimulus and the un-related neural activity sum linearly to create the recorded waveform; 2) the neural activity related to the external stimulus is uniform across all presentations of the stimulus; 3) the un-related neural activity fluctuates randomly across presentations of the stimulus and can be considered as a random sample of a stationary stochastic process. Figure 2.4 illustrates the averaging procedure by which ERPs are extracted from time-locked EEG epochs. For an extensive review of EEG and ERP recording and analysis, consult the work of Luck (2014) and Poeppel et al. (2012).

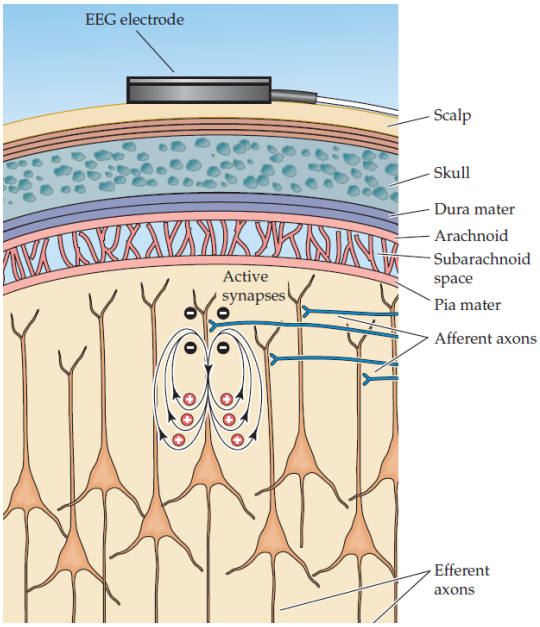

Figure 2.3 Schematic of the mechanism underlying EEG recordings from the scalp.
An electrode on the scalp measures the synaptic activity of a large population of neurons in the cerebral cortex. Many thousands of cells respond synchronously more or less at the same time generating small electrical fields that change over time (Purves, 2012).

2.2.1 Auditory Evoked Potentials

The study of human auditory electrophysiology is mainly conducted through auditory evoked potentials (AEPs) which, due to their contribution to the assessment of hearing as well as to the assessment of site of damage to the auditory system, have influenced the clinical diagnosis, treatment and management of hearing impairment (Fay, 2013).

Auditory evoked potentials are ERPs elicited to the presentation of acoustic stimuli. The time of occurrence, or latency, of the AEP after the start of the stimulus presentation, is an indicator of the anatomical location of its generating structure within the auditory pathway (i.e. how long it has taken for a particular nucleus of the auditory pathway to generate a bioelectrical signal after the stimulus was initiated). In terms of latency, AEPs can be categorized into early, middle, or late evoked potentials. The earlier the latency of the AEP the lower in the auditory pathway the stimulus is being processed (Picton, 2013). Figure 2.5 depicts this AEP categorization according to response latency and its association with the auditory pathway reviewed in Section 2.1.

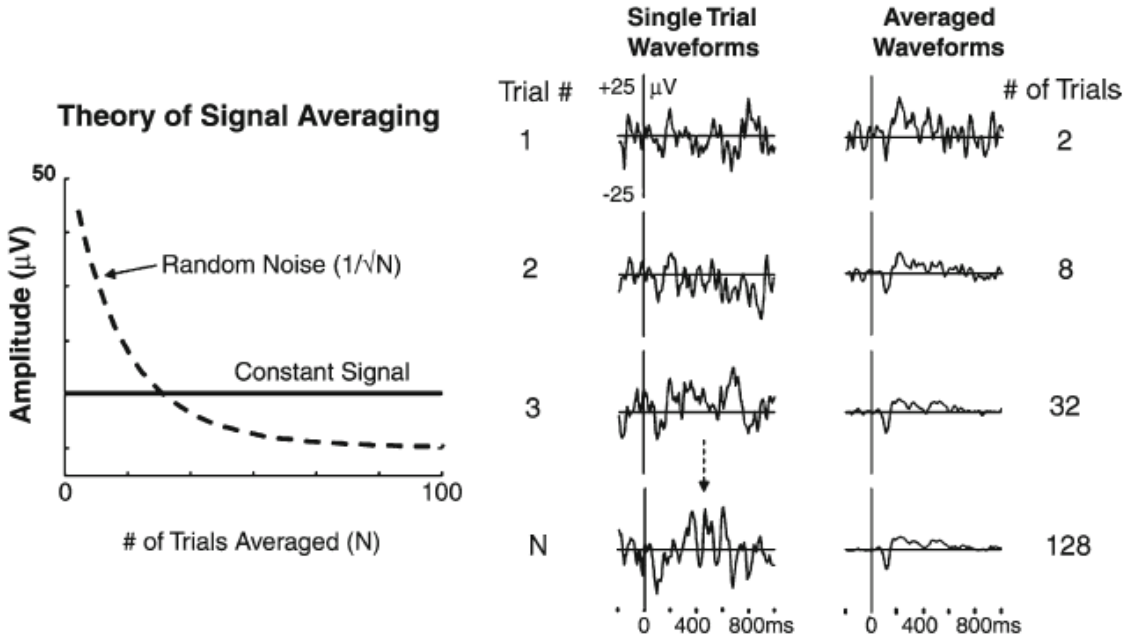

Figure 2.4 Averaging procedure to obtain ERPs from epochs of EEG data.
Signal averaging intends to increase the strength of a constant signal relative to random noise (left). Increasing the number of time-locked EEG epochs increases the signal-to-noise ratio of the resulting ERP waveform (Poeppel et al., 2012).

Early-latency AEPs occur between 1 to 12 milliseconds after the stimulus onset. As observed in Figure 2.5 (bottom left), they are characterized by a group of seven waves whose generators are located at the lowest portions of the auditory pathway, from the cochlear nerve to the inferior colliculus, hence, they are normally referred to as the auditory brainstem response (ABR). Waves I and II are associated with the auditory nerve; wave III is associated with the cochlear nucleus; wave IV represents the activity of the superior olivary complex; wave V is generated with contributions from the lateral lemniscus and the inferior colliculus; and waves VI and VII are believed to have

contributions from the thalamus (Møller and Jannetta, 1983). In human ABRs, only waves I, III and V are robust enough for use in clinical practice, being present from birth and mostly unaffected by attention, sleep or sedation (Fay, 2013). Together with the compound action potential (CAP), which is the intracranial recording analogous of wave II in the ABR (Møller and Jannetta, 1981), early-latency AEPs can be employed to assess the integrity of the auditory pathway, indicate the potential presence of tumours, and establish hearing thresholds in very young or uncooperative patients (Fay, 2013). Nowadays, ABRs are a de-facto test in neonatal hearing screening programs across the world, intended to diagnose hearing loss as early as possible in new-born babies (Patel and Feldman, 2011).

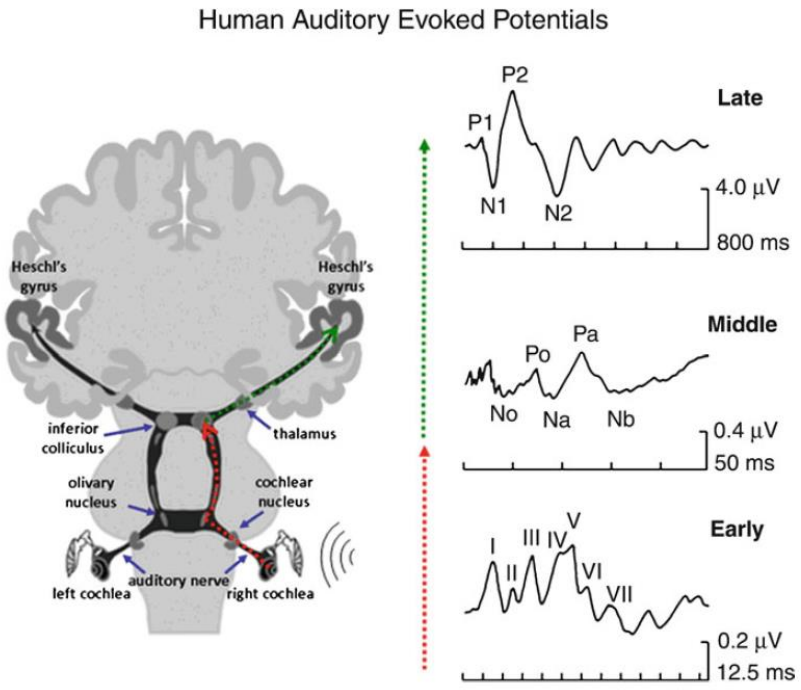

Figure 2.5 Schematic representation of the time-course of auditory evoked potentials and the progression of sound along the auditory pathway.
The timeline (with respect to stimulus onset) of auditory evoked potentials recorded from the midline central scalp region (Right) and their progression from early to late latency evoked potentials along the auditory ascending pathways (Left). Early AEPS comprise ABR waves I-VII, middle-latency components include waves No, Po, Na, Pa, and Nb whilst late-latency or cortical responses include the P1, N1, P2 and N2 components (Poeppel et al., 2012).

Following the ABR, middle-latency responses (MLRs) occur between 10 and 80 milliseconds after the stimulus onset. The Na and Pa components of the MLR are the most prominent and widely investigated, occurring at a latency around 30 milliseconds (Kraus and McGee, 1990). The generators of the MLR are a combination of auditory structures in the inferior colliculus and thalamus as well as structures outside the auditory

pathway such as the reticular formation and multi-sensory divisions of the thalamus (see Figure 2.5 middle left). MLRs can be an alternative for assessing hearing thresholds at low frequencies when the ABR approach is unsuccessful, and to evaluate damage to higher auditory pathways (Fay, 2013). Middle-latency responses have been shown to be useful in clinical situations other than hearing assessment such as in the evaluation of children with dyslexia and learning disabilities (Frizzo, 2015). Nonetheless, the MLR have shown developmental effects, due to the contribution of cortical and subcortical generators, not being fully developed until early adulthood (McGee and Kraus, 1996). This developmental trait hints at the complexity of the maturation of the auditory system beyond the perception of sound.

Late-latency evoked responses, also known as cortical auditory evoked potentials (CAEPs), are observed at latencies between 70 to 300 milliseconds with components identified as P1 (sometimes considered as part of the MLR response denoted Pb), N1, P2 and N2, as depicted in Figure 2.5 (top left) (Gelfand, 2016). The generation of these components is largely due to the activity in the temporal and frontal lobes of the cortex and some contributions from the limbic system (Gelfand, 2016). At later latencies, evoked potentials reflect the activity of structures which involve the integrative and attentional functions of the brain (i.e. higher-order processing) (Fay, 2013). Evoked responses occurring as a result of higher-order processing are less affected by the physical properties of the stimulus and more by the functional use that the processing structure has for it (i.e. they are mainly endogenous responses rather than exogenous responses like the ABR) and can be evoked by different sensory modalities such as visual and tactile (Sutton et al., 1967; Donchin et al., 1978). For this reason, CAEPs such as the N1-P2 complex show maturational effects, however, many components can be measured in children (Sussman et al., 2008; Choudhury and Benasich, 2011). Although the N1-P2 complex encodes low-level sound features like onset and pitch, it can also represent higher-level sound features brought by the spectral complexity of sounds (Shahin, 2011).

In addition to the N1-P2 complex described above, other endogenous CAEPs widely utilized are the P300, the N400 and the mismatch negativity (MMN). The latter, being of interest for the work presented in this thesis, will be described below. For a more extensive review of the P300, the N400 and other auditory endogenous responses refer to "The New Handbook of Auditory Evoked Potentials" by Hall (2007).

The MMN is an electrophysiological discrimination measure that occurs at latencies of about 150 to 275 milliseconds, and it is characterized by a negative deflection

bound to the detection of a signal that differs from a stream of preceding signals (Näätänen, 1995). Figure 2.6 (top) shows the averaged AEP to a train of frequent, or standard stimuli, contrasted to the averaged AEP to a rare, or deviant, stimuli (presented at random 20% of the time) and its derived MMN (bottom). The response to the differing signal occurs whether or not the subject is attending to the deviation (Naatanen, 1991). For this reason, it is thought that the MMN reflects automatic auditory discrimination (Naatanen et al., 2007). The generators of the MMN are thought to be located on the supra-temporal plane of the auditory cortex (Fay, 2013). It has been shown that the MMN is obtainable during sleep (Cheour-Luhtanen et al., 1995; Atienza and Cantero, 2001). This discrimination potential has been widely utilized when conducting basic research of auditory processing (Naatanen et al., 2007) under normal and disturbed circumstances (Naatanen et al., 2012).

Auditory evoked potentials have enabled clinicians and researchers to investigate the neurophysiological mechanisms of simple and complex auditory processing in a non-invasive manner. Whether it is to assess integrity of the auditory pathway or to investigate the functionality, integration and interpretation of speech sounds, AEPs represent an objective method to probe auditory function, development and maturation (Cheour-Luhtanen et al., 1995; Dehaene-Lambertz, 1997; Cheour et al., 1998a; Kral et al., 2002; Choudhury and Benasich, 2011).

2.3 Electrophysiology in Cochlear Implant Research

2.3.1 Evaluating CI Performance

The working principle of the CI was introduced in Chapter 1. It was highlighted that the correct programming, or fitting, of the CI parameters throughout the hearing rehabilitation period is crucial in order to achieve the desired positive outcomes from the implanted device. While behavioural estimations of stimulation thresholds lead to good results in the adult CI populations, these estimations may be far from optimal for children whose behavioural feedback is questionable (Cosetti and Roland, 2010).

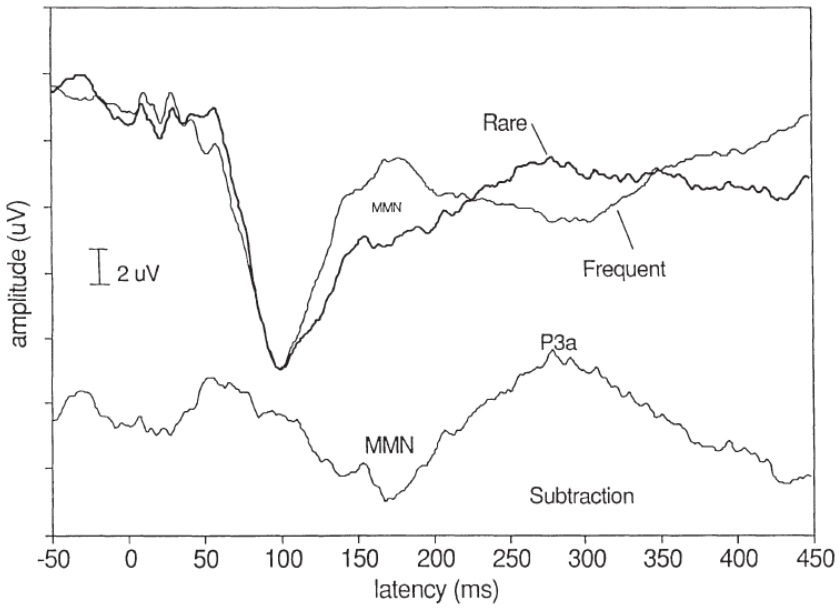

Figure 2.6 Mismatch negativity derived from a pure tone discrimination task.
CAEPs elicited in response to a series of frequent stimulus at 1 kHz and a rare stimulus at 1.5 kHz with a probability of 20% (top). The MMN (bottom) is derived from the subtraction of the rare minus the frequent CAEP (Fay, 2013).

The ability to record AEPs from CI users has had a great impact on the objective programming of CI parameters. To date, all or most CI devices have the capability to record early-latency AEPs from any of the intra-cochlear electrodes in the form of back telemetry (Zeng et al., 2008). Owing to the fact that these potentials are no longer elicited in response to an acoustic stimulus, but to an electric pulse instead, they are usually referred to as electrically evoked compound action potential (ECAP) and electrically evoked auditory brainstem response (EABR). ECAPs and EABRs are nowadays well established methods to assess auditory pathway integrity after implantation and estimation of stimulation thresholds for objective CI fitting (Shallop et al., 1990; Stollman et al., 1996; Shepherd and Javel, 1997; Gallego et al., 1998; Brown et al., 2000; Franck and Norton, 2001; Cafarelli Dees et al., 2005; Botros and Psarros, 2010; Hughes, 2010; Said Abdelsalam and Afifi, 2015).

However, as outlined in Section 2.2.1, early-latency potentials are mainly exogenous; they provide more information about the stimulus physical properties than that about the integrative and interpretative functions of higher-level cortical structures required for speech interpretation. Firszt et al. (2002b) conducted a study where 11 CI users were evaluated in terms of speech perception and physiological measures. Their findings suggest that the variability in speech perception scores of the participants relates to neurophysiological responses at higher cortical levels of the auditory pathway, namely

MLRs and CAEPs. In support of this evidence, Scheperle and Abbas (2015b) reported that while peripheral metrics, like the ECAP, provide valuable information about fitting parameters and speech perception, cortical measures of discriminability should be considered when comparing performance across individuals.

As cortical auditory evoked potentials present a better opportunity to investigate higher-order auditory processes (Garrido et al., 2009; Poeppel et al., 2012), and given the indication that they may provide a more observable link between neuro-electrophysiology and speech perception performance in CI users (Firszt et al., 2002b; Scheperle and Abbas, 2015b, a), they become the focus point of this thesis from this point forward.

2.3.2 Cortical Auditory Evoked Potentials in Cochlear Implant Users

N1-P2 Complex

It has been demonstrated that a cross-modal reorganization of the cortex can occur during the period of auditory depravation (Giraud et al., 2001b; Giraud et al., 2001a; Lee et al., 2001). This cross-modal plasticity signifies that other sensory modalities, such as vision, may take over a portion of the underutilised auditory cortex for their own sensory processing. Therefore, auditory recovery, especially speech understanding, may be more challenging after cochlear implantation in patients that have been deprived of auditory stimulation for a long time (Giraud et al., 2001b; Lee et al., 2001; Sharma et al., 2009).

The N1-P2 complex, previously described in Section 2.2.1, has been a neural biomarker helpful in determining auditory plasticity after CI implantation. A study conducted by Pantev et al. (2006) involving the follow-up of two CI paediatric users over a period of 2 years, suggests that N1 morphology changes during the first weeks after implantation and reaches close to normal maturity after six months of implantation. This is coherent with the work of Sharma et al. (2002) who demonstrated that the first months after implantation are a sensitive period for central auditory development in early implanted children. The work of Sandmann et al. (2015) corroborates this change in morphology through a longitudinal evaluation of CAEPs in a cohort of 11 adult bilateral CI users. Their findings suggest that bilateral cortical plasticity, although occurs promptly, may be limited by the length of sensory deprivation.

Similarly, the effects of cochlear implantation in single sided deafness and the benefit of performing sequential bilateral implantation (i.e. implanting two deaf ears simultaneously) have shown to have an impact on the cortical reorganization of the

auditory cortex, being neurophysiologically assessed via the N1-P2 complex (Gordon et al., 2013; Sharma et al., 2016).

Acoustic Change Complex

Another important aspect regarding CI performance evaluation is the ability to discriminate complex sound features. As an example, the ability to discriminate complex spectral patterns in sounds has been linked to speech perception performance in cochlear implant users (Henry et al., 2005; Litvak et al., 2007; Won et al., 2007). A particular CAEP recording paradigm, the acoustic change complex (ACC), can be employed to objectively measure sound discrimination abilities in CI users (Martin and Boothroyd, 2000; Friesen and Tremblay, 2006; Martin, 2007; Hoppe et al., 2010; Martin et al., 2010; Won et al., 2011b; He et al., 2012; Small and Werker, 2012; Martinez et al., 2013; Han and Dimitrijevic, 2015).

The ACC is an N1-P2 potential elicited in response to a change within an ongoing stimulus (e.g. a formant frequency change within a vowel). This complex can also be elicited by changes in intensity or by frequency modulations on a sustained sound. As observed in Figure 2.7, an 800 millisecond stimulus, containing the diphthong /ui/, elicits a P1-N1-P2 complex during the first detection of sound and an ACC upon the frequency formant change from the /u/ sound to the /i/ sound. Despite the fact that the recording of ACCs can be influenced by factors like training, inter stimuli intervals, and attention to the stimulation (Burkard et al., 2006), this potential has been employed successfully to evaluate central auditory processing. Brown et al. (2008) successfully recorded ACC responses in nine adult CI users demonstrating, for the first time, the feasibility of ACC acquisition by directly stimulating different intra-cochlear electrodes. Their findings suggest that the increasing amplitude of the potential in function of the separation of the stimulated electrodes may be an indication of central processing for spread of excitation. Contrasting with this finding, Hoppe et al. (2010) found no clear evidence of the relationship between electrophysiological electrode discrimination and behavioural results. However, they agreed with the idea that the ability to record ACCs from CI users was a promising approach for evaluating CI outcomes.

Spectral and temporal processing features of CI users, which have been found to play an important role in speech perception performance (Won et al., 2007), have been investigated utilising ACC paradigms. Won et al. (2014) investigated the relationship between electrophysiological and behavioural spectral ripple discrimination, finding a significant correlation between ACC amplitude and single-interval phase inversion

spectral ripple sounds, which in turn correlated significantly with speech perception in quiet and in noise. In a study investigating amplitude modulation detection, Han and Dimitrijevic (2015) suggest that the ACC also represents a novel approach to investigate temporal processing at the level of the cortex. Furthermore, their findings suggest that the ACC provides evidence of hemispheric specialisation for slow and fast stimuli.

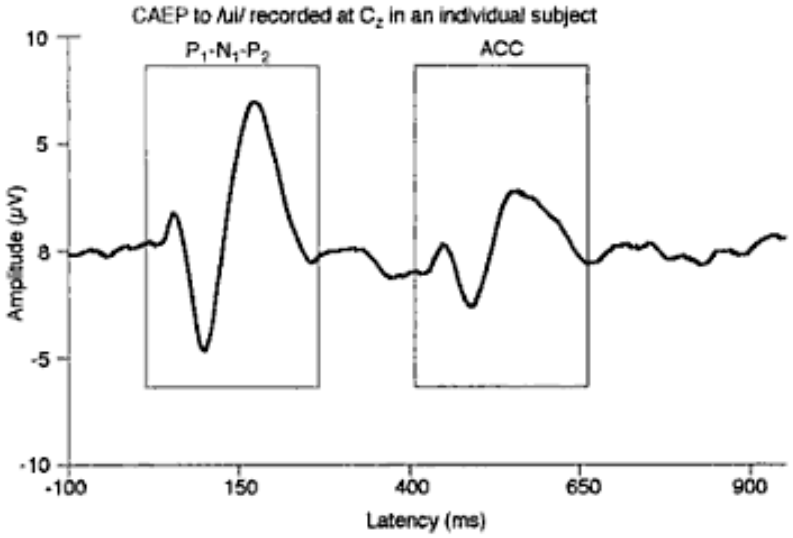

Figure 2.7 Acoustic Change Complex elicited to the diphthong /ui/.
Recording of CAEPs in an acoustic change complex (ACC) paradigm. Recorded at the midline central location (Cz), to a 800 ms long, diphthong sound. The vowel change is presented at 400 ms, eliciting a secondary N1-P2 complex with similar morphology as the one generated due to the onset of the sound (Burkard et al., 2006).

Mismatch Negativity

As described in Section 2.2.1, the MMN is an electrophysiological discrimination measure bound to the detection of a signal that differs from a stream of preceding signals. A number of studies have demonstrated the use of the MMN to evaluate different aspects of CI user performance. Zhang et al. (2011) measured adaptation of the MMN to pure pitch changes (1 kHz – 2 kHz) in 10 CI users. Their results suggest that poor performers exhibit a weak or absent MMN to pure tones, indicating that hearing deprivation not only affects cortical auditory processing but also cognitive processes. Another study performed by Torppa et al. (2012) measuring MMN to musical instrument changes in 30 CI children and 30 normal hearing controls demonstrated that musical discriminations in CI users is significantly poorer that in normal hearing controls.

Ponton et al. (2000) showed that despite having an abnormal N1 peak, the MMN was present in paediatric CI users who had good spoken language. Furthermore, they highlighted that the scalp distribution of the MMN was different between children with a CI and normal hearing children, being more contralateral lateralised in normal hearing

peers. In turn, Liang et al. (2014) described a maturational effect on the MMN measured at early stages of implantation in children. They showed an increase in amplitude and decrease of latencies around 3 to 6 months after implantation. This maturation was in line with an increase on ECAP responses, measured in parallel to the MMN, suggesting a rapid adaptation period in line with the one suggested by Pantev et al. (2006) and Sharma et al. (2002).

Thus far, it is clear that CAEPs provide an important tool when assessing cortical sound processing and cortical maturation after cochlear implantation. Not only can cortical evoked potentials be employed to program and assess CI performance, but they offer a unique opportunity to evaluate which aspects of cortical processing are responsible for said performance and pin-point where the deficiencies of the technology must be addressed. The continued utilisation of electrophysiological recordings in the clinic may represent an improvement of the management of deafness via cochlear implantation.

2.3.3 The Challenge of the CI Induced Artefact

Despite the fact that the possibility to record CAEPs via intra-cochlear electrodes using back telemetry has been demonstrated (Beynon et al., 2008; Beynon and Luijten, 2012; McLaughlin et al., 2012b), current hardware limitations hinder these methods from being readily implemented. Therefore, scalp recordings continue to be the gold standard for the acquisition of CAEPs in CI users.

As with any other active implantable device, such as pacemakers and deep brain stimulators, the CI induces an electrical artefact that obscures the naturally small neural signal recorded via scalp electrodes (see Figure 2.8 A, C and E). This electrical artefact is present regardless of the EEG configuration chosen, be it multi-channel or single-channel. To follow is a review of the different approaches to reduce the influence of the electrical artefact and to separate it from the desired neural response.

Multi-Channel Approach

The use of high density EEG recordings is common in research settings. The availability of multiple sensors allows for complex statistical methods to de-noise the EEG signals. There are many signal processing approaches that take advantage of multiple signal sources (i.e. multiple electrodes) aiming to reduce artefact contamination. Independent component analysis (ICA) is a method to statistically separate a signal into maximally independent components. This methodology entails choosing the independent

components that may be associated with a neural response and discard those that may relate to the artefact of the implant. Figure 2.8 shows the effect of applying ICA to attenuate CI artefact. The CI influence is present throughout the stimulation period and obscures the neural response (A, C, and E). After implementation, the typical N1-P2 response can be recovered from the contaminated data (B, D and F). ICA can be very time consuming due to the complex calculations required. Additionally, a rather high level of expertise is required in order to properly identify the appropriate components (Gilley et al., 2006).

Viola et al. (2012) proposed a semi-automated ICA methodology for analysing CI recordings. This method evaluates the independent components according to their temporal and spatial characteristics. The algorithm, named CI Artefact Correction (CIAC), is available as a processing toolbox for MATLAB. ICA is the most popular method for artefact cancellation in multi-channel EEG recordings when dealing with CI related artefacts (Marco-Pallares et al., 2005; Gilley et al., 2006; Debener et al., 2008; Gilley et al., 2008; Torppa et al., 2012).

An alternative to ICA is to apply linearly constraint minimum variance beamformers, which are a class of adaptive spatial filters that minimise the contribution of undesired sources (Wong and Gordon, 2009). This method requires high density EEG recordings in order to create a spatial map for the localisation of sources of interest.

The obvious shortcoming of multi-channel EEG acquisition is the long preparation time. The location of the CI coil and speech processor may also turn multi-channel EEG recordings into an unpleasant experience for the participant and discourage their use.

Single-Channel Approach

Single-channel EEG recordings only require the positioning of three electrodes: an electrode at the desired recording site, a reference electrode for differential measurement and a ground electrode for the system. This simpler and faster set-up may overcome the practical shortcomings of multi-channel EEG. However, none of the artefact reduction methods discussed previously can be applied to single-channel data.

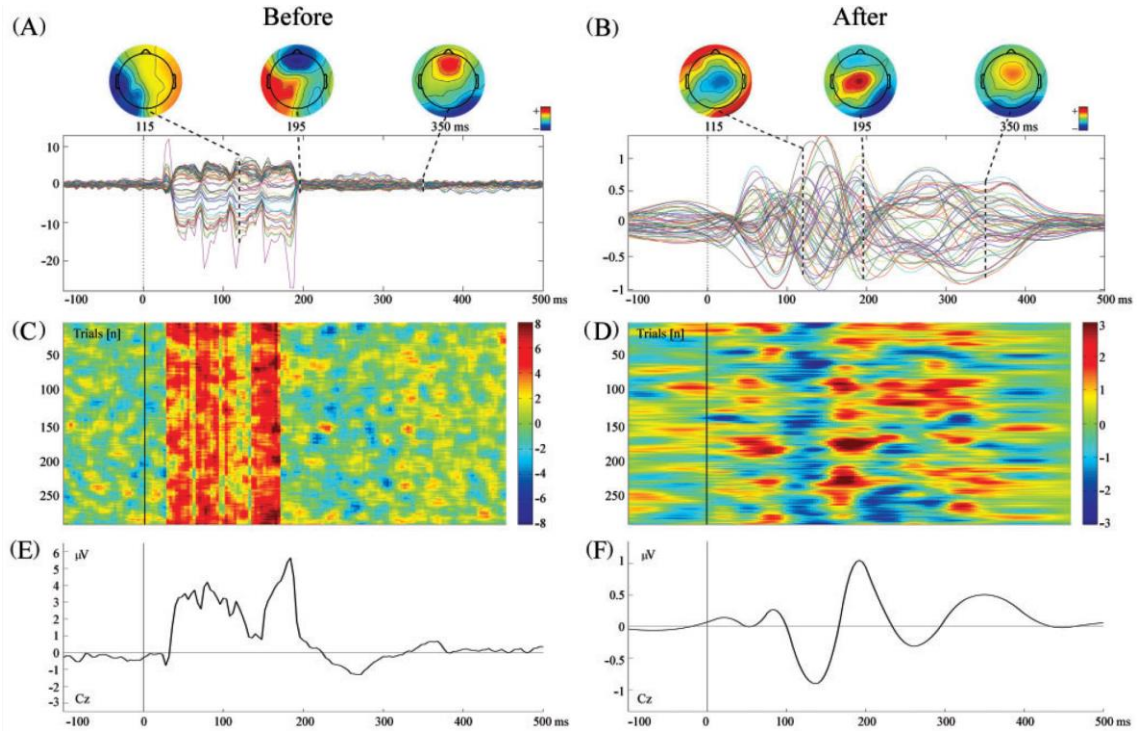

Figure 2.8 Representation of CI induced artefact and its removal via independent component analysis (Sandmann et al., 2009).
Auditory evoked potentials to target stimuli are illustrated before (A) and after (B) independent component analysis-based artefact reduction together with the voltage maps at N1, P2 and P3 latencies. Single trials and the corresponding grand average are illustrated before (C and E) and after (D and F) ICA-based artefact reduction.

Friesen and Picton (2010) were able to record the N1-P2 complex by randomising the inter-stimulus interval (ISI) of presentation between 3000 ms and 500 ms. When the ISI increases, the N1-P2 amplitude also increases due to the refractory properties of bioelectric potentials. However, the CI artefact remains the same for both ISIs, the stimuli presented at 3000 ms and the one presented at 500 ms. Consequently, subtracting the response to the 300 ms ISI stimuli from the 500 ms ISI stimuli allowed Friesen and Picton (2010) to eliminate the CI artefact from the signal. This artefact reduction method is bound to the N1-P2 complex and cannot be applied to other paradigms such as the ACC and the MMN as randomised ISIs will have an influence on these responses that is not associated with the presented stimuli.

More recently, Sinkiewicz et al. (2014) proposed a continuous wavelet transform (CWT) approach for CI artefact reduction that improved the outcome of the subtraction method. Additionally, a CWT-based artefact reduction could be employed to remove CI contamination from responses to speech stimuli, where the previous method could not.

2.4 Hypothesis and Research Questions

Following a review of the literature regarding the evaluation of cortical sound processing in CI users, it is clear that CAEPs are a promising tool for objectively assessing CI performance. However, a shortage of clinical application of these CAEPs was identified in the literature. Despite the fact that CAEPs were employed to investigate various aspects of auditory rehabilitation via cochlear implantation, there was no indication of a metric proposal that could be applied systematically in clinical practice. Furthermore, almost all studies were conducted under research settings utilising multi-channel EEG recordings which are not optimal for clinical applications.

With this in mind, the main hypothesis of this thesis states that the combination of objective electrophysiological metrics for assessment of CI performance together with a clinic-friendly single-channel EEG recording approach may be validated as a clinical tool when evaluating CI rehabilitation. In order to test this hypothesis, a number of research questions have been outlined.

2.4.1 Regarding the CI Induced Artefact in EEG Recordings

1. What would be the representation of the CI induced artefact if it was captured fully (i.e. recorded beyond the 512 Hz to 1024 Hz sampling frequency that most EEG research studies utilise)?
2. What would be the requirements for a single-channel EEG recording system to capture the full representation of the CI induced artefact?
3. Can the full representation of the CI induced artefact allow for an alternative attenuation approach that would effectively recover the neural response from the contaminated recording?

2.4.2 Regarding an Objective Metric to Assess CI Performance

4. Can discriminatory CAEPs like the ACC or the MMN be acquired via single-channel EEG recordings?
5. Can an objective electrophysiological metric of sound discrimination in CI users be derived from single-channel EEG recordings?
6. Do objective electrophysiological metrics relate to psychoacoustic behavioural metrics that relate to CI performance?

7. How does the re-development of CAEPs in newly implanted CI patients impact the ability to use objective metrics to assess CI performance?
8. Does the re-development of CAEPs relate to the changes in CI performance?
9. Are CI processing abilities like spectral discrimination dominated by hardware settings or does brain plasticity play a role in the development of these discrimination abilities?

To address these research questions, a number of studies will be presented in the following chapters of this thesis. These studies focus on the development of a single-channel methodology for acquisition and attenuation of CI induced artefact from CAEPs as well as the development and validation of objective electrophysiological metrics for assessment of CI performance in both experienced and newly implanted users.

Chapter 3 Cochlear Implant Artefact Attenuation in Cortical Auditory Evoked Potentials: A Single-Channel Approach

As described in Chapter 1, advances in CI technology now allows that a typical recipient of a modern CI can expect to understand speech in a quiet listening environment (for a review see Zeng et al. (2008) and Niparko (2009)). In spite of these advances there remains a large amount of variability in performance across users. Behavioural methods such as speech perception tests or non-speech based listening tests (Fu, 2002; Henry and Turner, 2003; Henry et al., 2005; Won et al., 2007) can be utilised to quantify this variability. However, behavioural methods are often not suitable for paediatric CI users and speech-based tests may not be the best way to assess the performance of new CI recipients while they are still learning to understand speech heard through their implants. It was mentioned in Chapter 2 that neural objective metrics of performance may provide a favourable alternative to behavioural testing for both these user groups. In addition to potentially improving the standard of treatment received by an individual CI user, the development of neural objective metrics of CI performance may also advance our understanding of the origins of the performance variability, by giving information on the underlying neural mechanisms. However, the development of such neural metrics has been hampered by the large CI related electrical artefact, which contaminates evoked potential recordings in these subjects, as described in Section 2.3.3.

Firszt et al. (2002b) found that cortical evoked potentials may be suitable for predicting speech perception outcomes for CI. However, to minimise the artefact, this study employed very short, simple stimuli which are unable to fully probe the complex processing that takes place in the auditory system. Utilising the multi-channel ICA approach, two recent studies by Zhang et al. (2010; 2011) showed how CAEPs obtained

using an MMN paradigm can provide utile information on CI functionality and that this information can be related to behavioural outcomes such as speech perception. One drawback of the ICA approach is that multi-channel data must be acquired, even when, as with the two studies by Zhang et al., most of the results and conclusions are based on artefact-free single-channel data. Having to acquire multi-channel data necessitates the purchase of expensive multi-channel acquisition systems, increases subject preparation time, as a full EEG cap must be attached and, for CI subjects, adds the difficulty of positioning the EEG cap over the behind-the-ear processor and magnetic link. For most clinical applications and many research questions, single-channel data are sufficient and subject preparation time significantly reduced. These practical considerations limit the applicability of the ICA-based artefact attenuation approach and motivate the development of a single-channel based artefact attenuation approach other than the ones described in Section 2.3.3.

To better understand the origin of the CI related artefact in CAEPs, a high-sample-rate, high-bandwidth, single-channel acquisition system was developed. The system required a temporal resolution high enough to clearly resolve each stimulation pulse. Utilising this system, it was possible to show that CAEPs recorded from CI subjects are generally composed of three components: a neural response component and two artefact components. Based on this signal composition, a three-stage artefact attenuation strategy was proposed. The high-frequency artefact (HFA) was found to be a direct representation of the stimulation pulses and was completely attenuated by a low-pass filter (stage 1). The low-frequency or DC artefact (DCA), often referred to as a 'pedestal' artefact, could be accentuated by an electrode impedance mismatch and in some subjects could be attenuated by balancing the impedance of the recording electrodes (stage 2). Based on the assumption that the DCA was caused by the stimulation pulses, a mathematical framework to obtain an estimate of the DCA and remove it from the CAEP was developed (stage 3). Finally, it was demonstrated how this single-channel approach could be also applied with low sample rate data (e.g. commercial systems) and that it could be used to measure N1-P2 amplitude growth functions for CI users.

3.1 Materials and Methods

3.1.1 Subjects

CAEPs were measured for 22 adult CI subjects (7 male, 15 female) at two separate locations: Hearing and Speech Laboratory, University of California Irvine (n=7) and Trinity Centre for Bioengineering, Trinity College Dublin (n=15). Experimental procedures were approved by The University of California Irvine's Institutional Review Board and the Ethical Review Board at Trinity College Dublin. Informed consent was obtained from all subjects. Subjects were aged between 20 and 79 (mean 55, standard deviation 17) years and used a device from one of the three main manufacturers (Cochlear n= 20, Advanced Bionics n=1, Med-El n=1). All subjects had monopolar stimulation strategies.

3.1.2 Stimuli

Stimuli consisted of tone bursts with frequencies of 250, 500 or 1000 Hz with durations of 100, 300 or 500 ms. Additionally, broadband noise stimuli (100 to 8000 Hz) were also used. Stimuli were presented at most comfortable level (MCL) and, when amplitude growth functions were collected, levels were decreased in equal decibel steps between MCL and threshold. Stimuli were generated in MATLAB (Mathworks, Natick, MA) at a sampling rate of 44.1 kHz and a 10 ms on and off cosine-squared ramp was applied. In Trinity College Dublin stimuli were presented through a standard PC soundcard and in University of California Irvine stimuli were presented through a DA converter (NI-USB 6221, National Instruments, Austin, TX). All stimuli were presented to the audio line-in on the subject's CI. To limit the effects of any unwanted background noise, the CI microphone volume and sensitivity were set to the minimum allowable values. At University of California Irvine subjects were seated in a sound booth and at Trinity Centre for Bioengineering subjects were seated in a quiet room. Subjects used their everyday speech processing strategy without any special adjustments other than changes to the microphone volume and sensitivity. This method of stimulation was chosen, as opposed to using a research interface to directly control the CI, because it represents a worst case scenario in terms of the CI artefact. It was reasoned that this would result in the development of a robust artefact attenuation approach that could be easily applied in different settings and with different modes of stimulation.

Stimuli were always presented monaurally through channel one on the PC sound card or DA converter. For all stimuli, a trigger pulse at stimulus onset was presented on channel two. This trigger pulse was used to synchronise stimulus presentation and CAEP recording.

3.1.3 Evoked Potential Recordings

A high temporal resolution EEG acquisition system was developed. It consisted of a high-bandwidth, low-noise, single-channel differential amplifier (SRS 560, Stanford Research Systems, Sunnyvale, CA) connected to a high sample rate AD converter (NI-USB 6221, National Instruments, Austin, TX). The sample rate on the AD converter was set to 125 kS/s, the low-pass filter on the amplifier was typically set to 100 kHz and the high-pass filter was set to either DC, 0.03 or 1 Hz. The filter roll-offs were set to 12 dB/Oct and the low-noise gain mode was selected. As standard, the gain on the amplifier was set to 2000. In most subjects at most stimulation levels this gain setting ensured that the amplifier did not saturate during stimulation. Occasionally, at the highest stimulation levels, the gain was reduced to 1000 to avoid amplifier saturation. To reduce 50/60 Hz mains noise the amplifier was disconnected from the mains and operated in battery mode. The dynamic range of the AD converter was set to ±10 V. Standard gold cup surface electrodes were used. An electrode placed at Cz was connected to the positive input on the amplifier, on the side opposite to the CI being tested, an electrode placed on the mastoid was connected to the negative input on the amplifier, and one placed on the collar bone was connected to the amplifier ground. This system was designed to allow the CI related artefact to be clearly sampled with only minimal distortion being caused by the acquisition system.

Channel one of the AD converter was connected to the output of the amplifier and channel two was connected to the stimulus trigger pulse mentioned in the previous section. Custom software written in MATLAB processed the output of the AD converter. Software detection of the trigger pulses allowed accurate synchronisation of the stimulus presentation with the recorded signal. The software performed online averaging, filtering, and visualisation of the CAEP and stored the raw data for offline analysis. Long epochs of 300 ms pre-stimulus to 800 ms post-stimulus were used. All digital filters mentioned below were applied to the long, averaged epochs. The extraction of long epochs

minimises any possible filter edge effects. For plotting and display purposes a shorter epoch of 100 ms pre-stimulus to 500 ms post-stimulus was selected.

3.1.4 Artefact Attenuation

CAEPs recorded with the high sample rate system in CI subjects were compared with typical CAEPs recorded in normal hearing subjects. This comparison showed that the signal (SIG) recorded in CI subjects consisted of a neural response component (NR) similar to that observed in normal hearing subjects in addition to two visually distinct artefact components, a high frequency artefact (HFA) and a low frequency artefact (DCA). Thus the recorded signal could be represented by the following equation, where *t* is time,

$$SIG(t) = NR(t) + HFA(t) + DCA(t)$$

Equation 3.1

Based on this signal composition a three stage, single-channel, artefact attenuation approach was developed. Each stage is explained in detail below and a block diagram outlining the approach is shown in Figure 3.1.

Stage 1: Low-Pass Filter

Single, un-averaged recordings of the response to one stimulus presentation showed that the HFA was a direct representation of the stimulation pulses (see Figure 3.2 A and D). The HFA was completely attenuated by a low-pass filter (Figure 3.2 C and F). The low-pass filter was implemented in the custom MATLAB software as a 2^{nd} order Butterworth filter with a cut-off frequency of 35 Hz and 12 dB/Oct slope. This filter was applied with a zero-phase forward and reverse digital filtering technique (filtfilt command, MATLAB). The HFA could also be attenuated by setting the hardware low-pass filter on the amplifier to 30 Hz with a 12 dB/Oct slope.

Stage 2: Impedance Balancing

After removal of the HFA, a DCA was observed in the CAEPs from some subjects (Figure 3.3). For some subjects this DCA could be attenuated by ensuring that the electrode impedances were balanced to within 1 kΩ (Figure 3.4). To do this, the high impedance electrode was firstly identified by comparison of the impedances measured between all combinations of the three electrodes. The high impedance electrode was then removed, the skin prepared again and the electrode replaced.

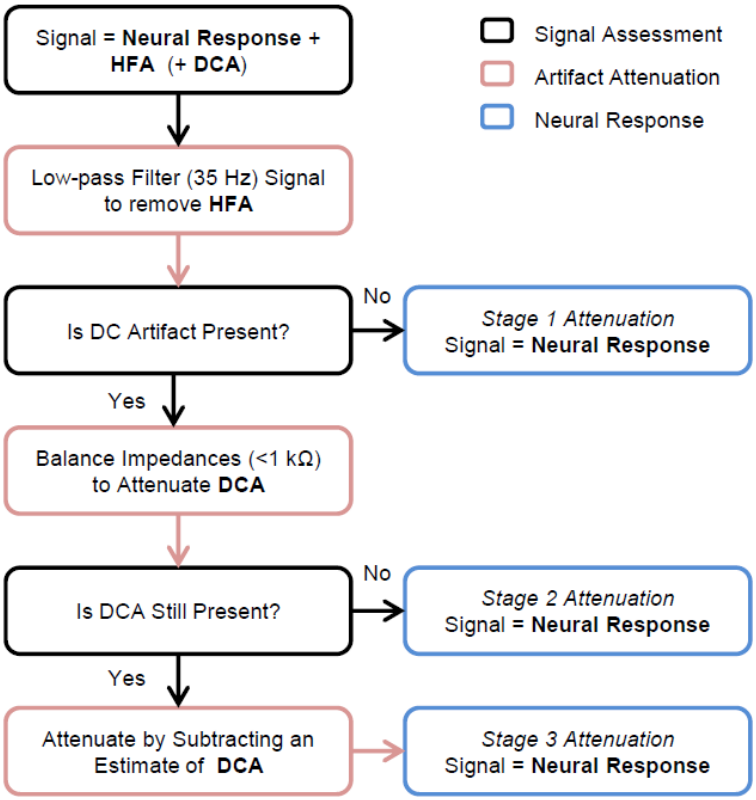

Figure 3.1 Flow chart showing three stage artefact attenuation approach.
The acquired signal (SIG) consisted of the neural response (NR) and two artefact components: a high frequency artefact (HFA) and a low frequency or DC artefact (DCA). A low-pass filter attenuated the HFA (stage 1). Balancing electrode impedances to within 1 kΩ attenuated the DCA in some subjects (stage 2). For the remaining subjects, the DCA could be estimated from the pulse amplitude or stimulus envelope and subtracted from the signal to leave the neural response (stage 3).

Stage 3: DCA Estimation

For some subjects, the DCA could not be fully attenuated by the impedance balancing. For these subjects, a DCA estimation method was applied. Examination of the DCA showed that it was related to the stimulation pulses, i.e. the onset and offset times of the DCA were similar to those of both the HFA and the stimulus, and the shape of the DCA was similar to that of the acoustic stimulus envelope and the HFA envelope. Given these observations, it is reasonable to assume that the DCA can be described by a function of both stimulation pulse amplitude (PA) and time (t),

$$DCA(t) = f(PA, t)$$

Equation 3.2

Examination of the DCA showed that this relationship was well approximated by a bivariate polynomial for all subjects,

$$DCA(t) = \sum_{ij} a_{ij} PA^i t^j$$

Equation 3.3

where a is a coefficient for each term in the polynomial and i and j determine the degree of the polynomial.

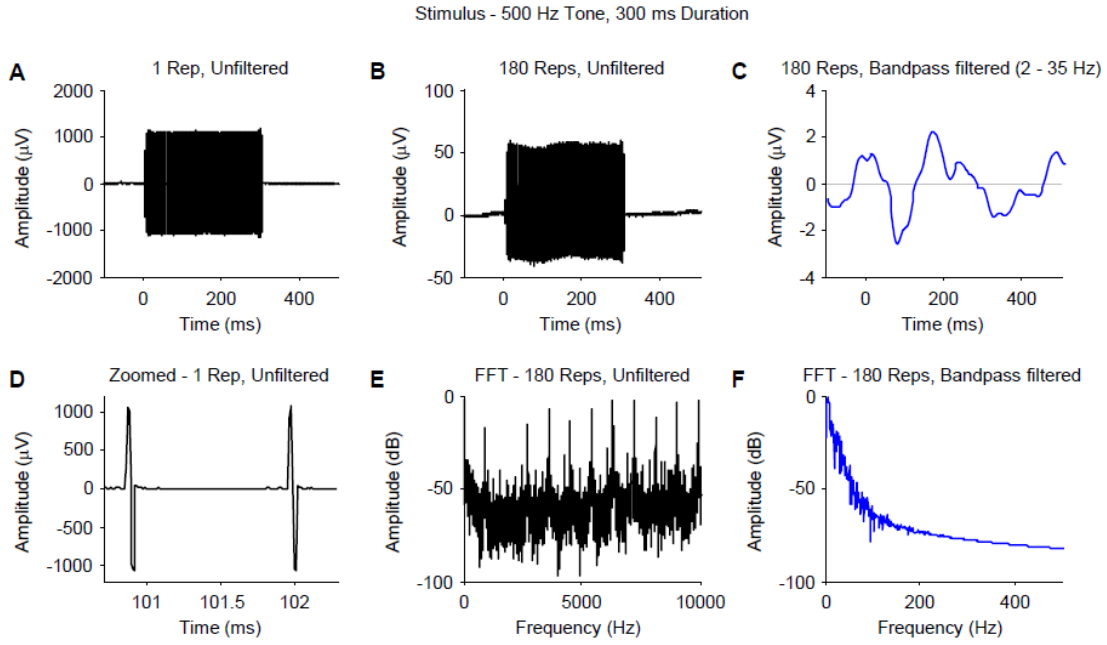

Figure 3.2 Low-pass filtering attenuation of high frequency artefact.
A) The large amplitude high frequency artefact is clearly visible after only one repetition. B) As the individual stimulation pulses do not sum in phase the high frequency artefact becomes smaller with more repetitions. The low frequency envelope is caused by the neural response. C) A band-pass (2 – 35 Hz) filter attenuates the high frequency artefact to leave the neural response. D) Zooming in on one repetition shows the individual stimulation pulses. E) The frequency spectrum of the unfiltered average data shows the high frequency artefact at the stimulation rate and harmonics. F) The frequency spectrum of the filtered data shows the effect of the band-pass 2nd order Butterworth filter.

The CI stimulation pulse generator and stimulus onset are not synchronised. Therefore, pulses across repetitions are slightly jittered, with the result that the PA in the averaged signal is smaller than in a single repetition (compare Figure 3.2 A and B). To create a pulse-synchronised averaged signal, a cross correlation between the first repetition and all other repetitions was performed. The maximum time lag in the cross correlation was limited to one time period of the stimulation rate. This determined the amount of jitter between repetitions which could then be applied as a small delay to each repetition to create a pulse-synchronised signal. An accurate measurement of PA could then be obtained from the pulse-synchronised signal.

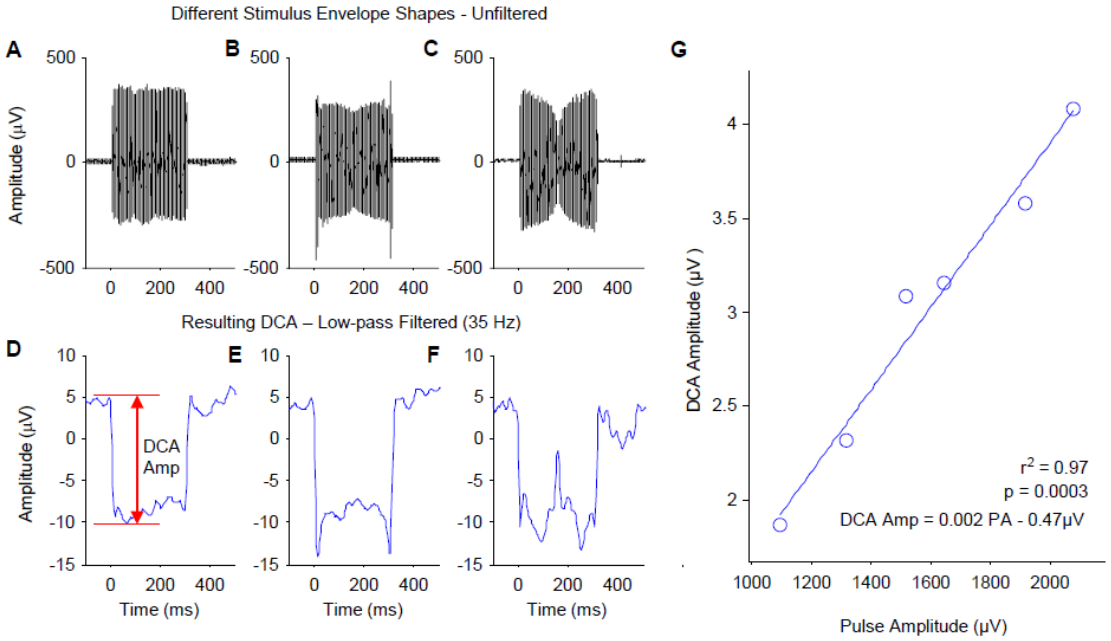

Figure 3.3 Relationship between DC artefact and pulse amplitude.
A-C) The unfiltered averaged response from one subject to three stimuli with different envelope shapes. The pulse amplitude follows the stimulus envelope shape. D-F) The low-pass filtered data show a DC artefact which is related to the shape of the pulse amplitude. G) Data from a different subject showing a linear relationship between DC artefact amplitude and pulse amplitude.

Figure 3.5 is a block diagram showing how the polynomial coefficients were estimated from the recorded signal to give an estimate of the DCA. Firstly, PA was measured from the unfiltered pulse-synchronised signal as a function time. Next, the averaged (non-synchronised) signal was low-pass filtered to remove the HFA, leaving just the NR and DCA,

$$SIG_f(t) = NR(t) + DCA(t)$$

Equation 3.4

The PA time series was filtered with a 2nd order digital Butterworth band-pass filter (compare the two upper right boxes in Figure 3.5). The cut-off frequencies and slopes of this digital band-pass filter were matched to cut-off frequencies and slopes of the filters applied to the signal: the high-pass setting used on the amplifier and low-pass used in the software for HFA attenuation. An estimate of the DCA was then obtained by fitting a bivariate polynomial to these data using the polyfitn function in MATLAB (available for download from the Mathworks File Exchange). In the polynomial fitting function, the two independent variables were given as PA and *t*, and the dependent variable was SIG_f. The parameters obtained from the fitting function, i.e. the coefficients *a*, could then be used in Equation 3.3, together with the PA time series, to obtain an

estimate of DCA (DCA_{est}). To obtain the neural response, the DCA was attenuated by subtracting DCA_{est} from SIG_f,

$$NR(t) \approx SIG_f(t) - DCA_{est}(t)$$

Equation 3.5

To obtain a measure of PA, it is necessary to have high sample rate data, for which the stimulation pulses are clearly resolved. Most commercially available acquisition systems cannot acquire data at these high sample rates. When a measure of PA is not available, a measure of the stimulus envelope (SE) can be substituted. For vocoder-based speech processing strategies the SE will be related to the PA via a compression function.

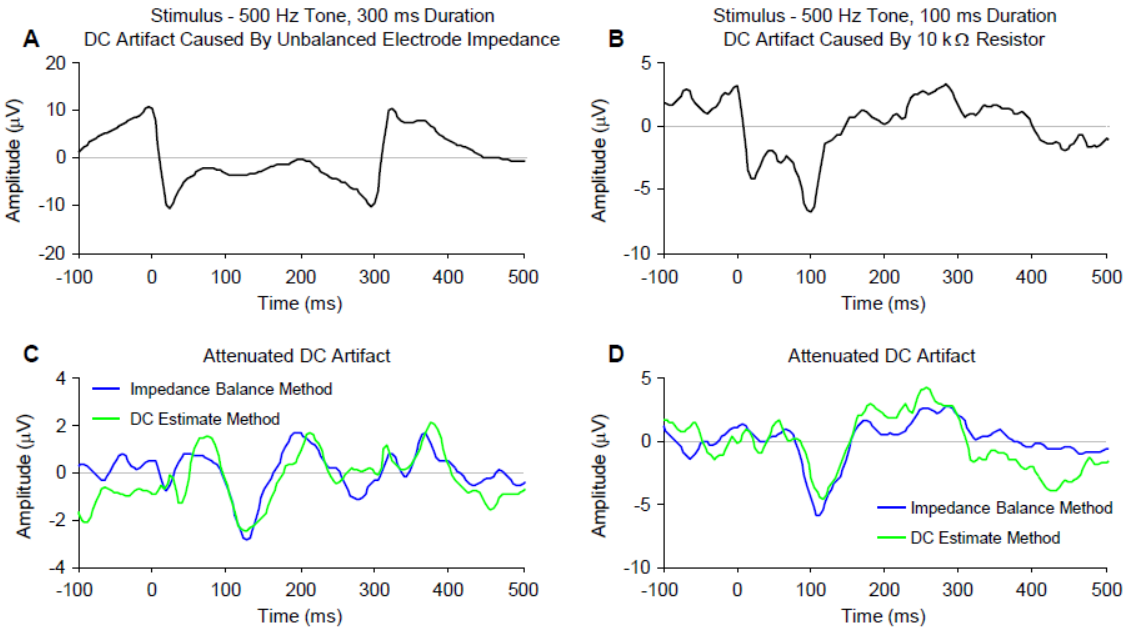

Figure 3.4 Effect of electrode impedance mismatch on the DC artefact.
The DC artefact can be caused by an impedance mismatch. A) A DC artefact was observed when the electrode impedances were unbalanced (Cz = 4.6, Mastoid = 2.9, Ground = 2.7 kΩ). B) Placing a 10 kΩ resistor between the Cz electrode and the amplifier also caused a DC artefact. C) Balancing the electrode impedances (Cz = 2.6, Mastoid = 2.6, Ground = 2.3 kΩ) attenuated the DC artefact (blue line). Applying the DC estimation method to the unbalanced data shown in panel A achieved a similar result (green line). D) Removing the resistor completely attenuated the DC artefact (blue line). Applying the DC estimation method to the unbalanced data shown in panel B achieved a similar result (green line).

Polynomial Degree

As a reminder, the degree (often referred to as order) of a polynomial is determined by the polynomial term with the largest degree, and that the degree of a polynomial term is determined by the sum of the exponents. Thus, a bivariate 3rd degree polynomial will contain PA^2 t and PAt^2 terms but not a PA^3t term. The degree of the polynomial which gave the best fit to the data was related to the number of non-linear

transformations between the PA (or SE) and the recorded signal. The results section shows the effects of different acquisition system settings, which influence these transformations, and suggests the appropriate polynomial degree to be used in each case.

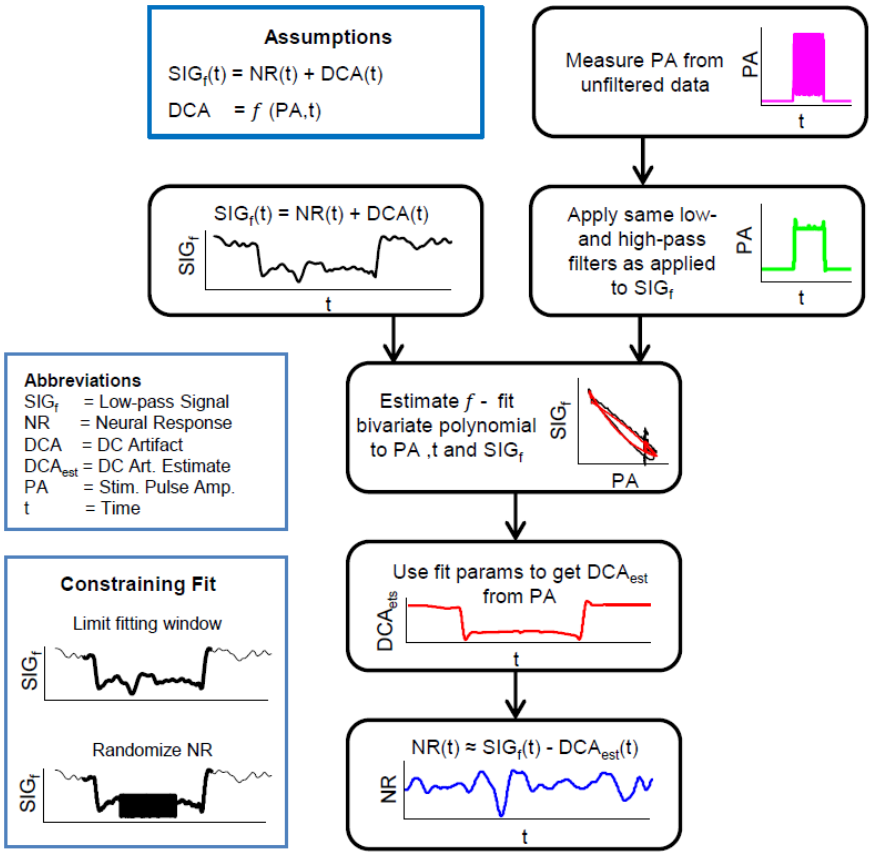

Figure 3.5 Flow-chart of the DC estimation derived from the stimulation pulses.
The DC artefact can be estimated from the stimulation pulse amplitude (measurable with high sample rate acquisition systems) or stimulus envelope (for low sample rate systems). The estimate of the DC artefact is subtracted from the low-pass filtered signal to leave the neural response.

Constraining the Fit

Equation 3.3 shows the approximated relationship between DCA, PA and *t*. PA and *t* are known but the coefficients *a* and DCA are unknown. As described above, to estimate the coefficients a bivariate polynomial was fitted to PA, *t* and SIG_f, where SIG_f contains both DCA and NR (see Equation 3.4). The most accurate estimate of DCA will be obtained when the fitting algorithm fits only the DCA component of SIG_f and not the NR component. A number of factors help constrain the fit to the DCA component only: 1) The PA (or SE) time series has a similar shape to the DCA. Conceptualising the estimation procedure as transforming this PA time series into the DCA_{est}, then the degree of the polynomial determines how non-linear this transformation will be. A polynomial

degree was selected that was high enough to characterise this transformation, but low enough to limit any fitting to the neural response. 2) Only a limited time window of the epoch, where the DCA is expected to occur, was used in the fitting procedure (see Figure 3.5 'Constraining Fit' inset). This time window was determined by the stimulus duration and the amplifier low-pass filter setting. If the amplifier low-pass filter was set to DC or 0.03 Hz, then the DCA was limited to the stimulus duration and only this portion of the epoch was used in the fitting procedure (thick line on upper plot in inset). A low-pass filter setting of 1 Hz caused the DCA to be smeared out in time, and here a time window from stimulus onset to epoch end was used in the fitting procedure. 3) Finally, during a time window when it was expected that the DCA would be flat, i.e. 30 ms after stimulus onset and 30 ms before stimulus offset, the order of elements in the SIG_f vector was randomised (see Figure 3.5 'Constraining Fit' inset, lower plot). The randomisation procedure preserves the main statistical properties of SIG_f during this time window (i.e. mean and standard deviation are unchanged) but removes temporal features of the NR, thus constraining the fitting procedure to the DCA component.

3.2 Results

3.2.1 Attenuation of High-Frequency Artefact

All subjects tested showed an HFA. Figure 3.2 shows an example of the HFA, which was generally in the mV range, and the low-pass filter procedure used to attenuate it. The high temporal resolution of the acquisition system allows us to see that the HFA was caused by the CI stimulation pulses (Figure 3.2 D). Averaging across repetitions caused a reduction in the HFA amplitude as the stimulation pulses in each repetition were not synchronised (Figure 3.2 B). The frequency spectrum of the averaged unfiltered signal (Figure 3.2 E) showed a strong component at the CI user's stimulation rate and its harmonics. The HFA could be completely attenuated for all subjects with a 35 Hz low-pass software filter (2^{nd} order Butterworth, Figure 3.2 F). Figure 3.2 C shows a CAEP collected from a CI subject after the HFA had been attenuated by filtering. The typical N1-P2 complex is visible. To examine how effective a hardware filter was at attenuating the HFA, CAEPs were collected from 3 subjects using a 30 Hz low-pass hardware filter on the amplifier (12 dB per octave). These were compared with CAEPs collected from the same subjects, during the same session, with a 100 kHz low-pass hardware filter and then subsequently digitally filtered with a low-pass 2^{nd} order Butterworth filter. The

effects of attenuating the HFA using hardware and software filters was found to be similar.

3.2.2 RF Coil Related Artefact

There are two possible sources of high frequency artefact when recording CAEPs from CI subjects: the stimulation pulses or the RF coil transmission. The close resemblance of temporal waveform of the HFA to that of the stimulation pulses suggests that, with this recording setup, the HFA is caused by the stimulation pulses and not the RF coil transmission. RF coil transmission is in the MHz range and so should be removed by the hardware filter on the amplifier. However, due to inadequate hardware filters, sub-harmonics or aliasing, it is possible that the RF coils elicit an artefact. The standard electrode configuration used a recording electrode on the mastoid contralateral to the CI. Since both the RF coil and stimulation pulse artefacts will decrease in amplitude with distance from the CI, this configuration helps minimise any artefact. To further investigate the possibility of an RF related artefact, data were collected with a modified electrode configuration: the contralateral mastoid electrode was moved to the mastoid ipsilateral to the CI. Examination of the unfiltered data, in both the temporal and spectral domains showed no evidence for an RF coil related artefact. The components present in data recorded with the standard electrode configuration were present in data recorded with an electrode on the ipsilateral mastoid.

To investigate this possibility that the DC artefact is caused by an RF coil related artefact and not the stimulation pulses, data were collected from one subject with a recording electrode on the ipsilateral mastoid, using stimuli with different shaped envelopes (Figure 3.3 A-F). Panels A, B and C show the unfiltered averaged data and panels D, E and F show the corresponding DC artefact after low-pass filtering. As part of the CI encoding strategies, the stimulus envelope is directly related to the stimulation pulse amplitude, while in the RF transmission, the amplitude of the stimulation pulses is not linearly encoded (Zeng et al., 2008). Therefore, if the DC artefact is caused by the RF coil transmission its shape will be unaffected by the stimulus envelope. Figure 3.3 A-F shows that this is not the case: the shape of the DC artefact clearly follows the fluctuations in the pulse amplitude, indicating that the DC artefact is dominated by a component caused by the stimulation pulses. However, the possibility that a small RF coil related component contributes to the DC artefact cannot be ruled out. Figure 3.3 G shows data

from a different subject recorded with the standard electrode configuration at different stimulation levels. Plotting DC artefact amplitude against pulse amplitude shows a clear linear relationship. Since pulse amplitude is not linearly encoded in the RF transmission, any RF artefact would not decrease with decreasing pulse amplitude.

3.2.3 Attenuation of DC Artefact

Attenuation by Impedance Balancing

After the HFA had been attenuated by low-pass filtering, the CAEPs for some subjects showed a DCA. Figure 3.4 A shows an example of a typical DCA, visible after low-pass filtering. In general, it was found that the size of the DCA was related to the size of the impedance mismatch between electrodes. Balancing electrode impedance reduced the size of the DCA and, in some cases, completely attenuated the DCA. For the CAEPs shown in Figure 3.4 A, where a large DCA is apparent, electrode impedances were Cz = 4.6 kΩ, Mastoid = 2.9 kΩ and Ground = 2.7 kΩ. Reducing the impedance on Cz to 2.6 kΩ completely attenuated the DCA (Figure 3.4, blue line). Applying a low-pass filter to remove the HFA and ensuring that electrode impedances were balanced to within 1 kΩ produced CAEPs that contained no visible artefacts for 27 % (n=6) of subjects tested. Of the 6 subjects who showed no visible artefact after low-pass filtering, 4 used CIs from Cochlear, 1 was a Med-El user and 1 was an Advanced Bionics users. For the remaining 73 % (n=16), even after impedance balancing, a DCA artefact was present. This DCA was removed using the DCA estimation procedure, the results of which are reported in the following section.

To further examine the cause of the DCA, 3 subjects who did not show a DCA were selected. In these subjects, after the electrode impedances had been balanced, a DCA could be created by adding a 10 kΩ resistor between one of the electrode leads and the amplifier (Figure 3.4 B). After the resistor was removed the DCA was not present (Figure 3.4 D, blue line).

The cases where the DCA artefact was present and could be removed by impedance balancing or when the DCA was created by adding a resistor provided a favourable method for validating the DCA estimation approach described below. The green lines in Figure 3.4 C and D show the CAEP obtained after applying the DCA estimation approach to the CAEP shown in Figure 3.4 A and B, respectively. The blue and green lines in Figure 3.4 C and D show good agreement in shape and peak timing,

indicating that the DCA artefact estimation approach attenuated the artefact just as effectively as the impedance balancing method.

Attenuation by DC Artefact Estimation

Figure 3.6 shows an example of the different stages in the DCA estimation approach and compares the CAEPs obtained using the PA and SE methods. Figure 3.6 A shows the PA measured as the difference between the minimum and maximum values of each pulse in the unfiltered signal (purple line). The same band-pass filter used on the signal (high-pass from the amplifier and low-pass used in software to remove the HFA) was then applied to the PA. The purple and green lines in Figure 3.6 A show the PA before and after filtering, respectively. The black line in Figure 3.6 B shows the filtered signal (NR + DCA) plotted against the filtered PA. A 3rd degree bivariate polynomial was fitted to these data (i.e. PA, t, and NR + DCA). There was good agreement between the fitted polynomial function (Figure 3.6 B, red line) and the data (black line). The coefficients estimated from the fit were used in Equation 3.3 to obtain an estimate of the DCA from the PA (Figure 3.6 E, red line). The blue line on Figure 3.6 E shows the NR, where the DCA has been attenuated by subtracting DCA_{est} (red line) from NR + DCA (black line).

With most commercial acquisition systems it is not possible to acquire data at a sample rate high enough to resolve individual stimulation pulses, making it difficult to obtain the measurement of PA shown in Figure 3.6 A. To accommodate data acquired with low sample rate systems, a method of estimating the DCA using the stimulus envelope (SE) was developed. To directly compare the two methods, the data shown in Figure 3.6 were down-sampled to 1250 S/s, simulating data acquired with a commercial acquisition system. The SE was obtained by rectifying and low-pass filtering (35 Hz, 2nd order Butterworth) the stimulus. As with the PA, the same band-pass filter as applied to the signal was then applied to the SE. The green line in Figure 3.6 C shows the band-pass filtered SE, which in this case is almost identical to the SE (purple line, not visible) because the amplifier high-pass filter cut-off frequency was close to DC (0.03 Hz) and its effect was negligible. However, as shown in Figure 3.7, when the cut-off frequency of the high-pass filter is further from DC, its effects become more significant, making it important to include this step. The black line of Figure 3.6 D shows the down-sampled filtered signal (NR + DCA) plotted against the SE. Here, the data (SE, t, and NR + DCA) were well fitted by a 4th degree bivariate polynomial (Figure 3.6 D, red line). In Equation 3.3, PA was substituted by SE and the coefficients determined from the fit were used to

obtain an estimate of DCA from SE and t. The NR, obtained by subtracting DCA_{est} from the down-sampled NR + DCA, is shown as the yellow line in Figure 3.6 E (offset from zero). The high sample rate NR (blue line) compares well with the low sample rate NR (yellow line). The high sample rate method gave an N1-P1 amplitude of 4.9 µV while the low sample rate method gave an N1-P1 amplitude of 4.2 µV. The high and low sample rate N1 latencies were 109 and 107 ms, respectively.

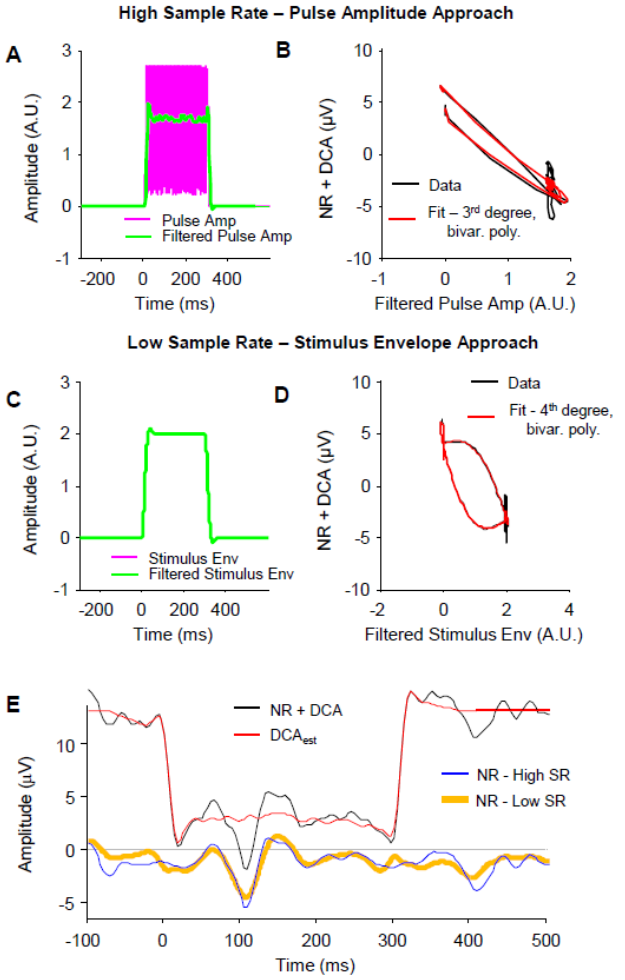

Figure 3.6 DC artefact attenuation.
A) *Stimulation pulse amplitude as a function of time (purple line) was band-pass (0.03 – 35 Hz) filtered (green line) with the same filter applied to the signal. B) Plot of the low-pass filtered signal (NR + DCA) against pulse amplitude (Data, black line). The relationship was well described by a 3rd degree bivariate polynomial (Fit, red line). C) With lower sample rate data, a measurement of stimulus envelope (purple line) provides a substitute for PA. The same filter that was applied to the signal, was applied to the stimulus envelope measurement (green line). D) Plot of the low-pass filtered signal (NR + DCA) against stimulus envelope (Data, black line).The relationship was well described by a 4th degree bivariate polynomial. E) Subtracting DCA_{est} artefact (red line, estimated from PA) from the low-pass filtered signal (NR + DCA, black line) leaves the NR. The blue line shows the NR obtained from the pulse amplitude approach and the orange line shows the NR obtained from the stimulus envelope approach.*

The data shown in Figure 3.5 and Figure 3.6 were collected using 300 ms duration tonal stimuli with a non-fluctuating envelope. Therefore, the onset and offset of the DC artefact did not overlap in time with the N1 response and the DC artefact was flat during the N1 response. The method was tested using shorter duration stimuli (100 ms tones with a non-fluctuating envelope) where the DC artefact offset overlaps in time with the N1 response. Figure 3.4 B and D clearly show that the DC estimation procedure robustly attenuates the artefact even when neural response and stimulus offset overlap in time. This set of experiments did not test the DC artefact estimation procedure using stimuli with low frequency fluctuating envelopes. It is expected that the procedure would need to be adjusted to robustly attenuate DC artefacts which fluctuate during the neural response of interest.

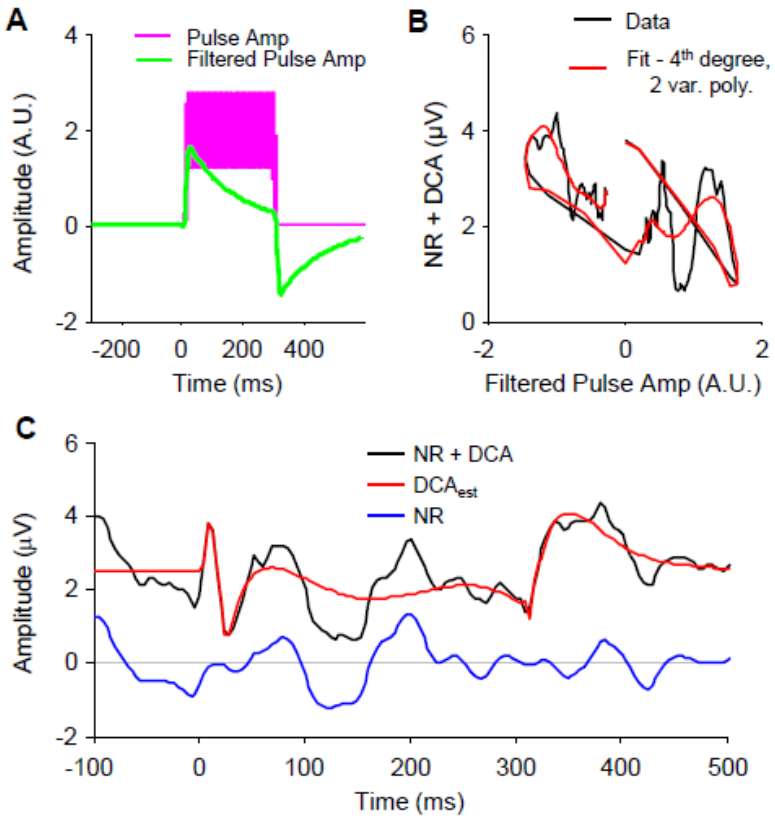

Figure 3.7 Non-linear distortion of the stimulation pulse amplitude.
A) Stimulation pulse amplitude as a function of time (purple line) was band-pass (1 – 35 Hz) filtered (green line) with the same filter applied to the signal. B) Plot of the low-pass filtered signal against pulse amplitude (Data, black line). The relationship is best described by a 4th degree polynomial (Fit, red line). C) Subtracting DCA$_{est}$ (red line) from the low-pass filtered signal (NR + DCA, black line) leaves the NR (blue line).

DC Artefact Estimation- Parameter Study

A study was undertaken to evaluate the effect of different parameter settings on the DC artefact estimation procedure. The green lines on Figure 3.8 A show the effect of changing the degree of the polynomial from 3 to 5, the effect constraining the fit (on or off), and the effect of including the amplifier high-pass filter setting (0.03 or 1 Hz). The effectiveness of the procedure was measured by calculating the sum of the squared differences (SSD) between the CAEP when the artefact was attenuated using the DC estimation procedure (green line, estimated for 12 parameter combinations) and the CAEP, measured using the same subject during the same recording session, when the artefact was attenuated using the impedance balancing procedure (blue line, measured once). Figure 3.8 B shows how this metric changes for different combinations of parameter settings. During this recording session the high-pass filter on the amplifier was set to 0.03 Hz. The parameter study shows that in this case the best artefact attenuation, utilising the DC estimation procedure, was achieved with a 3rd degree polynomial, applying the scrambling procedure, and filtering the PA with a high-pass setting that matched that used on the amplifier (i.e. 0.03 Hz).

In general, it was found that if the high-pass filter on the amplifier was set to DC or 0.03 Hz and the PA method was used, then the data (PA, t and NR + DCA) were well fitted by a 3rd degree polynomial. When the high-pass filter on the amplifier was set to DC or 0.03 Hz and the SE method was used, the data were best fitted with a 4th degree polynomial (Figure 3.6 C, D and E), the extra degree is accounting for the non-linear transformation between SE and PA. When the high-pass filter was set to 1 Hz, it produced a non-linear distortion of the DCA (Figure 3.7 C), i.e. the DCA became smeared out in time. Data acquired with these settings were best fitted by a 4th degree polynomial (Figure 3.7 A and B).

Amplitude Growth Functions

The single-channel three stage artefact attenuation reduced both the HFA and the DCA for all subjects tested. Out of the 22 subjects tested, 20 showed the typical N1-P2 complex in the CAEP. Two subjects did not show any significant peaks in the CAEP. To test the robustness of the approach, N1-P2 amplitude growth functions were collected for 6 of the 7 subjects tested at UC Irvine. Figure 3.9 shows the CAEP waveforms (blue lines) collected for one subject at MCL and at 7 other levels spaced in equal decibel steps down to threshold. N1 was defined as the minimum in the CAEP between 50 and 200 ms and P2 as the maximum occurring within 150 ms after N1. N1 and P2 are marked with blue

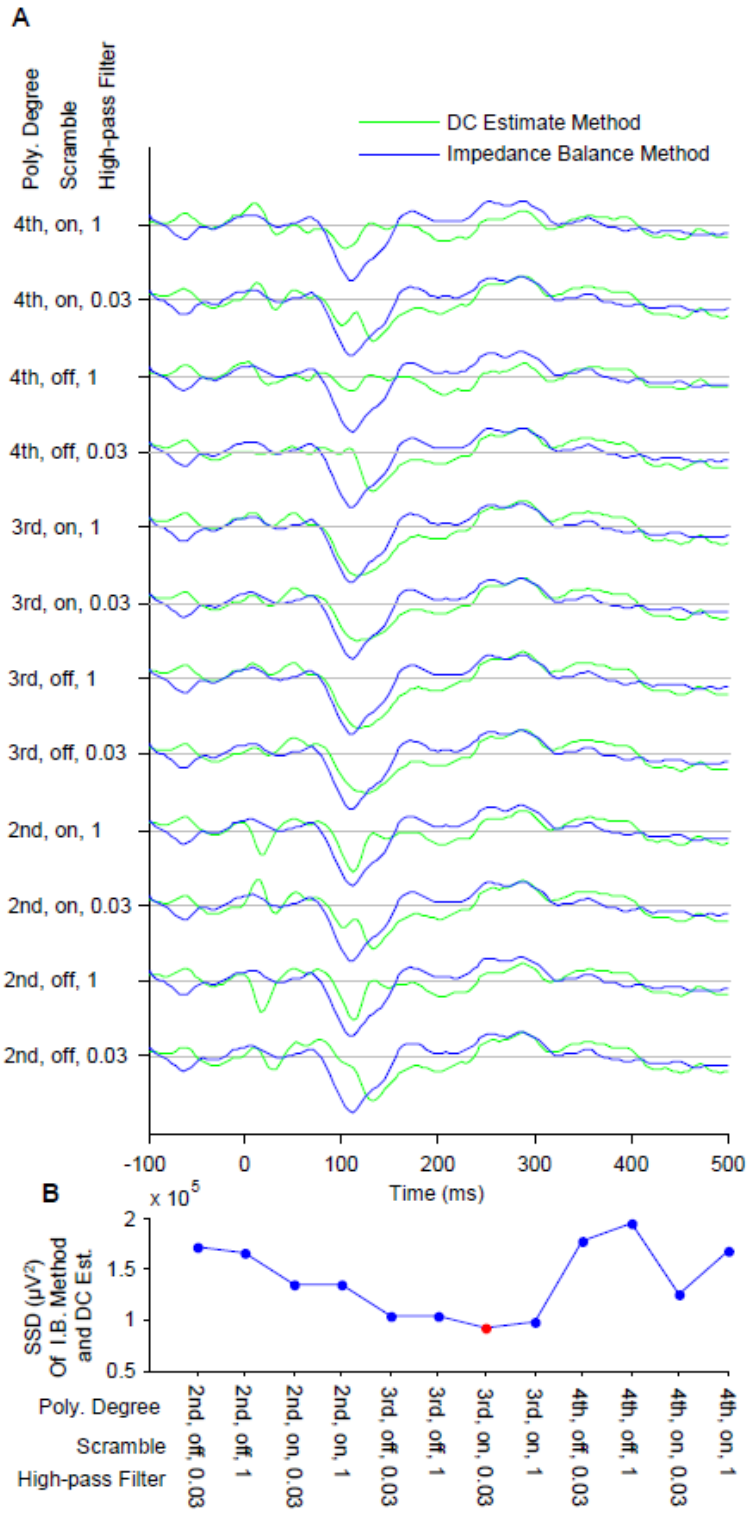

Figure 3.8 Parameter study for the DC artefact estimation procedure.
A) *The effect of changing polynomial degree, the scrambling procedure, and the filter applied to the PA, is shown for one CAEP (green lines, 12 parameter combinations). This is compared with a CAEP, collected in the same subject, where the artefact was attenuated using the impedance balancing method (blue lines, measured once). B) The sum of the squared differences (SSD) was calculated between the impedance balanced responses (blue line) and the DC estimation responses (green lines) for all the parameter combinations.*

circles in Figure 3.9. To calculate a noise floor for each CAEP, the standard error for each time point in a long epoch (300 ms pre-stimulus to 800 ms post-stimulus) was calculated from the un-averaged, artefact attenuated data. To do this, the DCA calculated from the average data was subtracted from each unaveraged epoch. This noise estimation approach is similar to that used by Elberling and Don (1984) to estimate the noise in ABR recordings. It was observed that the standard error did not vary a greatly as a function of time point, i.e. the standard error during time points with large neural response was similar to the standard error during time points with no neural response. Therefore, the standard error was averaged across all time points within one recording to provide a single-number quantification of the noise in a recording. A noise floor (Figure 3.9, grey lines) was defined at ± 1.5 times the mean standard error for the reason described below.

Figure 3.10 and Figure 3.11 show amplitude and latency metrics extracted from 10 N1-P2 amplitude growth functions measured from 10 different ears of 6 subjects. The stimuli were 300 ms duration tones with frequencies of 250, 500 or 1000 Hz. The difference in amplitude between the N1 and P2 peaks is shown as a function of stimulus level in Figure 3.10. Some N1-P2 amplitude growth functions had a linear shape (e.g. Figure 3.10 F), while others showed a plateau above a certain level (e.g. Figure 3.10 A). The shape was not always consistent between ears of the same subject (compare Figure 3.10 B and C). Note that these amplitude growth functions were collected by stimulating through the subjects' clinical processor and so they include the effects of the compression function used in the speech processing strategy. Figure 3.11 shows the latency of the N1 peak which either remained constant or showed an increase with decreasing level for all subjects. Only latencies where N1 amplitude was above the noise floor are shown. Taking the subject population as a whole, a value of 1.5 times the standard error was found to eliminate spurious N1 latency values at lower stimulation levels when the N1 amplitude became small. As a result of this criterion, there are often less points on Figure 3.11 than on the corresponding panel on Figure 3.10. For all 20 subjects, when stimulated at MCL, the mean N1-P2 amplitude was 5.4 (SD=2.1) μV and the mean N1 latency was 111 (SD=19) ms.

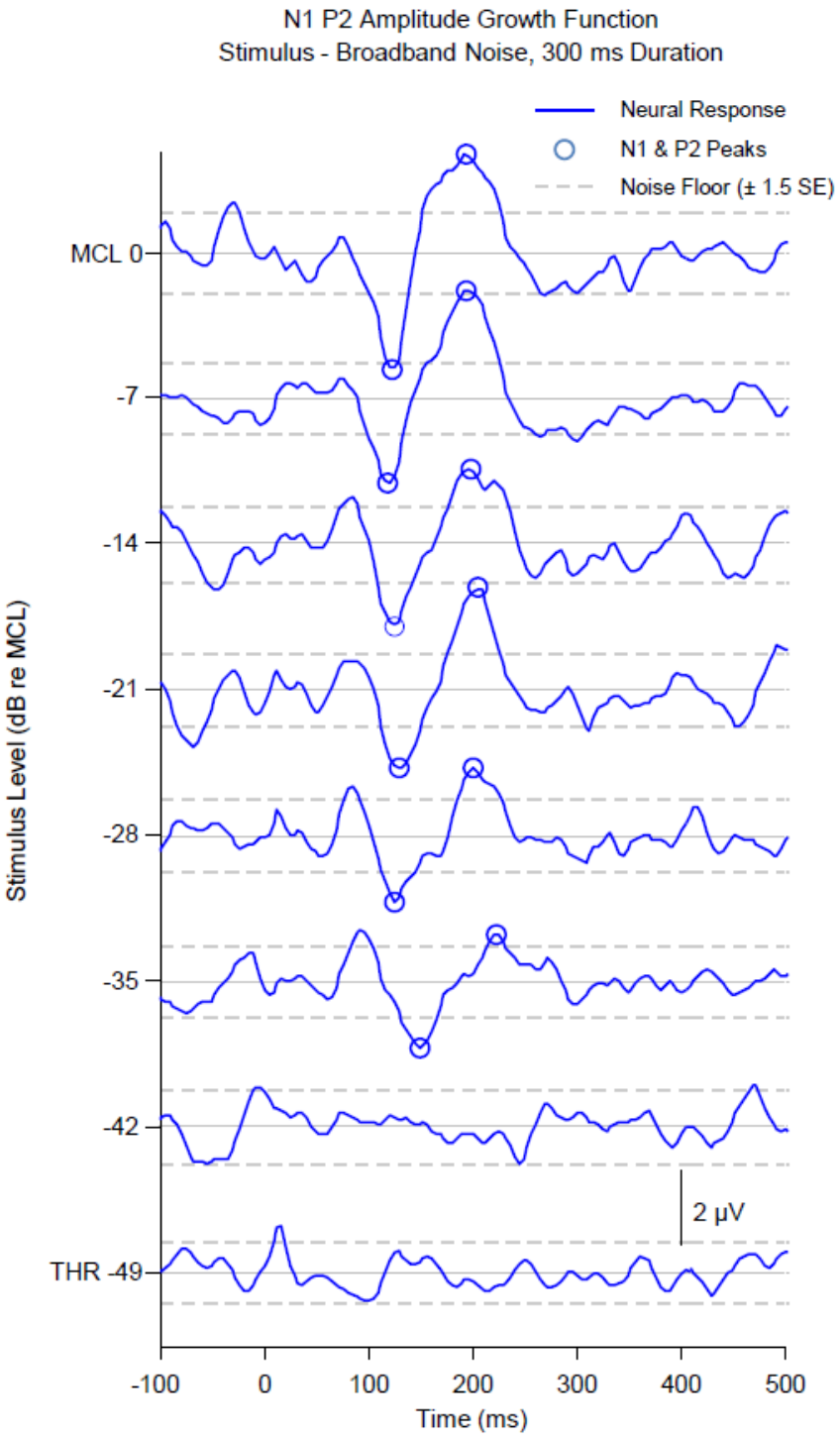

Figure 3.9 CAEP amplitude growth function.
CAEPs (blue lines) were obtained at 8 levels, equally spaced on a dB scale from most comfortable level (MCL) to threshold (THR). N1 and P2 peaks were extracted (open circles). The latency of the N1 peak was only considered significant if it was above a noise floor (dashed grey line).

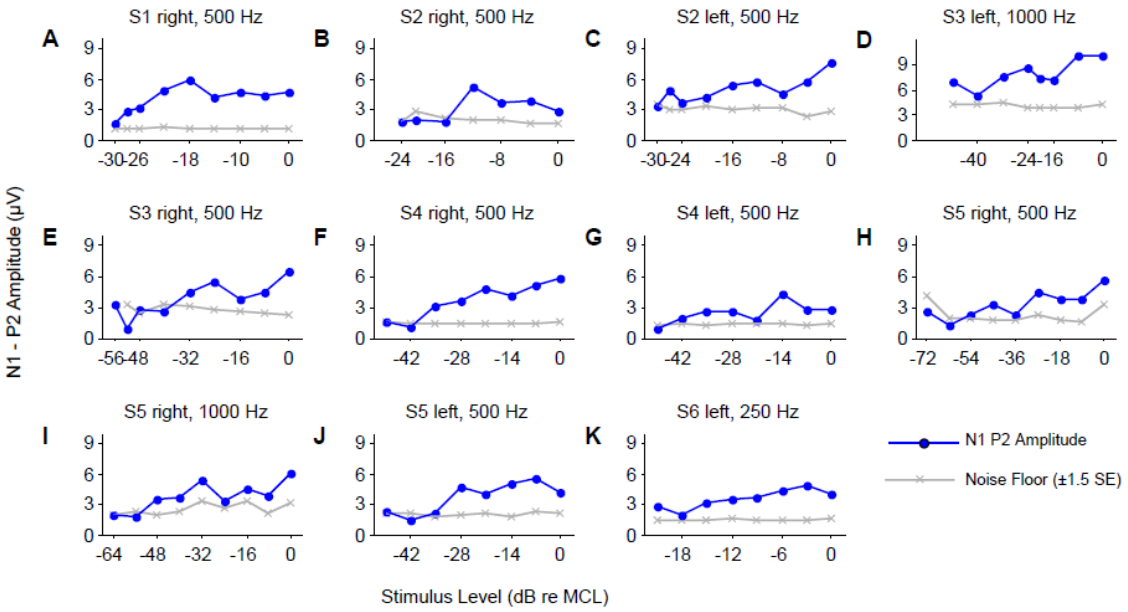

Figure 3.10 N1-P2 amplitude growth functions for all subjects.

3.3 Discussion

The reference to the term artefact attenuation, rather than artefact removal or cancelation, is preferred as it cannot be certified that the artefact (HFA or DCA) was completely removed. Successful attenuation of artefact was judged by visual inspection of the CAEP. However, three points provide reassurance that after the single channel artefact attenuation procedure has been applied, the effect of any remaining artefact on the neural response is negligible. Firstly, the impedance balancing procedure was used to validate the DCA estimation procedure. The CAEPs obtained using the DCA estimation procedure (Figure 3.4 C and D, green lines) show good agreement with the CAEP obtained using the impedance balancing method. Secondly, N1-P2 amplitudes and N1 latencies obtained at MCL are comparable to those reported in other studies. Viola et al. (2011) used the multi-channel ICA approach to measure CAEPs for 18 CI subjects. They reported a mean N1-P2 amplitude of 8.9 (± 4.1 standard deviation) µV and mean N1 latency of 132 (± 13.7 standard deviation) ms. Finally, the amplitude growth functions (Figure 3.9, Figure 3.10 and Figure 3.11) show that N1-P2 amplitudes increase and N1 latencies decrease with increasing level, as has been previously reported for normal hearing subjects (for a summary, see Picton et al. (1976)).

To follow is a list of recommendations for recording CAEPs for CI subjects, describing the best practice for applying the single channel approach; discussing potential causes of the DCA; and moving on to compare the single channel artefact attenuation

approach developed with other approaches used to attenuate the HFA and DCA. Finally, a discussion on the clinical utility of CAEPs for assessing CI functionality suggesting how the single channel approach may facilitate their application.

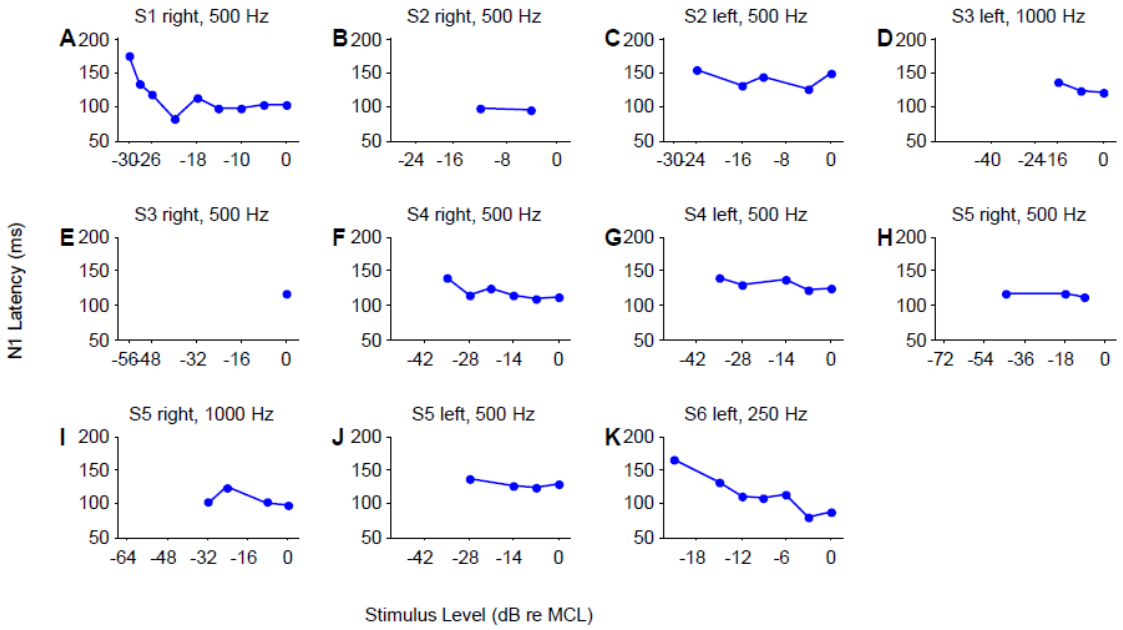

Figure 3.11 N1 latency functions for all subjects.

3.3.1 Recording Recommendations

As a first step to attenuating the DCA it is recommended to ensure that all electrode impedances are balanced to within 1 kΩ. If the DCA persists, setting the high-pass filter on the amplifier to DC or 0.03 Hz will give the clearest acquisition of the DCA and allow the most straightforward application of the DCA estimation approach. When available (i.e. with high sample rate systems), it is recommended to measure the PA to estimate and then attenuate the DCA. When the amplifier high-pass filter is at DC or 0.03 Hz, the data (PA, t and NR + DCA) are best fitted with a 3rd degree bivariate polynomial. If a measure of PA is not available (low sample rate systems), a measure of SE can be substituted and the bivariate polynomial degree should be increased by one to account for the extra non-linear transformation between PA and SE. If the data were acquired with the amplifier high-pass filter at 1 Hz, the bivariate polynomial degree should be increased by 1 to account for the non-linear effects of the filter.

3.3.2 Potential Causes of the DCA

With this recording system, the data show that the DCA is related to the stimulation pulse amplitude (Figure 3.3) and that an electrode impedance mismatch can cause a DCA (Figure 3.4). However, the mechanism by which these factors generate the DCA remains unknown. It is possible that unwanted capacitance effects cause the DCA. These capacitances could be located at the CI electrode-neuron interface or at the EEG electrode-scalp interface. The stimulation pulse may deposit charge on this capacitor which is slowly released, causing the DCA. For some subjects (n=6) the DCA can be removed by balancing the impedance of the scalp electrodes. In other subjects (n=16), even when the scalp electrode impedances are balanced, the DCA is still present. For these subjects the DCA may be caused by an internal impedance path mismatch (i.e. from CI electrode to EEG scalp electrode). For normal hearing subjects a scalp electrode impedance mismatch may result in noisier recordings but it does not typically cause a DCA. Therefore, in CI subjects the DCA is likely caused by the large amplitude stimulation pulses in combination with an impedance mismatch or capacitance effect. Further experiments are necessary to test these hypotheses.

The auditory sustained potential is a low-frequency, sustained, neural response with onset times of around 150 ms and amplitude up to 6 μV (Picton et al., 1978). It is possible that this auditory sustained potential contributes to the low frequency component which is labelled here as the DCA. Three pieces of evidence suggest that the DCA is dominated by artefact and not neural response: 1) The DCA has an onset time close to stimulus onset time while the sustained potential has a much later onset time. 2) The amplitude of the DCA can often be reduced by matching electrode impedances. 3) In some subjects, when electrode impedances are not matched, the amplitude of the DCA can be as large as 50 μV.

3.3.3 High-Frequency Artefact Attenuation

Most evoked potential studies using CI subjects utilise either a hardware or software low-pass filter with a cut-off frequency at around 50 or 35 Hz. The work presented here demonstrates that this low-pass filter will attenuate the HFA. Recent studies by Hofmann and Wouters (2010, 2012) used a high sample rate system to record auditory steady state responses from CI users. Their system could clearly resolve individual stimulation pulses, but rather than using a filtering approach, they showed that

locating each stimulation pulse and linearly interpolating through it also removed the HFA. An interpolation approach to removing the HFA would also work with the system developed here. However, in practice filtering is easier to implement and more robust.

3.3.4 DC Artefact Estimation Procedure

This study used tone or noise stimuli of 100, 300 or 500 ms in duration where the temporal envelope contained only very fast fluctuations and the low-frequency temporal envelope was non-fluctuating. This non-fluctuating, low frequency, stimulus envelope means that just after stimulus onset and just before stimulus offset, the DC artefact will be flat. Since it is known that the DC artefact will be flat in this period, the randomisation procedure described in *Constraining the Fit* can be applied. This will ensure that the fitting algorithm only fits to the mean amplitude (preserved by the randomisation procedure) and not to any neural response (destroyed by the randomisation procedure). To expand the DC estimation procedure to function with stimuli with a low-frequency fluctuating envelope, it would be necessary to remove the randomisation procedure. This was not tested in this set of experiments and more work is needed to investigate the feasibility of using the DC estimation procedure with stimuli with fluctuating envelopes.

3.3.5 Clinical Application of CAEPs for CI Users

A number of studies have indicated that cortical evoked potentials may be advantageous for predicting speech perception outcomes for CI subjects (Wable et al., 2000; Firszt et al., 2002b; Kelly et al., 2005; Zhang et al., 2011), more so than earlier evoked potential responses such as auditory nerve electric compound action potentials (ECAPs) or auditory brainstem responses (Miller et al., 2008). However, two factors appear to have limited the clinical application of cortical evoked potentials for CI subjects. The first factor is the CI related artefact. The ICA based approach is profitable in a research setting but, because of the necessity for multi-channel data, its practical application in a clinical setting is limited. This study provides a solution to this problem by showing how the CI related artefact can be attenuated using only single channel data, which are more easily obtained in a clinical setting. Recent work by our group (McLaughlin et al., 2012b) and Beynon et al (2008; 2012) has shown how CAEPs can be measured for CI subjects using the CI itself as a recording device, removing the need to attach scalp electrodes or have a dedicated CAEP acquisition system. Combining the

CAEP CI recording technique with this single channel artefact cancelation approach would greatly increase the ease of access to CAEPs: just as an ECAP can be measured directly from the CI, so too could CAEPs. The second factor hindering the application of cortical evoked potentials in clinical practice is that a stimulation paradigm or neural response that shows a strong correlation with speech perception in a large population of CI users has yet to be found. Firszt et al. (2002b) showed, in a small population of CI users, a significant correlation between speech perception in quiet and a measure of mid-latency Na-Pa amplitude normalised for different stimulation levels. Zhang et al. (2011) found that a mismatch negativity measure could discriminate between good and bad performers on a speech perception task. By eliminating the need for multi-channel recordings, thereby reducing recording times, the single channel approach should facilitate the study of larger populations of CI subjects and may help in the development of an improved neural objective measure of CI performance. Behaviourally, it has been shown that more complex stimuli, which probe the spectral discrimination of CI users, can be used to provide a reasonable estimate of speech perception (Henry and Turner, 2003; Henry et al., 2005; Won et al., 2007).

3.3.6 Conclusion

The single-channel artefact cancellation approach described here can successfully attenuate both the high-frequency artefact produced by a cochlear implant and the DC artefact. The main advantage of this approach is that only single channel data are needed, simplifying the hardware and software requirements. The single channel approach should facilitate research into CAEPs recorded from CI users and could help develop a clinically applicable objective neural metric of CI performance.

Key Points

- This Chapter addresses the research questions 1, 2, and 3, listed in Section 2.4
- A single-channel, high-resolution and high-sampling rate system has been developed to fully capture the influence of the CI electrical stimulation on EEG recordings.
- The CI induced electrical artefact can be characterised in terms of a high-frequency component, directly related to the device's stimulation pulse rate, and a low frequency component that, albeit its origin is uncertain, seems to be associated with the stimulation pulse amplitude of the device.
- A three-stage artefact attenuation approach was developed and can successfully recover the neural signal of interest from the CI artefact contaminated EEG recordings.
- The findings described in this Chapter were presented at the 7th International Symposium on Objective Measures in Auditory Implants, Amsterdam 2012.
- This Chapter has been published as: "Cochlear Implant Artifact Attenuation in Late Auditory Evoked Potentials: A Single Channel Approach". Hearing Research, 302:84-95. August 2013.

Chapter 4 Objective Assessment of Spectral Ripple Discrimination in Cochlear Implant Users via Cortical Auditory Evoked Potentials

It was mentioned in Section 1.2 that standardised sentence and word recognition tests are helpful for directly measuring speech perception in CI listeners. However, they cannot be used with pre-lingual children (a rapidly expanding user group (Waltzman and Roland, 2005)). Additionally, as highlighted in Chapter 3, speech-based tests may not be the best way to assess the performance of CI recipients while they are still learning to understand speech heard through their device.

Non-speech based evaluation methods aimed to evaluate the underlying mechanisms of speech recognition (e.g. spectral resolution) may provide a favourable alternative for the acute assessment of CI performance (Drennan et al., 2015). A spectral ripple discrimination test is a non-linguistic psychoacoustic method for probing a normal hearing listener's spectral resolution (Supin et al., 1997). A number of studies have shown that spectral ripple discrimination correlates with different aspects of speech perception and music perception in CI users (Henry et al., 2005; Litvak et al., 2007; Won et al., 2007; Jones et al., 2011; Drennan et al., 2015).

To measure spectral ripple discrimination thresholds in CI listeners, standard psychoacoustic threshold tracking methods are normally employed. CI listeners actively listen to a number of intervals containing either a standard stimulus or its ripple-phase inverted counterpart. They are requested to report which interval contained the inverted stimulus by, for example, pressing a button corresponding to the interval. This approach produces reliable results in adults. Although experienced researchers might be able to

apply an observer based psychoacoustic procedure to measure spectral ripple discrimination thresholds in infants (Horn et al., 2013), these standard psychophysical approaches are difficult to apply to special populations such as paediatric, pre-lingually deafened or non-compliant users in clinical practice.

An alternative to psychoacoustic methods is to employ an objective neural response, like the ones described in Section 2.3.2, to predict behavioural outcomes. An advantage of this approach is that listeners do not need to respond to the stimuli and often need not attend to the stimuli. A natural candidate for this approach is the MMN, as it has been previously proposed as an objective index of auditory discrimination for different clinical conditions (Naatanen et al., 2012). A detailed description of the MMN response can be found in Section 2.3.2.

The aim of this study was to utilise an unattended oddball paradigm to develop and validate a completely objective method for measuring spectral ripple discrimination thresholds in adult CI listeners, taking advantage of the single-channel acquisition set-up and the CI artefact attenuation methodology detailed in Chapter 3. An objective method for measuring spectral ripple discrimination thresholds would potentially provide an additional tool when standard psychophysical approaches are difficult to apply to certain CI populations.

4.1 Materials and Methods

4.1.1 Subjects

Nineteen adult CI listeners (6 male, 13 female) participated in the present study at two separate locations: Trinity Centre for Bioengineering, Trinity College Dublin (n=15) and Hearing and Speech Laboratory, University of California Irvine (n=4). One bilateral subject was evaluated separately for both ears yielding a total of 20 ears tested. Exclusion criteria applied to subjects under 18 years of age and subjects with cognitive or learning disabilities. There were no subjects withdrawn from this study. Subjects were aged between 31 and 79 years (mean 56, standard deviation 15). They used either a Cochlear (n=17), Med-El (n=1) or Advanced Bionics (n=1) implant (device details on implant type and usage experience are shown in Table 4.1). All subjects used monopolar stimulation mode.

Experimental procedures were approved by the Ethics (Medical Research) Committee at Beaumont Hospital, Beaumont, Dublin, the Ethical Review Board at Trinity

College Dublin and The University of California Irvine's Institutional Review Board. Written informed consent was obtained from all subjects.

4.1.2 Psychoacoustic Methods

Psychoacoustic Stimuli

Psychoacoustic spectral ripple discrimination thresholds were determined in all subjects using stimuli similar to that employed by Won et al. (Won et al., 2007). Stimuli were generated by summing 250 pure tones ranging from 250 to 5000 Hz. The amplitudes of the pure tones were determined by a full-wave rectified sinusoidal envelope on a logarithmic amplitude scale. The ripple peaks were spaced equally on a logarithmic frequency scale. The starting phases of the components were randomised for each presentation. The ripple stimuli were generated with 14 different densities, measured in ripples/octave. The ripple densities differed by ratios of 1.414 (0.125, 0.176, 0.250, 0.354, 0.500, 0.707, 1.000, 1.414, 2.000, 2.828, 4.000, 5.657, 8.000, and 11.314 ripples/octave). Standard and ripple-phase inverted stimuli were generated de novo in each trial run. For standard stimuli, the phase of the full-wave rectified sinusoidal spectral envelope was set to zero radians, and for phase-inverted stimuli, it was set to $\pi/2$. The stimuli were 500 ms in duration and 50 ms on and off cosine squared ramps were applied. Stimuli were filtered with a long-term, speech-shaped filter (Byrne et al., 1994). All stimuli were generated in MATLAB (MathWorks, Natick, MA) at 44.1 kHz and presented via a standard PC soundcard.

For both the psychoacoustic and electrophysiological testing, stimuli were presented via the audio line-in on the CI at the most comfortable level, determined for each subject using a 0 (silence) to 10 (too loud) loudness scale, with 6 being the most comfortable level. To limit the effects of any unwanted background noise the CI microphone volume and sensitivity were set to the minimum allowable values. Subjects used their everyday speech processing strategy without any special adjustments other than changes to the microphone volume and sensitivity. Stimuli were always presented monaurally.

Psychoacoustic Procedure

A two-down, one-up, three-alternative forced-choice (Levitt, 1971) paradigm was used to track the psychoacoustic spectral ripple discrimination threshold. Within one trial, two of the intervals were randomly selected to present the standard stimulus whilst the

remaining interval presented the inverted stimulus, with all three intervals having stimuli with the same number of ripples/octave. If the subject's spectral resolution is sharp enough to resolve the spectral peaks and valleys, they should hear a difference in the standard and inverted stimuli (Won et al., 2007; Jones et al., 2011). The subject was asked to select the interval which was different by pressing a button on a graphical user interface. After two consecutive correct responses, the number of ripples/octave was increased by a ratio of 1.414. As the number of ripples/octave increased, the standard and inverted stimuli began to sound more similar. After one incorrect response the number of ripples/octave was decreased to the previously tested value. A run was terminated after 13 reversals. The psychoacoustic spectral ripple discrimination threshold was defined as the mean of the last eight reversals on the three-alternative forced-choice threshold tracking function (Levitt, 1971). All subjects completed at least five repetitions of the test to minimise any learning or attention effects. The final threshold was taken as the mean of all completed tests.

4.1.3 CAEP Methods

CAEP Stimuli

The stimuli used in the electrophysiological paradigm were similar to those used in the psychoacoustic paradigm except that 4000 pure tones ranging from 100 to 8000 Hz were used to cover the full frequency range of the CI filter bank. The lower pure tone range in the psychoacoustic stimuli allowed for the stimuli to be generated and presented faster while still presenting some energy to the highest CI high-frequency band.

Standard and ripple phase-inverted stimuli with durations of either 300 or 500 ms and with 0.125, 0.25, 0.5, 1, 2, 4 and 8 ripples/octave were generated and stored. Examples of the stimuli characterisation at one and four ripples/octave can be seen in Figure 4.1. There was no significant difference for the presentation of 300 or 500 ms stimuli with respect to the CI artefact, therefore, data from both stimuli duration were pooled together for analysis. The same set of stored stimulus tokens were used for all presentations to all subjects. In Trinity College Dublin stimuli were presented via a standard PC soundcard (44.1 kHz sampling rate) and in University of California, Irvine stimuli were presented using a USB digital to analogue converter (DAC, 44.1 kHz sampling rate) (NI-USB 6221, National Instruments, Austin, TX).

Table 4.1 Psychoacoustic and neural discrimination thresholds.

Subject ID	Implant	Tested Ear	Years of CI Experience	Psychoacoustic Spectral Ripple Discrimination Threshold (RPO)	Neural Spectral Ripple Discrimination Threshold (RPO)		
					Positive Area	Negative Area	Total Area
UCI 01	Maestro	Left	2	0.574	0.420	0.398	0.434
UCI 02	Freedom	Right	5	1.403	1.008	0.900	0.989
UCI 03	Freedom	Left	9	2.210	3.202	6.335	5.974
UCI 03	Freedom	Right	1	1.542	2.085	1.188	2.407
UCI 04	Freedom	Right	4	2.595	1.252	0.659	1.045
TCD 01	Freedom	Left	3.5	1.158	1.793	0.665	0.763
TCD 02	Freedom	Left	4	0.381	0.193	0.337	0.225
TCD 03	Clarion 1.2	Right	12	0.948	0.909	0.589	0.953
TCD 04	Freedom	Left	7	0.618	0.248	0.221	0.237
TCD 05	Freedom	Left	5	2.172	2.957	2.861	2.987
TCD 06	Freedom	Right	1	0.658	*	*	*
TCD 07	Freedom	Right	1	0.778	*	0.161	0.150
TCD 08	CI512	Right	1	0.400	0.473	0.239	0.409
TCD 09	Freedom	Left	3.5	0.235	0.176	*	0.138
TCD 10	Freedom	Right	3.5	0.312	0.821	0.546	0.739
TCD 11	CI24RE	Right	9	1.113	0.489	0.833	0.782
TCD 12	Freedom	Right	4	0.931	1.618	1.497	1.597
TCD 13	CI24R	Left	8	0.463	*	0.461	0.482
TCD 14	CI24M	Right	12	1.503	1.717	1.870	1.827
TCD 15	Freedom	Left	5	0.240	*	*	*

RPO- Ripples per octave.

* Unable to estimate a neural spectral ripple discrimination threshold.

doi:10.1371/journal.pone.0090044.t001

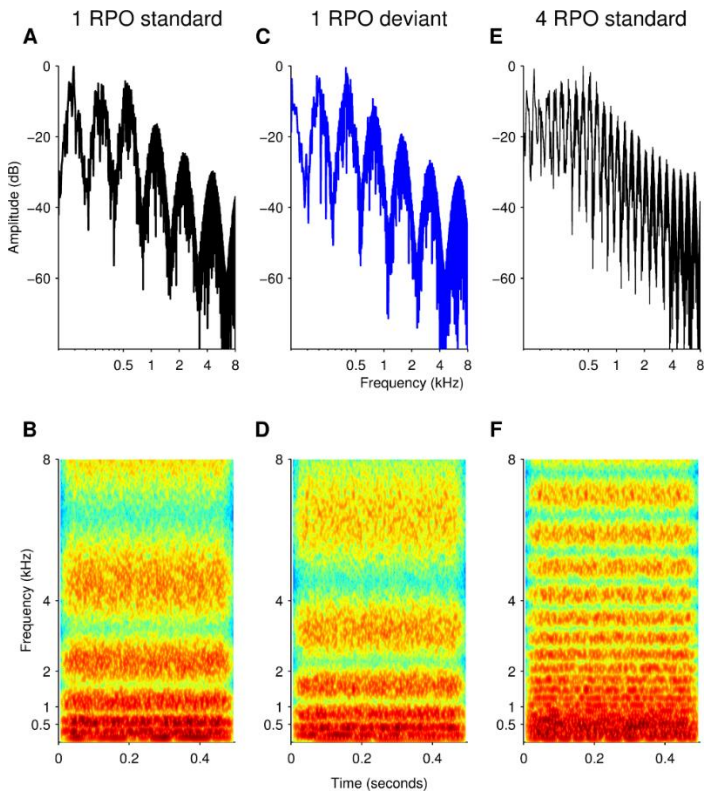

Figure 4.1 Spectral ripple stimuli characterisation.
(A) Frequency spectrum of a 500 ms standard stimulus with spectral peak density of one ripple per octave (RPO). One spectral peak can be clearly distinguished at the 0.5 – 1 kHz octave. Peak to valley amplitude of 30 dB as well as the high frequency attenuation of the speech-shaped filter can also be seen. (B) Spectrogram of the standard stimulus described, showing the frequency content of the stimulus along the 500ms duration. Spectral peak density of one RPO can clearly be resolved in the 4 – 8 kHz octave. (C) Frequency spectrum of the corresponding phase-inverted, or deviant, stimulus employed along with the standard stimulus at one RPO in an oddball paradigm. (D) Spectrogram of the deviant stimulus, showing the inversed frequency content along the 500ms duration with respect to the standard stimulus. (E) Frequency spectrum of a standard stimulus with spectral peak density of four RPO showing the increased spectral density with respect to the one RPO stimuli. (F) Spectrogram of the standard stimulus at four RPO. Spectral peak density of four RPO can clearly be resolved in the 4 – 8 kHz octave.

CAEP Acquisition

Figure 4.2 shows a schematic representation of the single-channel EEG acquisition set-up developed in Chapter 3. This configuration was employed in this study to record CAEPs elicited to the spectral ripple stimuli presented in an oddball paradigm. Standard gold cup surface electrodes were placed at Cz, on the mastoid and on the collarbone, these last two electrodes were placed contralateral to the CI location. Electrode impedances were always below 5 kΩ and care was taken to ensure that impedances were matched to within 1 kΩ to minimise low frequency artefacts as per the recommendations outlined in Section 3.3.1. The output of the amplifier was connected to one channel on the ADC. A trigger pulse generated simultaneously with the stimulus, and

presented on a separate channel, was connected to a second channel on the ADC and used to synchronise stimulus presentation and acquisition.

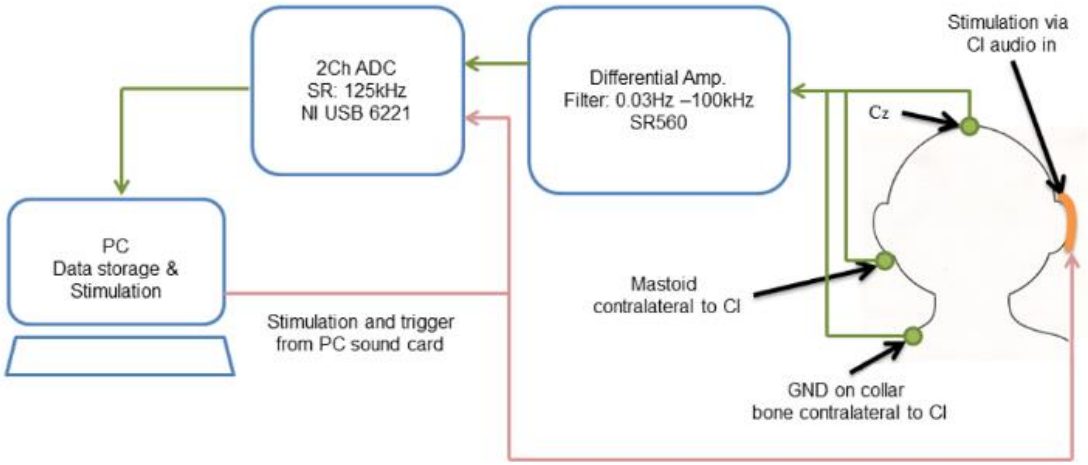

Figure 4.2 Single-channel acquisition set-up.
EEG is recorded from electrode position Cz, referenced to the mastoid contralateral to the tested ear and grounded on the collar bone. Stimulus and trigger presentation is done through the sound card of the computer. The trigger is fed to the ADC for event synchronization and the stimulus is presented via a personal audio cable to the auxiliary port of the subject's speech processor.

CAEP Procedure

Standard and ripple phase-inverted stimuli with the same number of ripples/octave were presented in an unattended oddball paradigm (see Figure 4.3). The deviant stimulus was the ripple phase-inverted stimulus, having an occurrence probability of 10%, and the standard stimulus was the non-inverted stimulus. The inter-onset interval for each stimulus presentation was one second. One run began with 20 presentations of the standard stimulus after which the deviant randomly occurred at least once in every 10 stimulus presentations, with the additional condition that a deviant was never to be followed by another deviant. The paradigm was repeated at least four times for every subject, each time using stimuli with a different number of ripples/octave. Subjects were instructed to ignore the stimulus and to minimise movement to avoid movement artefacts in the recordings. Each oddball paradigm lasted approximately 12 - 15 minutes. Subjects watched a silent captioned film and rest breaks were provided after each run or upon subject's request. EEG data collection lasted approximately one hour per subject. At Trinity Centre for Bioengineering the acquisition sessions took place in a dedicated EEG room, while at the University of California Irvine, the sessions took place in a sound booth.

CAEP Epoching

Raw EEG data were segmented into long epochs of 1100 ms, 300 ms pre- to 800 ms post-stimulus onset to avoid filter edge effects. Shorter epochs of 100 ms pre- to 500ms post-stimulus were used for plotting the data. A baseline correction of 150 ms pre-stimulus was applied in all filtered epochs. Epochs were classified as response to standard or deviant stimuli and averaged across presentations. Online averaging and artefact attenuation allowed the real time display of the evoked potential response to both standard and deviant stimuli. To speed up data collection a run was terminated when collecting more deviant responses did not significantly change the shape of the averaged deviant waveform. This change was evaluated by measuring the sum of squared differences of the averaged deviant epochs every time a new epoch was included, when the sum of squared differences stabilised at a low value it was determined that no significant change would be produced with the addition of more epochs. This was typically once 60 or 70 deviant responses were acquired, with a minimum of 50 deviants per run always being collected. A difference (or mismatch) waveform was calculated by subtracting the response to the standard stimuli from the response to the deviant stimuli (see Figure 4.3). The oddball paradigm was repeated using stimuli with different numbers of ripples/octave, yielding one difference waveform for each ripple/octave stimulus.

CAEP Artefact Attenuation

A 2nd order Butterworth band-pass filter (2-20 Hz, 12 dB/octave slope) was applied to the averaged standard and deviant responses (Figure 4.4 A and B single responses before filtering, Figure 4.4 C and D averaged responses after filtering) to eliminate the HFA described in Chapter 3. The filter was applied using a zero-phase forward and reverse digital filtering method (filtfilt command, MATLAB).

It was observed that, within a subject, the signal envelopes derived from the CI stimulation pulse sequence associated with the standard and deviant stimuli were similar (compare Figure 4.4 A and B). A cross-correlation of 112 sets of standard and deviant CI stimulation pulse sequences supported this observation (mean normalised correlation= 0.8871, standard deviation= 0.1597). This cross-correlation suggested that any low frequency artefact component was equally present in both the response to the standard and the response to the deviant (compare onset and offset artefacts in Figure 4.4 C and D), calculating the difference waveform adequately attenuated any low frequency artefact components, leaving a difference waveform dominated by neural response (Figure 4.4 E).

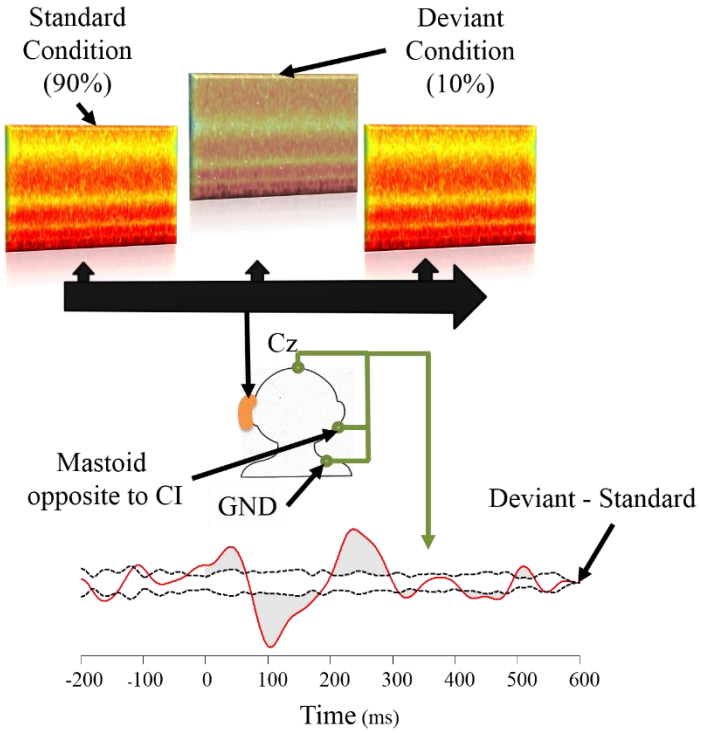

Figure 4.3 90-10 unattended oddball paradigm.
The standard condition was spectrally rippled noise stimuli at a specific RPO density. The deviant condition was the ripple phase-inverted version of the standard stimuli, having an occurrence probability of 10%. The difference waveform was calculated by subtracting the CAEP response to the standard stimuli from the CAEP response to the deviant stimuli and quantified as the area above or below the noise floor of the signal.

4.1.4 CAEP: Spectral Ripple Discrimination Thresholds

Hypothesis and Methodological Overview

If a listener can acoustically perceive a difference between a standard and deviant stimulus, the CAEP response to the deviant stimulus, when presented in an oddball paradigm, will differ in shape from that evoked by the standard stimulus (Picton et al., 2000; Naatanen et al., 2012). As mentioned in Section 2.3.2, the MMN is normally quantified by calculating a difference waveform, i.e. deviant response minus standard response. If the standard and deviant responses are the same, the difference waveform should be flat; while if they differ, the difference waveform will show oscillations. In practice the noise inherent in CAEP recordings means that even if the underlying standard and deviant waveforms are identical the difference waveform will still show some oscillations. Therefore, to calculate a neural discrimination threshold it was necessary to first quantify the amount of noise in the difference waveform and then define what quantifies a significant difference waveform response.

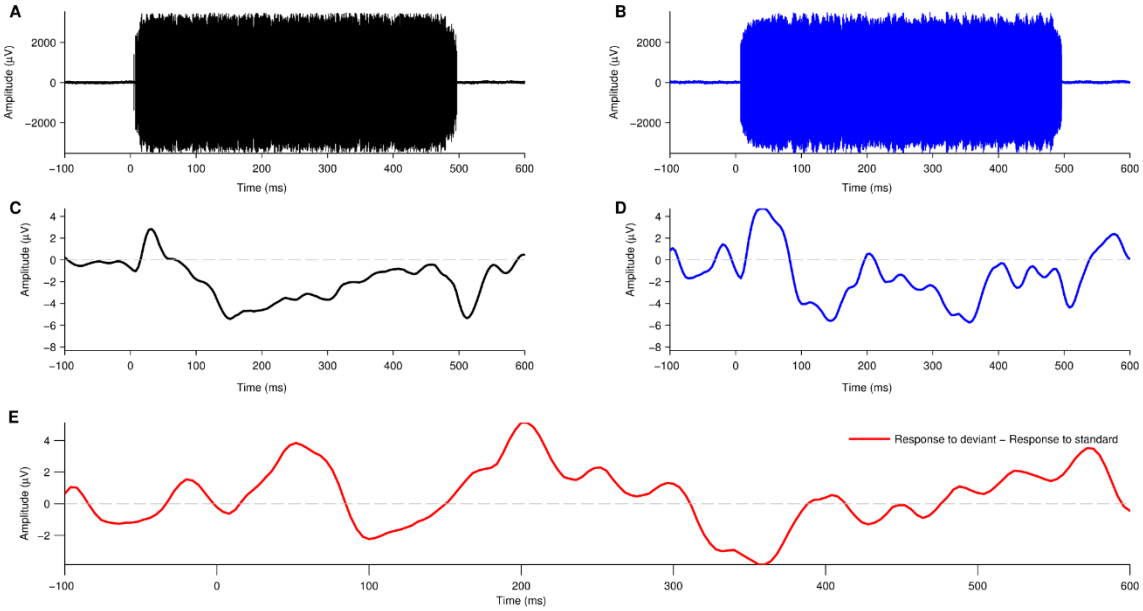

Figure 4.4 Artefact attenuation and CAEP extraction.
(A)-(B) Single EEG acquisition epoch of a 500 ms stimulus presented to a CI user. Data acquisition at a high-sampling rate (125 kHz) allows for the CI artefact to be clearly resolved from the recorded data as a high-frequency and large amplitude component present during the 500 ms of stimulus duration (standard in black, deviant in blue). (C)-(D) Applying a 2nd order Butterworth band-pass filter (2 – 20 Hz) to the averaged epochs, recorded from an oddball paradigm, it is possible to attenuate the CI artefact and extract the evoked potential (EP) elicited to each stimulus type (standard in black, deviant in blue). The N100, characteristic of AEPs, can be identified in both standard (C) and deviant (D) responses as a negative peak at around 100- 150 ms. In some cases, after filtering, a low-frequency artefact is present at stimulus onset and offset with similar shape and amplitude in both standard and deviant responses. (E) A difference waveform is calculated by subtracting the neural response elicited to the standard stimuli from the neural response elicited to the deviant stimuli. This method allows further attenuation of residual low-frequency artefacts.

Calculating the Difference Waveform Noise Floor

The noise present in one difference waveform was calculated by applying a bootstrap method to all the standard responses collected for that subject during that run. A randomly chosen sub-sample of 10% of all standard responses was chosen and averaged together to create a bootstrapped deviant response (Figure 4.5 A, blue line). The remaining 90% of the standard stimuli were then averaged together to create a bootstrapped standard response (Figure 4.5 A, black line). The bootstrapped deviant was subtracted from the bootstrapped standard to give a bootstrapped difference waveform (Figure 4.5 B, red line). If no noise were to be present in the recording this bootstrapped difference waveform would be completely flat. Thus, oscillations present in the bootstrapped difference waveform quantify the noise present in the recording. The bootstrap procedure was repeated to generate 54 separate bootstrapped difference waveforms. The noise floor was defined as the standard deviation of all bootstrapped

difference waveforms at each time point for positive and negative values (Figure 4.5 B, black lines).

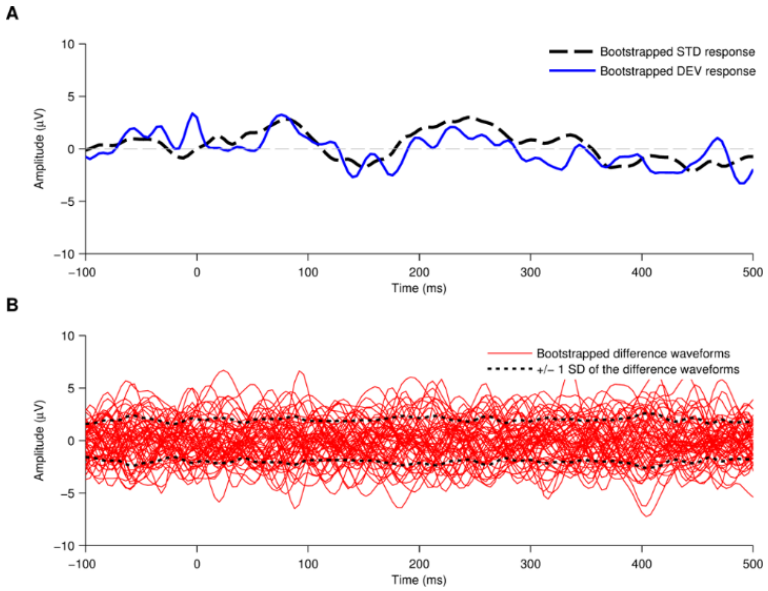

Figure 4.5 Noise-floor calculation of the neural response.
(A) The noise floor was calculated with a statistical bootstrap method. A random 10% sub-sample of epochs from the standard stimulus type was averaged to create a bootstrapped deviant response whilst the remaining epochs were averaged together to create a bootstrapped standard response. (B) A difference waveform was calculated by subtracting the bootstrapped standard response from the bootstrapped deviant response. This process was repeated 54 times, each time with a different randomly selected 10% sample of standard epochs. The noise floor of the signal was defined as +/- one standard deviation of the 54 resulting difference waveforms.

Defining a Significant Difference Waveform Response

To quantify the difference waveform, the area above the noise floor within a 90 to 450 ms time window was calculated. This time window allows for the expected CAEP components such as N1, P2, N2, P3 or MMN to be included in the analysis. Given that the difference waveform is defined as microvolts in function of time in milliseconds, the area above the noise floor is defined as microvolts times milliseconds ‘µVms’. A neural spectral ripple discrimination threshold was then defined as the point at which this area dropped below a predetermined significance level. As the aim of this study was to develop an objective CAEP test to accurately predict the psychoacoustic spectral ripple discrimination threshold, the significance level was determined by calculating the neural threshold for a range of different significance levels and selecting the significance level which gave the best correlation with the psychoacoustic threshold across all subjects. The ‘Defining a Significance Level’ subsection of Section 4.2.2, presents details of how this procedure was applied together with results from a validation study where data from all 19 subjects were randomly partitioned into two groups. One group was used to estimate

the significance level and the other group to test the accuracy of this significance level by predicting the psychoacoustic spectral ripple discrimination threshold.

4.2 Results

4.2.1 Psychoacoustic Spectral Discrimination Thresholds

Table 4.1 summarises the individual spectral ripple discrimination thresholds for all ears tested. The range (0.235 to 2.595 ripples/octave) and mean (1.012 ripples/octave) are in general agreement with previously reported values for spectral ripple discrimination in CI listeners (Henry and Turner, 2003; Henry et al., 2005; Won et al., 2007).

4.2.2 CAEP Spectral Ripple Discrimination Thresholds

CAEPs and Difference Waveform

Figure 4.6 A shows an example of CAEP waveforms recorded using an oddball paradigm in response to a 0.25 ripples/octave stimuli. The black line shows the response to the standard (standard spectral ripple stimulus) and the blue line the response to the deviant (inverted spectral ripple stimulus). This user reported hearing a difference between the standard and the deviant stimulus (psychoacoustic spectral ripple discrimination threshold of 2.210 ripples/octave) and correspondingly there was a marked difference in the response to the deviant. The deviant response has a larger P2 amplitude than the standard response. It also contains an N3 and P4 component which are not present in the standard response. Figure 4.6 B shows the difference waveform calculated by subtracting the standard from the deviant response. The P2, N3 and P4 differences are apparent in the difference waveform and, importantly, their peaks are above or below the noise-floor indicating that the neural response to the deviant is significantly different to the neural response to the standard.

To determine a neural spectral ripple discrimination threshold, responses to spectral ripple stimuli with an increasing number of ripples/octave were measured in all subjects. The standard and deviant responses for one subject to stimuli with 0.25, 0.5, 1 and 2 ripples/octave are shown in Figure 4.7 A. The large positivity, around 40 ms, present in all standard and deviant responses is probably an onset artefact. The standard responses to the 0.25, 0.5, 1 and 2 ripples/octave stimuli are similar. However, the deviant

responses change as the number of ripples/octave is increased. The deviant response to the 0.25 ripples/octave stimulus shows a large increase in the N1 and P2 component when compared with the standard response.

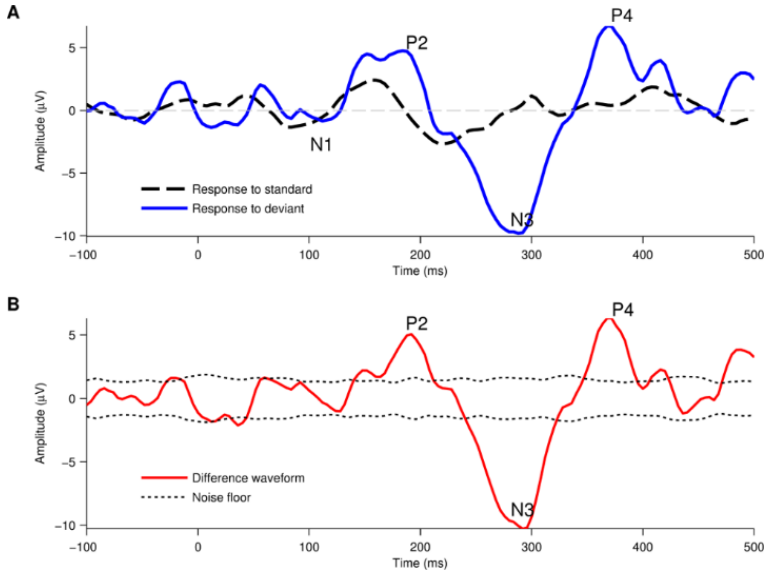

Figure 4.6 Difference waveform elicited to an oddball paradigm.
(A) CAEP responses elicited to 608 standard stimuli and 65 deviant stimuli at 0.25 RPO. When the standard and deviant stimuli are perceived as different sounds, the morphology of the neural response to the deviant stimuli (blue trace) is significantly different to the response to the standard stimuli (dashed, black trace). (B) The difference waveform represents the mismatch between the responses elicited to each stimulus type.

As the number of ripples/octave increases (and the stimuli begin to sound more alike) this N1-P2 difference becomes smaller and delayed, until at 2 ripples per octave the response to the deviant is essentially the same as the response to the standard. This subject had a psychoacoustic spectral ripple discrimination threshold of 1.503 ripples/octave. Figure 4.7 B shows the difference waveforms. Since the onset artefact (around 40 ms) was equally present in both standard and deviant responses it is significantly attenuated in the difference waveform. Calculating the area above and below the noise floor (shaded) within a 90-450 ms time window allows a quantification of the difference in the neural response to the standard and deviant stimuli. This area is large for 0.25 ripples/octave where the subject perceives a clear difference between the standard and deviant stimuli and is negligible at 2 ripples/octave where the subject reports that the standard and deviant stimuli sound the same.

Defining a Significance Level

In Figure 4.8, the area above and below the noise floor, and the total area, are plotted as a function of ripples/octave for the same subject shown in Figure 4.7. It is clear that as the number of ripples/octave increases, the area above and below the noise floor

decreases, i.e. the standard and deviant responses become similar. To allow the objective estimation of neural spectral ripple discrimination thresholds, a significance level (i.e. an area in microvolt times millisecond 'µVms') was defined as the threshold below which area differences between the standard and deviant response can be considered perceptually negligible.

A bootstrap method was employed to define and validate this significance level for the three different area measurements. The approach, described in detail below and in a flow chart in Figure 4.9 A, operated by first dividing the data into two groups. The first group (a determination group) was employed to determine one significance level for all members, which gave the best correlation with the known psychophysical thresholds. The second group (an estimation group) was then employed to test how well this significance level could estimate the known psychophysical threshold.

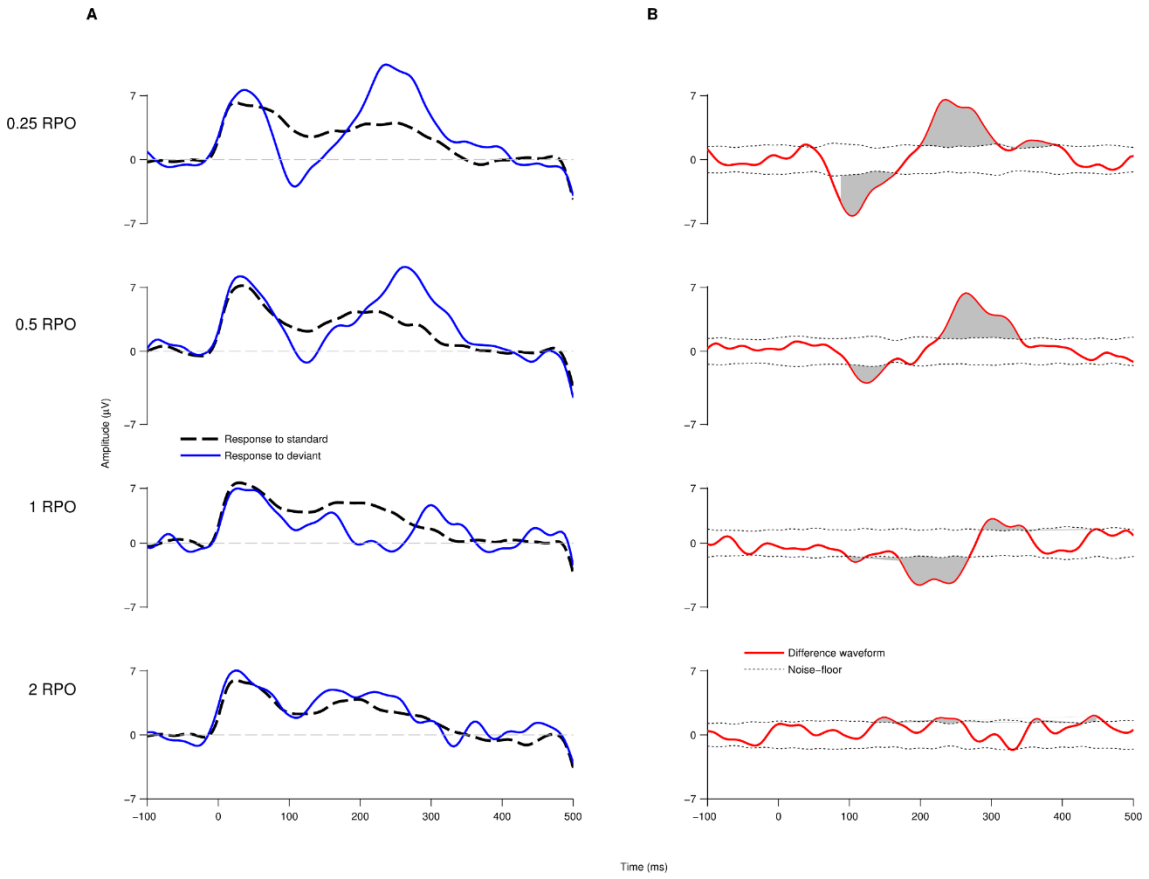

Figure 4.7 Sequential decrease of the difference waveform's area above the noise floor. *(A) CAEP traces of standard and deviant stimuli elicited at 0.25, 0.5, 1 and 2 RPO. As the spectral density increases, the neural responses to the standard and deviant stimuli become more similar. (B) The difference waveform at each spectral density shows a sequential decrease of the mismatch between the responses elicited to each stimulus type. The area above the noise floor of the signal (shaded grey) is taken as an indicator of said mismatch decrease.*

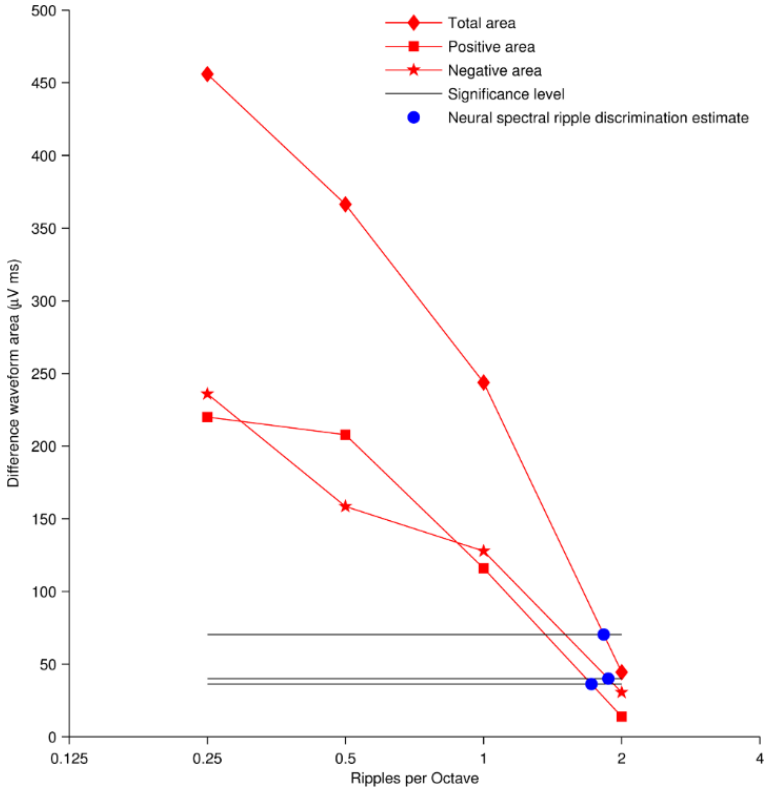

Figure 4.8 Estimation of the spectral ripple discrimination threshold based on the neural response.
The neural spectral ripple discrimination threshold is estimated as the point where the mismatch between the neural responses dropped below a set significance level. Thresholds were estimated with three different area-above-the-noise-floor measurements: positive area, negative area and total area above the noise floor.

Data from the 20 tested ears were separated into two groups: a determination and an estimation group. The determination group contained 12 randomly selected datasets whilst the estimation group contained the remaining 8 datasets. This partition ratio was chosen so that the estimation group represented more than a third of the total sample. Each dataset contained at least four measurements presenting stimuli with different ripples/octave. For the determination group, the neural spectral ripple discrimination threshold was calculated and linearly regressed with the measured psychoacoustic threshold for each subject. If the area never went below the significance level, the dataset was excluded. This regression was tested for a range of 19 different predetermined significance levels, ranging from 10 µVms to 100 µVms at 5 µVms increments, yielding 19 different (determination) R^2 and p-values (Figure 4.9 B). Significance levels, for which the regression yielded a p-value greater than 0.01 or which excluded more than two datasets, were discarded. From the remaining significance levels, the one that yielded the greatest regression R^2 was selected (Figure 4.9 B, red dot). The selected significance level was applied to the estimation group to determine the neural spectral ripple discrimination

threshold and then quantify, using linear regression, how well this predicted the psychophysical threshold (Figure 4.9 C). If this (estimation) regression yielded a p-value less than 0.05 with no dataset exclusions then the significance level was accepted. Otherwise, the significance level was rejected. One point on Figure 4.9 C represents one of the accepted estimation R^2 and p-values. Figure 4.9 C shows the p-values as a function of the regression R^2 value for the estimation group's linear regression.

This process was repeated, each time using a different random partitioning of the datasets into determination and estimation groups, until 20 significance levels that satisfied the criteria were generated (Figure 4.9 D). This shows that the significance level chosen performs accurately when estimating the psychoacoustic thresholds measured for each subject. The final significance level defined for this study was the average of the accepted significance levels. The entire process was repeated for the positive, negative and total area measurements.

For the total area the mean significance level was determined to be 70.4 µVms (17.7 standard deviation). Two tested ears did not yield a neural threshold (Figure 4.10 A). For one tested ear (TCD 06 in Table 4.1) the area above the noise floor for all recordings was below the significance level defined, and for the remaining exclusion (TCD15 in Table 4.1), the area above the noise floor did not drop below significance level. The mean neural threshold across 18 datasets was 1.230 ripples/octave (1.386 standard deviation).

For the positive area the mean significance level was determined to be 36.3 µVms (13.8 standard deviation). Four datasets did not yield a neural threshold using the positive area (Figure 4.10 B). The area above the noise floor from two tested ears (TCD 13 and TCD 15 in Table 4.1) did not drop below the significance level in any of the four recordings. Contrastingly, the area above the noise floor from the remaining two exclusions (TCD 06 and TCD07 in Table 4.1) was below the significance level in all four recordings. Hence, it was not possible to estimate the neural spectral ripple discrimination threshold. The mean neural threshold for the remaining 16 datasets was 1.121 ripples/octave (0.920 standard deviation).

For the negative area the mean significance level was determined to be 40 µVms (3.9 standard deviation). Three datasets did not yield a neural threshold (Figure 4.10 C). The area above the noise floor of three tested ears (TCD 06, TCD 09 and TCD15 in Table 4.1) was below the significance level in every recording, making it impossible to estimate a neural spectral ripple discrimination threshold with the defined significance level. The

mean neural threshold across 17 datasets was 1.116 ripples/octave (1.458 standard deviation). The individual neural thresholds for the positive, negative and total area are reported in Table 4.1.

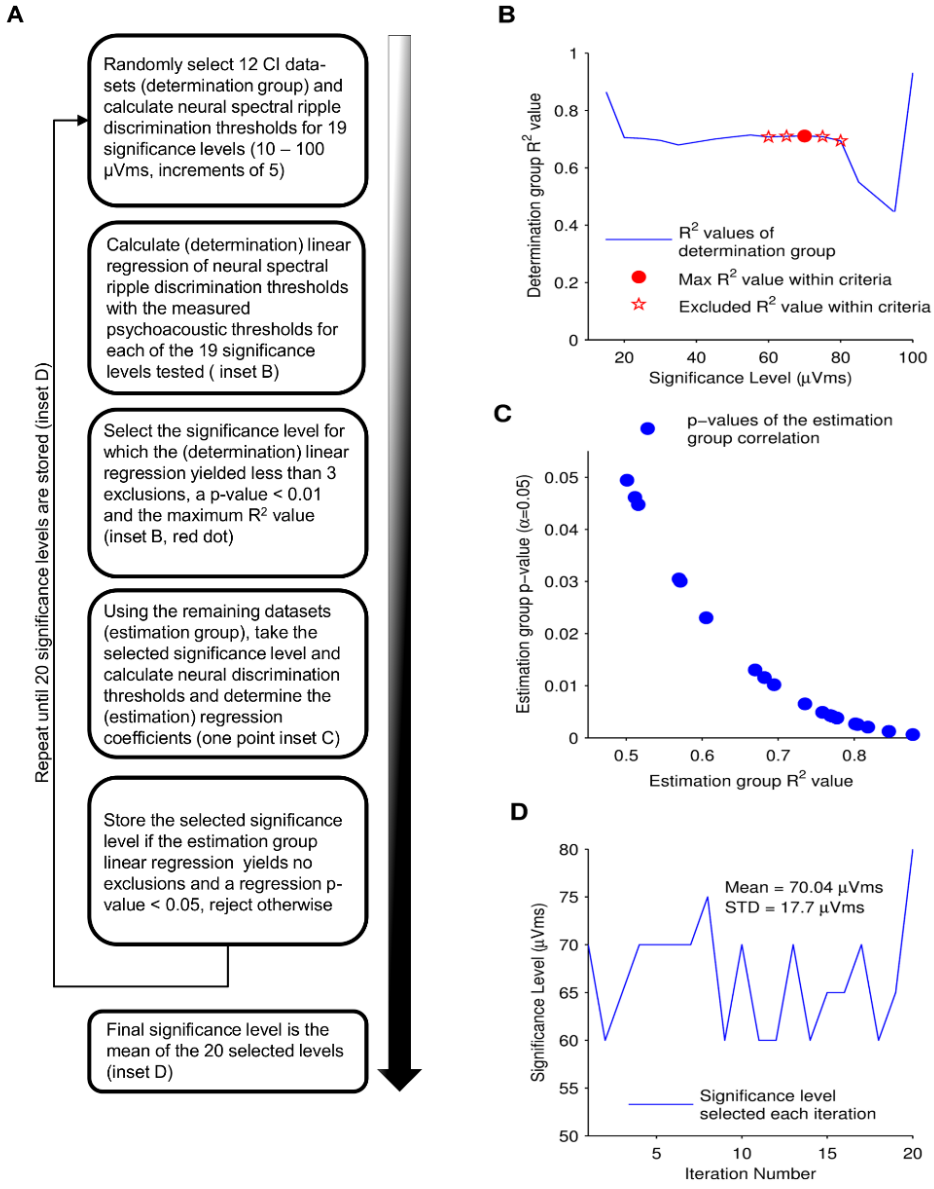

Figure 4.9 Bootstrapped determination of the significance level.
(A) Describes the progression of the bootstrapping method employed to determine the level at which neural spectral ripple discrimination thresholds were estimated and regressed with the measured psychoacoustic thresholds. (B) The square of the Pearson's correlation factor (R2) vs. the 19 significant levels tested on the determination group is plotted. The significance level that yields the maximum R2 value within the selection criteria, identified as the red point in the plot, is selected to continue with the bootstrap method, the rest are excluded (hollow stars). (C) The selected significance level is evaluated with estimation group. The regression's p-value plotted vs. the regression's R2 value resulting from the significance level evaluation on the estimation group for 20 bootstrap iterations. If the evaluation yields no exclusions and a p-value less than 0.05, the significance level is stored. (D) The bootstrap method is repeated to select 20 different significant levels. The mean of the selected values is employed as the final significance level.

Correlation between Psychoacoustic and Neural Thresholds

Linear regression of the psychoacoustic spectral ripple discrimination thresholds with the neural spectral ripple discrimination thresholds produced a Pearson's coefficient of determination (R^2) of 0.60 and p-value < 0.01 for total area (Fig. 9A), R^2 = 0.65 and p-value < 0.01 for the positive area (Fig. 9B), and R^2 = 0.50 and a p-value < 0.01 using the negative area (Fig. 9C).

Results from paired t-tests between psychoacoustic and neural thresholds, in all three area measurements, show no significant difference between the metrics: p-value = 0.75, t = 0.32 for positive area; p-value = 0.93, t = 0.09 for negative area; and p-value = 0.68, t = -0.41 for total area above the noise floor. A Steiger's Z test was performed to compare the correlations derived from the positive, negative and total area calculations. Results indicate that there is no statistically significant difference between: the positive area and negative area correlations (Z = 1.51, p-value > 0.05); the positive area and the total area correlations (Z = 1.14, p-value > 0.05) and; the negative area and the total area correlation (Z= -1.34, p-value > 0.05).

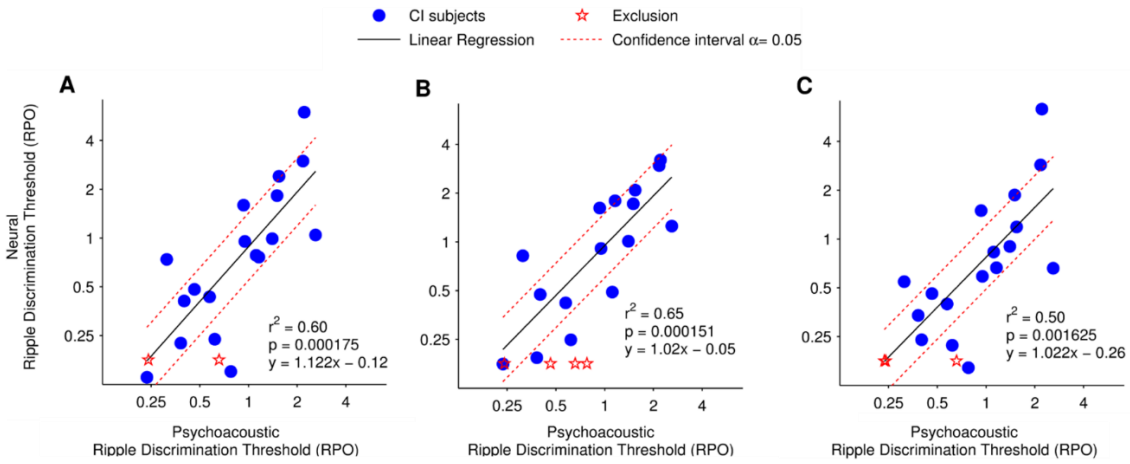

Figure 4.10 Correlation of neural and psychoacoustic spectral ripple discrimination thresholds.
Linear regression of the psychoacoustic spectral ripple discrimination thresholds with the neural spectral ripple discrimination thresholds for each of the analysed area above the noise floor measurements: (A) total area above the noise floor; (B) Positive area above the noise floor; and (C) negative area above the noise floor.

4.3 Discussion

The present study developed and validated a method to objectively assess spectral ripple discrimination in a population of CI listeners using an oddball EEG paradigm. Employing the clinically applicable single-channel set-up presented in Chapter 3, it was possible to acquire CAEP responses to standard and deviant stimuli in CI listeners.

Analysis of the difference waveform showed a strong correlation with behavioural spectral ripple discrimination thresholds, validating the utility of this approach as a clinical assessment tool.

4.3.1 Artefact Removal

It was possible to distinguish the expected N1-P2 complex from the CAEP traces. The large positivity at around 40 ms and negativity at around 500 ms after stimulus onset found in some subjects (see Figure 4.4 C and D) are most likely on-set and off-set artefacts caused by high-pass filtering of the low frequency (or pedestal) artefact component identified by Mc Laughlin et al. (McLaughlin et al., 2013) and others (Gilley et al., 2006; Wong and Gordon, 2009; Friesen and Picton, 2010; Viola et al., 2011) related to the CI's response to the stimuli. The 40 ms delay in the on-set artefact is caused by a combination of the rise time of the stimuli (50 ms), the CI processor delay (~5 to 8 ms as observed in single stimulus presentations, see Figure 4.4 A and B) and the high-pass filter characteristics. When present, on-set and off-set artefacts were equally present in both standard and deviant responses. Thus, the subtraction operation, employed to obtain a difference waveform, attenuated these artefacts. The analysis time window (90 to 450 ms) also minimised any potential artefact influence on the area measurement used to determine the neural spectral ripple discrimination threshold.

4.3.2 Objective Assessment of Neural Thresholds

Judging the presence or absence of a neural response in CAEPs (or in a difference waveform) is generally a subjective task. This study developed and validated an objective statistical approach to determine the point at which a response in the difference waveform became perceptually non-significant. Parts of this approach are similar to the integrated mismatch negativity metric developed by Ponton et al. (1997a) .Measuring the peak amplitude of specific components in the spectral ripple difference waveform is difficult because not all subject's responses exhibit a similar morphology (compare Figure 4.6 and Figure 4.7). The more general approach taken in this study, of measuring the area above or below a bootstrapped determined noise floor, avoids this difficulty. An area-, as opposed to peak-, based metric has the added advantage of reducing noise, an important consideration when using difference waveforms which are by definition noisier than the responses from which they are derived. To define a significance level, below which a

difference waveform area would be considered perceptually insignificant, a second bootstrap method was applied. Figure 4.9 C shows that, for 20 different data partitions, the selected significance level reasonably predicts the psychophysical thresholds of the estimation group. Additionally, variations of the significance level between around 20 and 80 µVms do not tend to produce large variations in the R^2 values (Figure 4.9 B), and most partitions of the data produce an estimate of the significance level close to 70 µVms (Figure 4.9 D). This shows that the good correlation between neural and psychophysical thresholds (Figure 4.10) is robust and is not simply dependent on subjectively selecting the appropriate significance level. The measurement of the positive, negative or total area between the noise floor and the difference waveform did not yield a significant difference when estimating spectral discrimination thresholds. However, using the total area, above the positive and negative noise floor, succeeded to estimate a spectral ripple discrimination threshold in the largest number of tested ears.

In cases where the cortical responses were too small compared to the noise floor, such as TCD06 and TCD15, it was difficult to estimate a neural spectral ripple discrimination threshold. While monitoring the impedance levels accordingly during the recording may reduce noise and CI artefact, small or unreliable CAEP responses from some subjects is a limitation when estimating neural spectral ripple discrimination thresholds. Reducing the noise in the signal as much as possible by limiting subject motion and external interference and increasing the stimulus presentation level may help get a better response in these subjects.

4.3.3 Potential Clinical Applications

The simple, yet robust, approach makes it feasible for application within a clinical environment, with faster and more comfortable acquisition than with high density EEG set-ups. The results presented in this study suggest that the single channel EEG acquisition and artefact attenuation is a reliable method for measuring CAEP responses to an oddball paradigm in CI users.

In addition to evaluating a CI subject's spectral resolution, it may also be possible to employ the method to fine tune a subject's frequency map. Typically, a CI processor would be loaded with a standard frequency map, i.e. predefined frequency bands assigned to each electrode of the CI. An objective metric for spectral resolution, such as the one presented in this study, could allow the evaluation of customised frequency maps, in

search of the map that allows the best spectral resolution. The time required to obtain spectral discrimination thresholds, approximately one hour, is a limiting factor for this potential application. However, being an objective metric, the possibility of an automated process may reduce the number of man-hours required for the task. Furthermore, the development of intra-cochlear recording methodologies that allow the recording of CAEPs without the additional EEG systems (Beynon et al., 2008; Beynon and Luijten, 2012; McLaughlin et al., 2012a) may benefit from objective metrics as a building block for the development of automated frequency tuning processes.

Current efforts to enhance spectral resolution via different electrode stimulation modalities, i.e. partial bipolar stimulation (pBP), tri-polar stimulation (TP) and partial tri-polar stimulation (pTP), benefit from psychoacoustic evaluation of frequency resolution (Landsberger and Srinivasan, 2009; Zhu et al., 2012; Wu and Luo, 2013). Objective assessment of spectral resolution using an oddball paradigm could be beneficial when evaluating different electrode stimulation modalities in CI populations where standard psychoacoustics cannot be performed such as young infants. The reliability of an oddball paradigm such as the mismatch negativity (MMN) has been reported successful in normal hearing and cochlear implant infant populations (Cheour et al., 1998b; Ponton et al., 2000; He et al., 2009). Evidence in literature suggests that the pitch discrimination characteristics of the MMN in infants is developed between two and four months of age (He et al., 2009).

Clinical applications involving the acquisition of CAEPs may be limited by the confounding factor of maturation changes during the longitudinal development of cortical potentials. The development of cortical auditory potentials can extend into adolescence (Ponton et al., 2000) and even after prolonged acoustic deprivation, cortical auditory potentials can be re-developed over a period of time (Pantev et al., 2006). Changes in the morphology, latency and amplitude of potentials over time represents an impediment when performing a within subject CAEP assessment. Trainor et al. (2003) identified changes in the EEG morphology of the MMN in young infants, with an age range of two, three, four and six months, suggesting that the difference at each age may be associated with layer-specific maturational processes in auditory cortex. However, the method developed in this study may overcome these limitations due to the robust nature of the oddball paradigm response and its applicability with different age populations as well as clinical conditions (Ponton et al., 2000; He et al., 2009; Naatanen et al., 2012). Despite maturational changes reflected by the EEG morphology of the MMN in young infants,

the cognitive change detection mechanism associated with the MMN has been proposed to be developed between two and four months of age (He et al., 2009).

Provided that a spectral ripple discrimination threshold could be obtained with an oddball paradigm at any stage of the cortical auditory potential maturation process, a within subject assessment can be conducted regardless of the developmental changes presented during the duration of the assessment. Nonetheless, determining the applicability of spectral rippled stimuli as well as the complexity of the paradigms and the presentation rate for younger populations requires further investigation.

4.3.4 Conclusions

The results presented in this study demonstrate that cortical responses to an oddball paradigm, utilising complex stimuli, can be recorded with a single channel EEG acquisition set-up from a CI population. This CAEP based method can provide an estimated spectral ripple discrimination threshold in adult CI listeners. Further research is required to investigate the relationship of the objective assessment of spectral resolution with speech perception scores, as well as to investigate the applicability of the proposed objective method in a population of paediatric CI recipients.

Key Points

- This Chapter builds towards the response to the research questions 4, 5 and 6 listed in Section 2.4.
- The single-channel EEG acquisition set-up presented in Chapter 3 was successfully employed to obtain MMWs with minimal influence from the CI artefact.
- An objective metric of spectral ripple discrimination was derived from MMWs elicited to a set of spectrally rippled noise stimuli in a cohort of experienced CI users.
- The neural-based objective metric of spectral ripple discrimination correlates well with discrimination measures derived behaviourally.
- Spectral ripple discrimination has been linked with speech perception performance. Thus, an objective metric for discrimination may be of significance in difficult-to-test CI cohorts.
- These findings were presented at 35th International Conference of the IEEE EMBS, Osaka 2013; and at the MidWinter Meeting- ARO, Baltimore 2013.
- The study presented in this Chapter is published in: "Objective Assessment of Spectral Ripple Discrimination in Cochlear Implant Listeners Using Cortical Evoked Potentials to an Oddball Paradigm". PLoS One, 9(3):e90044,March 2014

Chapter 5 The ACC as an Electrophysiological Correlate of Spectral Ripple Discrimination

Chapter 4 introduced a mismatch-based (referred here as mismatch waveform MMW) objective metric to estimate spectral discrimination abilities in CI users. While this metric correlated well with behavioural discrimination thresholds, the length of the acquisition time (i.e. one hour) was one of the potential caveats discussed in Section 4.1.3.

Nevertheless, we know from Chapter 2 that there are a number of CAEPs that can be evoked to investigate higher-order processing of complex sounds. The ACC, for example, has also been proposed to probe cortical discrimination abilities in normal hearing and CI populations (Martin and Boothroyd, 2000; Martin, 2007; Brown et al., 2008; Martin et al., 2010; Won et al., 2011b).

A study conducted by Won et al. (2011b) showed a correlation between electrophysiological and behavioural spectral ripple discrimination via single-interval change presentation (i.e. ACC for multi-channel electrophysiological discrimination and yes/no for behavioural discrimination) in normal hearing subjects under various vocoder conditions. Their results suggest that more frequency channels available enhance spectral ripple discrimination in normal hearing subjects. Interestingly, they showed that behavioural CI spectral ripple discrimination performance is comparable to that of normal hearing subjects with an eight channel vocoder. Furthermore, it validated the relationship suggested in Won et al. (2007) between spectral ripple discrimination and speech perception performance in noise for CI users.

The study presented here, explored the possibility to derive an objective metric of spectral ripple discrimination in CI users, based on an ACC paradigm in combination with the single-channel EEG acquisition and artefact attenuation approach described in

Chapter 3. A comparison between an ACC derived metric and the previously described MMW metric was conducted in order to evaluate the robustness of both potential tools. Giving the audiologist several options to objectively asses spectral ripple discrimination in CI users may encourage them to implement single-channel EEG recordings as a routine practice in clinic.

5.1 Materials and Methods

5.1.1 Subjects

Thirteen CI listeners (5 male, 8 female) volunteered for this study at two separate locations: Trinity Centre for Bioengineering, Trinity College Dublin (n=11) and Hearing and Speech Laboratory, University of California Irvine (n=2). Exclusion criteria applied to subjects under 18 years of age and subjects with cognitive or learning disabilities and implant switch-on date shorter than 6 months prior to the study. There were no subjects withdrawn from this study. Subjects were aged between 33 and 76 years (mean 53, standard deviation 14). They had either a Cochlear (n=12) or Advanced Bionics (n=1) implants. All subjects were had a monopolar stimulation mode strategy.

Experimental procedures were approved by the Ethics (Medical Research) Committee at Beaumont Hospital, Beaumont, Dublin, the Ethical Review Board at Trinity College Dublin and The University of California Irvine's Institutional Review Board. Written informed consent was obtained from all subjects.

5.1.2 Stimuli

Spectrally rippled broadband noise stimuli like those described in Section 4.1.3 were generated for this study. The broadband noise was created via summation of 4000 pure tones with frequencies from 100 Hz to 8,000 kHz. The spectral ripple was created with a full wave rectified sinusoidal envelope on a logarithmic amplitude scale and with maximum amplitude of 30 dB peak-to-valley (see Figure 4.1). Spectral peaks were equally distributed on a logarithmic frequency scale, and the number of spectral peaks per frequency octave defines the ripple density of the stimulus (RPO).

Two types of RPO stimuli configuration were generated and stored for presentation. Figure 5.1 shows an example of the spectrograms for a one RPO spectral ripple stimulus in each configuration. Standard and deviant stimuli for the MMW

paradigm (Figure 5.1 A) were 500 ms in duration. The deviant stimulus was spectrally inverted with respect to the standard stimulus. Acoustic change stimuli for the ACC paradigm were 2000 ms in duration with a spectral inversion at the mid-point (Figure 5.1 B). Spectral inversion was a phase shift of the sinusoidal ripple envelope of $\pi/2$. Stimuli were delivered electrically through the auxiliary input of the CI's speech processor at a most comfortable loudness level (MCL) defined for each subject on a scale from 0 (silence) to 10 (too loud), with 6 being the MCL.

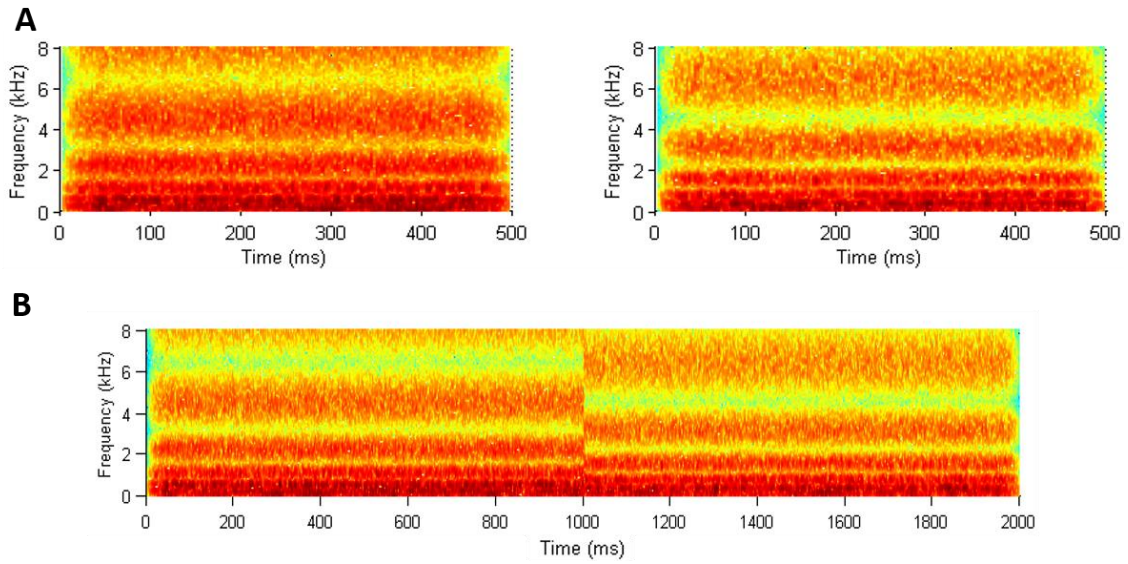

Figure 5.1 RPO stimuli configurations for the MMW and the ACC paradigms.
A) Stimulus spectrograms separate for standard (left) and deviant (right) presentation as employed in the MMW paradigm. Standard and deviant presentations had equal number of RPOs but inverted spectral content. B) Stimulus spectrogram of a fused spectral change presentation as employed in the acoustic change paradigm. Spectral inversion occurred at the midpoint of the simulus duration.

5.1.3 Electrophysiological Data Recording

Single-channel EEG recordings were acquired through the customised set-up previously described in Chapter 3. Electrodes were placed at the vertex (Cz) and the mastoid, contralateral with respect to the tested ear. The system ground was located at the collarbone. Figure 4.2 shows a graphical layout of the recording set-up.

5.1.4 Electrophysiological and Behavioural Paradigms

Mismatch Waveform Paradigm

A MMW was elicited by presenting a set of standard and deviant auditory stimuli in a 90-10 unattended oddball paradigm (as in Figure 4.3). The stimulus repetition rate was 1 Hz and the occurrence of a deviant presentation was random with a probability of

10%. At least four 15-minute recordings were acquired from each participant with different stimuli at different RPO levels. Recordings took place inside an electrically isolated room and participants were instructed to ignore the stimulus presentation and direct their attention to a silent, captioned film.

Behavioural spectral ripple discrimination thresholds were acquired through the implementation of the three-alternative forced-choice behavioural (3AFC) discrimination task described in Section 4.1.2. Briefly, a sequence of three stimuli was presented in one run, two of which were standard and one of which was the deviant. The subject had to identify the deviant stimulus by pressing on a graphical interface. The test ran, adaptively increasing in difficulty, until 13 reversals occurred. The spectral ripple discrimination threshold was calculated as the mean of the last eight reversal values. The final spectral ripple discrimination threshold was the average of five repetitions of this test.

Acoustic Change Complex Paradigm

The electrophysiological ACC was elicited to a successive presentation of 120 acoustic change stimuli as depicted in Figure 5.2. The stimulus presentation rate was 0.33 Hz with an inter-stimulus interval of one second. At least four 6-minute recordings were acquired from each participant with different stimuli at different RPO.

Behavioural acoustic change discrimination was determined via a single-interval psychoacoustic test (Won et al., 2011b). Acoustic change stimuli and non-change stimuli were presented randomly with a total of 120 presentations each. Upon stimulus presentation, the participant was asked to press a button on a graphical interface indicating 1 if there was no change in the stimulus or 2 if an acoustic change was present. At least four psychoacoustic tests were performed with the same RPO stimuli as in the electrophysiology paradigm. A psychometric curve was fitted to the behavioural results to determine psychoacoustic discrimination thresholds at the 70% correct mark.

5.1.5 Signal Processing

Mismatch Waveform Spectral Ripple Discrimination Thresholds

For the unattended oddball paradigm, raw EEG data were segmented into long epochs of 300 ms pre-stimulus to 800 ms post-stimulus onset. Epochs were separated into standard and deviant and averaged across each type. Averaged epochs were filtered with a pass-band (2-20 Hz) 2^{nd} order Butterworth filter. Baseline correction of 150 ms pre-stimulus was applied to the filtered epochs. MMW were calculated as the difference

waveform resulting from subtracting the standard response from the deviant response. The noise floor of the signal was calculated via a bootstrap difference waveform calculated from the standard epochs. The area under the curve of the MMW above and below (+/-) the noise floor was deemed as a significant response. MMW spectral ripple discrimination thresholds were calculated according to the methodology proposed in Section 4.1.4. Figure 5.3 illustrates how a clear MMW response to a spectral density of 0.25 RPO decreases as the spectral density increases to 0.5 RPO, 1 RPO and 2 RPO. The neural spectral discrimination threshold was defined as the point when the MMW area under the curve dropped below a significant level which was statistically derived from the data.

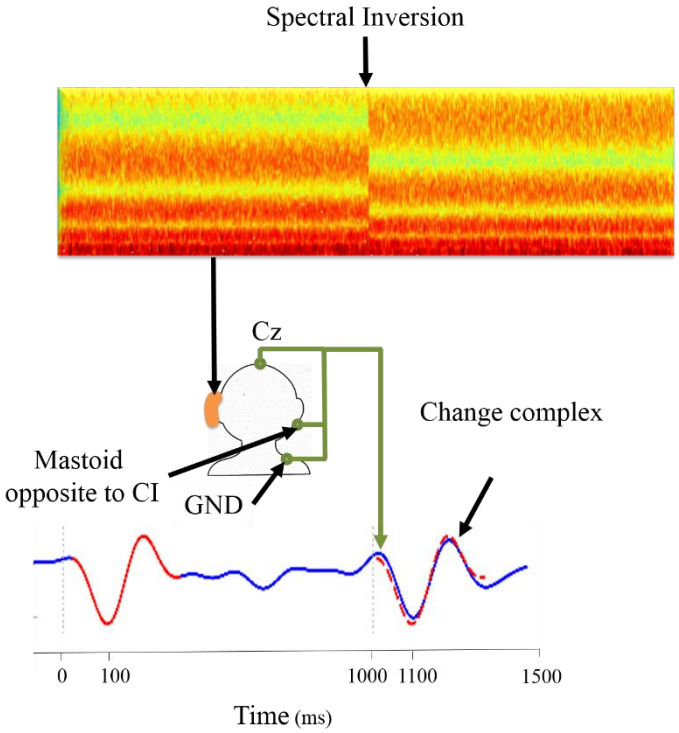

Figure 5.2 ACC electrophysiological paradigm.
Recording from Cz electrode location and referenced to the contralateral mastoid, a 2000 ms long RPO stimulus having a spectral inversion at the midpoint was presented in a sequence of 120 repetitions. The stimulus elicits an onset response at around 100 ms. If the spectral inversion is perceived, an ACC would be elicited at around 100 ms after the inversion.

Acoustic Change Complex Spectral Ripple Discrimination Thresholds

For the acoustic change complex paradigm, raw EEG data were segmented into long epochs of 300 ms pre-stimulus to 2500 ms post-stimulus onset to avoid filter edge effects. The three stage CI artefact attenuation procedure developed in Chapter 3 was applied to the ACC responses. Baseline correction of 150 ms pre-stimulus was applied to

the filtered epochs. Epochs were filtered with a pass-band (2-20 Hz) 2nd order Butterworth filter.

The ACC responses were quantified as a ratio of the stimulus onset response. The stimulus onset response is the characteristic N1-P2 complex reviewed in Section 2.3.2. The ACC response is generated approximately 100 ms after the spectral inversion is detected and it is similar in morphology to the N1-P2 complex, but smaller in amplitude. For each RPO density, the N1-P2 response was manually selected from a region of interest of 90 to 250 ms after stimulus onset. In order to identify the change response, a normalised version of the selected N1-P2 response was cross-correlated with the normalised region of interest of 1090 to 1250 ms after stimulus onset. The time stamp of maximum correlation was defined as the change response. Figure 5.4 illustrates this template search mechanism. N1-P2 responses were manually selected at each RPO density and the corresponding template was located after the acoustic change (i.e. 100 ms after spectral inversion). At RPO densities of 0.25 and 0.5 the change response was successfully located using a template search based on the onset response whereas at RPO densities of 1 and 4 no change response was identified. If the N1-P2 complex could not be successfully recognised from the signal, the recording at that RPO level was discarded.

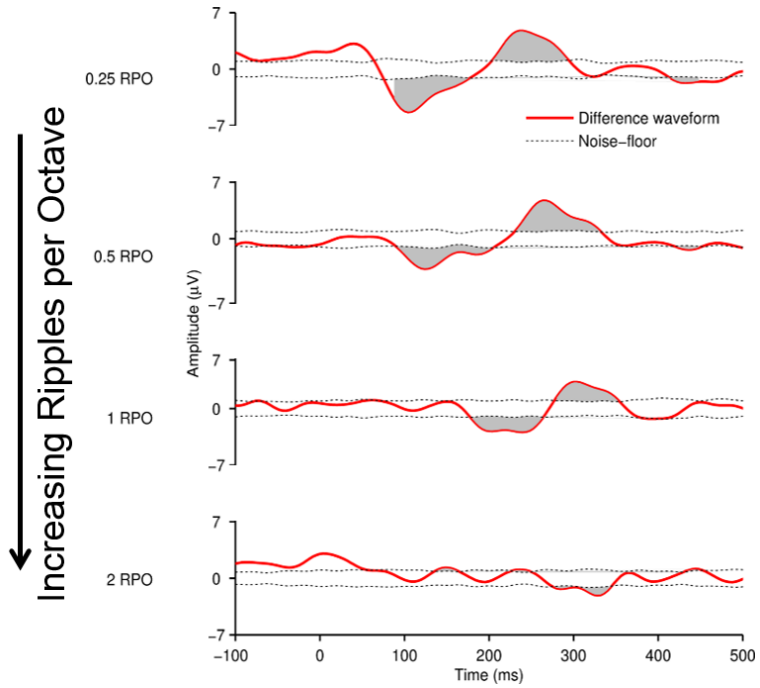

Figure 5.3 Decreasing MMW traces as a function of RPO density.
MMWs elicited to four different RPO stimuli. Amplitude of the difference waveform decreases as the ripple density increases from 0.25 to 2 RPOs.

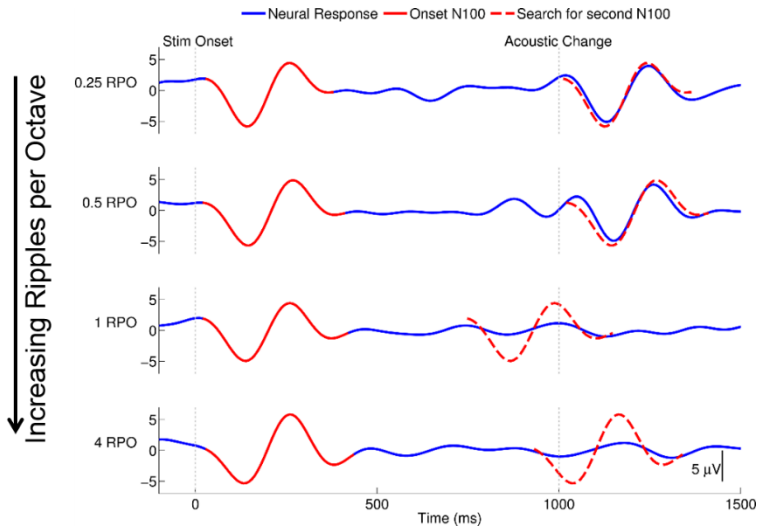

Figure 5.4 ACC responses elicited to a spectral inversion within a long spectral ripple sound.
Identifiable ACC (dashed red line) responses can be observed at 0.25 and 0.5 RPO densities while no ACC responses are evident at 1 and 4 RPO densities. If present, the ACC can be quantified in terms of the similarity to the onset N1-P2 complex (solid red line).

In order to estimate the amount of noise in the recording, the N1-P2 complex was cross-correlated with a randomly selected portion of the signal where no neural response was expected. Based on the average noise floor of each participant's recording, the neural spectral ripple discrimination threshold was defined as the RPO density where the ACC amplitude dropped below 11%. Figure 5.5 shows the manner in which the ACC amplitude decreases with respect to the onset response amplitude exemplary for subject 12. The ACC spectral ripple discrimination threshold for this particular subjects yields 0.964 RPO.

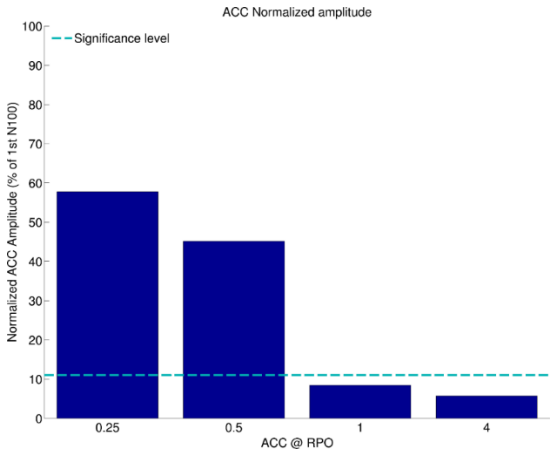

Figure 5.5 Decreasing normalised ACC amplitude with respect to the onset response as a function of spectral ripple density.
ACC responses are similar in morphology to the N1-P2 complex but they decrease in amplitude as the spectral inversion becomes more complex. A neural spectral ripple discrimination metric was defined as the point where the ACC response drops below 11% of the onset response amplitude.

5.2 Results

5.2.1 Behavioural Results

Table 5.1 summarises the individual results obtained for psychoacoustic and neural spectral ripple discrimination thresholds. Behavioural single-interval forced-choice task thresholds were in the range of 0.35 to 5.22 (mean= 1.74, standard deviation= 1.33) RPO. In two participants (i.e. S5 and S10) the fitting of the psychometric function was not possible due to ceiling effects. Figure 5.6 shows the individual psychometric functions to the performed single-interval forced-choice tasks at different RPO densities. The spectral ripple discrimination threshold was calculated at the 70% correct proportion to match the target proportion of the 3AFC task described in Chapter 4. Spectral discrimination thresholds for the same participants via the 3AFC paradigm were in the range of 0.24 to 2.60 (mean= 1.05, standard deviation= 0.73).

5.2.2 Electrophysiological Results

Neural estimates of spectral discrimination via the ACC paradigm could only be derived from seven participants with a mean threshold of 1.01 RPO (standard deviation= 0.72 RPO). Neural thresholds via the MMW paradigm were successfully derived from 11 participants with a mean threshold of 1.21 RPO (standard deviation= 0.89 RPO) (see Table 5.1).

Figure 5.7 shows the individual ACC response measurements for all 13 subjects. After accounting for the noise level of each individual recording, only S6, S7, S9, and S12 showed distinguishable ACC responses across 4 different RPO levels. For the rest of the subjects, one or more RPO levels had to be discarded as no significant ACC was detected.

Thresholds obtained through linear regression of behavioural results from the two psychoacoustic procedures were compared to the neural thresholds derived from the MMW and ACC paradigms in order to test the relationship among the metrics. The ACC correlation of the seven neural thresholds with the single-interval psychoacoustic thresholds was trending to statistical significance ($r^2 = 0.55$, p-value > 0.05). The MMW correlation of the 11 neural thresholds with the 3AFC psychoacoustic threshold was

statistically significant ($r^2 = 0.37$, p-value < 0.05). These correlations can be observed in Figure 5.8.

	Behavioural RPO Thresholds		Electrophysiological RPO Thresholds	
Subject ID	3AFC	Single-Interval	ACC	MMW
1	**1.54**	**2.408**	**1.987**	**2.407**
2	**2.59**	**5.226**	**1.83**	**1.045**
3	**1.158**	**1.44**	**0.312**	**0.763**
4	**0.948**	**0.621**	*	**0.9523**
5	**2.172**	*	*	**2.987**
6	**0.65**	**1.481**	*	*
7	**0.778**	**1.872**	*	**0.15**
8	**0.4**	**0.995**	*	**0.408**
9	**0.312**	**1.762**	**0.4819**	**0.739**
10	**0.931**	*	*	**1.597**
11	**0.463**	**0.351**	**0.193**	**0.482**
12	**1.503**	**0.702**	**0.964**	**1.827**
13	**0.24**	**2.303**	**1.29**	*

*, Not possible to determine

Table 5.1 Summary of individual behavioural and electrophysiological spectral ripple discrimination thresholds.

Pearson's correlations for the different threshold combination were carried out. Table 5.2 summarises the different relationships. A statistically significant correlation was found between the two psychoacoustic paradigms (i.e. 3AFC and Single-Interval; $r^2 = 0.438$, p-value = 0.028) and between the MMW and 3AFC discrimination thresholds ($r^2 = 0.379$, p-value = 0.049). A non-statistically significant, but trending, correlation was found between the two objective neural thresholds (i.e. MMW and ACC; $r^2 = 0.527$, p-value = 0.092) and between the ACC and single-interval discrimination thresholds ($r^2 = 0.551$, p-value = 0.056).

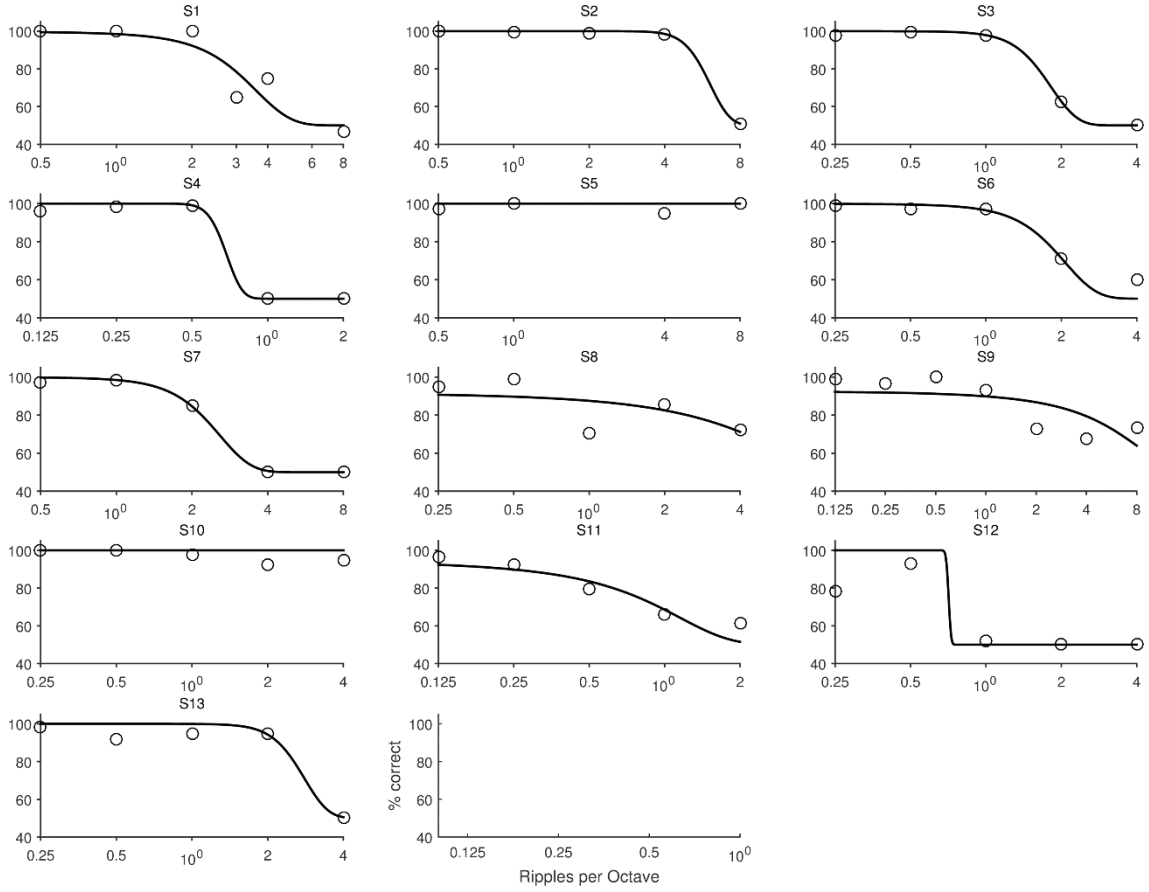

Figure 5.6 Individual behavioural psychometric functions fitted to the single-interval forced-choice discrimination task.
Psychometric functions were fitted to the single-interval forced-choice discrimination tasks at different RPO densities to estimate the behavioural discrimination thresholds. Ceiling effect was observed in subjects S5 and S10, where the fitting of the psychometric function was not possible.

5.3 Discussion

This study compared two different methods to objectively estimate spectral ripple discrimination in a population of CI users. The ACC was evaluated as a potential CAEP for assessing spectral ripple discrimination and was compared to the MMW method presented in Chapter 4. The findings confirm the robustness of the MMW as an objective metric of spectral ripple discrimination and presents the ACC as an additional objective metric.

5.3.1 Artefact Removal from ACC Single-Channel Recordings

It was possible to remove the characteristic CI artefact from the single-channel EEG recordings to long ACC stimulus presentations. This suggests that the artefact attenuation approach described in Chapter 3 could be applied to successfully extract

CAEPs from different presentation paradigms including N1-P2 complexes, MMW and ACC. The versatility to acquire different CAEPs with the same set-up may be of benefit for audiologists in the clinic, as it allows them to tailor the CAEP acquisition according to time, patient specific circumstances, and clinical goals.

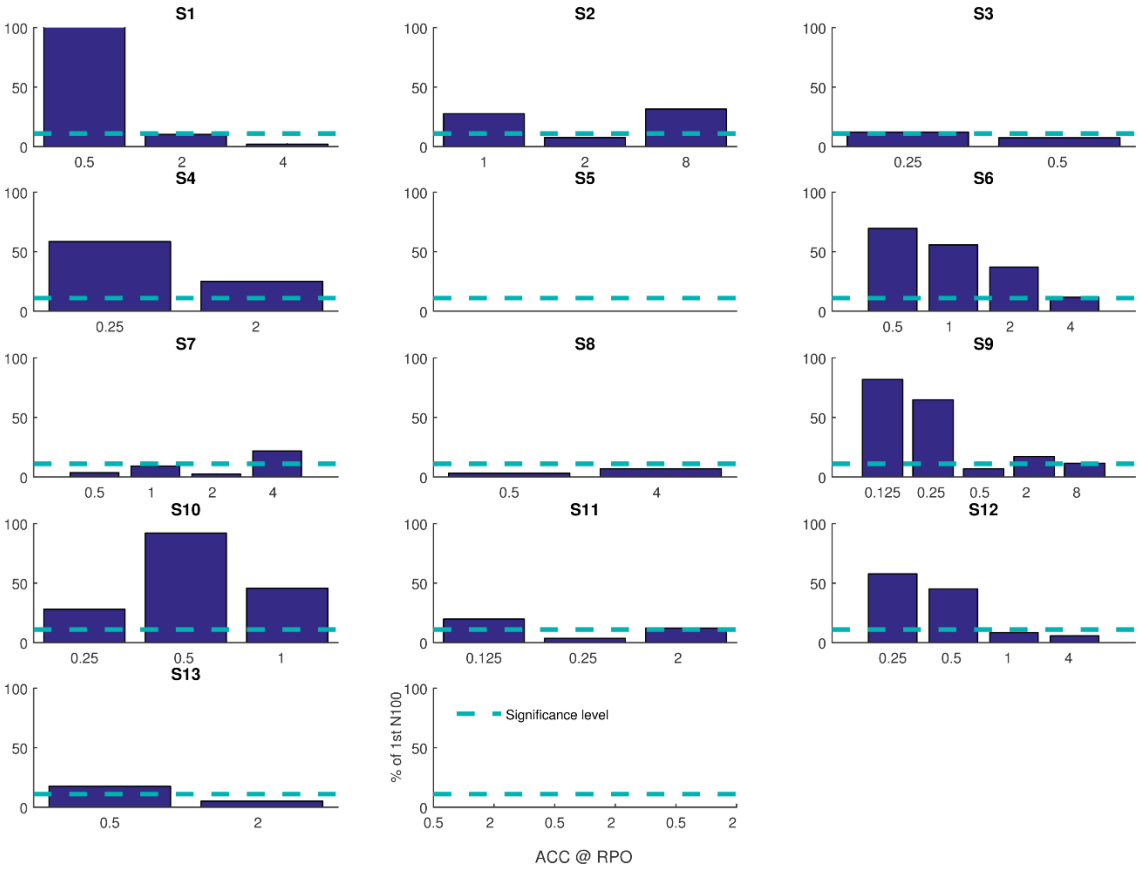

Figure 5.7 Individual ACC response measurements as a function of RPO density.

5.3.2 Deriving Spectral Ripple Discrimination Thresholds from ACC Recordings

Noise Level in Electrophysiological Recordings

If there was a high cross-correlation of the N1-P2 complex with a random selection of epoch signal where no neural response was expected, the recording was discarded due to a high presence of noise. For any given subject the noise level in the recordings showed variations across recordings (e.g. in Figure 5.7, S7 lost the recordings for 0.5, 1, and 8 RPO due to high noise level). This variation may be accounted for by the fact that the different ACC recordings were conducted in a random order at each session. Therefore, the events responsible for the high noise level in one recording (e.g. 1 RPO), could not be present in the following RPO level (i.e. 2RPO).

	3AFC	Single-Interval	MMW	ACC
3AFC		**r^2=0.434; p=0.028**	**r^2=0.379; p=0.049**	**r^2=0.384; p= 0.138**
Single-Interval			**r^2=0.027; p= 0.672**	**r^2=0.551; p=0.056**
MMW				**r^2=0.527; p= 0.092**
ACC				

Table 5.2 Pearson's correlation confusion matrix.

The effect of prolonged EEG recordings has been deemed detrimental for the signal-to-noise ratio of the electrophysiological response (Woodman, 2010). For the present study, EEG recordings were conducted over one session with a break for lunch. In such length of time and without a systematic check of electrode impedances, it is conceivable that the quality of the signals was poor during a portion of the session.

Furthermore, the increased number of recording paradigms in this study would have limited the number of stimuli presentations. It is possible that 120 repetitions for the ACC and 60 deviant repetitions for the MMW are not sufficient numbers of trials (Woodman, 2010). Even when CAEPs were successfully extracted from several subjects under these conditions, a low signal-to-noise ratio in combination with a limited number of stimuli presentations could explain the difficulty to derive electrophysiological spectral ripple discrimination thresholds in the subjects listed in

Table 5.1. However, it is conceivable that the lack of ACC responses in some participants is due to the high noise floor in the recording sessions, rather than to the recording paradigm; the MMW, recorded during the same session yielded better results (see Table 5.1).

Stimulus Representation at Electrode Level

In contrast to a study performed by Won et al. (2011b), in normal hearing participants, the stimulus presentation employed here was through direct input into each subject's CI processor. The lack of available information regarding the electrical voltage at the line-in input of the CI processor, for different manufacturers, makes it difficult to account for possible effects of the automatic gain control block within the front-end of the processors. It is possible that spectral ripple inversion may be clipped due to the 'fast

attack' of the automatic gain control in the speech processors, preventing an ACC response.

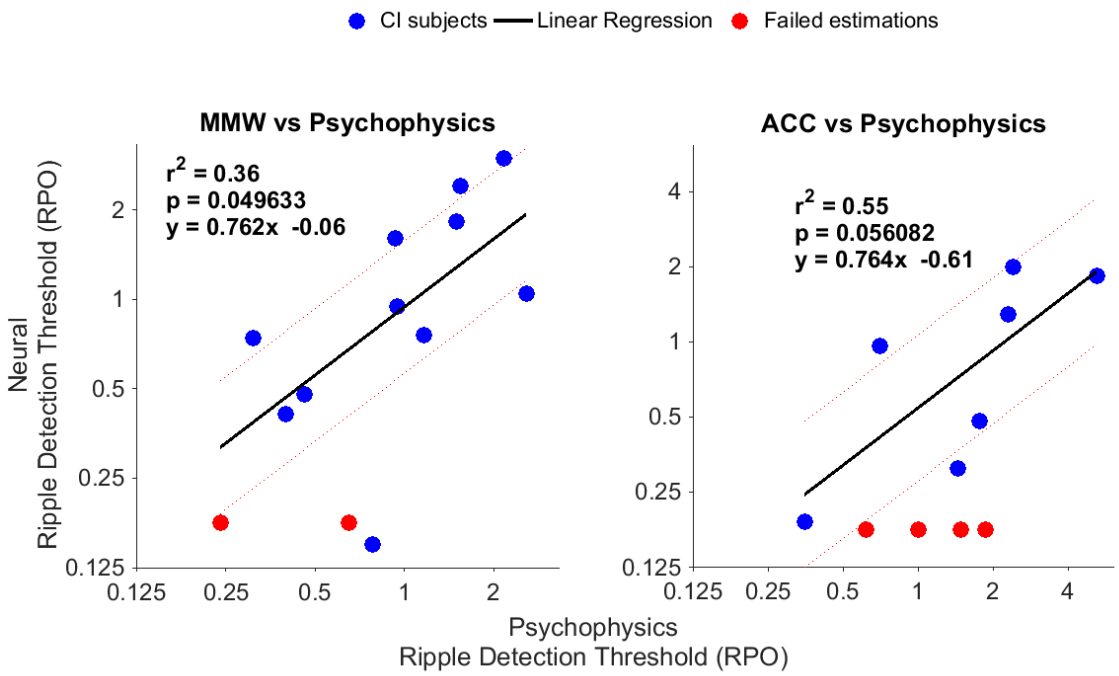

Figure 5.8 Correlation between the behavioural and neural spectral ripple discrimination.
Red lines inidcate 95% confidence intervals. ACC spectral ripple discrimination thresholds are shown on the right (r^2=0.55, p>0.05) and MMW spectral ripple discrimination thresholds on the left (r^2=0.36, p<0.05).

Figure 5.9 shows the electrodograms for four RPO densities according to the program in the CI processor of subject S3. The decreasing spectral inversion to increasing RPO densities is in line with the subject's behavioural results (see Figure 5.6). Although this suggests that the electrophysiological results for this particular subject were mainly influenced by noisy recordings and not a clipping of the stimuli by the processor, it also emphasizes the importance of each individual's programming and processing strategy when it comes to spectral ripple discrimination.

5.3.3 Correlation between Behavioural and Electrophysiological Spectral Ripple Discrimination Thresholds

A desirable advantage of the ACC paradigm over the MMW is the shorter acquisition time, six minutes for the ACC vs 15 minutes for the MMW (at a given RPO level). However, the representation of the spectral inversion in the ACC stimuli may generate additional temporal cues such as the switching on and off of stimulation electrodes allowing the CI patients to distinguish a change. An evidence of this effect

may be the ceiling effect found in two participants where they were able to discriminate changes in the sound at all RPO densities whereas their 3AFC tests indicated lower discrimination abilities.

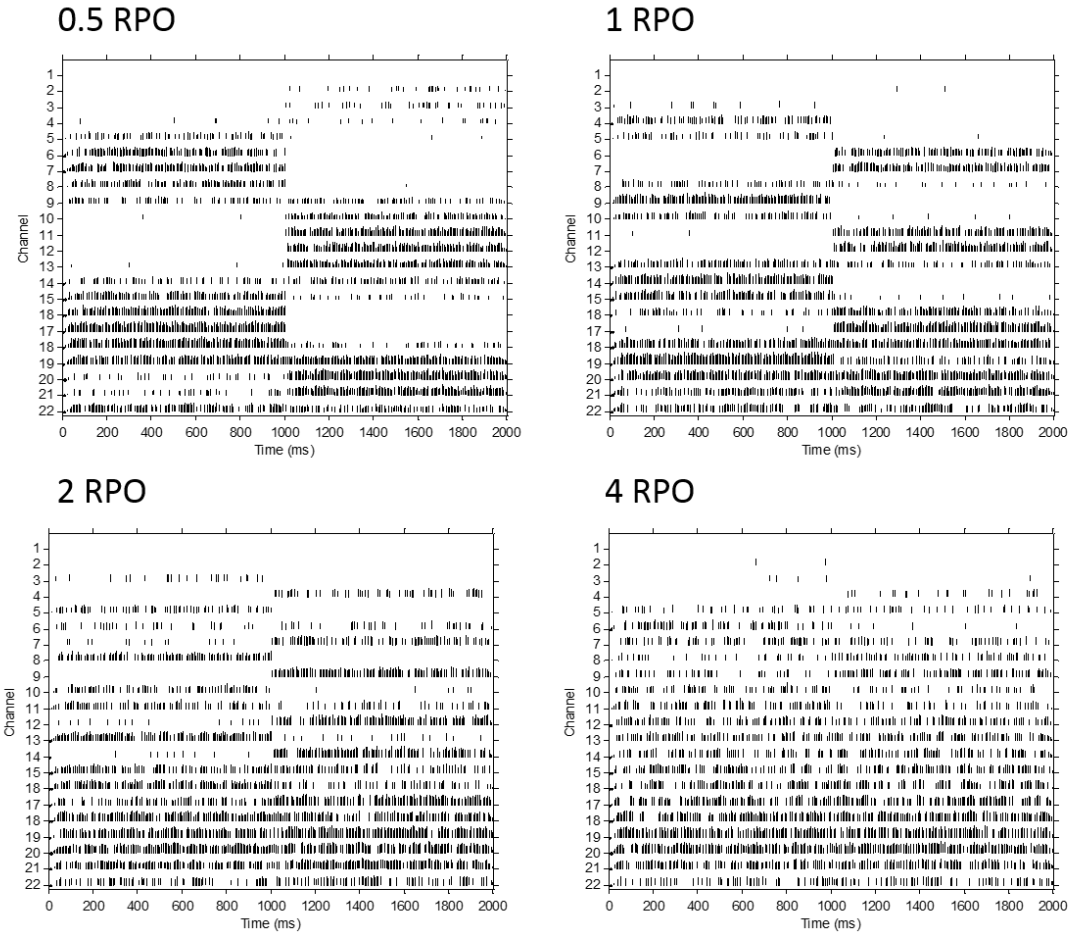

Figure 5.9 Electrodograms for ACC stimuli at four RPO densities.
Electrodograms derived from the Nucleus MATLAB Toolbox (NMT) for subject S3. There is a clear representation of spectral inversion at 0.5, 1, and 2 RPO densities, while at 4RPO the electrodogram shows no evidence of spectral inversion.

Nonetheless, Won et al. (2011b) provide an explanation for the differences in the two behavioural approaches. They suggest that the increased cognitive load of the 3AFC accounts for lower thresholds, whereas, the spectral inversion at the midpoint of the single interval stimuli serves as a direct comparison cue. The correlation between the single-interval and 3AFC behavioural approaches observed in this study supports their claim that, in spite of the fact that different auditory mechanisms could be summoned, the single-interval discrimination task is an adequate means to probe spectral ripple discrimination in CI users.

Despite the fact that the MMW was shown to be more robust for estimating objective spectral ripple discrimination thresholds, the trending correlation found

between the ACC estimated thresholds and the behavioural thresholds justifies the further exploration of the paradigm as a potential objective tool for assessing CI spectral ripple resolution.

5.3.4 Additional Potential Implementations of the ACC in CI Users

Recent approaches to record CAEPs through intra-cochlear electrodes have been successful for recording N1-P2 complexes through the implementation of back-telemetry (Beynon et al., 2008; Beynon and Luijten, 2012; McLaughlin et al., 2012b). Due to the current hardware restrictions, intra-cochlear recording of more complex CAEPs such as the MMW is not yet practical. However, preliminary work by our group has shown that it is possible to record ACC responses to different RPO stimuli in a bilateral CI user (Mc Laughlin et al., 2013). Figure 5.10 shows the comparison of intra-cochlear ACC recordings with respect to scalp ACC recordings from one bilateral CI user. This finding could lead to the development of automatic spectral ripple discrimination estimation that could enhance CI fitting procedures aiming for enhanced speech perception performance.

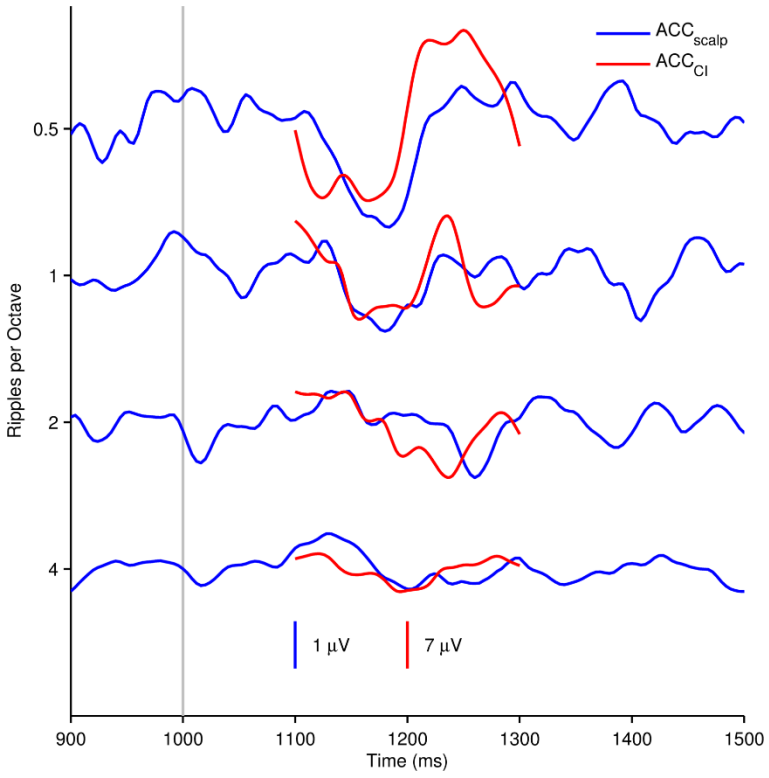

Figure 5.10 Intra-cochlear recording of ACC responses to four different RPO densities. *Intra-cochlear ACC recordings (red traces) compared to their scalp recorded counterpart (blue line). Recordings were acquired at four RPO densities (0.5, 1, 2, and 4 RPO) from one bilateral CI user.*

5.3.5 Conclusions

The present results suggest that it is possible to utilise the ACC in a single-channel EEG acquisition system as an alternative to estimate spectral ripple discrimination in some CI users. Despite its longer acquisition time, the MMW is more robust than the ACC measure in estimating the behavioural spectral resolution for the described stimulation protocol.

The addition of the ACC as an objective measure provides the audiologists in the clinic with more tools which could be employed depending on the particularities of each case. Furthermore, the possibility to record ACC via back-telemetry is a potential, novel application of the paradigm in automatic monitoring of CI performance.

Key Points

- This Chapter complements the response to the research questions 4, 5 and 6 listed in Section 2.4.
- It is possible to acquire ACC responses to spectral ripple stimuli in some CI users. These responses show a trend to correlate with behavioural spectral discrimination thresholds.
- The MMW spectral discrimination metric presented in Chapter 4 was more robust than the ACC paradigm when estimating spectral ripple discrimination thresholds.
- Spectral ripple discrimination can be measured intra-cochlearly via back-telemetry in combination with an ACC paradigm.
- These findings were presented at 35th International Conference of the IEEE EMBS, Osaka 2013; and at the MidWinter Meeting- ARO, Baltimore 2013.
- The study presented in this Chapter is published in: “Objective Assessment of Spectral Ripple Discrimination in Cochlear Implant Listeners Using Cortical Evoked Potentials to an Oddball Paradigm”. PLoS One, 9(3):e90044,March 2014

Chapter 6 Dynamics of Speech and Non-Speech Metrics in CI Users over One Year from Device Switch-On

Spectral resolution plays an important role for speech perception outcomes in CI users (Henry et al., 2005; Litvak et al., 2007; Won et al., 2007) and can be assessed with a non-linguistic spectral ripple discrimination test, which may be utilised to optimise rehabilitation processes in newly implanted CI recipients (Won et al., 2007; Drennan et al., 2014; Drennan et al., 2015). Chapter 4 and Chapter 5 demonstrate that spectral ripple discrimination can be objectively estimated utilising a mismatch paradigm and single-channel EEG. Nonetheless, the influence that the cortical reorganisation after implantation may have on this objective metric remains unexplored, as well as its correlation with speech perception performance in CI users.

Little is known about the development of spectral ripple discrimination abilities in newly implanted patients. Recent evidence suggests that the spectral ripple discrimination threshold remains unchanged during the first year of implantation, and thus, is a reliable predictor of the performance expected after one year of implantation (Drennan et al., 2015). This study presents a longitudinal follow-up of newly implanted CI recipients during their first year post-implantation. The aim of this study was to integrate previously developed tools into a clinical environment, addressing the following objectives: 1) To evaluate the clinical applicability of psychoacoustic, non-linguistic assessment of spectral ripple discrimination as an early predictor of speech perception performance; 2) To characterise the MMW based objective metric of spectral ripple discrimination; 3) To explore its correlation with speech perception outcomes.

6.1 Materials and Methods

6.1.1 Subjects

Ten adult, newly implanted CI recipients (5 male, 5 female) were recruited from the National Cochlear Implant Programme at Beaumont Hospital in Dublin, Ireland. Exclusion criteria applied to recipients under 18 years of age and/or with cognitive or learning disabilities. One subject opted out of the study during early stages, and thus, was excluded from the study analysis. The remaining nine subjects (4 male) were aged between 22 and 79 years (mean 55 ± 21 years). They used either a Cochlear Ltd. (n=4) or an Advanced Bionics (n=5) cochlear implant device. Table 6.1 summarises the demographics of the nine CI recipients that took part in this study.

Experimental procedures were approved by the Ethics (Medical Research) Committee at Beaumont Hospital, and the Ethical Review Board at Trinity College, The University of Dublin. Written informed consent was sought and signed by all participants.

6.1.2 Study Design

Subjects were asked to attend seven research sessions throughout the first year post-implantation. Research sessions were scheduled to match each subject's clinical appointments at switch-on date, one week, one month, three months, six months, nine months and one year after switch-on. All research sessions were conducted after the routine clinical assessment by the research team's audiologist. Subjects that could not complete at least four research sessions were excluded from the study analysis.

Each research session had a duration of two hours and 30 minutes and consisted on three test batteries: 1) Speech perception test under different listening conditions (i.e. in quiet and in 10 talker-babble noise at 10 dB, 5 dB SNR); 2) Four psychoacoustic runs of a spectral ripple discrimination task; 3) EEG data acquisition of CAEPs elicited to pure tone and spectral ripple stimuli.

All experimental tasks were implemented with sound presented via the audio line-in on the CI at the most comfortable level, determined for each subject on a 0 (silence) to 10 (too loud) loudness scale, 6 being the most comfortable level. To limit the effects of any unwanted background noise, a dedicated program with no audio mixing parameters (i.e. auxiliary audio only) was loaded into each subject's speech processor. Task related sounds were always presented monaurally.

Subject Number	Age at Implantation	Aetiology	Type	Implant Manufacturer	Speech Processor Model	Speech Processing Strategy
S1	**73yr, 8mo**	**Congenital**	**Progressive**	**Advance Bionics**	**Naida**	**HiRes Optima-S**
S2	**57yr, 9mo**	**Congenital**	**Progressive**	**Cochlear Ltd.**	**CP910**	**MP3000**
S3	**22yr, 2mo**	**Congenital**	**Progressive**	**Advance Bionics**	**Neptune**	**HiRes Optima-S**
S4	**34yr, 3mo**	**Congenital**	**Progressive**	**Cochlear Ltd.**	**CP910**	**ACE**
S5	**53yr, 6mo**	**Congenital**	**Progressive**	**Cochlear Ltd.**	**CP910**	**MP3000**
S6	**79yr, 1mo**	**Acquired**	**Progressive**	**Advance Bionics**	**Neptune**	**HiRes Optima-S**
S7	**72yr, 5mo**	**Acquired**	**Sudden**	**Advance Bionics**	**Naida**	**HiRes Optima-S**
S8	**73yr, 5mo**	**Acquired**	**Progressive**	**Cochlear Ltd.**	**CP910**	**MP3000**
S9	**30yr, 3mo**	**Congenital**	**Progressive**	**Advance Bionics**	**Naida**	**HiRes Optima-S**

Table 6.1 Subject demographics.

Research sessions took place inside a clinical assessment room assigned to the research study. The room had a standard office construction with neither sound proofing nor electrical isolation. The choice of the room specifications was deliberate. It was reasoned that an office room closely resembles a ‘real life’ clinical setting in which an assessment of this type would be conducted.

6.1.3 Stimuli

Spectrally rippled broadband noise stimuli like those described in Section 4.3.1 were generated for this study. The broadband noise was created via summation of 4000 pure tones with frequencies from 100 Hz to 8 kHz. The spectral ripple was created with a full wave rectified sinusoidal envelope on a logarithmic amplitude scale and with

maximum amplitude of 30 dB peak-to-valley (see Figure 4.1). Spectral peaks were equally distributed on a logarithmic frequency scale, and the number of spectral peaks per frequency octave defines the ripple density of the stimulus (RPO).

The same 'standard' and 'deviant' stimuli configuration as the one used in Chapter 4 and depicted in Figure 5.1A was employed in this study. Standard and deviant stimuli were 500 ms in duration with a 50 ms on / off cosine squared ramp applied to avoid undesired clicks during stimulation. The frequency content of the deviant stimulus was inverted with respect to the standard stimulus.

6.1.4 Speech Perception Test

Speech perception was assessed under three listening conditions: 1) Speech perception in quiet; 2) Speech perception in 10 talker-babble noise at 10dB SNR; 3) Speech perception in 10 talker-babble noise at 5dB SNR. For each condition, a different list from the AzBio sentence corpus was utilised (Spahr et al., 2012). The subjects were instructed to listen to one sentence at a time and repeat as many words from the sentence as were identified. The percentage of correctly recalled words in reference to the total number of words in the list was noted as the speech perception score for the corresponding listening condition.

6.1.5 Psychoacoustic Spectral Ripple Discrimination Thresholds

Behavioural spectral ripple discrimination thresholds (SRD) were acquired through the implementation of the 3AFC discrimination task described in Section 4.1.2. Briefly, a sequence of three stimuli was presented in one run, two of which were standard and one of which was the deviant. The subject had to identify the deviant stimulus by pressing on a graphical user interface. The test ran, adaptively (i.e. two-down / one-up) increasing in difficulty, until 13 reversals occurred. The spectral ripple discrimination threshold was calculated as the mean of the last eight reversal values. The final spectral ripple discrimination threshold was the average of four repetitions of this test.

6.1.6 Electrophysiological Data Recording

Single-channel EEG recordings were acquired through the customised set-up previously described in Chapter 3. Electrodes were placed at the vertex (Cz) and the

mastoid, contralateral with respect to the tested ear. The system ground was located at the collarbone. Figure 4.2 shows a graphical layout of the recording set-up.

In order to assess EEG data quality, auditory N1-P2 complexes were elicited to the repeated presentation of a 500 ms pure tone with an on / off cosine squared ramp of 50 ms. The frequency of the pure tone stimulus was 500 Hz and the inter-stimulus interval was one second. One block consisted of 160 repetitions of the pure tone. At least three blocks were recorded for each subject at a given session for a total of 480 stimulus repetitions per session. Raw EEG data were segmented in long epochs of 700 ms pre-stimulus onset to 1200 ms post-stimulus onset. CI artefact attenuation was applied according to the procedure outlined in Chapter 3. N1-P2 amplitude and latencies were manually determined from all subjects at each research session.

MMWs were elicited by means of an unattended oddball paradigm as the one described in Sections 4.1.3 and 5.1.4 (see Figure 4.3). However, for this study, spectral ripple densities were fixed at 0.25 RPO, 0.5 RPO, 1 RPO and 2 RPO. In total, four blocks at each ripple density were presented in a randomised order for each subject for a total of 584 standard and 56 deviant repetitions per spectral ripple density. Subjects were instructed to attend to a silent, captioned film, to ignore the presented stimuli and to keep body movements to a minimum to prevent motion artefacts in the data.

For each spectral ripple density, raw EEG data were segmented into epochs from 700 ms pre-stimulus to 1200 ms post-stimulus presentation. Epochs were filtered with a 2^{nd} order Butterworth band pass filter (2-20 Hz) created in MATLAB (MathWorks, Natick, MA) and averaged across standard and deviant conditions respectively. The averaged standard response was then subtracted from the deviant response to derive the mismatch waveforms (Naatanen et al., 2004). The area above and below one standard deviation of the noise floor of the signal, calculated as described in Section 4.1.4 and depicted in Figure 4.5, was noted for each spectral ripple density at each time-point.

6.2 Results

6.2.1 Data Analysis Framework

The dynamics of speech perception performance, spectral ripple discrimination and electrophysiological data was evaluated with a series of repeated measures analysis of variance (ANOVA) with contrast between conditions. Non-parametric Friedman tests were carried out to support the findings of the ANOVAs where data deviated from

normality. Pearson's correlation was utilised to evaluate the relationship between speech perception performance and spectral ripple discrimination. All statistical analyses were performed in IBM© SPSS© Statistics Version 22.

All nine subjects completed a minimum of four research sessions and every subject attended the sessions at one week, six months and one year after switch-on. Table 6.2 lists the full attendance per subject throughout the seven planned sessions. Due to the behaviour of the statistical software, which applies list-wise deletion of cases with a missing value, data attrition was required to complete the statistical analysis. Longitudinal interpolation was chosen as the method for data imputation due to its superior performance when dealing with missing values in longitudinal datasets (Twisk and de Vente, 2002).

Subject	Switch On	1 Week	1 Month	3 Months	6 Months	9 Months	1 Year
S1	X	X	X	X	X	X	X
S2	X	X	X	X	X	-	X
S3	X	X	X	X	X	-	X
S4	X	X	X	X	X	X	X
S5	X	X	X	-	X	X	X
S6	-	X	X	X	X	X	X
S7	X	X	X	X	X	X	X
S8	-	X	-	-	X	X	X
S9	X	X	X	X	X	X	X

X= Attended; - = Not attended

Table 6.2 Research session attendance per subject.

6.2.2 Speech Perception Performance

Figure 6.1 summarises the AzBio scores for all seven time-points and all three listening conditions (see Figure 6.1A for Quiet, B for 10 dB SNR and C for 5 dB SNR). A Shapiro-Wilk test of normality revealed that the normality assumption was violated in time-points where the AzBio scores were at floor level for the majority of the subjects. In those cases (time-points 1 – 3 in Figure 6.1A; 1 - 4 in B and 1 – 7 in C), the existence of a good performing subject would cause the data to be non-normally distributed. It was

reasoned that this behaviour was in line with expected behaviour for newly implanted patients and the ANOVA analysis was carried out in spite of violations to the normality assumption.

A 3 by 7 repeated measures ANOVA, with Greenhouse-Geisser correction accounting for sphericity violation, revealed a significant effect of time ($F_{(1.69, 13.55)} = 8.34$, $p < 0.001$), listening condition ($F_{(1.06, 8.52)} = 13.32$, $p < 0.001$), and an interaction between time and listening condition ($F_{(2.11, 16.87)} = 9.08$, $p < 0.001$) on AzBio scores, see Figure 6.2. The Bonferroni post-hoc tests for planned comparisons at switch-on, six months and one year after switch-on showed significant differences on AzBio scores across all listening conditions (Quiet vs 10 dB SNR, $p = 0.005$; Quiet vs 5 dB SNR, $p = 0.015$; and 10 dB SNR vs 5 dB SNR, $p = 0.038$). Significant differences in AzBio scores with respect to time-points were only observed between switch-on date and six months and one year respectively ($p = 0.012$ in both cases, Figure 6.2B).

Due to the previously mentioned non-normality of the AzBio scores, non-parametric tests were conducted to support the findings of the ANOVA. There was a statistically significant difference in AzBio scores depending on the time-point of testing ($\chi^2(6) = 7.600$, $p = 0.022$) and the listening condition ($\chi^2(6) = 7.600$, $p = 0.022$). A Wilcoxon test with Bonferroni correction for multiple comparisons ($\alpha=0.017$) confirmed the significant differences between AzBio scores at switch-on and six months ($Z = -2.52$, $p = 0.012$), switch-on and one year ($Z = -2.52$, $p = 0.012$), whilst no significant difference was found between speech perception scores at six months and one year ($Z = -1.40$, $p = 0.89$). A significant difference was found between speech perception scores obtained in quiet and speech perception scores obtained under ten-talker babble noise at both SNR ($Z=-2.52$, $p = 0.012$, in both cases). The findings of the non-parametric testing support the results from the ANOVA despite violating the assumption of normality.

6.2.3 Psychoacoustic Spectral Ripple Discrimination

Figure 6.3 summarises the psychoacoustic SRD thresholds across all seven time-points. A Shapiro-Wilk test of normality showed that all time-points except switch-on conform with the assumption of normality. The slight variation from normality at switch on was introduced by an outlier derived from the data attrition procedure and thus, it was considered a minor deviation.

A repeated measures ANOVA revealed a significant effect of time ($F_{(6,48)} = 5.81$, $p < 0.001$) on SRD thresholds. Figure 6.4 depicts The Bonferroni post-hoc tests for planned comparisons at switch-on, one month, six months and one year. A significant increase in SRD thresholds is observed from switch-on onwards (switch-on – one month, $p = 0.008$; switch-on – six months, $p = 0.002$; switch-on – one year, $p = 0.001$). There was an increase in SRD thresholds from one month onwards, however, this increase did not reach statistical significance.

6.2.4 Neural Spectral Ripple Discrimination

Figure 6.5 depicts the N1-P2 responses elicited to 480 stimuli repetitions of a 500 ms pure tone at 500 Hz. Each subject is plotted separately and each of the subject's time-point measurements are plotted with different colour traces. Visual inspection of N1-P2 responses shows that except for S5 and S8, the subjects in this cohort had predominantly weak responses. Inspection of the baseline portion of the plot (i.e. -100 ms to 0 ms in Figure 6.5) shows the signal-to-noise ratio is low in these subjects. In order to verify the existence of ERP responses in the collected data, the signal-to-noise ratio was increased (Light et al., 2010; Woodman, 2010). Signal-to-noise ratio was increased by pooling the average of all ERP responses from stimuli presented as the standard condition in each oddball paradigm. It was reasoned that, since no oddball response was expected from these standard responses and all standard stimuli consisted of spectrally rippled broadband noise, the pooled average of all responses would yield more prominent N1-P2 responses.

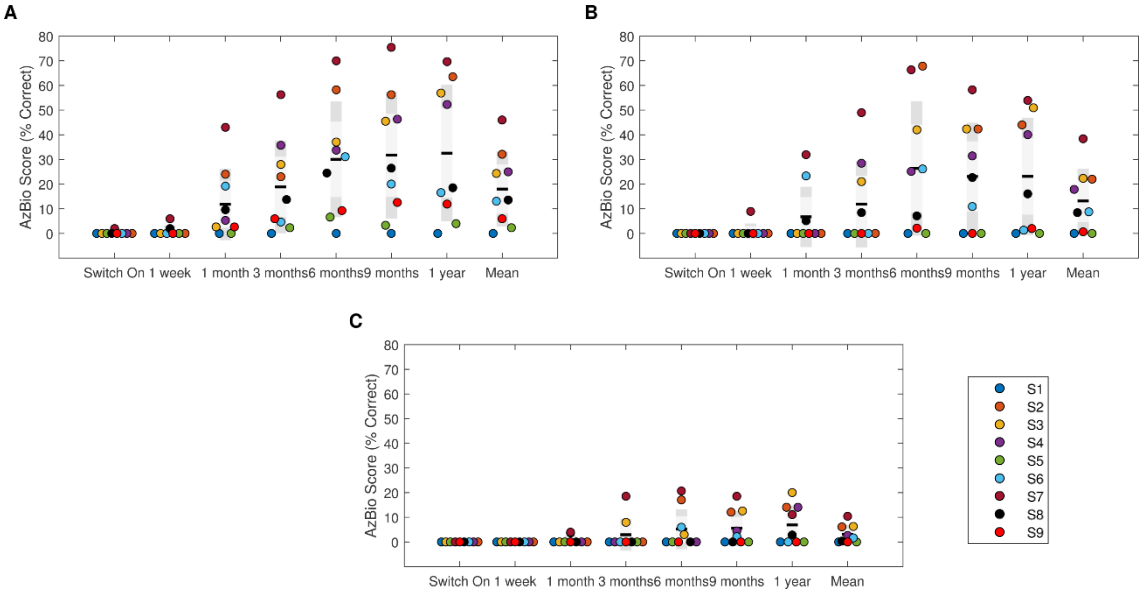

Figure 6.1 Summary of AzBio scores across all time-points and listening conditions.
AzBio scores represented as the percentage of words correctly repeated within a test list. (A) The individual and mean scores obtained in quiet listening condition. (B) The individual and mean scores obtained in ten talker babble noise at 10 dB SNR. (C) The individual and mean scores obtained in ten-talker babble noise at 5 dB SNR. Black lines indicate the mean of the population while the dark grey rectangles comprise the region after the 95% confidence interval.

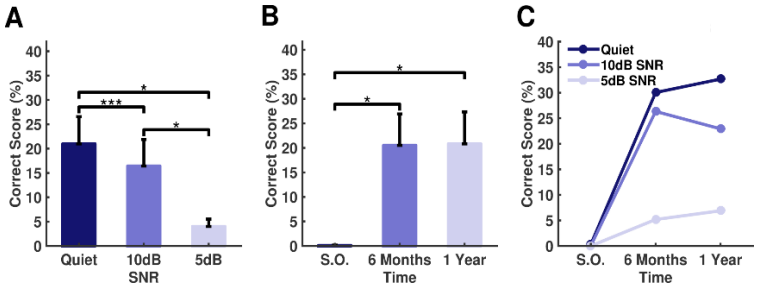

Figure 6.2 Effects of listening condition and time on AzBio scores.
(A) Effects of listening condition on speech perception; (B) Effects of time after switch-on on speech perception and; (C) Interactions of listening condition and time on speech perception. AzBio scores decrease linearly with increasing difficulty level and increase over time until reaching plateau at six months after switch-on.

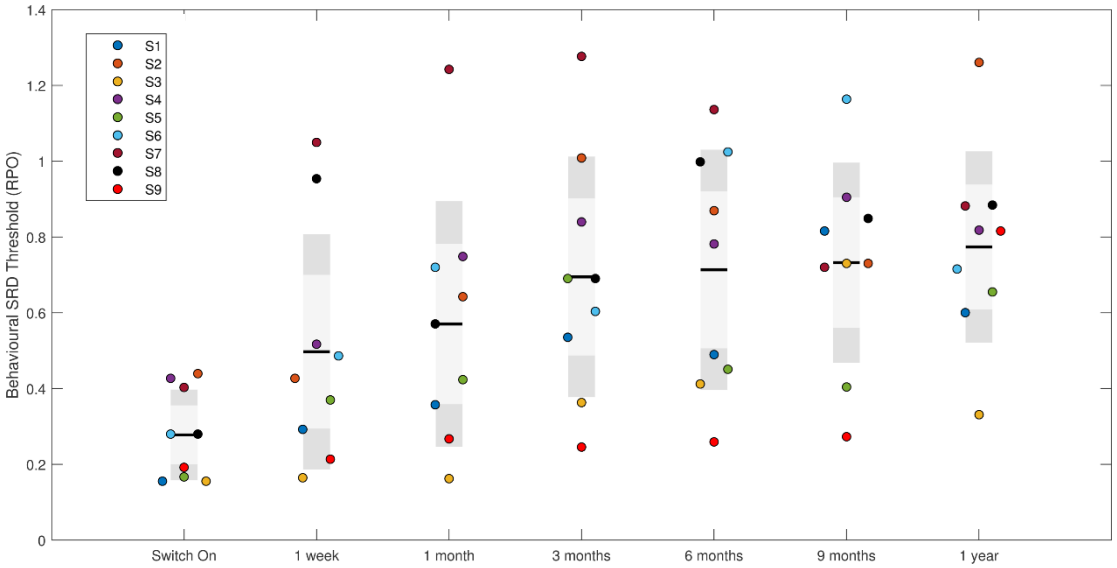

Figure 6.3 Summary of psychoacoustic spectral ripple discrimination thresholds across all time-points.
Individual scores and distribution characterisation of psychoacoustic spectral ripple discrimination thresholds from switch-on to one year after switch-on. Black lines indicate the mean of the population while the dark grey rectangles comprise the region outside the 95% confidence interval.

Figure 6.6 shows N1-P2 traces obtained by pooling the responses to the standard stimuli presented in the oddball paradigms. These spectral ripple N1-P2 responses are the result of 2,336 averages. Visual inspection of the pre-stimulus baseline shows an enhancement on signal-to-noise ratios, particularly in S1, S2, S3 and S4, compared to average of 480 pure tone stimuli. The nearly 5-fold increase in trial presentation between the ERPs presented in Figure 6.5 and Figure 6.6 had no positive effect for S9. It was determined that the quality of S9's neural responses were not suitable for analysis, therefore, they were omitted from the electrophysiological portion of the data analysis.

Figure 6.7 summarises the distribution of N1-P2 latencies and amplitudes throughout time. A Shapiro-Wilk test confirmed that the N1 and P2 latencies are normally distributed throughout all time-points. Figure 6.6 shows that S7 has the most delayed ERP response; which is reflected as the extreme value in all time-points in Figure 6.7A and Figure 6.7B. N1-P2 amplitudes showed a deviation from normality in the first four time-points which can be attributed to the evident outlier seen in Figure 6.7C corresponding to S5 in Figure 6.6.

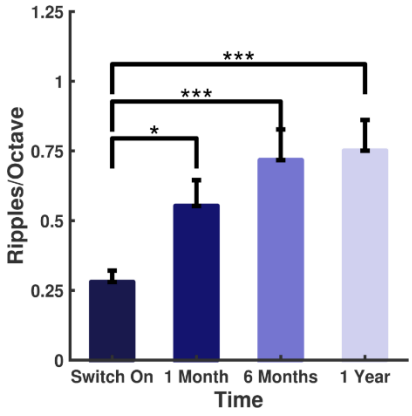

Figure 6.4 Effect of time on psychoacoustic spectral ripple discrimination.
Effect of time after switch-on on SRD thresholds assessed at 1 month, 6 months and one year. Significant differences are only observed with respect to switch-on.

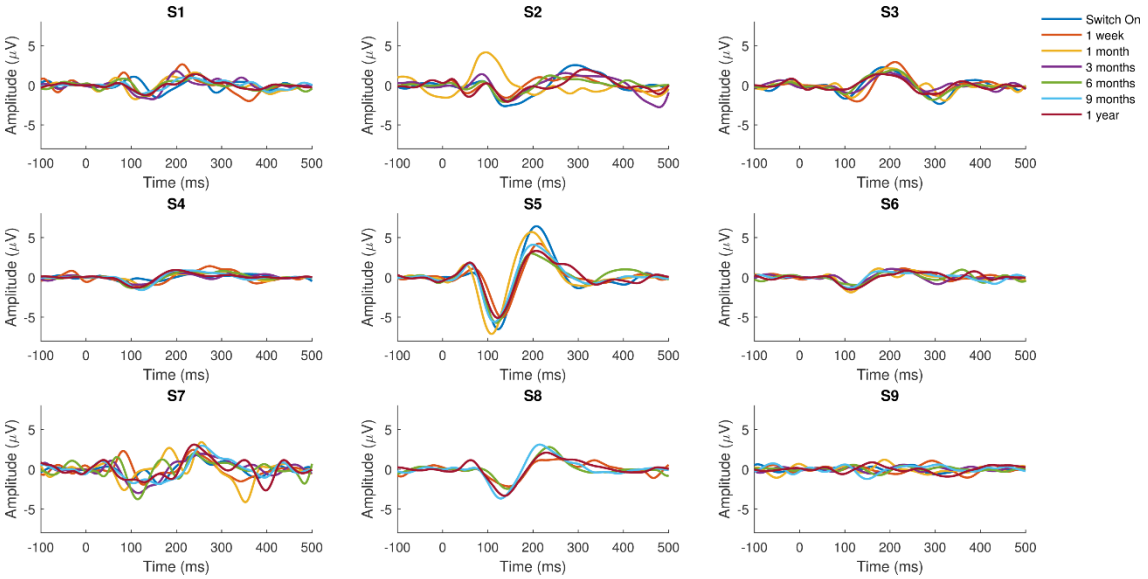

Figure 6.5 Pure tone N1-P2 responses for all subjects across time.
N1-P2 responses elicited to a 500 ms tone of 500 Hz. For each subject a total of 480 stimuli repetitions were recorded. EEG data processing and CI artefact attenuation was performed as described in Section 6.1.6. Different time-point responses are indicated by different colour traces.

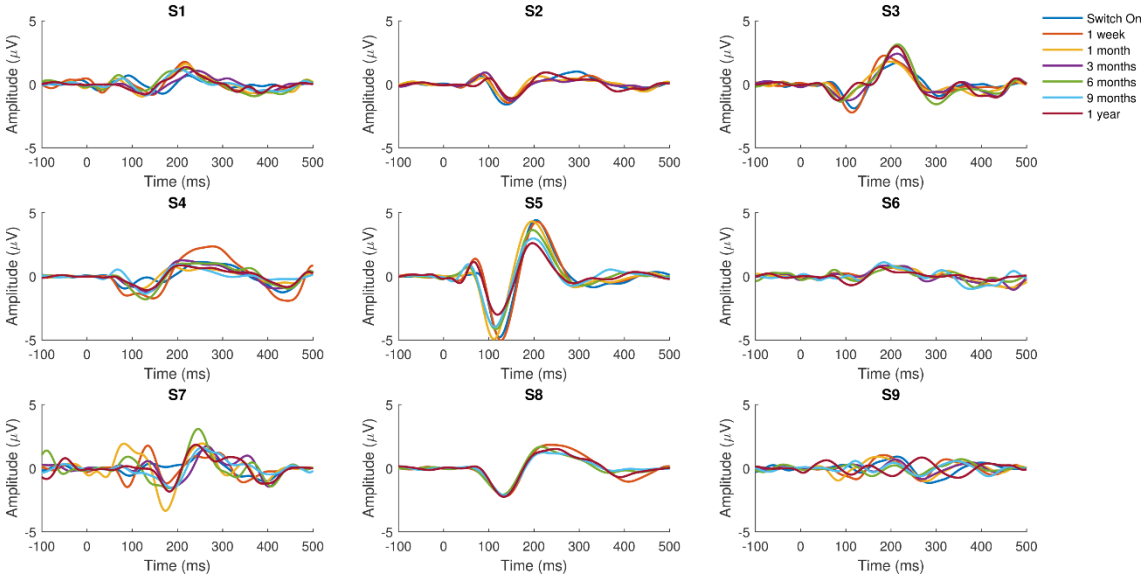

Figure 6.6 Spectral ripple N1-P2 responses for all subjects across time.
N1-P2 responses elicited to 500 ms spectrally rippled noise stimuli in the standard condition. For each subject a total of 2,336 standard stimuli presentations across spectral ripple densities were averaged. EEG data processing and CI artefact attenuation were performed as described in Section 6.1.6. Different time-point responses are indicated by different colour traces.

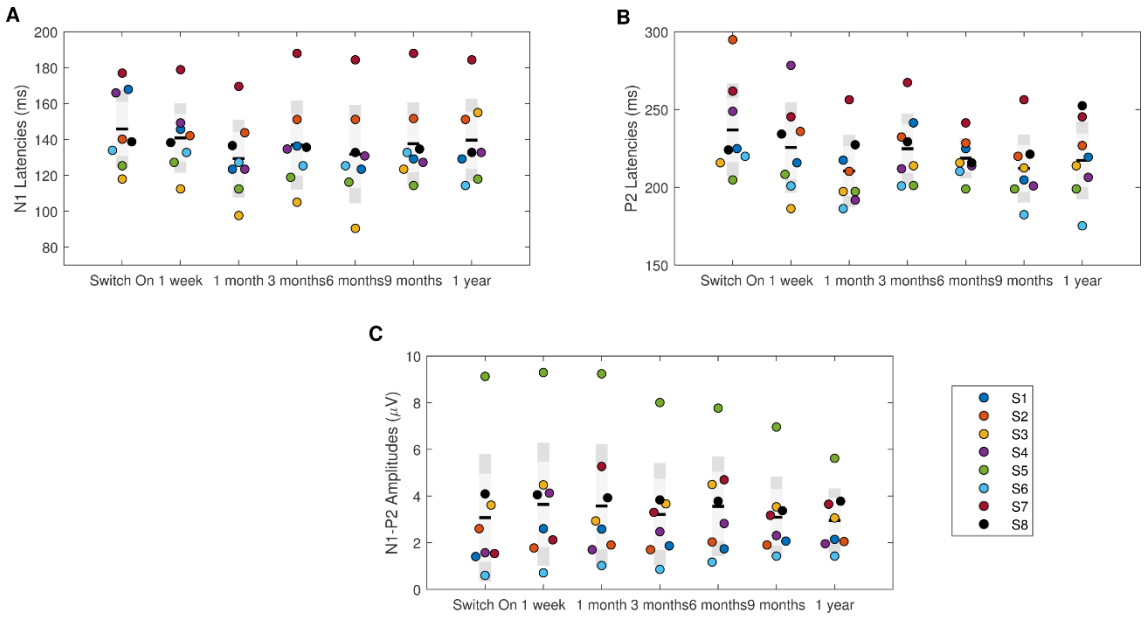

Figure 6.7 N1-P2 latencies and amplitude distributions across time.
N1-P2 complexes were visually inspected and (A) N1 latencies, (B) P2 latencies and (C) N1-P2 amplitudes were manually determined.

A Repeated measures ANOVA, with Greenhouse-Geisser correction accounting for sphericity violation, revealed no significant effects of time on N1 latencies ($F_{(1.72,13.74)} = 1.92$, $p = 0.187$), P2 latencies ($F_{(2.88,23.07)} = 2.53$, $p = 0.1$) nor N1-P2 amplitudes ($F_{(2.83,23.07)} = 2.53$, $p = 0.344$).

Figure 6.8 summarises the distribution of the MMW areas at the four different spectral ripple densities (i.e. 0.25 RPO (A), 0.5 RPO (B), 1 RPO (C) and 2 RPO (D)). MMW area data was logarithmically transformed to compensate for non-normality of data. However, at some time-points non-normality was still present after log transformations were carried out.

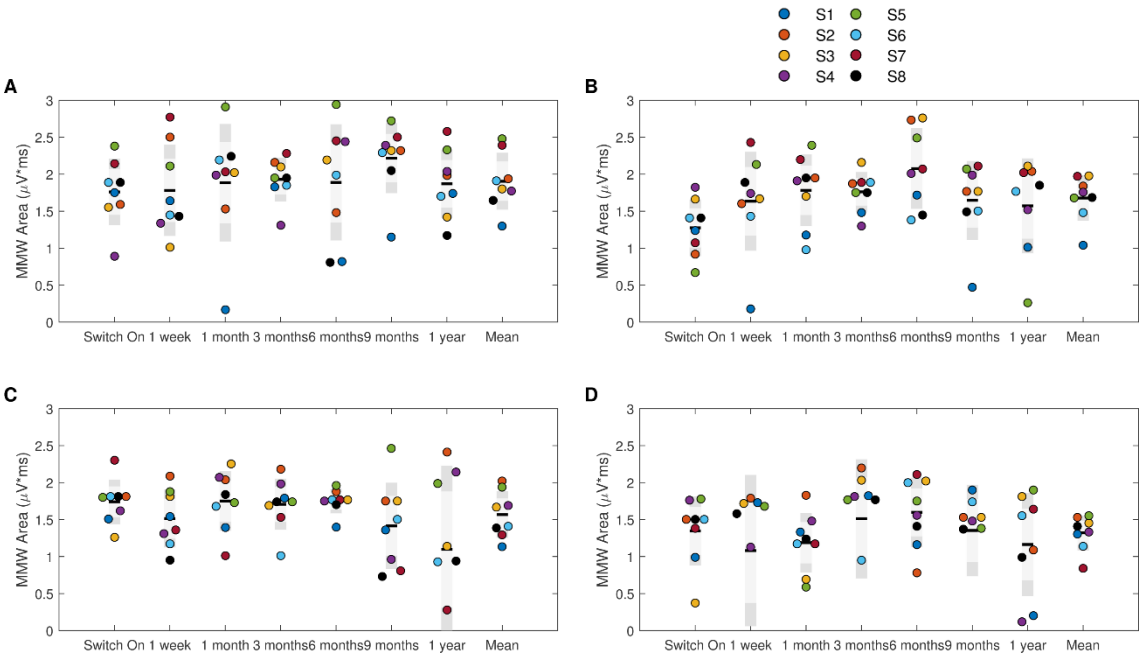

Figure 6.8 Distributions of MMW areas for all four spectral ripple densities across time. *Logarithmically transformed MMW area is plotted throughout all time points. Plots identify MMW areas for all four RPO densities: (A) 0.25 RPO; (B) 0.5 RPO; (C) 1 RPO; (D) 2 RPO.*

A 4 by 7 repeated measures ANOVA revealed a significant main effect only for ripple density ($F_{(3,24)} = 7.79$, $p < 0.005$). The Bonferroni post-hoc test revealed that there is a significant difference between log MMW area elicited at 0.25 RPO and log MMW area elicited at 2 RPO depicted in Figure 6.9A. The variations of the log MMW area under the curve over time (Figure 6.9B) were not significantly different.

A non-parametric Friedman test supports the findings of the ANOVA, highlighting a significant effect of RPO density on the MMW area ($\chi^2(3) = 9.45$, $p = 0.024$). A Wilcoxon test with Bonferroni correction for multiple comparisons ($\alpha = 0.012$) revealed an almost significant difference between MMW area at 0.25 RPO and 2 RPO ($Z = -2.52$, $p = 0.017$).

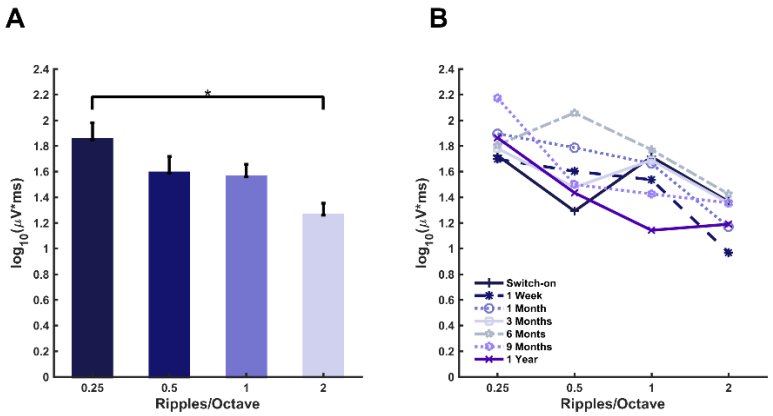

Figure 6.9 Effect of spectral ripple density and time on MMW area.
(A) Effect of ripple density on log transformed MMW area under the curve; (B) Variations of MMW area under the curve over time were shown to be non-significant

Figure 6.10 summarises the distribution of neural spectral ripple discrimination thresholds obtained from the MMW data as outlined in Chapter 4. A Shapiro-Wilk test for normality revealed that the neural threshold has a normal distribution throughout time except at the six months time-point. A repeated measures ANOVA, with Greenhouse-Geisser correction accounting for sphericity violation, revealed no significant effects of time on neural spectral ripple discrimination thresholds ($F_{(1.48, 2.96)} = 1.31$, $p = 0.370$).

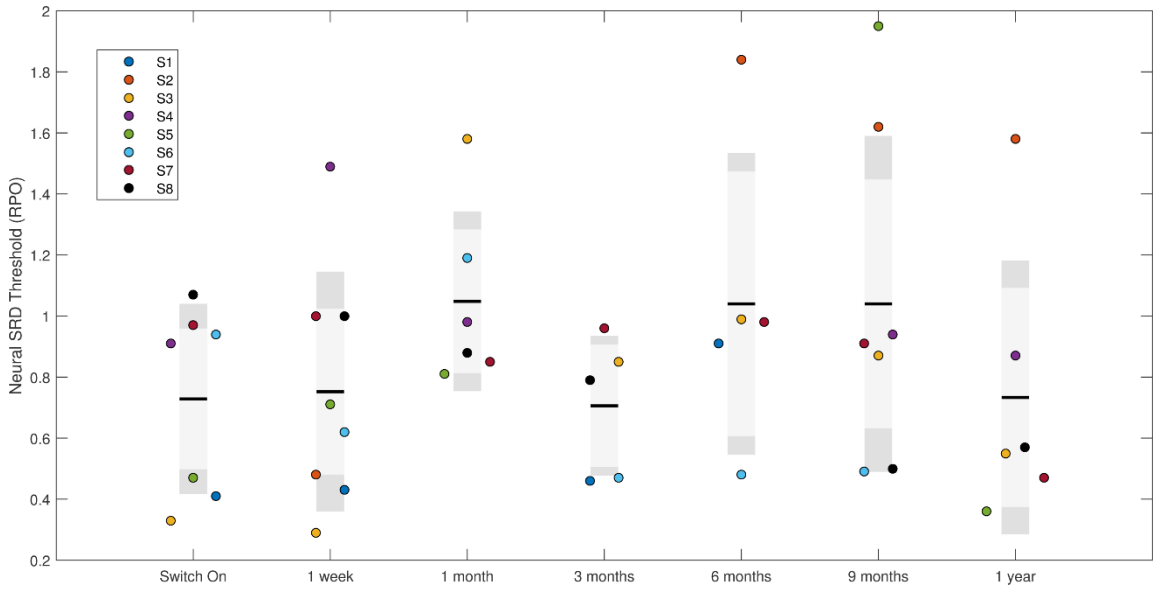

Figure 6.10 Distribution of neural spectral ripple discrimination thresholds across all time-points.
Individual estimates and distribution characterisation of neural spectral ripple discrimination thresholds from switch-on to one year after switch-on. Black lines indicate the mean of the population while the dark grey rectangles comprise the region outside the 95% confidence interval.

6.2.5 Relationship between Speech Perception and Spectral Ripple Discrimination

Linear regression analysis revealed that psychoacoustic SRD thresholds correlated with AzBio scores in all three listening conditions. **Table** 6.3 summarises the correlation for psychoacoustic SRD thresholds and AzBio scores for the three listening conditions and throughout the seven time-points. With exception of switch-on date, nine months and one year, SRD correlates with speech perception in quiet at the same time-point.

It is to be noted that SRD at switch-on correlates with speech perception at six months, nine months and one year in the quiet listening condition. Switch-on SRD also showed a significant correlation with speech perception in ten-talker babble noise at 10 dB SNR during six and nine months. A non-significant but trending correlation was found between AzBio scores in ten-talker babble noise at 10 dB SNR at one year and in ten-talker babble noise at 5 dB SNR at six and nine months after switch-on.

Figure 6.11 depicts the correlation between SRD thresholds at switch-on and speech perception performance 6 months after switch-on. In the quiet listening condition (Figure 6.11A) and in ten-talker babble noise at 10 dB SNR (Figure 6.11B) a significant correlation was revealed (r^2 = 0.6, p = 0.01 and r^2 = 0.47, p = 0.04, respectively). A trending non-significant relationship (r^2 = 0.41, p = 0.063) was found between SRD and AzBio scores in ten-talker babble noise at 5 dB SNR (Figure 6.11C).

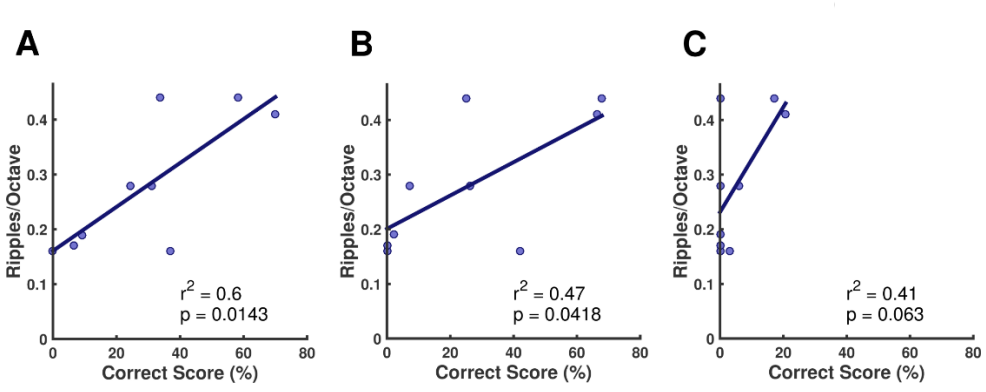

Figure 6.11 Relationship between psychoacoustic spectral ripple discrimination and speech perception performance.
Correlation between psychoacoustic SRD at switch-on and AzBio scores at six months in all listening conditions: (A) quiet; (B) in ten-talker babble noise at 10 dB SNR and; (C) in noise at 5 dB SNR

Quiet	SRD\AzBio	Switch on	1 Week	1 Month	3 Months	6 Months	9 Months	1 Year
	Switch on	***p*= 0.28** **r^2= 0.17**	***p*= 0.17** **r^2= 0.25**	*p*= 0.04 r^2= 0.48	***p*= 0.09** **r^2= 0.36**	*p*= 0.01 r^2= 0.59	*p*= 0.02 r^2= 0.55	*p*= 0.03 r^2= 0.50
	1 Week		*p*< 0.01 r^2= 0.77	*p*= 0.02 r^2= 0.55	***p*= 0.06** **r^2= 0.41**	***p*= 0.13** **r^2= 0.29**	*p*= 0.03 r^2= 0.52	***p*= 0.41** **r^2= 0.10**
	1 Month			*p*= 0.01 r^2= 0.66	***p*= 0.08** **r^2= 0.37**	*p*= 0.05 r^2= 0.45	*p*= 0.01 r^2= 0.62	***p*= 0.20** **r^2= 0.22**
	3 Months				*p*= 0.03 r^2= 0.50	*p*= 0.02 r^2= 0.56	*p*= 0.03 r^2= 0.50	***p*= 0.10** **r^2= 0.34**
	6 Months					*p*= 0.04 r^2= 0.46	*p*= 0.04 r^2= 0.48	***p*= 0.27** **r^2= 0.18**
	9 Months						***p*= 0.46** **r^2= 0.08**	***p*= 0.69** **r^2= 0.02**
	1 Year							***p*= 0.31** **r^2= 0.14**

10 dB SNR	SRD\AzBio	Switch on	1 Week	1 Month	3 Months	6 Months	9 Months	1 Year
	Switch on	-	***p*= 0.29** **r^2= 0.16**	***p*= 0.36** **r^2= 0.12**	***p*= 0.27** **r^2= 0.17**	*p*= 0.04 r^2= 0.46	*p*= 0.03 r^2= 0.53	***p*= 0.08** **r^2= 0.37**
	1 Week		*p*= 0.04 r^2= 0.49	*p*= 0.03 r^2= 0.5	***p*= 0.06** **r^2= 0.41**	***p*= 0.39** **r^2= 0.10**	*p*= 0.01 r^2= 0.61	***p*= 0.41** **r^2= 0.10**
	1 Month			*p*= 0.03 r^2= 0.52	***p*= 0.11** **r^2= 0.31**	***p*= 0.14** **r^2= 0.28**	*p*= 0.01 r^2= 0.66	***p*= 0.31** **r^2= 0.14**
	3 Months				***p*= 0.10** **r^2= 0.34**	*p*= 0.05 r^2= 0.44	*p*= 0.02 r^2= 0.58	***p*= 0.14** **r^2= 0.28**
	6 Months					***p*= 0.14** **r^2= 0.29**	*p*= 0.02 r^2= 0.59	***p*= 0.34** **r^2= 0.13**
	9 Months						***p*= 0.34** **r^2= 0.13**	***p*= 0.71** **r^2= 0.02**
	1 Year							***p*= 0.39** **r^2= 0.11**

5 dB SNR	SRD\AzBio	Switch on	1 Week	1 Month	3 Months	6 Months	9 Months	1 Year
	Switch on	-	-	***p*= 0.41** **r^2= 0.10**	***p*= 0.67** **r^2= 0.03**	***p*= 0.06** **r^2= 0.41**	***p*= 0.11** **r^2= 0.32**	***p*= 0.22** **r^2= 0.20**
	1 Week		-	***p*= 0.06** **r^2= 0.44**	***p*= 0.08** **r^2= 0.37**	***p*= 0.19** **r^2= 0.23**	***p*= 0.07** **r^2= 0.41**	***p*= 0.97** **r^2= 0.00**
	1 Month			*p*= 0.04 r^2= 0.49	***p*= 0.28** **r^2= 0.16**	***p*= 0.06** **r^2= 0.41**	*p*= 0.02 r^2= 0.55	***p*= 0.74** **r^2= 0.02**
	3 Months				***p*= 0.17** **r^2= 0.26**	*p*= 0.01 r^2= 0.61	*p*= 0.02 r^2= 0.55	***p*= 0.47** **r^2= 0.08**
	6 Months					***p*= 0.08** **r^2= 0.37**	***p*= 0.09** **r^2= 0.36**	***p*= 0.75** **r^2= 0.01**
	9 Months						***p*= 0.68** **r^2= 0.03**	***p*= 0.74** **r^2= 0.02**
	1 Year							***p*= 0.57** **r^2= 0.05**

- = Not possible to evaluate

Table 6.3 Confusion tables for correlation values between psychoacoustic SRD and AzBio Scores.

Quiet	SRD\AzBio	Switch on	1 Week	1 Month	3 Months	6 Months	9 Months	1 Year
	Switch on	***p*= 0.24 r^2= 0.05**	***p*= 0.14 r^2= 0.00**	***p*= 0.53 r^2= 0.06**	***p*= 0.53 r^2= 0.05**	***p*= 0.92 r^2= 0.00**	***p*= 0.23 r^2= 0.03**	***p*= 0.80 r^2= 0.04**
	1 Week		***p*= 0.20 r^2= 0.31**	***p*= 0.68 r^2= 0.22**	***p*= 0.19 r^2= 0.34**	***p*= 0.69 r^2= 0.32**	***p*= 0.16 r^2= 0.32**	***p*= 0.66 r^2= 0.24**
	1 Month			***p*= 0.86 r^2= 0.03**	***p*= 0.49 r^2= 0.20**	***p*= 0.80 r^2= 0.09**	***p*= 0.47 r^2= 0.14**	***p*= 0.69 r^2= 0.13**
	3 Months				***p*= 0.54 r^2= 0.02**	***p*= 0.53 r^2= 0.17**	***p*= 0.34 r^2= 0.09**	***p*= 0.69 r^2= 0.10**
	6 Months					***p*= 0.17 r^2= 0.09**	***p*= 0.78 r^2= 0.12**	***p*= 0.19 r^2= 0.26**
	9 Months						***p*= 0.99 r^2= 0.35**	***p*= 0.51 r^2= 0.34**
	1 Year							***p*= 0.07 r^2= 0.53**

10 dB SNR	SRD\AzBio	Switch on	1 Week	1 Month	3 Months	6 Months	9 Months	1 Year
	Switch on	-	***p*= 0.40 r^2= 0.05**	***p*= 0.11 r^2= 0.01**	***p*= 0.25 r^2= 0.09**	***p*= 0.60 r^2= 0.00**	***p*= 0.19 r^2= 0.04**	***p*= 0.78 r^2= 0.07**
	1 Week		***p*= 0.54 r^2= 0.23**	***p*= 0.66 r^2= 0.14**	***p*= 0.15 r^2= 0.28**	***p*= 0.89 r^2= 0.16**	***p*= 0.18 r^2= 0.29**	***p*= 0.69 r^2= 0.21**
	1 Month			***p*= 0.55 r^2= 0.01**	***p*= 0.31 r^2= 0.15**	***p*= 0.99 r^2= 0.04**	***p*= 0.51 r^2= 0.14**	***p*= 0.62 r^2= 0.16**
	3 Months				***p*= 0.31 r^2= 0.00**	***p*= 0.67 r^2= 0.23**	***p*= 0.25 r^2= 0.15**	***p*= 0.54 r^2= 0.09**
	6 Months					***p*= 0.40 r^2= 0.21**	***p*= 0.79 r^2= 0.16**	***p*= 0.25 r^2= 0.30**
	9 Months						***p*= 0.92 r^2= 0.30**	***p*= 0.60 r^2= 0.29**
	1 Year							***p*= 0.10 r^2= 0.49**

5 dB SNR	SRD\AzBio	Switch on	1 Week	1 Month	3 Months	6 Months	9 Months	1 Year
	Switch on	-	-	***p*= 0.11 r^2= 0.37**	***p*= 0.52 r^2= 0.07**	***p*= 0.75 r^2= 0.02**	***p*= 0.47 r^2= 0.09**	***p*= 0.48 r^2= 0.09**
	1 Week		-	***p*= 0.72 r^2= 0.02**	***p*= 0.83 r^2= 0.01**	***p*= 0.86 r^2= 0.01**	***p*= 0.52 r^2= 0.07**	***p*= 0.94 r^2= 0.00**
	1 Month			***p*= 0.51 r^2= 0.08**	***p*= 0.43 r^2= 0.11**	***p*= 0.59 r^2= 0.05**	***p*= 0.71 r^2= 0.02**	***p*= 0.50 r^2= 0.08**
	3 Months				***p*= 0.06 r^2= 0.47**	***p*= 0.64 r^2= 0.04**	***p*= 0.27 r^2= 0.20**	***p*= 0.79 r^2= 0.01**
	6 Months					***p*= 0.06 r^2= 0.50**	***p*= 0.47 r^2= 0.09**	***p*= 0.27 r^2= 0.20**
	9 Months						***p*= 0.92 r^2= 0.00**	***p*= 0.57 r^2= 0.06**
	1 Year							***p*= 0.09 r^2= 0.41**

- = Not possible to evaluate

Table 6.4 Confusion tables for correlation values between neural SRD and AzBio Scores.

Quiet	MMWarea\AzBio	Switch on	1 Week	1 Month	3 Months	6 Months	9 Months	1 Year
	Switch on	**p= 0.67 r^2= 0.17**	**p= 0.92 r^2= 0.25**	**p= 0.58 r^2= 0.48**	**p= 0.97 r^2= 0.36**	**p= 0.97 r^2= 0.59**	**p= 0.55 r^2= 0.55**	**p= 0.61 r^2= 0.50**
	1 Week		**p= 0.15 r^2= 0.77**	**p= 0.23 r^2= 0.55**	p= 0.02 r^2= 0.41	**p= 0.15 r^2= 0.29**	**p= 0.11 r^2= 0.52**	**p= 0.22 r^2= 0.10**
	1 Month			**p= 0.67 r^2= 0.66**	p= 0.04 r^2= 0.37	**p= 0.48 r^2= 0.45**	**p= 0.47 r^2= 0.62**	**p= 0.39 r^2= 0.22**
	3 Months				**p= 0.74 r^2= 0.50**	**p= 0.31 r^2= 0.56**	**p= 0.77 r^2= 0.50**	**p= 0.45 r^2= 0.34**
	6 Months					**p= 0.48 r^2= 0.46**	**p= 0.98 r^2= 0.48**	**p= 0.20 r^2= 0.18**
	9 Months						**p= 0.14 r^2= 0.08**	**p= 0.13 r^2= 0.02**
	1 Year							p= 0.04 r^2= 0.14

10 dB SNR	MMWarea \AzBio	Switch on	1 Week	1 Month	3 Months	6 Months	9 Months	1 Year
	Switch on	-	**p= 0.61 r^2= 0.05**	**p= 0.86 r^2= 0.01**	**p= 0.72 r^2= 0.02**	**p= 0.92 r^2= 0.00**	**p= 0.59 r^2= 0.05**	**p= 0.52 r^2= 0.07**
	1 Week		**p= 0.23 r^2= 0.23**	**p= 0.36 r^2= 0.14**	**p= 0.07 r^2= 0.45**	**p= 0.33 r^2= 0.16**	**p= 0.12 r^2= 0.36**	**p= 0.25 r^2= 0.21**
	1 Month			**p= 0.82 r^2= 0.01**	**p= 0.13 r^2= 0.33**	**p= 0.63 r^2= 0.04**	**p= 0.47 r^2= 0.09**	**p= 0.32 r^2= 0.16**
	3 Months				**p= 0.93 r^2= 0.00**	**p= 0.23 r^2= 0.23**	**p= 0.75 r^2= 0.02**	**p= 0.46 r^2= 0.09**
	6 Months					**p= 0.25 r^2= 0.21**	**p= 0.88 r^2= 0.00**	**p= 0.16 r^2= 0.30**
	9 Months						**p= 0.18 r^2= 0.28**	**p= 0.17 r^2= 0.29**
	1 Year							p= 0.05 r^2= 0.49

5 dB SNR	MMWarea \AzBio	Switch on	1 Week	1 Month	3 Months	6 Months	9 Months	1 Year
	Switch on	-	-	**p= 0.92 r^2= 0.00**	**p= 0.73 r^2= 0.02**	**p= 0.36 r^2= 0.14**	**p= 0.91 r^2= 0.00**	**p= 0.33 r^2= 0.16**
	1 Week		-	**p= 0.43 r^2= 0.11**	**p= 0.12 r^2= 0.35**	**p= 0.35 r^2= 0.14**	**p= 0.20 r^2= 0.26**	**p= 0.46 r^2= 0.09**
	1 Month			**p= 0.65 r^2= 0.04**	**p= 0.25 r^2= 0.21**	**p= 0.58 r^2= 0.05**	**p= 0.52 r^2= 0.07**	**p= 0.50 r^2= 0.08**
	3 Months				**p= 0.25 r^2= 0.21**	**p= 0.31 r^2= 0.17**	**p= 0.56 r^2= 0.06**	**p= 0.47 r^2= 0.09**
	6 Months					**p= 0.50 r^2= 0.08**	**p= 0.84 r^2= 0.01**	**p= 0.47 r^2= 0.44**
	9 Months						**p= 0.25 r^2= 0.22**	**p= 0.25 r^2= 0.22**
	1 Year							**p= 0.10 r^2= 0.39**

- = Not possible to evaluate

Table 6.5 Confusion tables for correlation values between MMW area at 0.5 RPO and AzBio Scores.

Linear regression analysis revealed a significant correlation between psychoacoustic SRD thresholds and neural thresholds at nine months and one year after switch-on (r^2 = 0.50, p = 0.05 and r^2 = 0.57, p = 0.03, respectively). The correlation between psychoacoustic SRD thresholds and neural thresholds is summarised in **Table** 6.6. Furthermore, a trending non-significant correlation was found between neural SRD thresholds and speech perception performance one year after switch-on for all listening conditions (r^2 = 0.53, p = 0.07; r^2 = 0.49, p = 0.10 and r^2 = 0.41, p = 0.09, respectively). Similarly, MMW area at 0.5 RPO was significantly correlated with AzBio scores in the quiet and in ten-talker babble noise at 10 dB SNR listening conditions one year after switch-on (r^2 = 0.53, p = 0.04 and r^2 = 0.49, p = 0.05, respectively). A trending non-significant correlation was found between MMW area at 0.5 RPO and speech perception performance one year after switch-on and ten-talker babble noise at 5 dB SNR listening condition (r^2 = 0.39, p = 0.10). **Table** 6.4 and **Table** 6.5 summarise the correlations between neural SRD thresholds and speech perception as well as MMW area at 0.5 RPO and speech perception in all listening conditions.

Psychoacoustic SRD\Neural SRD	Switch on	1 Week	1 Month	3 Months	6 Months	9 Months	1 Year
Switch on	***p*= 0.63 r^2= 0.04**	***p*= 0.11 r^2= 0.36**	***p*= 0.65 r^2= 0.04**	***p*= 0.60 r^2= 0.05**	***p*= 0.59 r^2= 0.05**	***p*= 0.61 r^2= 0.05**	***p*= 0.07 r^2= 0.44**
1 Week		***p*= 0.11 r^2= 0.37**	***p*= 0.90 r^2= 0.00**	***p*= 0.28 r^2= 0.19**	***p*= 0.61 r^2= 0.04**	***p*= 0.83 r^2= 0.01**	***p*= 0.96 r^2= 0.00**
1 Month			***p*= 0.84 r^2= 0.01**	***p*= 0.99 r^2= 0.00**	***p*= 0.97 r^2= 0.00**	***p*= 0.90 r^2= 0.00**	***p*= 0.70 r^2= 0.03**
3 Months				***p*= 0.91 r^2= 0.00**	***p*= 0.56 r^2= 0.06**	***p*= 0.43 r^2= 0.11**	***p*= 0.29 r^2= 0.18**
6 Months					***p*= 0.90 r^2= 0.00**	***p*= 0.69 r^2= 0.03**	***p*= 0.74 r^2= 0.02**
9 Months						*p*= 0.05 r^2= 0.50	***p*= 0.58 r^2= 0.05**
1 Year							*p*= 0.03 r^2= 0.57

- = Not possible to evaluate

Table 6.6 Confusion table for correlation values between psychoacoustic SRD and neural SRD

6.3 Discussion

6.3.1 Dynamics of Speech Perception Performance

Speech perception performance was assessed through the AzBio open-set test battery included in the minimum speech test battery (MSTB) developed by Spahr et al. (2012). Results suggest that speech perception performance in newly implanted patients stabilises over the first six months after device activation (see Figure 6.2). These results are in line with the reported speech rehabilitation time-frames in the literature (Krueger et al., 2008; Lenarz et al., 2012; Massa and Ruckenstein, 2014). Furthermore, the significant interaction found among different listening conditions, depicted in Figure 6.2C**,** indicates that speech perception in noise develops at a slower rate than speech perception in quiet conditions.

It is to be noted that the speech material utilised in this study was recorded in American English. There was no evidence found in the literature to indicate an expected difference in AzBio test performance with respect to English language variations (i.e. British English, Irish English, American English, etc.). Nonetheless, self-reported feedback from the participating subjects highlighted difficulties to comprehend the unfamiliar rate of articulation. This should be considered as a confounding factor when interpreting the lower average scores of this cohort vs the average scores reported by Massa and Ruckenstein (2014). However, the large variability observed within this subject cohort (Figure 6.1) rather suggests a mixture of good and poor performers.

6.3.2 Dynamics of Psychoacoustic Spectral Ripple Discrimination

Mean psychoacoustic spectral ripple discrimination ranged from 0.22 to 0.82 ripples / octave across time-points. These results are in line with SRD thresholds previously reported in Chapter 4and those reported by Won et al. (2007). However, these thresholds are in the low-end when compared to those reported by Drennan et al. (2015). In that study, Drennan et al. (2015) performed a longitudinal evaluation (starting at one month after device switch one) of behavioural, non-linguistic tests such as spectral ripple discrimination, temporal modulation detection and Schroeder-phase discrimination. Their findings suggest that SRD threshold could be used as an acute measure of CI performance as it did not show significant changes within time frame of their study. The results presented in this study partly support this claim.

There were no significant differences found in SRD one month after switch-on onwards as depicted in Figure 6.4. However, there was a significant difference found from switch-on to one month. The novelty factor of having the implant just turned on, may account for the difference in performance. SRD thresholds obtained one week after switch-on onwards show no significant difference (ANOVA- $F_{(2.34, 18.70)} = 2.83$, $p = 0.07$). Despite having the device just switched-on, all subjects were able to perform the SRD task after one training run. This evidence contributes to the idea that SRD could be performed earlier than one month to assess CI performance.

6.3.3 Dynamics of Electrophysiological Data

As it was discussed in Section 4.3.3, clinical applications of CAEP methods may be limited by the known maturational changes of cortical potentials (Ponton et al., 2000). It has been shown that even after prolonged acoustic deprivation, cortical auditory potentials can re-develop over a period of time in both paediatric and adult CI populations (Sharma et al., 2002; Bauer et al., 2006; Pantev et al., 2006; Gilley et al., 2008; Sharma et al., 2009; Sharma et al., 2016).

This study evaluates the dynamics of single-channel electrophysiology longitudinally over the period of one year after device switch-on. The results reported in Section 6.2.4 and depicted in Figure 6.7 revealed that there were no significant changes identified, in this CI population, with respect to N1-P2 latencies and amplitudes across time. Contrastingly to what is reported in the literature, Figure 6.6 depicts rather unchanged N1-P2 responses for the majority of the subjects. Two major factors may account for this contrasting result. The first being that some of the evidence or CI cortical plasticity and re-organisation are based on high density EEG (Gilley et al., 2008; Sharma et al., 2016) or MEG (Pantev et al., 2006) recordings, allowing the possibility to evaluate inter-hemispheric differences and dipole localisation. The electrophysiological data recorded in this study is limited by the low dimensionality provided from the single-channel set-up.

The second major factor that could explain the results from this study lies in the demographics of the CI cohort. Discussions regarding cortical plasticity in CI users focus mainly on paediatric populations (Bauer et al., 2006; Gilley et al., 2008; Sharma et al., 2009; Sharma et al., 2016) and the P1 potential, which is the predecessor of the N1 potential in normal developing children (Ponton et al., 1996). This suggests that there is

a de facto ongoing maturational process expected in these studies. Changes in morphology of CAEPs in adults may be more affected by the type of hearing impairment, duration of deafness and the use of hearing devices pre-implantation.

MMW areas were logarithmically transformed as an attempt to account for the non-normal behaviour of the data. This non-normality may have derived from the low signal-to-noise ratio in the EEG recordings, leading to spurious measurements of MMW area. The low signal-to-noise ratio in this study is a combination of the recording environment and the paradigm design. In contrast to the study presented in Chapter 4, EEG recordings were not conducted in a dedicated and electrically isolated room, instead, recordings were conducted in an ordinary office space allocated to the research at the clinic. The choice of the recording environment was deliberate, as it was reasoned that it was representative of real clinical conditions. Additionally, due to the number of spectral ripple densities to be tested and based on the results from the studies in Chapter 4 and Chapter 5, the number of deviants acquired per condition was limited to 56. This number is around four times less than the recommended number of deviants required to obtain reliable mismatch responses from normal hearing experiments (i.e. 225) (Light et al., 2010; Woodman, 2010). Impact of number of repetitions on CAEP signal-to-noise ratio can be seen from Figure 6.5 and Figure 6.6.

6.3.4 Relationship between Spectral Ripple Discrimination and Speech Perception Performance

The results of this study suggest that clinical assessment of spectral ripple discrimination immediately at switch-on can be applied as a predictor of speech perception performance in quiet and in noise at six months, nine months and one year after implantation. This result is in line with recent evidence suggesting that the spectral ripple discrimination abilities are an acute measure of spectral discrimination abilities, which don't seem to change over time (Drennan et al., 2015). Spectral resolution seems to be determined by the implant and implant placement within the cochlea (Drennan et al., 2010; Jones et al., 2011; Won et al., 2011a; Won et al., 2012). No learning effect takes place in contrast to speech perception which has a development period before stabilising around six months.

The correlation found between neural spectral ripple discrimination and behavioural spectral ripple discrimination, as well as the trending correlation with speech perception performance in quiet and in the ten-talker babble noise one year after device

switch-on, suggests that neural estimates of spectral ripple discrimination may require longer maturation time when assessing CI performance. Additionally, the significant correlation found between MMW area at 0.5 RPO and AzBio scores, highlights the possibility to optimise electrophysiological data by focusing in a particular spectral ripple density rather than four as was the case in this study.

6.3.5 Implications for Future Clinical Applications

As a first field trial, this study demonstrated the possibility to record single-channel electrophysiological data from CI users longitudinally within a clinical environment. There is a need for optimisation of the electrophysiological paradigms to account for low signal-to-noise ratio in the data and maximise the number of trials recorded.

All research sessions were conducted after the clinical fitting session. The cognitive expenditure associated with the clinical appointment as well as the time-of-day effect (Hines, 2004) may have had a detrimental effect on the overall session performance. This can be accounted for by interleaving the research sessions in different days throughout the year. Since there was no significant effect of time identified on spectral ripple discrimination metrics, it is possible to reduce the number of sessions.

6.3.6 Conclusions

This study evaluated the clinical applicability of non-linguistic and objective assessment of spectral ripple discrimination as an early predictor of speech perception performance in newly implanted CI users over the first year after implantation within a clinical environment. The previously developed tools for acquisition of artefact free EEG presented in Chapter 4 and for the objective assessment of SRD via MMWs presented in Chapter 5, were successfully integrated in clinical practice. Results from the objective MMW assessment of spectral ripple discrimination showed indications of a central contribution to the discrimination of different spectral ripple densities whilst no significant change on MMW area under the curve was observed over time. Factors such as the length of the research session and subject's cognitive depletion after the routine clinical assessment may account for the variability of the MMWs. This study demonstrated the clinical applicability of non-linguistic spectral ripple discrimination tests as early predictors of speech perception performance in CI users. Clinical spectral

ripple discrimination testing from switch-on date may be advantageous for optimisation of hearing rehabilitation by predicting speech perception outcomes six months in advance.

Key Points

- This study aimed to address the research questions 7, 8 and 9 listed in Section 2.4.
- Neural spectral ripple discrimination thresholds may require a maturation time longer that one year after device switch-on.
- Psychoacoustic spectral ripple discrimination as early as switch-on day correlates with speech perception performance six months in advance.
- It is possible to record single-channel CAEPs longitudinally in a population fo CI users within a clinical environment.
- Optimisation of the neural spectral ripple discrimination clinical protocol is required in order to account for low signal-to-noise ratio of the neural recordings as well as for cognitive depletion from the preceding clinical assessment.
- These findings were presented at the 8th International Symposium on Objective Measures in Auditory Implants, Toronto 2012; the 8th Speech in Noise Workshop, Groningen 2016; the 22nd Bioengineering in Ireland Conference, Galway 2016; and at the MidWinter Meeting- ARO, San Diego 2016.

Chapter 7 Exploring Objective Metrics of Temporal Processing in CI users

The studies presented in Chapter 4, Chapter 5 and Chapter 6 were oriented towards the development and validation of an objective electrophysiological metric for assessment of spectral ripple discrimination. The importance of spectral resolution for speech perception performance in quiet and in noisy listening situations has been highlighted in Chapter 4. However, speech perception performance depends on both spectral and temporal processing abilities (Shannon et al., 1995; Fu, 2002; Zeng, 2004; Zeng et al., 2005; Winn et al., 2016). Particularly, temporal fine structure has been associated with voice recognition, segregation of competing talkers and speech intelligibility in noisy conditions (Lorenzi et al., 2006; Hopkins et al., 2008). As mentioned in Section 1.2 a number of new speech processing strategies have been proposed to better represent the temporal fine structure of sound through electric hearing.

Various objective metrics for CI temporal processing abilities have been investigated in recent literature. He et al. (2013) investigated CAEPS such as the N1-P2 and the ACC in response to temporal gaps of various lengths in a train of stimuli. The reported results demonstrated the potential of the method as an objective measure of gap detection abilities in CI users, but lacked a direct comparison with behavioural thresholds. The MMN has also been employed as an objective metric for gap detection abilities in a normal hearing population (Kujala et al., 2001). Additionally, experimental evidence of the electrically evoked auditory steady state response, also known as the amplitude modulation following response, has demonstrated its potential as an objective measure of amplitude modulation detection ability in CI users (Hofmann and Wouters, 2010, 2012; Luke et al., 2015). Similarly, Han and Dimitrijevic (2015) investigated the potential of the ACC as an objective metric for temporal processing when assessing amplitude

modulation detection and hemispheric lateralization. However, the above mentioned metrics fail to probe the ability to discriminate temporal fine structure conveyed by the CI processing strategies.

Schroeder-phase harmonic complexes have recently been proposed as a potential means to behaviourally measure temporal fine structure discrimination abilities in CI users (Drennan et al., 2008; Drennan and Rubinstein, 2008; Drennan et al., 2010; Won et al., 2010; Golub et al., 2012; Jung et al., 2012; Won et al., 2012; Imennov et al., 2013). Schroeder-phase harmonic complexes (Schroeder, 1970) are sound pairs that have equal frequency spectra, minimal amplitude modulations, and different temporal fine structures.

Drennan et al. (2008) investigated how the Schroeder-phase discrimination scores are correlated with consonant-nucleus-consonant word scores, speech perception in noise, and spectral ripple discrimination scores in 24 users. It was found that Schroeder-phase discrimination scores at several fundamental frequencies were significantly correlated to consonant-nucleus-consonant word scores and speech perception scores under noise listening conditions.

Won et al. (2010a) analysed the correlation between Schroeder-phase discrimination and music perception. Their findings suggest that Schroeder-phase discrimination correlate to timbre recognition ($r=0.37$, $p=0.03$). Furthermore, Schroeder-phase discrimination has been used in paediatric populations (Jung et al. 2012) and as a means to evaluate temporal fine structure representation of different speech processing strategies (Drennan et al. 2010; Imennov et al. 2013).

This study explored the feasibility to assess temporal fine structure processing of CI users employing Schroeder-phase harmonic complexes and a MMW paradigm, like the one introduced in Chapter 3. An unattended objective assessment of temporal processing based on CAEPs may be relevant in a clinical environment, specifically for paediatric user groups. Additionally, it may provide new insights into temporal processing that may benefit the development of new CI processing strategies. This study was conducted as part of the M.Sc. qualification of Ms. Anne M. Leijsen. The study design and data analysis pipeline were defined by the author whilst the data collection and analysis was carried out by Ms. Anne M. Leijsen.

7.1 Materials and Methods

7.1.1 Subjects

Six CI listeners (4 male, 2 female) volunteered for this study at Trinity Centre for Bioengineering, Trinity College Dublin. Exclusion criteria applied to subjects under 18 years of age, subjects with cognitive or learning disabilities, and implant switch-on date shorter than 6 months prior to the study. There were no subjects withdrawn from this study. Subjects were aged between 27 and 74 years (mean 55). All subjects were unilateral implant recipients from a single manufacturer (i.e. Cochlear Ltd.) and at least 2.5 years of listening experience with their device. Subject demographics are summarised in Table 7.1.

Experimental procedures were approved by the Ethics (Medical Research) Committee at Beaumont Hospital, Beaumont, Dublin, and the Ethical Review Board at Trinity College Dublin. Written informed consent was obtained from all subjects.

7.1.2 Stimulus Generation and Presentation

Schroeder-phase harmonic complexes were generated in MATLAB by a summation of equal-amplitude sinusoidal harmonics with predetermined fundamental frequencies of 50, 100, 200 and 400 Hz, in which the harmonic phases were determined by:

$$\boldsymbol{\theta_{n=\pm\pi\cdot n(n+1)/N}}$$

Equation 7.1

where θ_n is the phase of the *n*-th harmonic, *n* is the *n*-th harmonic, *N* is the total number of harmonics in the complex and with the positive or negative sign indicating the construction of Schroeder-phase stimuli, respectively. Figure 7.1 shows an example of the Schroeder-phase harmonic complex for a fundamental frequency of 50 Hz. It can be observed that the positive and negative Schroeder-phase harmonic stimuli have opposing fine structure representation while maintaining the same frequency content. Higher fundamental frequencies result in a higher temporal complexity of the stimulus. All stimuli had a sample frequency of 44.1 kHz and duration of 500 ms. A 50 ms cosine squared ramp was applied to avoid clicks at the onset and offset of the stimulus. With the

purpose of restraining the frequency content to five kHz in all cases, the number of harmonics at each individual fundamental frequency (f0) was defined as 5000 / f0.

Stimuli were delivered electrically through the auxiliary input of the CI's speech processor at the MCL defined for each subject on a scale from 0 (silence) to 10 (too loud), with 6 being the MCL.

Subject ID	Sex	Age (yrs.)	Ear of implant	CI experience (yrs.)	Implant type
SCI03	**M**	**66**	**Right**	**13**	**Nucleus 5**
SCI05	**M**	**74**	**Left**	**10**	**Nucleus 5**
SCI06	**M**	**70**	**Right**	**2.5**	**Nucleus 5**
SCI07	**F**	**39**	**Left**	**7**	**Nucleus Freedom**
SCI08	**F**	**51**	**Left**	**7**	**Nucleus Freedom**
SCI09	**M**	**27**	**Left**	**11**	**Nucleus 5**

Table 7.1 Subject Demogrpahics.

7.1.3 Psychoacoustic Measure

Psychoacoustic (PA) Schroeder-phase discrimination abilities were obtained by a four-interval two-alternative forced choice test similar to the one described by Drennan et al. (2008). For each trial, four Schroeder-phase stimuli of the same fundamental frequency (e.g. 50 Hz, 100 Hz, 200 Hz or 400 Hz) were presented interleaved with 100ms of silence. A positive Schroeder-phase stimulus was presented randomly in either the second or the third interval, the rest of the intervals consisted of a negative Schroeder-phase stimulus. The subjects were asked to choose either the second or the third stimulus according to what they identified as different. Following each trial, visual feedback of the correct answer was provided. Each fundamental frequency was randomly presented 24 times, resulting in test blocks of 96 trials. The percentage correct was calculated for each block and each fundamental frequency. Each subject completed a total of four test blocks and the final PA discrimination score was the average of the last 3 blocks.

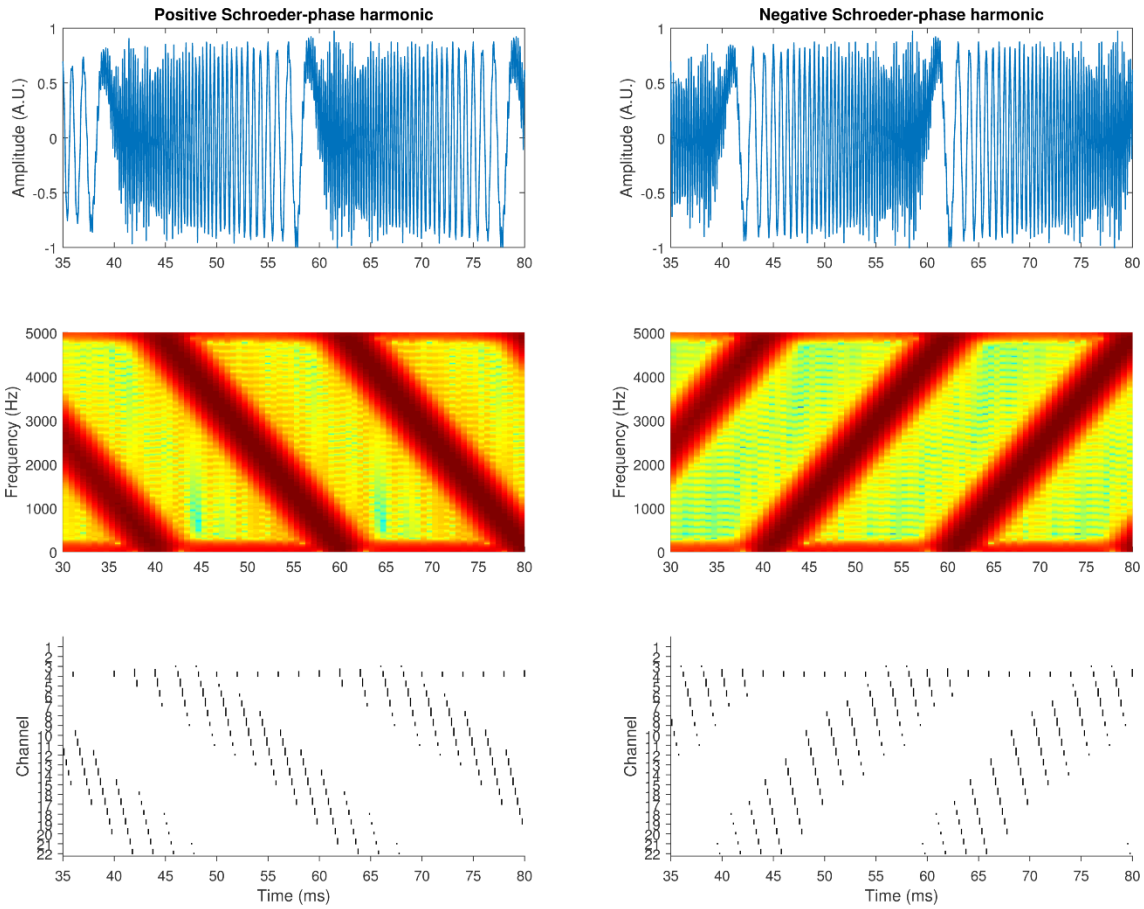

Figure 7.1 Representation of the Schroeder-phase harmonic complex.
Time plots (top), spectrograms (mid) and electrodograms (bottom) of a Schroeder-phase harmonic complex with a fundamental frequency of 50 Hz. Positive Schroeder-phase harmonic (left column) and negative Schroeder-phase harmonic complexes (right column) generate opposite fine structures while preserving the same overall frequency content. Electrodograms were simulated through the NMT toolbox and an ACE processing strategy.

7.1.4 Cortical Auditory Evoked Potential Recordings

CAEPs were obtained utilising the customised single-channel set-up developed in Chapter 3. Electrodes were placed at the vertex (Cz) and the mastoid, contralateral with respect to the tested ear. The system ground was located at the collar bone. Figure 4.2shows a graphical layout of the recording set-up. Impedances were ensured to be lower than 5 kΩ.

As discussed in Chapter 3, the CI's electrical artefact is closely related to the envelope of the sound being processed. It was mentioned in Section 3.3that the developed artefact attenuation methodology was bound to stimuli with a flat envelope such as pure tone stimuli or spectrally rippled noise stimuli utilised in Chapter 4, Chapter 5 and Chapter 6. The recorded electrical artefact from the Schroeder-phase harmonic complex stimuli was observed to be relatively flat, as shown in Figure 7.2 A, and thus, the

implementation of the CI artefact attenuation method previously developed was possible, see Figure 7.2 B and C.

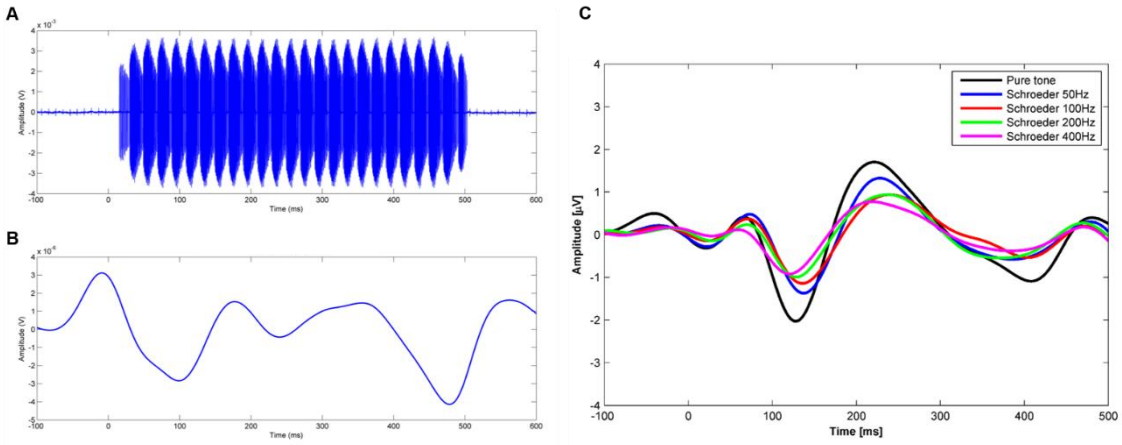

Figure 7.2 CI artefact representation of Schroeder-phase stimuli via the single-channel EEG acquisition set-up.
A) Representation of the CI electrical artefact associated with Schroeder-phase stimuli, captured with a high resolution single-channel EEG set-up. B) Low-pass filtering (10 Hz) of the high frequency artefact reveals the neural response together with onset and offset artefacts. D) Recovered neural responses to pure tone and Schroeder-phase stimuli after implementation of the CI artefact attenuation method proposed in Chapter 3.

Positive and negative Schroeder-phase stimuli of the same fundamental frequency were presented in an unattended oddball paradigm where the standard stimulus was presented with a probability of 90% whilst the deviant stimulus was presented 10% of the times. The ISI was kept constant at one second. Subjects were instructed to attend to a captioned silent film during the recording and asked to keep body movements to a minimum. Four 15 minute recordings were conducted, each at a different fundamental frequency for the Schroeder-phase stimuli (i.e. 50 Hz, 100 Hz, 200 Hz and 400 Hz). The order in which the different fundamental frequencies were presented was randomised to avoid undesired data trends.

7.1.5 Data Analysis

Raw EEG data were epoched from 800ms pre-stimulus to 800ms post-stimulus onset and baseline corrected with a window of 250 ms pre-stimulus. The CI artefact was attenuated following the methods from Chapter 3. EEG epochs were filtered with a 2nd order Butterworth band-pass (2 Hz -10 Hz) filter and shortened to 100 ms pre-stimulus onset to 500 ms post-stimulus onset for analysis.

Difference waveforms were calculated by subtracting the average response to the standard from the average response to the deviant stimuli. To define significant peaks and

troughs in the difference waveform, a noise floor was calculated using a bootstrap method, as previously described in Section 4.1.4. The area above and below the noise floor level was considered a significant MMW area (measured in µV*ms).

Single subject and group mean MMW areas and psychoacoustic (PA) scores were analysed for correlation employing a Spearman's rank-order correlation test.

7.2 Results

Group average of the behavioural results derived from the PA paradigm indicate that Schroeder-phase discrimination abilities were of 64 % ± 16.8 %, 67% ± 18.1 %, 56 % ± 11.9 % and 51% ± 9.1% (mean ± SD) for the 50 Hz, 100 Hz, 200 Hz and 400 Hz Schroeder-phase stimuli, respectively. Figure 7.3 shows the individual performance of each CI user, as well as the intra-subject variability throughout the last 3 runs of the psychoacoustic task. Although temporal complexity of the stimuli was expected to increase with increasing fundamental frequencies of the Schroeder-phase harmonic complexes, a non-monotonic relationship was found between the individual PA scores and the fundamental frequencies. However, a repeated measures ANOVA with assumed sphericity (Mauchly's Test of Sphericity, $\chi^2(5) = 5.578$, $p = 0.364$) revealed no statistically significant difference between the average scores.

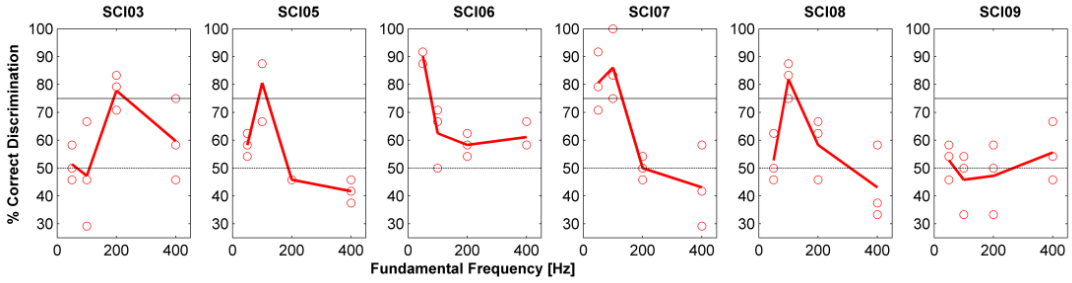

Figure 7.3 Individual psychoacoustic scores across four fundamental frequencies.
Mean scores are denoted by the red line. Individual scores from the second, third and fourth psychoacoustic runs are denoted by open circles. Horizontal lines mark the chance and 75 % level respectively.

MMW areas of the group mean CAEP responses were calculated to be 9.8 µV*ms, 0 µV*ms, 0.006 µV*ms and 0 µV*ms for the 50 Hz, 100 Hz, 200 Hz and 400 Hz Schroeder-phase stimuli, respectively (see Figure 7.4). No significant correlation was revealed between the average MMW areas and the average PA scores ($r^2 = 0.258$, $n = 4$, $p = 0.742$).

7.3 Discussion

7.3.1 CI Artefact Attenuation for Temporally Complex Stimuli

As depicted in Figure 7.2, Schroeder-phase harmonic complexes were shown to have a suitable construction for application in single-channel CI EEG recordings. The temporal modulation embedded in the stimuli generates an electrical artefact that can be treated as a flat envelope when recorded at a high sampling frequency (i.e. 125 kHz). This allows for the attenuation methodology proposed in Chapter 3 to successfully attenuate the presence of artefact contamination and recover the clean neural response of interest. The CI's electrical artefact is closely related to the envelope of the sound being processed. However, more research is required investigating the applicability of the system in slower temporal modulations where the stimulus artefact can no longer be estimated as a flat envelope.

7.3.2 Psychoacoustic Schroeder-Phase Discrimination

The psychoacoustic Schroeder-phase discrimination test employed in this study aimed to replicate the work presented by Drennan et al. (2008). In contrast to their results of Schroeder-phase discrimination at 50 Hz, 100 Hz, 200 Hz and 400 Hz (84%, 80%, 67% and 58% respectively), the scores reported in this study for the same tested frequencies (64%, 67%, 56% and 51% respectively) are notably lower. Several factors may account for these contrasting results.

Firstly, one of the divergent aspects of this study when compared to the behavioural study conducted by Drennan et al. (2008) is the stimulus presentation method. Here, direct sound delivery through the CI's auxiliary input was chosen over free-field presentation. Bypassing the microphone of the device decreases the amount of environmental noise when sound treated rooms are not available, however, if the voltage presented at the direct input exceeds the specification voltage for the knee-point of the automatic gain control stage of the CI processors, there is high risk of undesired compression being applied to the stimuli. Due to the proprietary nature of the information, the specifications of these knee-point voltages were not known at the time of this study and thus, there is no guarantee that the stimuli delivered to the subjects were exactly as intended.

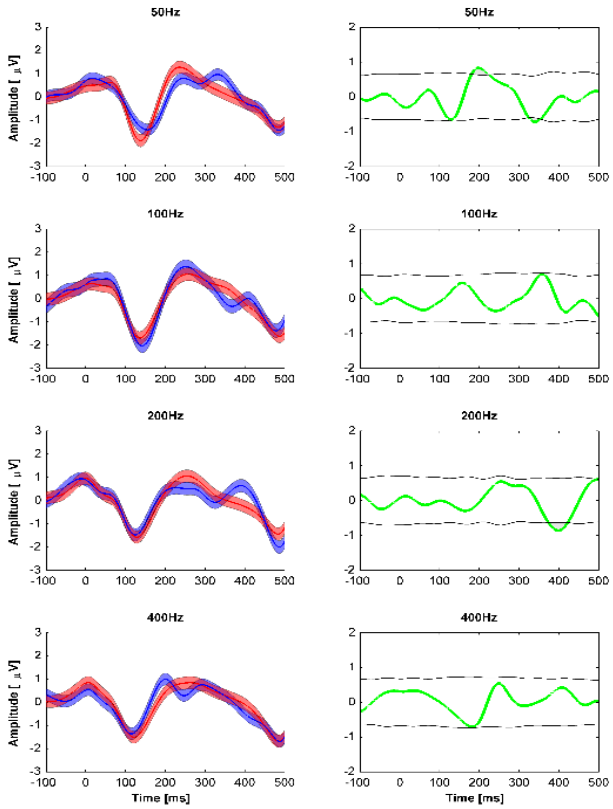

Figure 7.4 MMW group means for all four Schroeder-phase fundamental frequencies. *Group mean responses and their standard error to the standard (negative) (red, left column) and deviant (positive) (blue, left column) Schroeder-phase stimuli and their corresponding difference waveforms (green, right column). MMW areas were absent or minimal.*

Secondly, the subject demographics in terms of speech processors and stimulation pulse rates may impact the Schroeder-phase discrimination tasks. The higher stimulation pulse rate on different speech processing strategies (e.g. 1800 Hz for HiRes vs 1100 Hz for ACE) may have a critical impact on the temporal representation of positive and negative Schroeder-phase stimuli. In line with this, Drennan et al. (2010) showed that behavioural Schroeder-phase discrimination abilities were influenced by the choice of speech processing strategy when comparing two Advanced Bionics processing strategies at different stimulation pulse rates.

Lastly, it is possible that lack of agreement of the results presented in this study with respect to other literature may be influenced by the number of data points available for the comparison (e.g. six subjects vs 24 subjects in Drennan et al. (2008)).

7.3.3 MMW Elicited to Schroeder-Phase Harmonic Complex Pairs

Group average MMW areas were non-existent at any of the four different fundamental frequencies tested. These results are in line with the poor performance of the

subject populations in the psychoacoustic task. Figure 7.3 shows the trial by trial result of the psychoacoustic tests administered to each subject. The majority of the data points hoover around chance level, an indication that the discrimination performance on average is poor. This, in turn, would explain the extremely low MMW areas recorded (see Figure 7.4) and suggests that they are a consequence of the inability of the subjects to discriminate the Schroeder-phase stimuli at the tested fundamental frequencies. There is no indication in the literature of minimal detectable contrast with respect to MMW and Schroeder-phase harmonic complexes. Further investigations should be conducted to establish the discrimination thresholds at which a MMW may be elicited.

7.3.4 Conclusions

The main aim of this study was to investigate an objective assessment of temporal processing abilities in CI users employing Schroeder-phase harmonic complexes as probe stimuli. It was shown that the construction of Schroeder-phase harmonic complexes is appropriate for eliciting CAEPs in CI users with the single-channel approach described in Chapter 3. However, the poor discrimination performance of the small cohort of CI users that participated in this study may have prevented the acquisition of MMW. Therefore, the discussion that can be drawn from the electrophysiological paradigm applied in this study as an objective metric of temporal fine structure discrimination is limited. Further research is required in an expanded cohort of subjects with better behavioural Schroeder-phase discrimination abilities in order to probe the proposed objective metric in both good and bad performers. A more extensive population with a larger number of good performers could contribute to the analysis of Schroeder-phase discrimination sensitivity and MMW occurrence.

Key Points

- This chapter contributes to the answer for research questions 4, 5, and 6 listed in Section 2.4.
- Schroeder-phase harmonic complexes can be utilised to elicit artefact attenuated CAEPs in CI users via a single-channel EEG set-up like the one proposed in Chapter 3.
- The cohort of CI users that took part in this study showed poor behavioural Schroeder-phase discrimination abilities, which was reflected in the absence of MMWs at 50 Hz, 100 Hz 200 Hz and 400 Hz.
- These findings were presented at the 8th International Symposium on Objective Measures in Auditory Implants, Toronto 2014; and at the 7th International IEEE/EMBS Conference on Neural Engineering, Montpellier, 2015.
- The study presented in this Chapter is published in: "An Approach to Develop an Objective Measure of Temporal Processing in Cochlear Implant Users Based on Schroeder-Phase Harmonic Complexes". 7th International IEEE/EMBS Conference on Neural Engineering. 2015:699-702. 2015

Chapter 8 General Discussion

8.1 Thesis Summary

The studies presented in this thesis aimed to investigate the applicability of single-channel electroencephalography as an objective metric of speech perception performance in cochlear implant users. As it was outlined in Chapter 1, current metrics of CI performance rely on behavioural methods. While successful, these methods fall short in situations where the patient cannot provide a reliable feedback.

A number of objective metrics have been established and are currently being used to determine some of the fitting parameters of the CI device such as comfort and threshold levels of stimulation. These objective metrics are associated mainly with the sensory responses to stimulation and may not provide sufficient insights into the higher order processes involved in speech perception. The relevance of EEG recordings in CI users lies in the ability to probe higher order processes that may be relevant for speech perception. Chapter 2 provides numerous examples of how EEG has been used to probe auditory processes in CI users. However, there is a need to reduce the complexity of EEG based approaches in order for it to be a practical option for clinicians and audiologists in a clinical environment.

Section 2.4outlines a number of research questions that were formulated in order to address the objective of this thesis; and a series of studies were conducted to formulate a response to these research questions. The motivation to use sound processing features, such as spectral ripple discrimination and temporal fine structure discrimination, stem from psychoacoustic literature where these features have been associated with speech perception performance in CI populations. The electrophysiological investigation of these features was carried out throughout the studies reported in this thesis. All thesis objectives and aims were examined by the studies and are further outlined within this chapter.

8.2 Main Findings of the Thesis

The studies detailed in this thesis demonstrate that CAEP potentials can be acquired via single-channel EEG methods; and may be employed to objectively estimate spectral ripple discrimination abilities in CI users employing different EEG paradigms. Furthermore, it was found that CAEP potentials could be recorded longitudinally in the clinic during the first year of rehabilitation post implantation, with minimal interference of the CI induced artefact, via single-channel recordings. Additionally, a link was established between spectral ripple discrimination abilities and speech perception performance at different time points during the first year of CI rehabilitation. The importance of the research findings and the lessons learnt from this thesis will now be critically discussed in relation to the research questions previously posed in Chapter 2.

8.2.1 Dealing with the CI Induced Artefact in EEG recordings

A factor that appears to have limited the clinical application of cortical evoked potentials for CI subjects is the CI related artefact. Artefact removal approaches, such as ICA (Gilley et al., 2006; Viola et al., 2012) and beamforming (Wong and Gordon, 2009), are profitable in a research setting but, because of the necessity for multi-channel data, their practical application in a clinical setting is limited. The study presented in Chapter 3 provides a solution to this problem by showing how the CI related artefact can be attenuated using single-channel data, which are more easily obtained in a clinical setting.

Chapter 3 provides a comprehensive characterisation of the CI induced artefact. It was shown that the CI could be characterised in terms of a high-frequency component, directly related to the device's stimulation pulse rate, and a low frequency component that, albeit its origin is uncertain, seems to be associated with the stimulation pulse amplitude of the device. Single-channel recording recommendations were provided to minimize the influence of the artefact; and a three stage artefact attenuation methodology was developed to retrieve clean neural responses from contaminated data.

The artefact attenuation methodology takes advantage of the high sampling rate capabilities of the proposed set-up. This feature allows for the resolution of individual CI stimulation pulses which can later be filtered out. Hofmann and Wouters (2010, 2012) also proposed a high sampling rate methodology to deal with the CI induced artefact. However, they employ a linear interpolation between each stimulation pulse rather than a filtering approach. An interpolation approach to remove the high frequency artefact

would also work with the system developed in Chapter 3. However, a filtering approach is easier to implement, eliminating the need to select individual stimulation pulses.

The single-channel artefact attenuation approach described in Chapter 3 can successfully attenuate both the high-frequency artefact produced by a cochlear implant and the DC artefact. The main advantage of this approach is that only single-channel data are needed, simplifying the hardware and software requirements. The single-channel approach is aimed at facilitating research into CAEPs recorded from CI users with minimal interference from the device induced artefact.

8.2.2 Development of Objective Metrics of CI performance

A number of studies have indicated that cortical evoked potentials may be advantageous for predicting speech perception outcomes for CI subjects (Wable et al., 2000; Firszt et al., 2002b; Kelly et al., 2005; Zhang et al., 2011), more so than earlier evoked potential responses such as auditory nerve electric compound action potentials (ECAPs) or auditory brainstem responses (Miller et al., 2008). Behaviourally, it has been shown that more complex stimuli, such as spectrally rippled broadband noise, which probe the spectral discrimination of CI users, can be used to provide a reasonable estimate of speech perception (Henry and Turner, 2003; Henry et al., 2005; Won et al., 2007).

The study carried out in Chapter 4, developed and validated a method to objectively assess spectral ripple discrimination in a population of CI listeners using an oddball EEG paradigm (Naatanen et al., 2007). It was possible to acquire CAEP responses to standard and deviant stimuli in CI listeners and the analysis of the difference waveform showed a strong correlation with behavioural spectral ripple discrimination thresholds. In order to avoid subjectivity by manually selecting the difference waveform area, a statistical approach was developed involving the noise-floor of the recorded signals. This statistical approach can be comparable to the one proposed by Ponton et al. (1997b) known as the integrated mismatch negativity.

In Chapter 5, the ACC is presented as an alternative EEG paradigm that may facilitate the objective assessment of spectral ripple discrimination. However, that study showed that the MMW outperforms the ACC approach. The ACC has been shown to be a simple, time-efficient way to assess spectra ripple discrimination in normal hearing listeners (Won et al., 2011b). Nonetheless, when presenting the stimuli directly into the line-in port of the speech processors, the lack of available information regarding the

electrical voltage at the line-in input for different manufacturers makes it difficult to account for possible effects of the automatic gain control block within the front-end of the processors. This makes it difficult to assess if the representation of the ACC stimuli is as desired or if the response elicited is due to the pure effect of the spectral inversion rather than a temporal cue arising from the stimulation of different electrodes within the cochlea.

Speech perception performance depends on both spectral and temporal processing abilities (Shannon et al., 1995; Fu, 2002; Zeng, 2004; Zeng et al., 2005; Winn et al., 2016). Specifically, temporal fine structure has been associated with voice recognition, segregation of competing talkers and speech intelligibility in noisy conditions (Lorenzi et al., 2006; Hopkins et al., 2008). As mentioned in Section 1.2, a number of new speech processing strategies have been proposed to better represent the temporal fine structure of sound through electric hearing. Chapter 7investigates an objective assessment of temporal processing abilities in CI users, employing Schroeder-phase harmonic complexes as probe stimuli. It was shown that it is possible to acquire CAEPs elicited to complex stimuli that differed in temporal fine structure. However, the poor discrimination performance of the small cohort of CI users that participated in that study may have prevented the acquisition of MMW. Further research is required in an expanded cohort of subjects with better behavioural Schroeder-phase discrimination abilities in order to probe the proposed objective metric in both good and bad performers.

8.2.3 Longitudinal Evaluation of Objective Metrics of CI Performance

Clinical applications involving the acquisition of CAEPs may be limited by the confounding factor of maturation changes during the longitudinal development of cortical potentials. The development of cortical auditory potentials can extend into adolescence (Ponton et al., 2000) and even after prolonged acoustic deprivation, cortical auditory potentials can be re-developed over a period of time (Pantev et al., 2006). Changes in the morphology, latency and amplitude of potentials over time represents an impediment when performing a within subject longitudinal CAEP assessment. Trainor et al. (2003) identified changes in the EEG morphology of the MMW in young infants, with an age range of two, three, four and six months, suggesting that the difference at each age may be associated with layer-specific maturational processes in auditory cortex. However, the MMW metric developed in Chapter 4 may overcome these limitations due to the robust

nature of the oddball paradigm response and its applicability with different age populations as well as clinical conditions (Ponton et al., 2000; He et al., 2009; Naatanen et al., 2012). Despite maturational changes reflected by the EEG morphology of the MMW in young infants, the cognitive change detection mechanism associated with the MMW has been proposed to be developed between two and four months of age (He et al., 2009).

Chapter 6 evaluated the dynamics of single-channel electrophysiology longitudinally over the period of one year after device switch-on. The results revealed that there were no significant changes identified, in this CI population with respect to N1-P2 latencies and amplitudes across time. Two major factors may account for this contrasting result. The first being that some of the evidence of CI cortical plasticity and re-organisation are based on high density EEG (Gilley et al., 2008; Sharma et al., 2016) or MEG (Pantev et al., 2006) recordings, allowing the possibility to evaluate inter-hemispheric differences and dipole localisation. This is not possible with the single-channel approach favoured in this thesis.

The second major factor that could explain the results from that study lies in the demographics of the CI cohort. Discussions regarding cortical plasticity in CI users focus mainly on paediatric populations (Bauer et al., 2006; Gilley et al., 2008; Sharma et al., 2009; Sharma et al., 2016) and the P1 potential, which is the predecessor of the N1 potential in normal developing children (Ponton et al., 1996). This suggests that there is an ongoing maturational process expected in these studies. Changes in morphology of CAEPs in adults may be more affected by the type of hearing impairment, duration of deafness and the use of hearing devices pre-implantation.

The correlation found between neural spectral ripple discrimination and behavioural spectral ripple discrimination, as well as the trending correlation with speech perception performance in quiet and in the ten-talker babble noise one year after device switch-on, suggests that neural estimates of spectral ripple discrimination may require longer maturation time when assessing CI performance. Additionally, the significant correlation found between MMW area at 0.5 RPO and AzBio scores, highlights the possibility to optimise electrophysiological data acquisition by focusing in a particular spectral ripple density rather than four as was the case in that study.

8.3 Limitations of the Research

The low number of participants typically associated with single site studies in CI populations (i.e. Chapter 6 and Chapter 7), represents a limitation when drawing meaningful conclusions from the performed studies. This limitation is typical of prospective studies involving CI populations from a single clinic, contrasting with retrospective studies where sufficient number patient records are available for analysis (Raman et al., 2011). The methods employed throughout the studies in this thesis have the advantage of being easy to replicate in different locations (i.e. Chapter 3, Chapter 4 and Chapter 5). The findings presented un this thesis could potentially benefit from the involvement of multiple clinics sharing a common interest in research oriented towards objective metrics of CI performance.

All the studies carried out as part of this thesis were conducted using the direct input as means to deliver sounds to the research subjects. While this stimulus presentation mode can be beneficial when cancelling out undesired external noise, each CI manufacturer has proprietary circuitry that makes it difficult to account for possible effects of the automatic gain control blocks within the front-end of the speech processors. More controllable stimulus presentation methods should be favoured in order to avoid undesired confounds derived from the unexpected stimulus alterations. Employing dedicated research tools for direct stimulation of the electrode array (e.g. the NIC from Cochlear Ltd. or the BEDSC from Advance Bionics) or free-field sound presentation could be potential solutions to this limitation.

The rigorous statistical approach taken in this thesis may have resulted in metrics that are less than perfectly sensitive to real effects. In Chapter 5, the dismissal of RPO levels due to the noise-correlation cut-off may have been too rigorous on the ACC metric, resulting in less successfully estimated neural SRD thresholds for comparison with behavioural thresholds. In Chapter 6, the bootstrapping method to employed to detect significant MMW areas may have been to strict and over restricted emerging responses within the first year after device activation. This in turn could have led to failed estimations and large threshold variabilities as observed in Figure 6.10.

Another limitation of this thesis is the amount of data available for analysis. Inherently, reducing the dimensionality of EEG from high density recordings (e.g. 32+ channels) to a single-channel acquisition, which is an advantage of this approach in terms of set-up practicality, reduces the versatility of the data. Despite the fact that high density

recordings may focus on a single sensor location for the final analysis, the ability to explore different locations to ensure maximum signal strength can greatly benefit the analysis output. Independent of the quality of the recording, if the location of the of the single-channel electrodes is not in the optimal place, the resulting data may not suitable for analysis. The addition of one or two extra recording channels could provide more flexibility to the recording set-up while maintaining simplicity and high resolution capabilities.

8.4 Clinical Impact of the Research

Providing the clinicians and audiologists with clinically viable objective means for assessing CI performance can be of great benefit for optimising rehabilitation pathways in patients where reliable feedback is not present. Current efforts to enhance spectral resolution via different electrode stimulation modalities, i.e. partial bipolar stimulation (pBP), tri-polar stimulation (TP) and partial tri-polar stimulation (pTP), benefit from psychoacoustic evaluation of frequency resolution (Landsberger and Srinivasan, 2009; Zhu et al., 2012; Wu and Luo, 2013). Objective assessment of spectral resolution via electrophysiology could be beneficial when evaluating different electrode stimulation modalities in CI populations where standard psychoacoustics cannot be performed such as young infants.

Recent approaches to record CAEPs through intra-cochlear electrodes have been successful for recording N1-P2 complexes through the implementation of back-telemetry (Beynon et al., 2008; Beynon and Luijten, 2012; McLaughlin et al., 2012b). Preliminary work by our group has shown that it is possible to record ACC responses to different RPO stimuli in a bilateral CI user (Mc Laughlin et al., 2013). This finding could lead to the development of automatic spectral ripple discrimination estimation that could enhance CI fitting procedures aiming for enhanced speech perception performance.

Furthermore, behavioural results found in Chapter 6 suggest that clinical assessment of spectral ripple discrimination immediately at switch-on can be applied as a predictor of speech perception performance in quiet and in noise at six months, nine months and one year after implantation. This result is in line with recent evidence suggesting that the spectral ripple discrimination abilities are an acute measure of spectral discrimination abilities, which don't seem to change over time (Drennan et al., 2015). Spectral resolution seems to be determined by the implant and implant placement within

the cochlea (Drennan et al., 2010; Jones et al., 2011; Won et al., 2011a; Won et al., 2012). No learning effect takes place in contrast to speech perception which has a development period before stabilising around six months. Clinical spectral ripple discrimination testing from switch-on date may be advantageous for the optimisation of hearing rehabilitation by predicting speech perception outcomes six months in advance.

8.5 Conclusions

The research questions posed in Chapter 2 have been answered through the course of five studies. The body of research from this thesis provides a method to acquire CAEPs from single-channel EEG recordings, outlining recommendations and a methodology to deal with the CI induced artefact. It has also established the possibility to objectively assess CI spectral ripple discrimination abilities through the implementation of EEG paradigms. The tools developed within this thesis have been implemented in a clinical environment where it was shown that the acquisition of CAEPs in clinic is feasible.

Providing clinicians and audiologists with an additional set of tools for objectively assessing CI performance can be beneficial to patients where standard behavioural methods are not reliable.

References

Abbas PJ, Brown CJ (1988) Electrically evoked brainstem potentials in cochlear implant patients with multi-electrode stimulation. Hear Res 36:153-162.

Atienza M, Cantero JL (2001) Complex sound processing during human REM sleep by recovering information from long-term memory as revealed by the mismatch negativity (MMN). Brain Res 901:151-160.

Bauer PW, Sharma A, Martin K, Dorman M (2006) Central auditory development in children with bilateral cochlear implants. Archives of Otolaryngology-Head & Neck Surgery 132:1133-1136.

Bear MF, Connors BW, Paradiso MA (2007) Neuroscience: Exploring the brain: Lippincott Williams & Wilkins.

Berger H (1929) Über das Elektrenkephalogramm des Menschen. Archiv für Psychiatrie und Nervenkrankheiten 87:527-570.

Beynon AJ, Luijten B (2012) Intracorporeal cortical telemetry (ICT): capturing EEG with a CI. In: 7th International Symposium on Objective Measures in Cochlear and Brainstem Implants, p 24. Amsterdam.

Beynon AJ, Luijten B, Snik AF (2008) The cochlear implant as an EEG-system: a feasibility study to measure evoked potentials beyond the ecap. In: 10th International Conference on Cochlear Implants and Other Implantable Auditory Technologies. San Diego.

Botros A, Psarros C (2010) Neural response telemetry reconsidered: I. The relevance of ECAP threshold profiles and scaled profiles to cochlear implant fitting. Ear Hear 31:367-379.

Brown CJ, Hughes ML, Luk B, Abbas PJ, Wolaver A, Gervais J (2000) The relationship between EAP and EABR thresholds and levels used to program the nucleus 24 speech processor: Data from adults. Ear and Hearing 21:151-163.

Brown CJ, Etler C, He S, O'Brien S, Erenberg S, Kim JR, Dhuldhoya AN, Abbas PJ (2008) The electrically evoked auditory change complex: preliminary results from nucleus cochlear implant users. Ear Hear 29:704-717.

Burkard RF, Don M, Eggermont JJ (2006) Auditory Evoked Potentials: Basic Principles and Clinical Application: Lippincott Williams & Wilkins.

Byrne D, Dillon H, Tran K, Arlinger S, Wilbraham K, Cox R, Hagerman B, Hetu R, Kei J, Lui C (1994) An international comparison of long-term average speech spectra. The Journal of the Acoustical Society of America 96:2108.

Cafarelli Dees D et al. (2005) Normative findings of electrically evoked compound action potential measurements using the neural response telemetry of the Nucleus CI24M cochlear implant system. Audiol Neurootol 10:105-116.

Campbell J, Sharma A (2016) Visual Cross-Modal Re-Organization in Children with Cochlear Implants. PLoS One 11:e0147793.
Cheour-Luhtanen M, Alho K, Kujala T, Sainio K, Reinikainen K, Renlund M, Aaltonen O, Eerola O, Näätänen R (1995) Mismatch negativity indicates vowel discrimination in newborns. Hearing Research 82:53-58.
Cheour M, Alho K, Ceponiene R, Reinikainen K, Sainio K, Pohjavuori M, Aaltonen O, Naatanen R (1998a) Maturation of mismatch negativity in infants. International journal of psychophysiology : official journal of the International Organization of Psychophysiology 29:217-226.
Cheour M, Alho K, Ceponiene R, Reinikainen K, Sainio K, Pohjavuori M, Aaltonen O, Naatanen R (1998b) Maturation of mismatch negativity in infants. International Journal of Psychophysiology 29:217-226.
Choudhury N, Benasich AA (2011) Maturation of auditory evoked potentials from 6 to 48 months: prediction to 3 and 4 year language and cognitive abilities. Clinical neurophysiology : official journal of the International Federation of Clinical Neurophysiology 122:320-338.
Clark G (2006) Cochlear Implants: Fundamentals and Applications: Springer New York.
Conti G, Gallus R, Fetoni AR, Martina BM, Muzzi E, Orzan E, Bastanza G (2016) Early definition of type, degree and audiogram shape in childhood hearing impairment. Acta Otorhinolaryngologica Italica 36:21-28.
Cooper H, Craddock L (2005) Cochlear Implants: A Practical Guide.
Cosetti M, Roland JT (2010) Cochlear Implantation in the Very Young Child: Issues Unique to the Under-1 Population. Trends in Amplification 14:46-57.
Davis A, McMahon CM, Pichora-Fuller KM, Russ S, Lin F, Olusanya BO, Chadha S, Tremblay KL (2016) Aging and Hearing Health: The Life-course Approach. Gerontologist 56 Suppl 2:S256-267.
Davis PA (1939) Effects of acoustic stimuli on the waking human. Journal of Neurophysiology 2:494-499.
Debener S, Hine J, Bleeck S, Eyles J (2008) Source localization of auditory evoked potentials after cochlear implantation. Psychophysiology 45:20-24.
Dehaene-Lambertz G (1997) Electrophysiological correlates of categorical phoneme perception in adults. Neuroreport 8:919-924.
Dimitrijevic A, John MS, Picton TW (2004) Auditory steady-state responses and word recognition scores in normal-hearing and hearing-impaired adults. Ear Hear 25:68-84.
Donchin E, Ritter W, McCallum WC (1978) Cognitive psychophysiology: The endogenous components of the ERP. Event-related brain potentials in man:349-411.
Drennan WR, Rubinstein JT (2008) Music perception in cochlear implant users and its relationship with psychophysical capabilities. Journal of Rehabilitation Research and Development 45:779-789.
Drennan WR, Longnion JK, Ruffin C, Rubinstein JT (2008) Discrimination of Schroeder-phase harmonic complexes by normal-hearing and cochlear-implant listeners. Jaro-Journal of the Association for Research in Otolaryngology 9:138-149.
Drennan WR, Anderson ES, Won JH, Rubinstein JT (2014) Validation of a Clinical Assessment of Spectral-Ripple Resolution for Cochlear Implant Users. Ear and Hearing 35:E92-E98.
Drennan WR, Won JH, Timme AO, Rubinstein JT (2015) Nonlinguistic Outcome Measures in Adult Cochlear Implant Users Over the First Year of Implantation. Ear and hearing.

Drennan WR, Won JH, Nie K, Jameyson E, Rubinstein JT (2010) Sensitivity of psychophysical measures to signal processor modifications in cochlear implant users. Hearing Research 262:1-8.
Elberling C, Don M (1984) Quality estimation of averaged auditory brainstem responses. Scandinavian audiology 13:187-197.
Fay RR (2013) The Mammalian Auditory Pathway: Neurophysiology: Springer New York.
Firszt JB, Chambers RD, Kraus, Reeder RM (2002a) Neurophysiology of cochlear implant users I: effects of stimulus current level and electrode site on the electrical ABR, MLR, and N1-P2 response. Ear Hear 23:502-515.
Firszt JB, Chambers, Rd, Kraus N (2002b) Neurophysiology of cochlear implant users II: comparison among speech perception, dynamic range, and physiological measures. Ear Hear 23:516-531.
Franck KH, Norton SJ (2001) Estimation of psychophysical levels using the electrically evoked compound action potential measured with the neural response telemetry capabilities of cochlear corporation's CI24M device. Ear and Hearing 22:289-299.
Friesen LM, Tremblay KL (2006) Acoustic change complexes recorded in adult cochlear implant listeners. Ear Hear 27:678-685.
Friesen LM, Picton TW (2010) A method for removing cochlear implant artifact. Hear Res 259:95-106.
Frizzo ACF (2015) Auditory evoked potential: a proposal for further evaluation in children with learning disabilities. Frontiers in Psychology 6:788.
Fu QJ (2002) Temporal processing and speech recognition in cochlear implant users. Neuroreport 13:1635-1639.
Gallego S, Frachet B, Micheyl C, Truy E, Collet L (1998) Cochlear implant performance and electrically-evoked auditory brain-stem response characteristics. Electroencephalography and clinical neurophysiology 108:521-525.
Garrido MI, Kilner JM, Stephan KE, Friston KJ (2009) The mismatch negativity: A review of underlying mechanisms. Clinical Neurophysiology 120:453-463.
Gelfand SA (2016) Hearing: An introduction to psychological and physiological acoustics: CRC Press.
Gilley PM, Sharma A, Dorman MF (2008) Cortical reorganization in children with cochlear implants. Brain Res 1239:56-65.
Gilley PM, Sharma A, Dorman M, Finley CC, Panch AS, Martin K (2006) Minimization of cochlear implant stimulus artifact in cortical auditory evoked potentials. Clinical neurophysiology : official journal of the International Federation of Clinical Neurophysiology 117:1772-1782.
Giraud AL, Truy E, Frackowiak R (2001a) Imaging plasticity in cochlear implant patients. Audiol Neurootol 6:381-393.
Giraud AL, Price CJ, Graham JM, Truy E, Frackowiak RS (2001b) Cross-modal plasticity underpins language recovery after cochlear implantation. Neuron 30:657-663.
Golub JS, Won JH, Drennan WR, Worman TD, Rubinstein JT (2012) Spectral and Temporal Measures in Hybrid Cochlear Implant Users: On the Mechanism of Electroacoustic Hearing Benefits. Otology & Neurotology 33:147-153.
Gordon KA, Wong DDE, Papsin BC (2013) Bilateral input protects the cortex from unilaterally-driven reorganization in children who are deaf. Brain 136:1609-1625.
Groenen PA, Beynon AJ, Snik AF, van den Broek P (2001) Speech-evoked cortical potentials and speech recognition in cochlear implant users. Scandinavian audiology 30:31-40.
Hall JW (2007) New Handbook of Auditory Evoked Responses: Pearson.

Han JH, Dimitrijevic A (2015) Acoustic change responses to amplitude modulation: a method to quantify cortical temporal processing and hemispheric asymmetry. Front Neurosci 9:38.
Hansen JT, Koeppen BM, Netter FH, Craig JA, Perkins J (2002) Atlas of Neuroanatomy and Neurophysiology: Selections from the Netter Collection of Medical Illustrations: Icon Custom Communication.
He C, Hotson L, Trainor LJ (2009) Maturation of cortical mismatch responses to occasional pitch change in early infancy: Effects of presentation rate and magnitude of change. Neuropsychologia 47:218-229.
He S, Grose JH, Buchman CA (2012) Auditory discrimination: the relationship between psychophysical and electrophysiological measures. Int J Audiol 51:771-782.
He S, Grose JH, Teagle HF, Woodard J, Park LR, Hatch DR, Buchman CA (2013) Gap detection measured with electrically evoked auditory event-related potentials and speech-perception abilities in children with auditory neuropathy spectrum disorder. Ear Hear 34:733-744.
Henry BA, Turner CW (2003) The resolution of complex spectral patterns by cochlear implant and normal-hearing listeners. J Acoust Soc Am 113:2861-2873.
Henry BA, Turner CW, Behrens A (2005) Spectral peak resolution and speech recognition in quiet: normal hearing, hearing impaired, and cochlear implant listeners. J Acoust Soc Am 118:1111-1121.
Hines CB (2004) Time-of-Day Effects on Human Performance. Catholic Education: A Journal of Inquiry and Practice 7:390-413.
Hofmann M, Wouters J (2010) Electrically evoked auditory steady state responses in cochlear implant users. Journal of the Association for Research in Otolaryngology : JARO 11:267-282.
Hofmann M, Wouters J (2012) Improved electrically evoked auditory steady-state response thresholds in humans. JARO - Journal of the Association for Research in Otolaryngology 13:573-589.
Hopkins K, Moore BCJ, Stone MA (2008) Effects of moderate cochlear hearing loss on the ability to benefit from temporal fine structure information in speech. The Journal of the Acoustical Society of America 123:1140-1153.
Hoppe U, Wohlberedt T, Danilkina G, Hessel H (2010) Acoustic change complex in cochlear implant subjects in comparison with psychoacoustic measures. Cochlear implants international 11 Suppl 1:426-430.
Horn D, Werner L, Rubinstein JT, Won JH (2013) Spectral Ripple Discrimination in Infants: Effect of Ripple Depth and Envelope Phase Randomization. In: Association for Research in Otolaryngology, 36th Annual Midwinter Meeting. Baltimore.
HSE (2011) HSE National Audiology Review. In: Health Service Executive.
Hughes ML (2010) Fundamentals of Clinical ECAP Measures in Cochlear Implants: Part 1: Use of the ECAP in Speech Processor Programming (2nd Ed.). In: Audiology Online.
Huinck W, Mylanus EA (2016) Education level mediates the outcome of cochlear implantation in the elderly. In: 14th International Conference in Cochlear Implants (Alliance ACI, ed). Toronto
Imennov NS, Won JH, Drennan WR, Jameyson E, Rubinstein JT (2013) Detection of acoustic temporal fine structure by cochlear implant listeners: Behavioral results and computational modeling. Hearing Research 298:60-72.

Jones GL, Drennan WR, Rubinstein JT (2011) Relationship between channel interaction and spectral-ripple discrimination in cochlear implant users. J Acoust Soc Am 129:2656.

Jung KH, Won JH, Drennan WR, Jameyson E, Miyasaki G, Norton SJ, Rubinstein JT (2012) Psychoacoustic Performance and Music and Speech Perception in Prelingually Deafened Children with Cochlear Implants. Audiology and Neuro-Otology 17:189-197.

Kelly AS, Purdy SC, Thorne PR (2005) Electrophysiological and speech perception measures of auditory processing in experienced adult cochlear implant users. Clinical Neurophysiology 116:1235-1246.

Kral A, Hartmann R, Tillein J, Heid S, Klinke R (2002) Delayed maturation and sensitive periods in the auditory cortex. Audiology and Neurotology 6:346-362.

Kraus N, McGee T (1990) Clinical applications of the middle latency response. J Am Acad Audiol 1:130-133.

Krueger B, Joseph G, Rost U, Strau-Schier A, Lenarz T, Buechner A (2008) Performance groups in adult cochlear implant users: speech perception results from 1984 until today. Otology & Neurotology 29:509-512.

Kujala T, Kallio J, Tervaniemi M, Naatanen R (2001) The mismatch negativity as an index of temporal processing in audition. Clinical Neurophysiology 112:1712-1719.

Landsberger DM, Srinivasan AG (2009) Virtual channel discrimination is improved by current focusing in cochlear implant recipients. Hearing Research 254:34-41.

Lee DS, Lee JS, Oh SH, Kim SK, Kim JW, Chung JK, Lee MC, Kim CS (2001) Cross-modal plasticity and cochlear implants. Nature 409:149-150.

Lenarz M, Sönmez H, Joseph G, Büchner A, Lenarz T (2012) Long-term performance of cochlear implants in postlingually deafened adults. Otolaryngology--Head and Neck Surgery 147:112-118.

Levitt H (1971) Transformed up-down methods in psychoacoustics. J Acoust Soc Am 49:Suppl 2:467+.

Liang M, Zhang X, Chen T, Zheng Y, Zhao F, Yang H, Zhong Z, Zhang Z, Chen S, Chen L (2014) Evaluation of auditory cortical development in the early stages of post cochlear implantation using mismatch negativity measurement. Otol Neurotol 35:e7-14.

Light GA, Williams LE, Minow F, Sprock J, Rissling A, Sharp R, Swerdlow NR, Braff DL (2010) Electroencephalography (EEG) and event-related potentials (ERPs) with human participants. Current protocols in neuroscience / editorial board, Jacqueline N Crawley [et al] Chapter 6:Unit 6 25 21-24.

Litvak LM, Spahr AJ, Saoji AA, Fridman GY (2007) Relationship between perception of spectral ripple and speech recognition in cochlear implant and vocoder listeners. Journal of the Acoustical Society of America 122:982-991.

Loizou PC (1999) Introduction to cochlear implants. Ieee Engineering in Medicine and Biology Magazine 18:32-42.

Lorenzi C, Gilbert G, Carn H, Garnier S, Moore BCJ (2006) Speech perception problems of the hearing impaired reflect inability to use temporal fine structure. Proceedings of the National Academy of Sciences 103:18866-18869.

Luck SJ (2014) An introduction to the event-related potential technique: MIT press.

Luke R, Van Deun L, Hofmann M, van Wieringen A, Wouters J (2015) Assessing temporal modulation sensitivity using electrically evoked auditory steady state responses. Hear Res 324:37-45.

Marco-Pallares J, Grau C, Ruffini G (2005) Combined ICA-LORETA analysis of mismatch negativity. NeuroImage 25:471-477.
Martin BA (2007) Can the acoustic change complex be recorded in an individual with a cochlear implant? Separating neural responses from cochlear implant artifact. Journal of the American Academy of Audiology 18:126-140.
Martin BA, Boothroyd A (2000) Cortical, auditory, evoked potentials in response to changes of spectrum and amplitude. J Acoust Soc Am 107:2155-2161.
Martin BA, Tremblay KL, Korczak P (2008) Speech evoked potentials: from the laboratory to the clinic. Ear Hear 29:285-313.
Martin BA, Boothroyd A, Ali D, Leach-Berth T (2010) Stimulus presentation strategies for eliciting the acoustic change complex: increasing efficiency. Ear Hear 31:356-366.
Martinez AS, Eisenberg LS, Boothroyd A (2013) The Acoustic Change Complex in Young Children with Hearing Loss: A Preliminary Study. Semin Hear 34:278-287.
Massa ST, Ruckenstein MJ (2014) Comparing the Performance Plateau in Adult Cochlear Implant Patients Using HINT and AzBio. Otology & Neurotology 35:598-604.
Mc Laughlin M, Lopez Valdes A, Reilly RB, Zeng FG (2013) Expanding Cochlear Implant Neural Response Measurement Capabilities to Cortical Potentials. In: Conference on Implantable Auditory Prostheses. Lake Tahoe, CA.
McGee T, Kraus N (1996) Auditory development reflected by middle latency response. Ear Hear 17:419-429.
McLaughlin M, Lu T, Dimitrijevic A, Zeng FG (2012a) Towards a Closed-Loop Cochlear Implant System: Application of Embedded Monitoring of Peripheral and Central Neural Activity. Neural Systems and Rehabilitation Engineering, IEEE Transactions on 20:443-454.
McLaughlin M, Lu T, Dimitrijevic A, Zeng FG (2012b) Towards a closed-loop cochlear implant system: Application of embedded monitoring of peripheral and central neural activity. IEEE Transactions on Neural Systems and Rehabilitation Engineering 20:443-454.
McLaughlin M, Lopez Valdes A, Reilly RB, Zeng FG (2013) Cochlear Implant Artifact Attenuation in Late Auditory Evoked Potentials: A Single Channel Approach. Hearing research In Press.
Miller CA, Brown CJ, Abbas PJ, Chi SL (2008) The clinical application of potentials evoked from the peripheral auditory system. Hearing Research 242:184-197.
Moeller MP, McCleary E, Putman C, Tyler-Krings A, Hoover B, Stelmachowicz P (2010) Longitudinal Development of Phonology and Morphology in Children with Late-Identified Mild-Moderate Sensorineural Hearing Loss. Ear and hearing 31:625-635.
Møller AR, Jannetta PJ (1981) Compound action potentials recorded intracranially from the auditory nerve in man. Experimental neurology 74:862-874.
Møller AR, Jannetta PJ (1983) Interpretation of brainstem auditory evoked potentials: results from intracranial recordings in humans. Scandinavian audiology 12:125-133.
Mosnier I, Bebear JP, Marx M, Fraysse B, Truy E, Lina-Granade G, Mondain M, Sterkers-Artieres F, Bordure P, Robier A, Godey B, Meyer B, Frachet B, Poncet-Wallet C, Bouccara D, Sterkers O (2015) Improvement of cognitive function after cochlear implantation in elderly patients. JAMA Otolaryngol Head Neck Surg 141:442-450.

Naatanen R (1991) Mismatch negativity outside strong attentional focus: a commentary on Woldorff et al. (1991). Psychophysiology 28:478-484.
Naatanen R, Pakarinen S, Rinne T, Takegata R (2004) The mismatch negativity (MMN): towards the optimal paradigm. Clinical neurophysiology : official journal of the International Federation of Clinical Neurophysiology 115:140-144.
Naatanen R, Paavilainen P, Rinne T, Alho K (2007) The mismatch negativity (MMN) in basic research of central auditory processing: a review. Clinical neurophysiology : official journal of the International Federation of Clinical Neurophysiology 118:2544-2590.
Naatanen R, Kujala T, Escera C, Baldeweg T, Kreegipuu K, Carlson S, Ponton C (2012) The mismatch negativity (MMN)--a unique window to disturbed central auditory processing in ageing and different clinical conditions. Clinical neurophysiology : official journal of the International Federation of Clinical Neurophysiology 123:424-458.
Näätänen R (1995) The mismatch negativity: A powerful tool for cognitive neuroscience. Ear & Hearing 16:6-18.
NICDC (2016) Cochlear Implants. In: NIH Publicatio No. 00-4798.
Niparko JK (2009) Cochlear implants: principles & practices: Lippincott Williams & Wilkins.
Pantev C, Dinnesen A, Ross B, Wollbrink A, Knief A (2006) Dynamics of auditory plasticity after cochlear implantation: a longitudinal study. Cereb Cortex 16:31-36.
Patel H, Feldman M (2011) Universal newborn hearing screening. Paediatrics & Child Health 16:301-305.
Picton T (2013) Hearing in time: evoked potential studies of temporal processing. Ear Hear 34:385-401.
Picton T, Woods DL, Baribeau-Braun J, Healey TM (1976) Evoked potential audiometry. J Otolaryngol 6:90-119.
Picton TW, Woods DL, Proulx GB (1978) Human auditory sustained potentials. I. The nature of the response. Electroencephalography and clinical neurophysiology 45:186-197.
Picton TW, Alain C, Otten L, Ritter W, Achim A (2000) Mismatch negativity: different water in the same river. Audiol Neurootol 5:111-139.
Poeppel D, Overath T, Popper A, Fay RR (2012) The Human Auditory Cortex: Springer New York.
Ponton CW, Don M, Eggermont JJ, Kwong B (1997a) Integrated mismatch negativity (MMN< sub> i</sub>): a noise-free representation of evoked responses allowing single-point distribution-free statistical tests. Electroencephalography and Clinical Neurophysiology/Evoked Potentials Section 104:143-150.
Ponton CW, Don M, Eggermont JJ, Kwong B (1997b) Integrated mismatch negativity (MMNi): a noise-free representation of evoked responses allowing single-point distribution-free statistical tests (vol 104, pg 143, 1997). Evoked Potentials-Electroencephalography and Clinical Neurophysiology 104:381-382.
Ponton CW, Don M, Eggermont JJ, Waring MD, Masuda A (1996) Maturation of human cortical auditory function: differences between normal-hearing children and children with cochlear implants. Ear Hear 17:430-437.
Ponton CW, Eggermont JJ, Don M, Waring MD, Kwong B, Cunningham J, Trautwein P (2000) Maturation of the mismatch negativity: Effects of profound deafness and cochlear implant use. Audiology and Neuro-Otology 5:167-185.

Purves DA, G.J; Fitzpatrick, D; Hall, W.C.; LaMantia, A.S.; White, L.E. (2012) NEUROSIENCE. Sunderland, MA: Sinauer Associates, Inc.

Raman G, Lee J, Chung M, Gaylor JM, Sen S, Rao M, Lau J (2011) Effectiveness of Cochlear Implants in Adults with Sensorineural Hearing Loss: Technology Report. Agency for Healthcare Research and Quality. US Department of Health & Human Services

In. Rockville, Maryland: Agency for Healthcare Research and Quality.

Said Abdelsalam NM, Afifi PO (2015) Electric auditory brainstem response (E-ABR) in cochlear implant children: Effect of age at implantation and duration of implant use. Egyptian Journal of Ear, Nose, Throat and Allied Sciences 16:145-150.

Sandmann P, Plotz K, Hauthal N, de Vos M, Schonfeld R, Debener S (2015) Rapid bilateral improvement in auditory cortex activity in postlingually deafened adults following cochlear implantation. Clinical neurophysiology : official journal of the International Federation of Clinical Neurophysiology 126:594-607.

Sandmann P, Eichele T, Buechler M, Debener S, Jäncke L, Dillier N, Hugdahl K, Meyer M (2009) Evaluation of evoked potentials to dyadic tones after cochlear implantation. Brain 132:1967-1979.

Sandmann P, Kegel A, Eichele T, Dillier N, Lai W, Bendixen A, Debener S, Jancke L, Meyer M (2010) Neurophysiological evidence of impaired musical sound perception in cochlear-implant users. Clinical neurophysiology : official journal of the International Federation of Clinical Neurophysiology 121:2070-2082.

Scheperle RA, Abbas PJ (2015a) Peripheral and Central Contributions to Cortical Responses in Cochlear Implant Users. Ear Hear 36:430-440.

Scheperle RA, Abbas PJ (2015b) Relationships Among Peripheral and Central Electrophysiological Measures of Spatial and Spectral Selectivity and Speech Perception in Cochlear Implant Users. Ear Hear 36:441-453.

Schnupp J, Nelken I, King A (2011) Auditory Neuroscience: Making Sense of Sound: MIT Press.

Schroeder M (1970) Synthesis of low-peak-factor signals and binary sequences with low autocorrelation (Corresp.). IEEE Transactions on Information Theory 16:85-89.

Shahin AJ (2011) Neurophysiological influence of musical training on speech perception. Front Psychol 2:126.

Shallop JK, Beiter AL, Goin DW, Mischke RE (1990) Electrically Evoked Auditory Brain-Stem Responses (Eabr) and Middle Latency Responses (Emlr) Obtained from Patients with the Nucleus Multichannel Cochlear Implant. Ear Hear 11:5-15.

Shannon RV, Zeng F-G, Kamath V, Ekelid M (1995) Speech Recognition with PrimarilyTemporal Cues. Science 270:303-304.

Sharma A, Dorman MF, Spahr AJ (2002) A sensitive period for the development of the central auditory system in children with cochlear implants: implications for age of implantation. Ear Hear 23:532-539.

Sharma A, Nash AA, Dorman M (2009) Cortical development, plasticity and re-organization in children with cochlear implants. J Commun Disord 42:272-279.

Sharma A, Glick H, Campbell J, Torres J, Dorman M, Zeitler DM (2016) Cortical Plasticity and Reorganization in Pediatric Single-sided Deafness Pre- and Postcochlear Implantation: A Case Study. Otol Neurotol 37:e26-34.

Shepherd RK, Javel E (1997) Electrical stimulation of the auditory nerve. I. Correlation of physiological responses with cochlear status. Hear Res 108:112-144.

Sinkiewicz D, Friesen L, Ghoraani B (2014) Analysis of cochlear implant artifact removal techniques using the continuous wavelet transform. In: 2014 36th Annual

International Conference of the IEEE Engineering in Medicine and Biology Society, pp 5482-5485.
Small SA, Werker JF (2012) Does the ACC have potential as an index of early speech discrimination ability? A preliminary study in 4-month-old infants with normal hearing. Ear Hear 33:e59-69.
Spahr AJ, Dorman MF, Litvak LM, Van Wie S, Gifford RH, Loizou PC, Loiselle LM, Oakes T, Cook S (2012) Development and validation of the AzBio sentence lists. Ear Hear 33:112-117.
Stollman MHP, Snik AFM, Hombergen G, Nieuwenhuys R, tenKoppel P (1996) Detection of the binaural interaction component in the auditory brainstem response. British Journal of Audiology 30:227-232.
Supin A, Popov VV, Milekhina ON, Tarakanov MB (1997) Frequency-temporal resolution of hearing measured by rippled noise. Hear Res 108:17-27.
Sussman E, Steinschneider M, Gumenyuk V, Grushko J, Lawson K (2008) The maturation of human evoked brain potentials to sounds presented at different stimulus rates. Hear Res 236:61-79.
Sutton S, Tueting P, Zubin J, John ER (1967) Information delivery and the sensory evoked potential. Science 155:1436-1439.
Swanepoel D, Hugo R (2004) Estimations of auditory sensitivity for young cochlear implant candidates using the ASSR: preliminary results. Int J Audiol 43:377-382.
Torppa R, Salo E, Makkonen T, Loimo H, Pykalainen J, Lipsanen J, Faulkner A, Huotilainen M (2012) Cortical processing of musical sounds in children with Cochlear Implants. Clinical neurophysiology : official journal of the International Federation of Clinical Neurophysiology 123:1966-1979.
Trainor L, McFadden M, Hodgson L, Darragh L, Barlow J, Matsos L, Sonnadara R (2003) Changes in auditory cortex and the development of mismatch negativity between 2 and 6 months of age. International Journal of Psychophysiology 51:5-15.
Tseng C-C, Hu L-Y, Liu M-E, Yang AC, Shen C-C, Tsai S-J (2016) Risk of depressive disorders following sudden sensorineural hearing loss: A nationwide population-based retrospective cohort study. Journal of Affective Disorders 197:94-99.
Twisk J, de Vente W (2002) Attrition in longitudinal studies: how to deal with missing data. Journal of clinical epidemiology 55:329-337.
Viola FC, Thorne JD, Bleeck S, Eyles J, Debener S (2011) Uncovering auditory evoked potentials from cochlear implant users with independent component analysis. Psychophysiology 48:1470-1480.
Viola FC, De Vos M, Hine J, Sandmann P, Bleeck S, Eyles J, Debener S (2012) Semi-automatic attenuation of cochlear implant artifacts for the evaluation of late auditory evoked potentials. Hear Res 284:6-15.
Visram AS, Innes-Brown H, El-Deredy W, McKay CM (2015) Cortical auditory evoked potentials as an objective measure of behavioral thresholds in cochlear implant users. Hear Res 327:35-42.
Wable J, Van Den Abbeele T, Gallégo S, Frachet B (2000) Mismatch negativity: A tool for the assessment of stimuli discrimination in cochlear implant subjects. Clinical Neurophysiology 111:743-751.
Waltzman SB, Roland JT (2005) Cochlear implantation in children younger than 12 months. Pediatrics 116:E487-E493.
WHO (2015) Deafness and Hearing Impairment. In: Fact Sheet No.300: World Trade Organization.

Winn MB, Won JH, Moon IJ (2016) Assessment of Spectral and Temporal Resolution in Cochlear Implant Users Using Psychoacoustic Discrimination and Speech Cue Categorization. Ear Hear.

Won JH, Drennan WR, Rubinstein JT (2007) Spectral-ripple resolution correlates with speech reception in noise in cochlear implant users. Journal of the Association for Research in Otolaryngology : JARO 8:384-392.

Won JH, Drennan WR, Kang RS, Rubinstein JT (2010) Psychoacoustic Abilities Associated With Music Perception in Cochlear Implant Users. Ear and Hearing 31:796-805.

Won JH, Nie K, Drennan WR, Rubinstein JT (2012) Maximizing the Spectral and Temporal Benefits of Two Clinically Used Sound Processing Strategies for Cochlear Implants. Trends in Amplification 16:201-210.

Won JH, Jones GL, Drennan WR, Jameyson EM, Rubinstein JT (2011a) Evidence of across-channel processing for spectral-ripple discrimination in cochlear implant listeners. J Acoust Soc Am 130:2088-2097.

Won JH, Clinard CG, Kwon S, Dasika VK, Nie K, Drennan WR, Tremblay KL, Rubinstein JT (2011b) Relationship Between Behavioral and Physiological Spectral-Ripple Discrimination. JARO-Journal of the Association for Research in Otolaryngology 12:375-393.

Won JH, Humphrey EL, Yeager KR, Martinez AA, Robinson CH, Mills KE, Johnstone PM, Moon IJ, Woo J (2014) Relationship among the physiologic channel interactions, spectral-ripple discrimination, and vowel identification in cochlear implant users. J Acoust Soc Am 136:2714-2725.

Wong DD, Gordon KA (2009) Beamformer suppression of cochlear implant artifacts in an electroencephalography dataset. IEEE transactions on bio-medical engineering 56:2851-2857.

Wong DJ, Moran M, O'Leary SJ (2016) Outcomes After Cochlear Implantation in the Very Elderly. Otol Neurotol 37:46-51.

Woodman GF (2010) A Brief Introduction to the Use of Event-Related Potentials (ERPs) in Studies of Perception and Attention. Attention, perception & psychophysics 72:10.3758/APP.3772.3758.2031.

Wu C-C, Luo X (2013) Current Steering with Partial Tripolar Stimulation Mode in Cochlear Implants. Jaro-Journal of the Association for Research in Otolaryngology 14:213-231.

Zeng F-G, Rebscher S, Harrison W, Sun X, Feng H (2008) Cochlear implants: system design, integration, and evaluation. IEEE reviews in biomedical engineering 1:115-142.

Zeng F-G, Nie K, Stickney GS, Kong Y-Y, Vongphoe M, Bhargave A, Wei C, Cao K (2005) Speech recognition with amplitude and frequency modulations. Proceedings of the National Academy of Sciences of the United States of America 102:2293-2298.

Zeng FG (2004) Trends in cochlear implants. Trends Amplif 8:1-34.

Zeng FG, Grant G, Niparko J, Galvin J, Shannon R, Opie J, Segel P (2002) Speech dynamic range and its effect on cochlear implant performance. Journal of the Acoustical Society of America 111:377-386.

Zhang F, Anderson J, Samy R, Houston L (2010) The adaptive pattern of the late auditory evoked potential elicited by repeated stimuli in cochlear implant users. Int J Audiol 49:277-285.

Zhang F, Hammer T, Banks HL, Benson C, Xiang J, Fu QJ (2011) Mismatch negativity and adaptation measures of the late auditory evoked potential in cochlear implant users. Hear Res 275:17-29.
Zhu Z, Tang Q, Zeng F-G, Guan T, Ye D (2012) Cochlear-implant spatial selectivity with monopolar, bipolar and tripolar stimulation. Hearing Research 283:45-58.

Appendices

Appendix A Journal Publications

Hearing Research 302 (2013) 84–95

Contents lists available at SciVerse ScienceDirect

Hearing Research

journal homepage: www.elsevier.com/locate/heares

Research paper

Cochlear implant artifact attenuation in late auditory evoked potentials: A single channel approach

Myles Mc Laughlin [a,b,*], Alejandro Lopez Valdes [b], Richard B. Reilly [b], Fan-Gang Zeng [a]

[a] Hearing and Speech Laboratory, University of California Irvine, USA
[b] Neural Engineering Group, Trinity College Dublin, Ireland

ARTICLE INFO

Article history:
Received 10 December 2012
Received in revised form
7 May 2013
Accepted 12 May 2013
Available online 28 May 2013

ABSTRACT

Recent evidence suggests that late auditory evoked potentials (LAEP) provide a useful objective metric of performance in cochlear implant (CI) subjects. However, the CI produces a large electrical artifact that contaminates LAEP recordings and confounds their interpretation. Independent component analysis (ICA) has been used in combination with multi-channel recordings to effectively remove the artifact. The applicability of the ICA approach is limited when only single channel data are needed or available, as is often the case in both clinical and research settings. Here we developed a single-channel, high sample rate (125 kHz), and high bandwidth (0–100 kHz) acquisition system to reduce the CI stimulation artifact. We identified two different artifacts in the recording: 1) a high frequency artifact reflecting the stimulation pulse rate, and 2) a direct current (DC, or pedestal) artifact that showed a non-linear time varying relationship to pulse amplitude. This relationship was well described by a bivariate polynomial. The high frequency artifact was completely attenuated by a 35 Hz low-pass filter for all subjects ($n = 22$). The DC artifact could be caused by an impedance mismatch. For 27% of subjects tested, no DC artifact was observed when electrode impedances were balanced to within 1 kΩ. For the remaining 73% of subjects, the pulse amplitude was used to estimate and then attenuate the DC artifact. Where measurements of pulse amplitude were not available (as with standard low sample rate systems), the DC artifact could be estimated from the stimulus envelope. The present artifact removal approach allows accurate measurement of LAEPs from CI subjects from single channel recordings, increasing their feasibility and utility as an accessible objective measure of CI function.

1. Introduction

Advances in cochlear implant (CI) technology now mean that a typical recipient of a modern CI can expect to understand speech in a quiet listening environment (for a review see Zeng et al., 2008). In spite of these advances there remains a large amount of variability in performance across users. Behavioral methods such as speech perception tests or non-speech based listening tests (Fu, 2002; Henry and Turner, 2003; Henry et al., 2005; Won et al., 2007) can be used to quantify this variability. However, behavioral methods are often not suitable for pediatric CI users and speech-based tests may not be the best way to assess the performance of new CI recipients while they are still learning to understand speech heard through their implants. Neural based objective metrics of performance may provide a useful alternative to behavioral testing for both these user groups. In addition to potentially improving the standard of treatment received by an individual CI user, the development of neural objective metrics of CI performance may also advance our understanding of the origins of the performance variability, by giving information on the underlying neural mechanisms. However, the development of such neural metrics has been hampered by the large CI related electrical artifact, which contaminates evoked potential recordings in these subjects.

Firszt et al. (2002) found that cortical evoked potentials may be useful for predicting speech perception outcomes for CI. However, to minimize the artifact, this study used very short simple stimuli which are unable to fully probe the complex processing that takes place in the auditory system. Gilley et al. (2006) proposed a method for attenuating the artifact caused by longer duration stimuli. They showed how independent component analysis (ICA) could be used to recover late auditory evoked potentials (LAEP) from multi-channel data. Utilizing the multi-channel ICA approach, two recent studies by Zhang et al. (2010, 2011) showed how LAEPs

* Corresponding author. 110 Medical Sciences E, University of California Irvine, Irvine, CA 92697, USA. Tel.: +1 949 282 7667.
E-mail address: myles.mclaughlin@uci.edu (M. Mc Laughlin).

0378-5955/$ – see front matter © 2013 Elsevier B.V. All rights reserved.
http://dx.doi.org/10.1016/j.heares.2013.05.006

obtained using a mismatch negativity paradigm can provide useful information on CI functionality and that this information can be related to behavioral outcomes such as speech perception. One drawback of the ICA approach is that multi-channel data must be acquired, even when, as with the two studies by Zhang et al., most of the results and conclusions are based on artifact-free single-channel data. Having to acquire multi-channel data necessitates the purchase of expensive multi-channel acquisition systems, increases subject preparation time, as a full EEG cap must be attached and, for CI subjects, adds to the difficulty of positioning the EEG cap over the behind-the-ear processor and magnetic link. For most clinical applications and many research questions, single-channel data are sufficient and subject preparation time much shorter. These practical considerations limit the applicability of the ICA-based artifact attenuation approach and led us to develop a single-channel based artifact attenuation approach.

To better understand the origin of the CI related artifact in LAEPs we developed a high-sample-rate, high-bandwidth, single-channel acquisition system with a temporal resolution high enough to clearly resolve each stimulation pulse. Here, we used this acquisition system to show that LAEPs recorded from CI subjects are generally composed of three components: a neural response component and two artifact components. Based on this signal composition, we proposed a three-stage artifact attenuation strategy (Fig. 1). The high frequency artifact (HFA) was found to be a direct representation of the stimulation pulses and was completely attenuated by a low-pass filter (stage 1). The low frequency or DC artifact (DCA), often referred to as a 'pedestal' artifact, could be accentuated by an electrode impedance mismatch and in some subjects could be attenuated by balancing the impedance of the recording electrodes (stage 2). Based on the assumption that the DCA was caused by the stimulation pulses, we developed a mathematical framework to obtain an estimate of the DCA and remove it from the LAEP (stage 3). Finally, we demonstrated how this single-channel approach could be also be applied with low sample rate data (commercial systems) and that it could be used to measure N1–P1 amplitude growth functions for CI users.

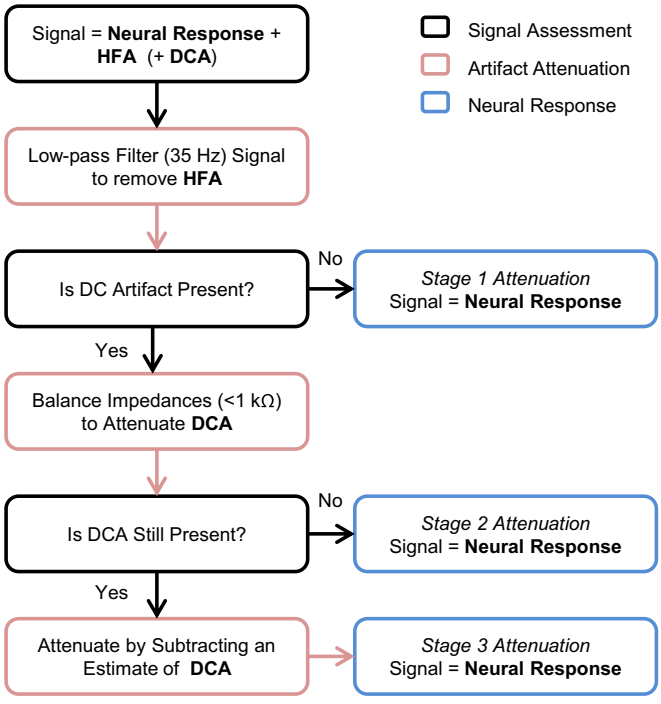

Fig. 1. Flow chart showing three stage artifact attenuation approach. The acquired signal (SIG) consisted of the neural response (NR) and two artifact components: a high frequency artifact (HFA) and a low frequency or DC artifact (DCA). A low-pass filter attenuated the HFA (stage 1). Balancing electrode impedances to within 1 kΩ attenuated the DCA for some subjects (stage 2). For the remaining subjects, the DCA could be estimated from the pulse amplitude or stimulus envelope and subtracted from the signal to leave the neural response (stage 3).

2. Material and methods

2.1. Subjects

LAEPs were measured for 22 adult CI subjects (7 male, 15 female) at two separate locations: Hearing and Speech Laboratory, University of California Irvine ($n = 7$) and Trinity Centre for Bioengineering, Trinity College Dublin ($n = 15$). Experimental procedures were approved by The University of California Irvine's Institutional Review Board and the Ethical Review Board at Trinity College Dublin. Informed consent was obtained from all subjects. Subjects were aged between 20 and 79 (mean 55, standard deviation 17) years and used a device from one of the three main manufacture's (Cochlear $n = 20$, Advanced Bionics $n = 1$, Med-El $n = 1$). All devices used monopolar stimulation strategies.

2.2. Stimuli

Stimuli consisted of tone bursts with frequencies of 250, 500 or 1000 Hz with durations of 100, 300 or 500 ms. Broadband noise stimuli (100–8000 Hz) were also used. Stimuli were presented at most comfortable level (MCL) and, when amplitude growth functions were collected, levels were decreased in equal decibel steps between MCL and threshold. Stimuli were generated in Matlab (Mathworks, Natick, MA) at a sampling rate of 44.1 kHz and a 10 ms on and off cosine squared ramp was applied. In Trinity College Dublin stimuli were presented through a standard PC soundcard and in University of California Irvine stimuli were presented through a DA converter (NI-USB 6221, National Instruments, Austin, TX). All stimuli were presented to the audio line in on the subject's CI. To limit the effects of any unwanted background noise, the CI microphone volume and sensitivity were set to the minimum allowable values. At University of California Irvine subjects were seated in a sound booth and at Trinity Centre for Bioengineering subjects were seated in a quiet room. Subjects used their everyday speech processing strategy without any special adjustments other than changes to the microphone volume and sensitivity. This method of stimulation was chosen, as opposed to using a research interface to directly control the CI, because it represents a worst case scenario in terms of the CI artifact. It was reasoned that this would result in the development of a robust artifact attenuation approach that could be easily applied in different settings and with different modes of stimulation.

Stimuli were always presented monaurally through channel one on the PC sound card or DA converter. For all stimuli, a trigger pulse at stimulus onset was presented on channel two of the output device. This trigger pulse was used to synchronize stimulus presentation and LAEP recording.

2.3. Evoked potential recordings

A high temporal resolution EEG acquisition system was developed. It consisted of a high bandwidth, low noise, single-channel differential amplifier (SRS 560, Stanford Research Systems, Sunnyvale, CA) connected to a high sample rate AD converter (NI-USB 6221, National Instruments, Austin, TX). The sample rate on the AD converter was set to 125 kS/s, the low-pass filter on the amplifier was typically set to 100 kHz and the high-pass filter was set to either DC, 0.03 Hz or 1 Hz. The filter roll-offs were set to 12 dB/Oct

and the low-noise gain mode was selected. Usually, the gain on the amplifier was set to 2000. For most subjects at most stimulation levels this gain setting ensured that the amplifier did not saturate during stimulation. Occasionally, at the highest stimulation levels, the gain was reduced to 1000 to avoid amplifier saturation. To reduce 50/60 Hz mains noise the amplifier was disconnected from the mains and operated in battery mode. The dynamic range on the AD converter was set to ±10 V. Standard gold cup surface electrodes were used. An electrode placed at Cz was connected to the positive input on the amplifier. On the side opposite to the CI being tested, an electrode placed on the mastoid was connected to the negative input on the amplifier, and one placed on the collar bone was connected to the amplifier ground. This system was designed to allow the CI related artifact to be clearly sampled with only minimal distortion being caused by the acquisition system.

Channel one on the AD converter was connected to the output of the amplifier and channel two was connected to the stimulus trigger pulse mentioned in the previous section. Custom software written in Matlab processed the output of the AD converter. Detection of the trigger pulses in software allowed accurate synchronization of the stimulus presentation with the recorded signal. The software performed online averaging, filtering, and visualization of the LAEP and stored the raw data for offline analysis. Long epochs of 300 ms pre-stimulus to 800 ms post-stimulus were used. All digital filters mentioned below were applied to the long, averaged, epochs. The use of long epochs minimizes any possible filter edge effects. For plotting and display purposes a shorter epoch of 100 ms pre-stimulus to 500 ms post-stimulus was used.

2.4. Artifact attenuation

LAEPs recorded with the high sample rate system using CI subjects were compared with typical LAEPs recorded using normal hearing subjects. This comparison showed that the signal (SIG) recorded in CI subjects consisted of a neural response component (NR), similar to that observed for normal hearing subjects, in addition to two visually distinct artifact components, a high frequency artifact (HFA) and a low frequency artifact (DCA). Thus the recorded signal could be represented by the following equation, where t is time,

$$\mathrm{SIG}(t) = \mathrm{NR}(t) + \mathrm{HFA}(t) + \mathrm{DCA}(t) \quad (1)$$

Based on this signal composition we developed a three stage, single-channel, artifact attenuation approach. Each stage is explained in detail below and a block diagram outlining the approach is shown in Fig. 1.

2.4.1. Stage 1: low-pass filter

Single, unaveraged recordings of the response to one stimulus presentation showed that the HFA was a direct representation of the stimulation pulses (see Fig. 2A and D). The HFA was completely attenuated by a low-pass filter (Fig. 2C and F). The low-pass filter was implemented in the custom Matlab software as a 2nd order Butterworth filter with a cutoff frequency of 35 Hz and 12 dB/Oct slope. This filter was applied using a zero-phase forward and reverse digital filtering technique (filtfilt command, Matlab). The HFA could also be attenuated by setting the hardware low-pass filter on the amplifier to 30 Hz with a 12 dB/Oct slope.

2.4.2. Stage 2: impedance balancing

After removal of the HFA a DCA was observed in the LAEPs from some subjects (Fig. 3). For some subjects this DCA could be attenuated by ensuring that the electrode impedances were balanced to within 1 kΩ (Fig. 4). To do this, the high impedance electrode was first identified by comparison of the impedances measured between all combinations of the three electrodes. The high impedance electrode was then removed, the skin prepared again and the electrode replaced.

2.4.3. Stage 3: DCA estimation

For some subjects, the DCA could not be fully attenuated by the impedance balancing. For these subjects, a DCA estimation method

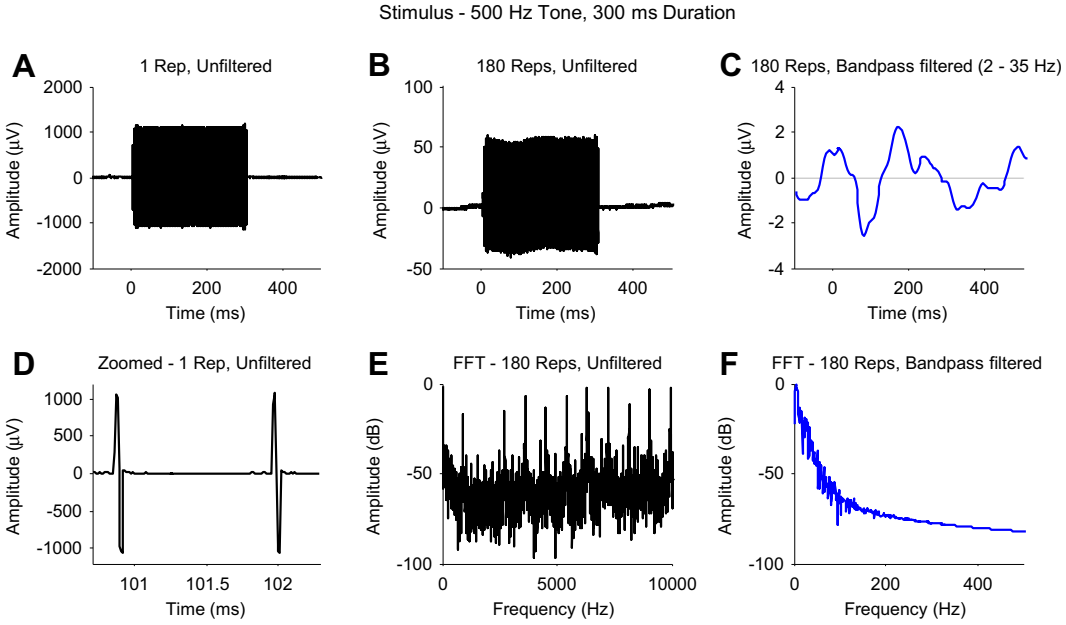

Fig. 2. A low-pass filter removed the high frequency artifact. A) The large amplitude high frequency artifact is clearly visible after only one repetition. B) As the individual stimulation pulses do not sum in phase the high frequency artifact becomes smaller with more repetitions. The low frequency envelope is caused by the neural response. C) A band-pass (2–35 Hz) filter attenuates the high frequency artifact to leave the neural response. D) Zooming in on one repetition shows the individual stimulation pulses. E) The frequency spectrum of the unfiltered average data shows the high frequency artifact at the stimulation rate and harmonics. F) The frequency spectrum of the filtered data shows the effect of the band-pass 2nd order Butterworth filter.

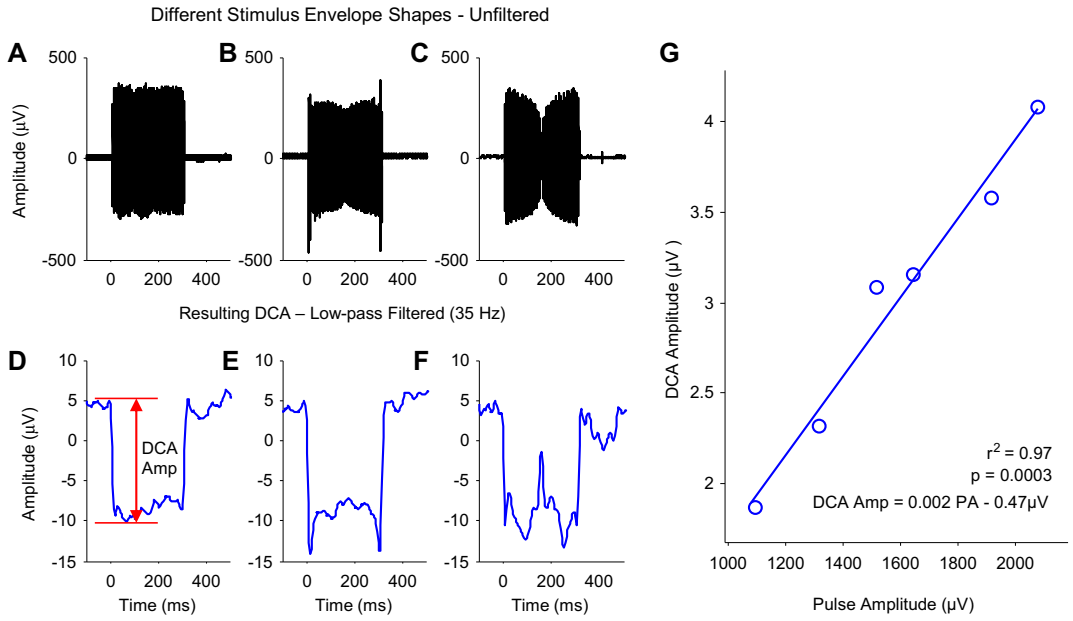

Fig. 3. DC artifact is related to pulse amplitude. A–B) The unfiltered averaged response from one subject to three stimuli with different envelope shapes. The pulse amplitude follows the stimulus envelope shape. E–F) The low-pass filtered data show a DC artifact which is related to the shape of the pulse amplitude. G) Data from a different subject showing a linear relationship between DC artifact amplitude and pulse amplitude.

was applied. Examination of the DCA showed that it was related to the stimulation pulses, i.e. the onset and offset times of the DCA were similar to those of both the HFA and the stimulus, and the shape of the DCA was similar to that of the acoustic stimulus envelope and the HFA envelope. Given these observations, it is reasonable to assume that the DCA can be described by a function of both stimulation pulse amplitude (PA) and time (t),

$$\mathrm{DCA} = f(\mathrm{PA}, t) \tag{2}$$

Examination of the DCA showed that this relationship was well approximated by a bivariate polynomial for all subjects,

$$\mathrm{DCA} = \sum_{ij} a_{ij} \mathrm{PA}^i t^j, \tag{3}$$

where a is a coefficient for each term in the polynomial and i and j determine the degree of the polynomial.

The CI stimulation pulse generator and stimulus onset are not synchronized. Therefore, pulses across repetitions are slightly jittered, with the result that the PA in the averaged signal is smaller than in a single repetition (compare Fig. 2A and B). To create a pulse-synchronized averaged signal, a cross correlation between the first repetition and all other repetitions was performed. The

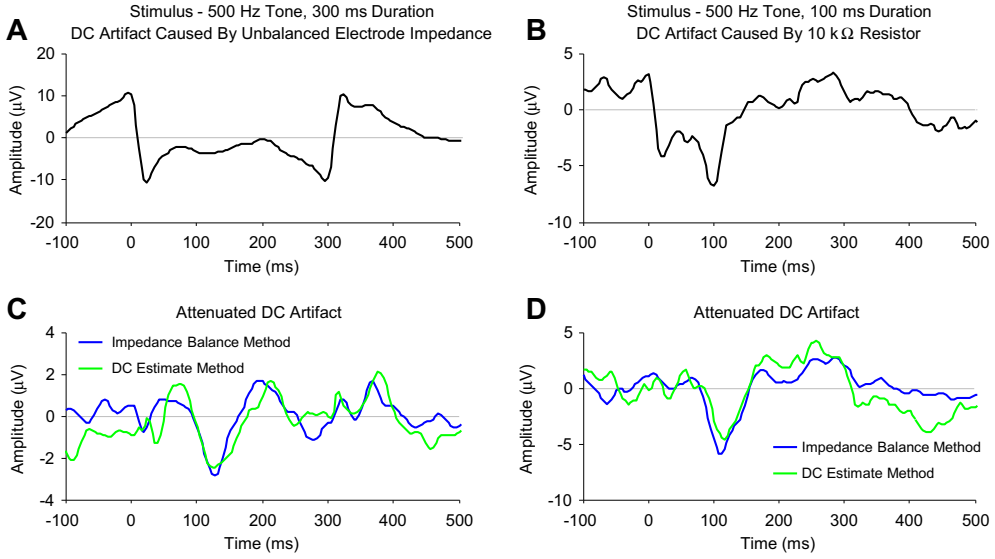

Fig. 4. The DC artifact can be caused by an impedance mismatch. A) A DC artifact was observed when the electrode impedances were unbalanced (Cz = 4.6, Mastoid = 2.9, Ground = 2.7 kΩ). B) Placing a 10 kΩ resistor between the Cz electrode and the amplifier also caused a DC artifact. C) Balancing the electrode impedances (Cz = 2.6, Mastoid = 2.6, Ground = 2.3 kΩ) attenuated the DC artifact (blue line). Applying the DC estimation method to the unbalanced data shown in panel A achieved a similar result (green line). D) Removing the resistor completely attenuated the DC artifact (blue line). Applying the DC estimation method to the unbalanced data shown in panel B A achieved a similar result (green line). (For interpretation of the references to colour in this figure legend, the reader is referred to the web version of this article.)

maximum time lag in the cross correlation was limited to one time period of the stimulation rate. This determined the amount of jitter between repetitions, which could then be applied as a small delay to each repetition to create a pulse-synchronized signal. An accurate measurement of PA could then be obtained from the pulse-synchronized signal.

Fig. 5 is a block diagram showing how the polynomial coefficients were estimated from the recorded signal to give an estimate of the DCA. Firstly, PA was measured from the unfiltered pulse-synchronized signal as a function of time. Next, the averaged (non-synchronized) signal was low-pass filtered to remove the HFA, leaving just the NR and DCA,

$$\mathrm{SIG_f}(t) = \mathrm{NR}(t) + \mathrm{DCA}(t) \quad (4)$$

The PA time series was filtered with a 2nd order digital Butterworth band-pass filter (compare the two upper right boxes on Fig. 5). The cut-off frequencies and slopes of this band-pass digital filter were matched to the cut-off frequencies and slopes of the filters applied to the signal: the high-pass setting used on the amplifier and low-pass used in the software for HFA attenuation. An estimate of the DCA was then obtained by fitting a bivariate polynomial to these data using the polyfitn function in Matlab (available for download from the Mathworks File Exchange). In the polynomial fitting function, the two independent variables were given as PA and t, and the dependent variable was $\mathrm{SIG_f}$. The parameters obtained from the fitting function, i.e. the coefficients a, could then be used in Eq. (3), together with the PA time series, to obtain an estimate of DCA ($\mathrm{DCA_{est}}$). To obtain the neural response, the DCA was attenuated by subtracting $\mathrm{DCA_{est}}$ from $\mathrm{SIG_f}$,

$$\mathrm{NR}(t) \approx \mathrm{SIG_f}(t) - \mathrm{DCA_{est}}(t) \quad (5)$$

To obtain a measure of PA, it is necessary to have high sample rate data, for which the stimulation pulses are clearly resolved. Most commercially available acquisition systems cannot acquire data at these high sample rates. When a measure of PA is not available, a measure of the stimulus envelope (SE) can be substituted. For vocoder-based speech processing strategies the SE will be related to the PA via a compression function.

2.4.3.1. Polynomial degree. We remind the reader that the degree (often referred to as order) of a polynomial is determined by the polynomial term with the largest degree, and that the degree of a polynomial term is determined by the sum of the exponents. Thus, a bivariate 3rd degree polynomial will contain PA^2t and $\mathrm{PA}t^2$ terms but not a PA^3t term. The degree of the polynomial which gave the best fit to that data was related to the number of non-linear transformations between the PA or SE and the recorded signal. The results section shows the effects of different acquisition system settings which influence these transformations and suggests the appropriate polynomial degree to be used in each case.

2.4.3.2. Constraining the fit. Eq. (3) shows the approximated relationship between DCA, PA and t. PA and t are known but the coefficients a and DCA are unknown. As described above, to estimate the coefficients a bivariate polynomial was fitted to PA, t and $\mathrm{SIG_f}$, where $\mathrm{SIG_f}$ contains both DCA and NR (see Eq. (4)). The most accurate estimate of DCA will be obtained when the fitting algorithm fits only the DCA component of $\mathrm{SIG_f}$ and not the NR component. A number of factors help constrain the fit to the DCA component only:

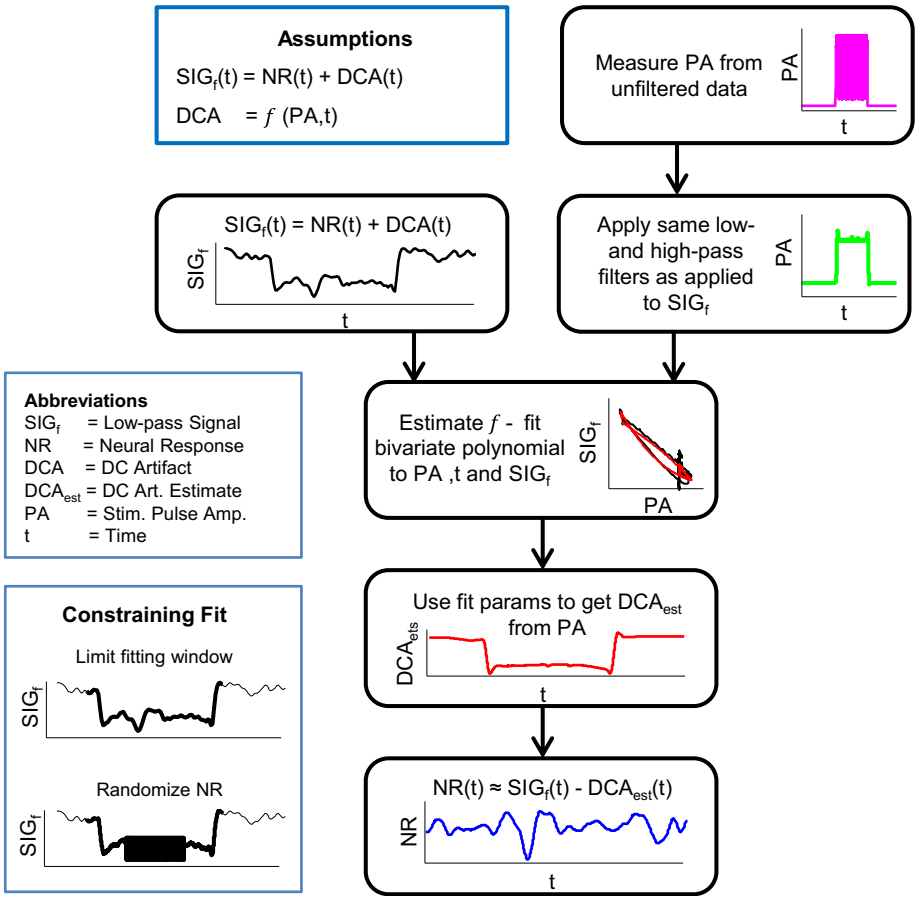

Fig. 5. Flow chart showing how the DC artifact can be estimated from the stimulation pulse amplitude (measurable with high sample rate acquisition systems) or stimulus envelope (for low sample rate systems). The estimate of the DC artifact is subtracted from the low-pass filtered signal to leave the neural response.

1) The PA (or SE) time series has a similar shape to the DCA. If we conceptualize the estimation procedure as transforming this PA time series into the DCA_{est}, then the degree of the polynomial determines how non-linear this transformation will be. A polynomial degree was selected that was high enough to characterize this transformation but low enough to limit any fitting to the neural response. 2) Only a limited time window of the epoch, where the DCA is expected to occur, was used in the fitting procedure (see Fig. 5 'Constraining Fit' inset). This time window was determined by the stimulus duration and the amplifier low-pass filter setting. If the amplifier low-pass filter was set to DC or 0.03 Hz, then the DCA was limited to the stimulus duration and only this portion of the epoch was used in the fitting procedure (thick line on upper plot in inset). A low-pass filter setting of 1 Hz caused the DCA to be smeared out in time, and here a time window from stimulus onset to epoch end was used in the fitting procedure. 3) Finally, during a time window when it was expected that the DCA would be flat, i.e. 30 ms after stimulus onset and 30 ms before stimulus offset, the order of elements in the SIG_f vector was randomized (see Fig. 5 'Constraining Fit' inset, lower plot). The randomization procedure preserves the main statistical properties of SIG_f during this time window (i.e. mean and standard deviation are unchanged) but removes temporal features of the NR, thus constraining the fitting procedure to the DCA component.

3. Results

3.1. Attenuation of high frequency artifact

All subjects tested showed a HFA. Fig. 2 shows an example of the HFA, which was generally in the mV range, and the low-pass filter procedure used to attenuate it. The high temporal resolution of the acquisition system allows us to see that the HFA was caused by the CI stimulation pulses (Fig. 2D). Averaging across repetitions caused a reduction in the HFA amplitude as the stimulation pulses in each repetition were not synchronized (Fig. 2B). The frequency spectrum of the averaged unfiltered signal (Fig. 2E) showed a strong component at that user's stimulation rate and its harmonics. The HFA could be completely attenuated for all subjects with a 35 Hz low-pass software filter (2nd order Butterworth, Fig. 2F). Fig. 2C shows an LAEP collected from a CI subject after the HFA had been attenuated by filtering. The typical N1–P2 complex is visible. To examine how effective a hardware filter was at attenuating the HFA, LAEPs were collected from 3 subjects using a 30 Hz low-pass hardware filter on the amplifier (12 dB per octave). These were compared with LAEPs collected from the same subjects, during the same session, with a 100 kHz low-pass hardware filter and then subsequently digitally filtered with a low-pass 2nd order Butterworth filter. The effects of attenuating the HFA using the hardware and software filters were found to be similar.

3.2. RF coil related artifact

There are two possible sources of high frequency artifact when recording LAEPs from CI subjects: the stimulation pulses or the RF coil transmission. The close resemblance of the temporal waveform of the HFA to that of the stimulation pulses suggests that, with this recording setup, the HFA is caused by the stimulation pulses and not the RF coil transmission. RF coil transmission is in the MHz range and so should be removed by the hardware filter on the amplifier. However, due to inadequate hardware filters, sub-harmonics or aliasing, it is possible that the RF coils causes an artifact. The standard electrode configuration used a recording electrode on the mastoid contralateral to the CI. Since both the RF coil and stimulation pulse artifacts will decrease in amplitude with distance from the CI, this configuration helps minimize any artifact. To further investigate the possibility of an RF related artifact, we collected data with a modified electrode configuration: the contralateral mastoid electrode was moved to the mastoid ipsilateral to the CI. Examination of the unfiltered data in both the temporal and spectral domains showed no evidence for a RF coil related artifact (see Supplementary Fig. 1 for a comparison of the amplitude spectra). The components present in data recorded with the standard electrode configuration were present in data recorded with an electrode on the ipsilateral mastoid.

To investigate this possibility that the DC artifact is caused by an RF coil related artifact and not the stimulation pulses, we collected data from one subject with a recording electrode on the ipsilateral mastoid, using stimuli with different shaped envelopes (Fig. 3A–F). Panels A, B and C show the unfiltered averaged data and panels D, E and F show the corresponding DC artifact after low-pass filtering. We know from CI encoding strategies (Zeng et al., 2008) that the stimulus envelope is directly related to the stimulation pulse amplitude, while in the RF transmission the amplitude of the stimulation pulses in not linearly encoded. Therefore, if the DC artifact is caused by the RF coil transmission its shape will be unaffected by the stimulus envelope. Fig. 3A–F shows that this is not the case: the shape of the DC artifact clearly follows the fluctuations in the pulse amplitude, indicating that the DC artifact is dominated by a component caused by the stimulation pulses. However, we cannot rule out the possibility that a small RF coil related component contributes to the DC artifact. Fig. 3G shows data from a different subject recorded with the standard electrode configuration at different stimulation levels. Plotting DC artifact amplitude against pulse amplitude shows a clear linear relationship. Since pulse amplitude is not linearly encoded in the RF transmission, any RF artifact would not decrease with decreasing pulse amplitude.

3.3. Attenuation of DC artifact

3.3.1. Attenuation by impedance balancing

After the HFA had been attenuated by low-pass filtering, the LAEPs for some subjects showed a DCA. Fig. 4A shows an example of a typical DCA, visible after low-pass filtering. In general, it was found that the size of the DCA was related to the size of the impedance mismatch between electrodes. Balancing electrode impedance reduced the size of the DCA and, in some cases, completely attenuated the DCA. For the LAEPs shown in Fig. 4A, where a large DCA is apparent, electrode impedances were Cz = 4.6 kΩ, Mastoid = 2.9 kΩ and Ground = 2.7 kΩ. Reducing the impedance on Cz to 2.6 kΩ completely attenuated the DCA (Fig. 4, blue line). Applying a low-pass filter to remove the HFA and ensuring that electrode impedances were balanced to within 1 kΩ produced LAEPs that contained no visible artifacts for 27% ($n = 6$) of subjects tested. Of the 6 subjects who showed no visible artifact after low-pass filtering, 4 used CIs from Cochlear, 1 was a Med-El user and 1 was an Advanced Bionics users. For the remaining 73% ($n = 16$), even after impedance balancing, a DCA artifact was present. This DCA was removed using the DCA estimation procedure, the results of which are reported in the following section.

To further examine the cause of the DCA, we selected 3 subjects who did not show a DCA. In these subjects, after the electrode impedances had been balanced, a DCA could be created by adding a 10 kΩ resistor between one of the electrode leads and the amplifier (Fig. 4B). After the resistor was removed the DCA was not present (Fig. 4D, blue line).

The cases where the DCA artifact was present and could be removed by impedance balancing or when the DCA was created by adding a resistor provided a useful method for validating the DCA estimation approach described below. The green lines in Fig. 4C and

D show the LAEPs obtained after applying the DCA estimation approach to the LAEPs shown in Fig. 4A and B, respectively. The blue and green lines in Fig. 4C and D show good agreement in shape and peak timing, indicating that the DCA artifact estimation approach attenuated the artifact just as effectively as the impedance balancing method.

3.3.2. Attenuation by DC artifact estimation

Fig. 6 shows an example of the different stages in the DCA estimation approach and compares the LAEPs obtained using the PA and SE methods. Fig. 6A shows the PA measured as the difference between the minimum and maximum values of each pulse in the unfiltered signal (purple line). The same band-pass filter used on the signal (high-pass from the amplifier and low-pass used in software to remove the HFA) was then applied to the PA. The purple and green lines in Fig. 6A show the PA before and after filtering, respectively. The black line in Fig. 6B shows the filtered signal (NR + DCA) plotted against the filtered PA. A 3rd degree bivariate polynomial was fitted to these data (i.e. PA, *t*, and NR + DCA). There was good agreement between the fitted polynomial function (Fig. 6B, red line) and the data (black line). The coefficients estimated from the fit were used in Eq. (3) to obtain an estimate of the DCA from the PA (Fig. 6E, red line). The blue line in Fig. 6E shows the NR, where the DCA has been attenuated by subtracting DCA_{est} (red line) from NR + DCA (black line). Supplementary Fig. 2 shows a three dimensional representation of the dataset before (NR + DCA) and after (NR) the attenuation of the DCA, where amplitude is coded as a color, repetitions are plotted on the *y* axis and time on the *x* axis. It is apparent that the DCA is present across different repetitions and that it is synchronized with stimulus onset and offset.

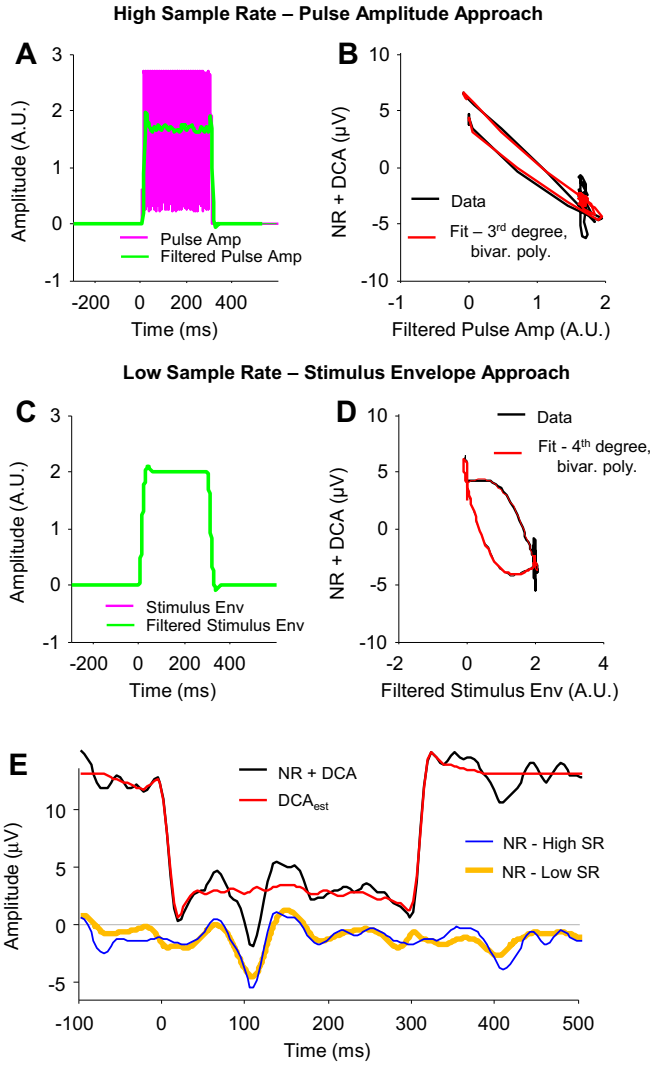

Fig. 6. DC artifact attenuation. A) Stimulation pulse amplitude as a function of time (purple line) was band-pass (0.03–35 Hz) filtered (green line) with the same filter applied to the signal. B) Plot of the low-pass filtered signal (NR + DCA) against pulse amplitude (Data, black line). The relationship was well described by a 3rd degree bivariate polynomial (Fit, red line). C) With lower sample rate data a measurement of stimulus envelope (purple line) is substituted for PA. The same filter that was applied to the signal was applied to the stimulus envelope measurement (green line). D) Plot of the low-pass filtered signal (NR + DCA) against stimulus envelope (Data, black line). The relationship was well described by a 4th degree bivariate polynomial. E) Subtracting DCA_{est} artifact (red line, estimated from PA. Stimulus envelope estimate not shown) from the low-pass filtered signal (NR + DCA, black line) leaves the NR. The blue line shows the NR obtained from the pulse amplitude approach and the orange line shows the NR obtained from the high stimulus envelope approach. (For interpretation of the references to colour in this figure legend, the reader is referred to the web version of this article.)

With most commercial acquisition systems it is not possible to acquire data at a sample rate high enough to resolve individual stimulation pulses, making it difficult to obtain the measurement of PA shown in Fig. 6A. To accommodate data acquired with low sample rate systems, we developed a method of estimating of the DCA using the stimulus envelope (SE). To directly compare the two methods, the data shown in Fig. 6 were downsampled to 1250 S/s, simulating data acquired with a commercial acquisition system. The SE was obtained by rectifying and low-pass filtering (35 Hz, 2nd order Butterworth) the stimulus. As with the PA, the same band-pass filter as applied to the signal was then applied to the SE. The green line in Fig. 6C shows the band-pass filtered SE, which in this case is almost identical to the SE (purple line, not visible) because the amplifier high-pass filter cutoff frequency was close to DC (0.03 Hz) and its effect was negligible. However, as shown in Fig. 7, when the cutoff frequency of the high-pass filter is further from DC its effects become more significant, making it important to include this step. The black line of Fig. 6D shows the downsampled filtered signal (NR + DCA) plotted against the SE. Here, the data (SE, *t*, and NR + DCA) were well fitted by a 4th degree bivariate polynomial (Fig. 6D, red line). In Eq. (3), PA was substituted by SE and the coefficients determined from the fit were used to obtain an estimate of DCA from SE and *t*. The NR, obtained by subtracting DCA_{est} from the downsampled NR + DCA, is shown as the yellow line in Fig. 6E (offset from zero). The high sample rate NR (blue line) compares well with the low sample rate NR (yellow line). The high sample rate method gave an N1–P1 amplitude of 4.9 μV while the low sample rate method gave an N1–P1 amplitude of 4.2 μV. The high and low sample rate N1 latencies were 109 and 107 ms, respectively.

The data shown in Figs. 6 and 7 were collected using 300 ms duration tonal stimuli with a non-fluctuating envelope. Therefore, the onset and offset of the DC artifact did not overlap in time with the N1 response and the DC artifact was flat during the N1 response. The method was tested using shorter duration stimuli (100 ms tones with a non-fluctuating envelope) where the DC artifact offset overlaps in time with the N1 response. Fig. 4B and D clearly show that the DC estimation procedure robustly attenuates the artifact even when neural response and stimulus offset overlap in time. This set of experiments did not test the DC artifact estimation procedure using stimuli with low frequency fluctuating envelopes. It is expected that the procedure would need to be adjusted to robustly attenuate DC artifacts which fluctuate during the neural response of interest.

3.3.3. DC artifact estimation – parameter study

A study was undertaken to evaluate the effect of different parameter settings on the DC artifact estimation procedure. The

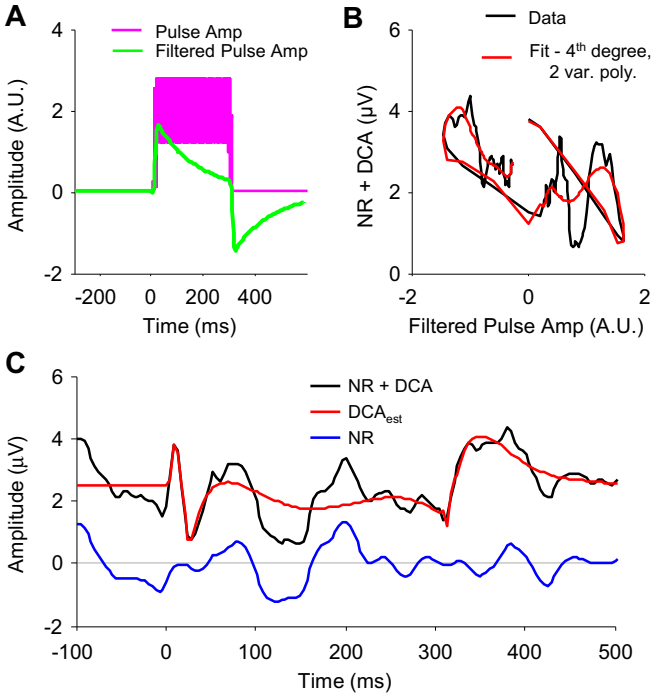

Fig. 7. Effect of the amplifier high-pass filter on the DC artifact. A) Stimulation pulse amplitude as a function of time (purple line) was band-pass (1–35 Hz) filtered (green line) with the same filter applied to the signal. B) Plot of the low-pass filtered signal against pulse amplitude (Data, black line). The relationship is best described by a 4th degree polynomial (Fit, red line). C) Subtracting DCA_{est} (red line) from the low-pass filtered signal (NR + DCA, black line) leaves the NR (blue line). (For interpretation of the references to colour in this figure legend, the reader is referred to the web version of this article.)

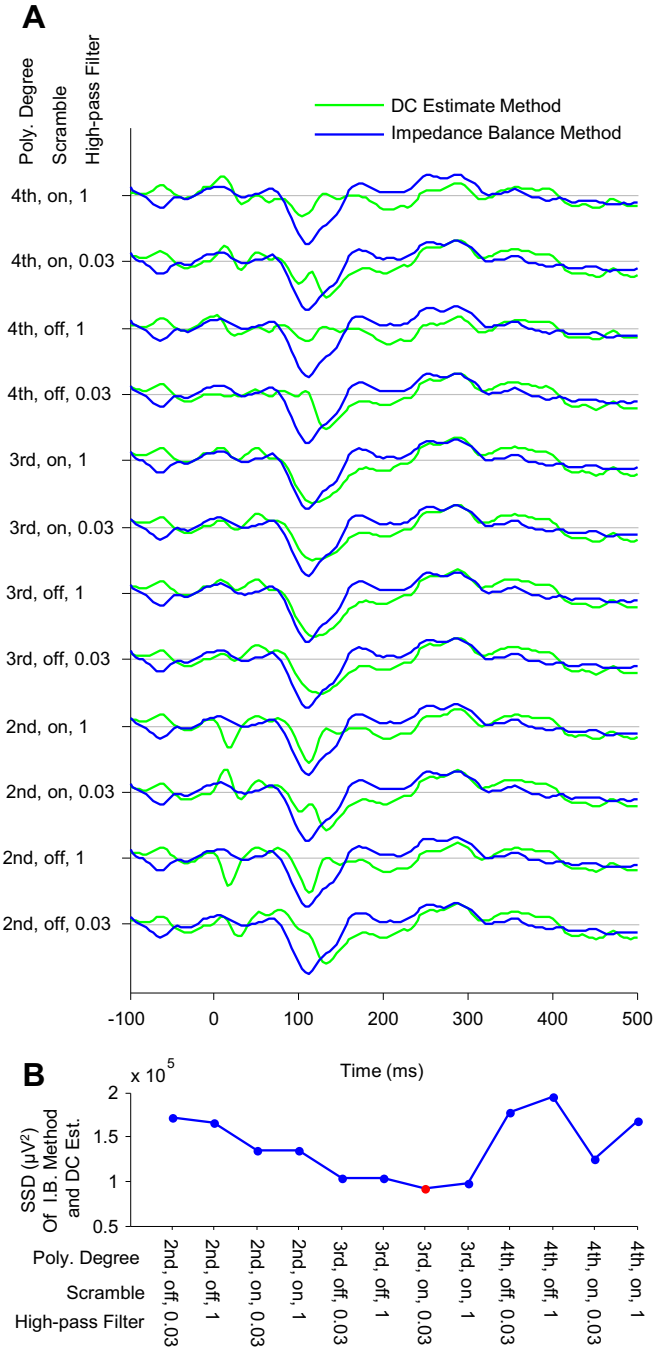

Fig. 8. Parameter study of DC artifact estimation procedure. A) The effect of changing polynomial degree, the scrambling procedure, and the filter applied to the PA, is shown for one LAEP (green lines, 12 parameter combinations). This is compared with an LAEP, collected from the same subject, where the artifact was attenuated using the impedance balancing method (blue lines, measured once). B) The sum of the squared differences (SSD) was calculated between the blue line and each of the lines for the different parameter combinations. (For interpretation of the references to colour in this figure legend, the reader is referred to the web version of this article.)

green lines in Fig. 8A show the effect of changing the degree of the polynomial from 2 to 4, the effect of the scrambling procedure (on or off), and the effect of including the amplifier high-pass filter setting (0.03 or 1 Hz). The effectiveness of the procedure was measured by calculating the sum of the squared differences (SSD) between the LAEP when the artifact was attenuated using the DC estimation procedure (green line, estimated for 12 parameter combinations) and the LAEP, measured using the same subject during the same recording session, when the artifact was attenuated using the impedance balancing procedure (blue line, measured once). Fig. 8B shows how this metric changes for different combinations of parameter settings. During this recording session the high-pass filter on the amplifier was set to 0.03 Hz. The parameter study shows that in this case the best artifact attenuation, using the DC estimation procedure, was achieved with a 3rd degree polynomial, applying the scrambling procedure, and filtering the PA with a high-pass setting that matched that used on the amplifier (i.e. 0.03).

In general, it was found that if the high-pass filter on the amplifier was set to DC or 0.03 Hz and the PA method was used, then the data (PA, *t* and NR + DCA) were well fitted by a 3rd degree polynomial. When the high-pass filter on the amplifier was set to DC or 0.03 Hz and the SE method was used, the data were best fitted with a 4th degree polynomial (Fig. 6C–E), the extra degree here accounting for the non-linear transformation between SE and PA. When the high-pass filter was set to 1 Hz, it produced a non-linear distortion of the DCA (Fig. 7C), i.e. the DCA became smeared out in time. Data acquired with these settings were best fitted by a 4th degree polynomial (Fig.7A and B).

3.4. Amplitude growth functions

The single-channel three stage artifact attenuation attenuated both the HFA and the DCA for all subjects tested. Out of the 22 subjects tested, 20 showed the typical N1–P2 complex in the LAEP. Two subjects did not show any significant peaks in the LAEP. To test the robustness of the approach, N1–P2 amplitude growth functions were collected for 6 of the 7 subjects tested at UC Irvine.

Fig. 9 shows the LAEP waveforms (blue lines) collected for one subject at MCL and at 7 other levels spaced in equal decibel steps down to threshold. N1 was defined as the minimum in the LAEP between 50 and 200 ms and P2 as the maximum occurring within 150 ms after N1. N1 and P2 are marked with blue circles in Fig. 9. To calculate a noise floor for each LAEP, the standard error for each time point in a long epoch (300 ms pre-stimulus to 800 ms post-stimulus) was calculated from the un-averaged, artifact attenuated, data. To do this the DCA calculated from the averaged data was subtracted from each un-averaged epoch. This noise estimation approach is similar to that used by Elberling and Don (1984) to estimate the noise in ABR recordings. It was observed that the standard error did not vary a lot as a function of time point, i.e. the standard error during time points with large neural response was similar to standard error during time points with no neural response. Therefore, the standard error was averaged across all time points within one recording to provide a single-number quantification of the noise in a recording. A noise floor (Fig. 9, gray lines) was defined at ±1.5 times the mean standard error, for the reason described below.

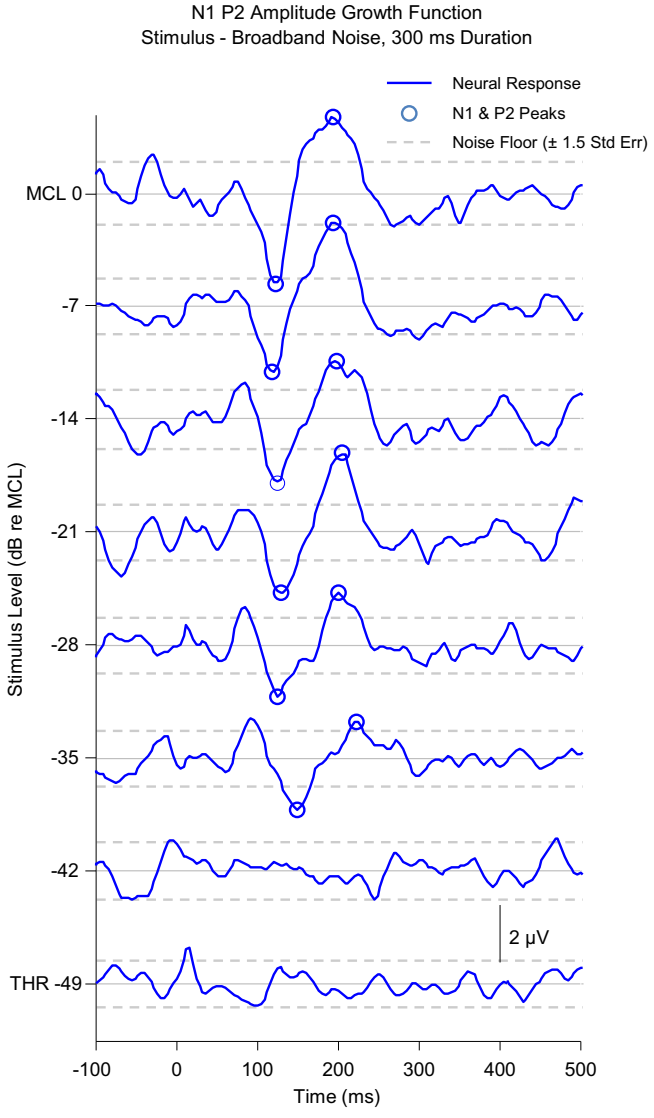

Fig. 9. LAEP amplitude growth function. LAEPs (blue lines) were obtained at 8 levels, equally spaced on a dB scale from most comfortable level (MCL) to threshold (THR). N1 and P2 peaks were extracted (open circles). The latency of the N1 peak was only considered significant if was above a noise floor (dashed gray line). (For interpretation of the references to colour in this figure legend, the reader is referred to the web version of this article.)

Figs. 10 and 11 show amplitude and latency metrics extracted from 11 N1–P2 amplitude growth functions measured from 10 different ears of 6 subjects. The stimuli were 300 ms duration tones with frequencies of 250, 500 or 1000 Hz. The difference in amplitude between the N1 and P2 peaks is shown as a function of stimulus level in Fig. 10. Some N1–P2 amplitude growth functions had a linear shape (e.g. Fig. 10F), while others showed a plateau above a certain level (e.g. Fig. 10A). The shape was not always consistent between ears of the same subject (compare Fig. 10B and C). Note that these amplitude growth functions were collected by stimulating through the subject's clinical processor and so they include the effects of the compression function used in the speech processing strategy. Fig. 11 shows the latency of the N1 peak, which either remained constant or showed an increase with decreasing level for all subjects. Only latencies where N1 amplitude was above the noise floor are shown. Taking the subject population as a whole, a value of 1.5 times the standard error was found to eliminate spurious N1 latency values at lower stimulation levels when the N1 amplitude became small. As a result of this criterion, there are often less points on Fig. 11 than on the corresponding panel on Fig. 10. For all 20 subjects, when stimulated at MCL, the mean N1–P2 amplitude was 5.4 (SD = 2.1) µV and the mean N1 latency was 111 (SD = 19) ms.

4. Discussion

We use the term artifact attenuation, rather than artifact removal or cancellation, as we cannot be certain that the artifact (HFA or DCA) was completely removed. Successful attenuation of artifact was judged by visual inspection of the LAEP. However, three points provide reassurance that, after the single channel artifact attenuation procedure has been applied, the effect of any remaining artifact on the neural response is negligible. Firstly, the impedance balancing procedure was used to validate the DCA estimation procedure. The LAEPs obtained using the DCA estimation procedure (Fig. 4C and D, green lines) shows good agreement with the LAEP obtained using the impedance balancing method. Secondly, N1–P2 amplitudes and N1 latencies obtained at MCL are comparable to those reported in other studies. Viola et al. (2011) used the multi-channel ICA approach to measure LAEPs for 18 CI subjects. They reported a mean N1–P2 amplitude of 8.9 (±4.1 standard deviation) µV and mean N1 latency of 132 (±13.7 standard deviation) ms. Finally, the amplitude growth functions (Figs. 9–11) show that N1–P2 amplitudes increase and N1 latencies decrease with increasing level, as has been previously reported for normal hearing subjects (for a summary, see Picton et al., 1976).

Below we give a list of recommendations for recording LAEPs for CI subjects and describe the best practice for applying the single channel approach. We discuss potential causes of the DCA. We then compare our single channel artifact attenuation approach with other approaches used to attenuate the HFA and DCA. Finally, we discuss the clinical use of LAEPs for assessing CI functionality and suggest how the single channel approach may facilitate their application.

4.1. Recording recommendations

As a first step to attenuating the DCA we recommend ensuring that all electrode impedances are balanced to within 1 kΩ. If the DCA persists, setting the high-pass filter on the amplifier to DC or 0.03 Hz will give the clearest acquisition of the DCA and allow the most straightforward application of the DCA estimation approach. When available (i.e. with high sample rate systems), we

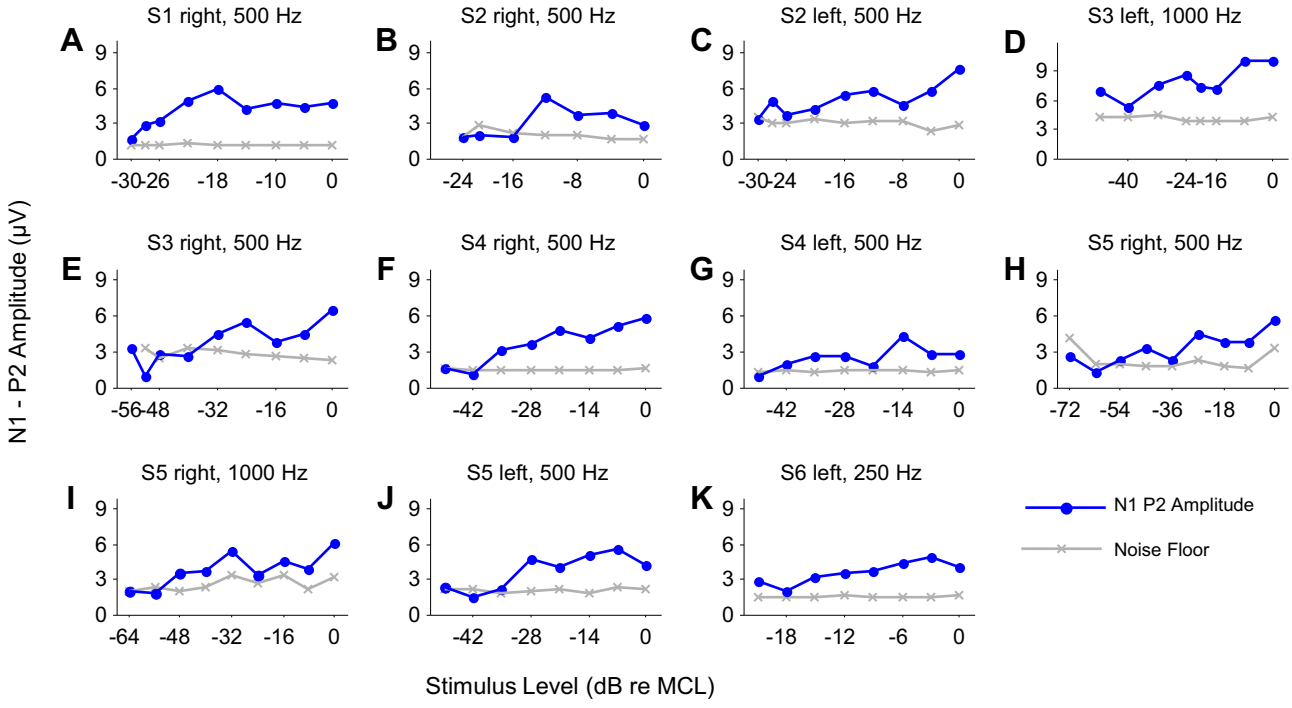

Fig. 10. N1–P2 amplitude growth functions for all subjects.

recommend using a measure of PA to estimate and then attenuate the DCA. When the amplifier high-pass filter is at DC or 0.03 Hz, the data (PA, *t* and NR + DCA) are best fitted with a 3rd degree bivariate polynomial. If a measure of PA is not available (low sample rate systems), a measure of SE can be substituted and the bivariate polynomial degree should be increased by one to account for the extra non-linear transformation between PA and SE. If the data were acquired with the amplifier high-pass filter at 1 Hz, the bivariate polynomial degree should be increased by 1 to account for the non-linear effects of the filter.

4.2. Potential causes of the DCA

With this recording system, the data show that the DCA is related to the stimulation pulse amplitude (Fig. 3) and that an electrode impedance mismatch can cause a DCA (Fig. 4). However,

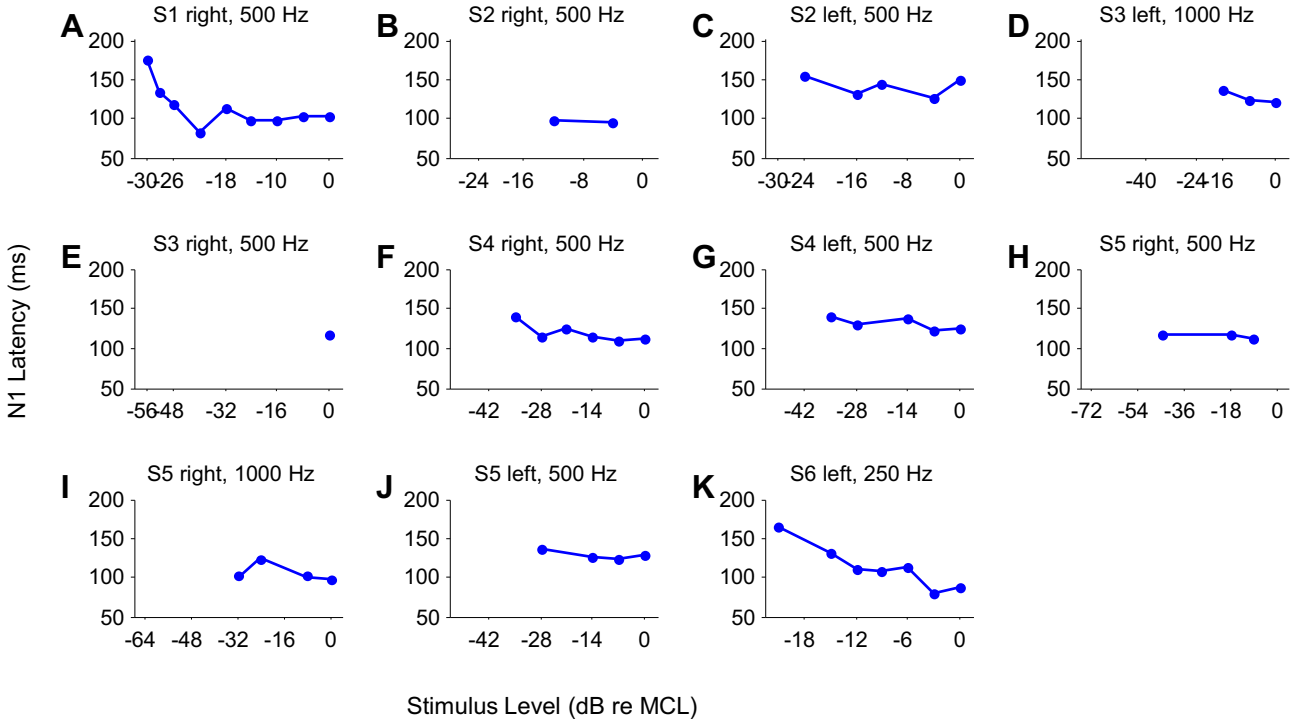

Fig. 11. N1 latency functions for all subjects.

we do not know the mechanism by which these factors cause or generate the DCA. It is possible that unwanted capacitance effects cause the DCA. These capacitances could be located at the CI electrode–neuron interface or at the EEG electrode–scalp interface. The stimulation pulse may deposit charge on this capacitor which is slowly released, causing the DCA. For some subjects ($n = 6$) the DCA can be removed by balancing the impedance of the scalp electrodes. For other subjects ($n = 16$), even when the scalp electrode impedances are balanced, the DCA is still present. For these subjects the DCA may be caused by an internal impedance path mismatch (i.e. from CI electrode to EEG scalp electrode). For normal hearing subjects a scalp electrode impedance mismatch may result in noisier recordings but it does not typically cause a DCA. Therefore, for CI subjects the DCA is likely caused by the large amplitude stimulation pulses in combination with an impedance mismatch or capacitance effect. Further experiments are necessary to test these hypotheses.

The auditory sustained potential is a low frequency, sustained, neural response with onset times of around 150 ms and amplitude to 6 μV (Picton et al., 1978). It is possible that this auditory sustained potential contributes to the low frequency component which we label as the DCA. Three pieces of evidence suggest that the DCA is dominated by artifact and not neural response: 1) The DCA has an onset time close to stimulus onset time while the sustained potential has a much later onset time. 2) The amplitude of the DCA can often be reduced by matching electrode impedance. 3) For some subjects, when electrode impedances are not matched, the amplitude of the DCA can be as large as 50 μV.

4.3. High frequency artifact attenuation

Most evoked potential studies using CI subjects use either a hardware or software low-pass filter with a cutoff frequency at around 50 or 35 Hz. The work presented here demonstrates that this low-pass filter will attenuate the HFA. Recent studies by Hofmann and Wouters (2010, 2012) used a high sample rate system to record auditory steady state responses from CI users. Their system could clearly resolve individual stimulation pulses, but rather than using a filtering approach, they showed that locating each stimulation pulse and linearly interpolating through it also removed the HFA. An interpolation approach to removing the HFA would also work with the system developed here. However, in practice filtering is easier to implement and more robust.

4.4. DC artifact estimation procedure

This study used tone or noise stimuli of 100, 300 or 500 ms duration where the temporal envelope contained only very fast fluctuations and the low frequency temporal envelope was non-fluctuating. This non-fluctuating, low frequency, stimulus envelope means that, just after stimulus onset and just before stimulus offset, the DC artifact will be flat. Since we know that the DC artifact will be flat in this period we can apply the randomization procedure described in Methods 2.4.3, *Constraining the Fit*. This will ensure that the fitting algorithm only fits to the mean amplitude (preserved by the randomization procedure) and not to any neural response (destroyed by the randomization procedure). To expand the DC estimation procedure to function with stimuli with a low frequency fluctuating envelope it would be necessary to remove the randomization procedure. This was not tested in this set of experiments and more work is needed to investigate the feasibility of using the DC estimation procedure with stimuli with fluctuating envelopes.

4.5. Clinical application of LAEP to CI users

A number of studies have indicated that cortical evoked potentials may be useful for predicting speech perception outcomes for CI subjects (Wable et al., 2000; Firszt et al., 2002; Kelly et al., 2005; Zhang et al., 2011), more so than earlier evoked potential responses such as auditory nerve electric compound action potentials (ECAPs) or auditory brainstem responses (Miller et al., 2008). However, two factors appear to have limited the clinical application of cortical evoked potentials for CI subjects. The first factor is the CI related artifact. The ICA based approach is useful in a research setting but, because of the necessity for multi-channel data, its practical application in a clinical setting is limited. This study provides a solution to this problem by showing how the CI related artifact can be attenuated using only single channel data, which are more easily obtained in a clinical setting. Recent work by our group, Mc Laughlin et al. (2012) and Beynon et al. (2008, 2012) has shown how LAEPs can be measured for CI subjects using the CI itself as a recording device, removing the need to attach scalp electrodes or have a dedicated LAEP acquisition system. Combining the LAEP CI recording technique with this single channel artifact cancellation approach would greatly increase the ease of access to LAEPs: just as an ECAP can be measured directly from the CI, so too could LAEPs. The second factor hindering the use of cortical evoked potentials in clinical use is that a stimulation paradigm or neural response that shows a strong correlation with speech perception in a large population of CI users has yet to be found. Firszt et al. (2002) showed, for a small population of CI users, a significant correlation between speech perception in quiet and a measure of mid-latency Na–Pa amplitude normalized for different stimulation levels. Zhang et al. (2011) found that a mismatch negativity measure could discriminate between good and bad performers on a speech perception task. By eliminating the need for multi-channel recordings, thereby reducing recording times, the single channel approach should facilitate the study of larger populations of CI subjects and may help in the development of an improved neural objective measure of CI performance. Behaviorally, it has been shown that more complex stimuli which probe the spectral discrimination of CI user can be used to provide a reasonable estimate of speech perception (Henry and Turner, 2003; Henry et al., 2005; Won et al., 2007). A preliminary study by our group has shown that combining this single channel artifact cancellation approach with a mismatch negativity paradigm using spectrally rippled stimuli can provide an objective neural estimate of a CI user's spectral discrimination (Mc Laughlin et al., 2013).

5. Conclusions

The single channel artifact cancellation approach described here can successfully attenuate both the high-frequency artifact produced by a cochlear implant and the DC artifact. The main advantage of this approach is that only single channel data are needed, simplifying the hardware and software requirements. The single channel approach should facilitate research into LAEPs recorded from CI users and could help develop a clinically applicable objective neural metric of CI performance.

Acknowledgments

We gratefully acknowledge the generosity of John D'Errico for contributing the polyfitn function to the Matlab File Exchange. We thank all the cochlear implant subjects who participated in the experiments. We also thank the two reviewers and the associate editor for their helpful comments and suggestions. This work was

partly supported by a Marie-Curie International Outgoing Fellowship (FP7 IOF 253047).

Appendix A. Supplementary data

Supplementary data related to this article can be found at http://dx.doi.org/10.1016/j.heares.2013.05.006.

References

Beynon, A., Luijten, B., 2012. Intracorporeal cortical telemetry (ICT): capturing EEG with a CI. In: 7th International Symposium on Objective Measures in Cochlear and Brainstem Implants. Amsterdam, p. 24.

Beynon, A., Luijten, B., Snik, A., 2008. The cochlear implant as an EEG-system: a feasibility study to measure evoked potentials beyond the ecap. In: 10th International Conference on Cochlear Implants and Other Implantable Auditory Technologies. San Diego.

Elberling, C., Don, M., 1984. Quality estimation of averaged auditory brainstem responses. Scand. Audiol. 13, 187–197.

Firszt, J.B., Chambers, R.D., Kraus, N., 2002. Neurophysiology of cochlear implant users II: comparison among speech perception, dynamic range, and physiological measures. Ear Hear. 23, 516–531.

Fu, Q.-J., 2002. Temporal processing and speech recognition in cochlear implant users. Neuroreport 13, 1635–1639.

Gilley, P.M., Sharma, A., Dorman, M., Finley, C.C., Panch, A.S., Martin, K., 2006. Minimization of cochlear implant stimulus artifact in cortical auditory evoked potentials. Clin. Neurophysiol. 117, 1772–1782.

Henry, B.A., Turner, C.W., 2003. The resolution of complex spectral patterns by cochlear implant and normal-hearing listeners. J. Acoust. Soc. Am. 113, 2861–2873.

Henry, B.A., Turner, C.W., Behrens, A., 2005. Spectral peak resolution and speech recognition in quiet: normal hearing, hearing impaired, and cochlear implant listeners. J. Acoust. Soc. Am. 118, 1111–1121.

Hofmann, M., Wouters, J., 2010. Electrically evoked auditory steady state responses in cochlear implant users. J. Assoc. Res. Otolaryngol. 11, 267–282.

Hofmann, M., Wouters, J., 2012. Improved electrically evoked auditory steady-state response thresholds in humans. J. Assoc. Res. Otolaryngol. 13, 573–589.

Kelly, A.S., Purdy, S.C., Thorne, P.R., 2005. Electrophysiological and speech perception measures of auditory processing in experienced adult cochlear implant users. Clin. Neurophysiol. 116, 1235–1246.

Mc Laughlin, M., Lopez Valdes, Alejandro, Viani, L., Walshe, P., Smith, J., Reilly, R.B., Zeng, F.-G., 2013. A spectrally rippled noise mismatch negativity paradigm for objectively assessing speech perception in cochlear implant users. In: 36th Annual Midwinter Meeting Abstract Book. Baltimore, p. 184.

Mc Laughlin, M., Lu, T., Dimitrijevic, A., Zeng, F.-G., 2012. Towards a closed-loop cochlear implant system: application of embedded monitoring of peripheral and central neural activity. IEEE Trans. Neural Syst. Rehabil. Eng. 20, 443–454.

Miller, C.A., Brown, C.J., Abbas, P.J., Chi, S.-L., 2008. The clinical application of potentials evoked from the peripheral auditory system. Hear. Res. 242, 184–197.

Picton, T.W., Woods, D.L., Baribeau-Braun, J., Healey, T.M., 1976. Evoked potential audiometry. J. Otolaryngol. 6, 90–119.

Picton, T.W., Woods, D.L., Proulx, G.B., 1978. Human auditory sustained potentials. I. The nature of the response. Electroencephalogr. Clin. Neurophysiol. 45, 186–197.

Viola, F.C., Thorne, J.D., Bleeck, S., Eyles, J., Debener, S., 2011. Uncovering auditory evoked potentials from cochlear implant users with independent component analysis. Psychophysiology 48, 1470–1480.

Wable, J., Van den Abbeele, T., Gallégo, S., Frachet, B., 2000. Mismatch negativity: a tool for the assessment of stimuli discrimination in cochlear implant subjects. Clin. Neurophysiol. 111, 743–751.

Won, J.H., Drennan, W.R., Rubinstein, J.T., 2007. Spectral-ripple resolution correlates with speech reception in noise in cochlear implant users. J. Assoc. Res. Otolaryngol. 8, 384–392.

Zeng, F.-G., Rebscher, S., Harrison, W.V., Sun, X., Feng, H., 2008. Cochlear implants: system design, integration and evaluation. IEEE Rev. Biomed. Eng. 1, 115–142.

Zhang, F., Anderson, J., Samy, R., Houston, L., 2010. The adaptive pattern of the late auditory evoked potential elicited by repeated stimuli in cochlear implant users. Int. J. Audiol. 49, 277–285.

Zhang, F., Hammer, T., Banks, H.-L., Benson, C., Xiang, J., Fu, Q.-J., 2011. Mismatch negativity and adaptation measures of the late auditory evoked potential in cochlear implant users. Hear. Res. 275, 17–29.

OPEN ACCESS Freely available online

PLOS ONE

Objective Assessment of Spectral Ripple Discrimination in Cochlear Implant Listeners Using Cortical Evoked Responses to an Oddball Paradigm

Alejandro Lopez Valdes[1]*, Myles Mc Laughlin[1,2], Laura Viani[3], Peter Walshe[3], Jaclyn Smith[3], Fan-Gang Zeng[2], Richard B. Reilly[1]

1 Trinity Centre for Bioengineering, Trinity College, Dublin, Ireland, **2** Hearing and Speech Laboratory, University of California Irvine, Irvine, California, United States of America, **3** National Cochlear Implant Programme, Beaumont Hospital, Dublin, Ireland

Abstract

Cochlear implants (CIs) can partially restore functional hearing in deaf individuals. However, multiple factors affect CI listener's speech perception, resulting in large performance differences. Non-speech based tests, such as spectral ripple discrimination, measure acoustic processing capabilities that are highly correlated with speech perception. Currently spectral ripple discrimination is measured using standard psychoacoustic methods, which require attentive listening and active response that can be difficult or even impossible in special patient populations. Here, a completely objective cortical evoked potential based method is developed and validated to assess spectral ripple discrimination in CI listeners. In 19 CI listeners, using an oddball paradigm, cortical evoked potential responses to standard and inverted spectrally rippled stimuli were measured. In the same subjects, psychoacoustic spectral ripple discrimination thresholds were also measured. A neural discrimination threshold was determined by systematically increasing the number of ripples per octave and determining the point at which there was no longer a significant difference between the evoked potential response to the standard and inverted stimuli. A correlation was found between the neural and the psychoacoustic discrimination thresholds ($R^2 = 0.60$, $p < 0.01$). This method can objectively assess CI spectral resolution performance, providing a potential tool for the evaluation and follow-up of CI listeners who have difficulty performing psychoacoustic tests, such as pediatric or new users.

Citation: Lopez Valdes A, Laughlin MM, Viani L, Walshe P, Smith J, et al. (2014) Objective Assessment of Spectral Ripple Discrimination in Cochlear Implant Listeners Using Cortical Evoked Responses to an Oddball Paradigm. PLoS ONE 9(3): e90044. doi:10.1371/journal.pone.0090044

Editor: Jyrki Ahveninen, Harvard Medical School/Massachusetts General Hospital, United States of America

Received August 23, 2013; **Accepted** January 28, 2014; **Published** March 5, 2014

Funding: This work was supported by a Higher Education Authority (HEA) Graduate Research Education Program in Engineering (GREP-Eng) scholarship to Alejandro Lopez Valdes, an EU FP7 Marie Curie International Outgoing Fellowship to Myles Mc Laughlin and the National Institutes of Health, the United States Department of Health and Human Services (P30 DC008369). The funders had no role in study design, data collection and analysis, decision to publish, or preparation of the manuscript.

Competing Interests: The authors have declared that no competing interests exist.

* E-mail: lopezvaa@tcd.ie

Introduction

A cochlear implant (CI) can partially restore hearing in deaf individuals, allowing most listeners to obtain 70–80% correct sentence perception in quiet [1]. A CI is now the standard treatment for severe to profound deafness worldwide, with infants as young as 6 months being considered for implantation [2]. In spite of this success, there remains a large amount of variability in speech perception outcomes among CI listeners. While factors such as duration of deafness, age at onset of deafness or duration of CI use affect performance [3,4], they cannot completely account for all the observed variability [5–10]. Factors such as temporal and spectral processing capabilities also contribute to speech perception outcomes [11–14]. To help understand the causes of this performance variability, and to improve clinical evaluation and follow-up of CI listeners, there is a need for tests which can objectively quantify performance in both pediatric and adult populations.

Standardized sentence and word recognition tests are useful for directly measuring speech perception in CI listeners. However, they cannot be used with pre-lingual children (a rapidly expanding user group), nor do they directly asses underlying mechanisms of speech recognition (i.e. spectral resolution). A spectral ripple discrimination test is a non-linguistic psychoacoustic method for probing a normal hearing listener's spectral resolution [15]. A number of studies have now shown that spectral ripple discrimination correlates with different aspects of speech perception and music perception in CI users [13,14,16,17].

To measure spectral ripple discrimination thresholds in CI listeners, standard psychoacoustic threshold tracking methods are normally employed. CI listeners actively listen to a number of intervals containing either a standard stimulus or its ripple-phase inverted counterpart. They are requested to report which interval contained the inverted stimulus by, for example, pressing a button corresponding to the interval. This approach produces reliable results in adults. Although experienced researchers might be able to use an observer based psychoacoustic procedure to measure spectral ripple discrimination thresholds in infants [18], these standard psychophysical approaches are difficult to apply to special populations such as pediatric, pre-lingually deafened or non-compliant users in clinical practice.

An alternative to psychoacoustic methods is to employ an objective neural response to predict behavioral outcomes. An

advantage of this approach is that listeners do not need to respond to the stimuli and often need not attend to the stimuli. Neural responses from the auditory nerve and brainstem in CI listeners have been shown to correlate reasonably well with threshold and comfort stimulation levels [19–22], while cortical evoked potentials have been shown to correlate with higher level outcomes such as speech perception [23–26], musical perception and auditory plasticity [27–32]. In particular, mismatch negativity (MMN) responses have been proposed as an objective index of auditory discrimination for different clinical conditions [33]. The MMN response can be obtained, via an unattended oddball paradigm, as the evoked potential difference between a frequently presented stimulus (standard) and a less frequently and randomly presented different stimulus (deviant or oddball).

The aim of this study was to use an unattended oddball paradigm to develop and validate a completely objective method for measuring spectral ripple discrimination thresholds in adult CI listeners. An objective method for measuring spectral ripple discrimination thresholds would potentially provide an additional tool when standard psychophysical approaches are difficult to apply to certain CI populations.

Materials and Methods

Subjects and Ethics Statement

Subjects. Nineteen adult CI listeners (6 male, 13 female) participated in the present study at two separate locations: Trinity Centre for Bioengineering, Trinity College Dublin (n = 15) and Hearing and Speech Laboratory, University of California Irvine (n = 4). One bilateral subject was evaluated separately for both ears yielding a total of 20 ears tested. Exclusion criteria applied to subjects under 18 years of age and subjects with cognitive or learning disabilities. There were no subjects withdrawn from this study. Subjects were aged between 31 and 79 years (mean 56, standard deviation 15). They used either a Cochlear (n = 17), Med-El (n = 1) or Advanced Bionics (n = 1) implants (device details on implant type and usage experience are shown in Table 1). All subjects used monopolar stimulation mode.

Ethics Statement

Experimental procedures were approved by the Ethics (Medical Research) Committee at Beaumont Hospital, Beaumont, Dublin, the Ethical Review Board at Trinity College Dublin and The University of California Irvine's Institutional Review Board. Written informed consent was obtained from all subjects.

Psychoacoustic Methods

Psychoacoustic Stimuli. Psychoacoustic spectral ripple discrimination thresholds were determined in all subjects using stimuli similar to that employed by Won et al. [14]. Stimuli were generated by summing 250 pure tones ranging from 250 to 5000 Hz. The amplitudes of the pure tones were determined by a full-wave rectified sinusoidal envelope on a logarithmic amplitude scale. The ripple peaks were spaced equally on a logarithmic frequency scale. The starting phases of the components were randomized for each presentation. The ripple stimuli were generated with 14 different densities, measured in ripples/octave. The ripple densities differed by ratios of 1.414 (0.125, 0.176, 0.250, 0.354, 0.500, 0.707, 1.000, 1.414, 2.000, 2.828, 4.000, 5.657, 8.000, and 11.314 ripples/octave). Standard and ripple-phase inverted stimuli were generated de novo in each trial run. For standard stimuli, the phase of the full-wave rectified sinusoidal spectral envelope was set to zero radians, and for phase-inverted stimuli, it was set to $\pi/2$. The stimuli were 500 ms in duration and 50 ms on and off cosine squared ramps were applied. Stimuli were filtered with a long-term, speech-shaped filter [34]. All stimuli were generated in MATLAB (MathWorks, Natick, MA) at 44.1 kHz and presented via a standard PC soundcard.

For both the psychoacoustic and evoked potential testing, stimuli were presented via the audio line-in on the CI at the most comfortable level, determined for each subject using a 0 (silence) to 10 (too loud) loudness scale, with 6 being the most comfortable level. To limit the effects of any unwanted background noise the CI microphone volume and sensitivity were set to the minimum allowable values. Subjects used their everyday speech processing strategy without any special adjustments other than changes to the microphone volume and sensitivity. Stimuli were always presented monaurally.

Psychoacoustic Procedure. A two-down, one-up, three-alternative forced-choice [35] paradigm was used to track the psychoacoustic spectral ripple discrimination threshold. Within one trial, two of the intervals were randomly selected to present the standard stimulus whilst the remaining interval presented the inverted stimulus, with all three intervals having stimuli with the same number of ripples/octave. If the subject's spectral resolution is sharp enough to resolve the spectral peaks and valleys, they should hear a difference in the standard and inverted stimuli [14,17]. The subject was asked to select the interval which was different by pressing a button on a graphical interface. After two consecutive correct responses, the number of ripples/octave was increased by a ratio of 1.414. As the number of ripples/octave increased the standard and inverted stimuli began to sound more similar. After one incorrect response the number of ripples/octave was decreased to the previously tested value. A run was terminated after 13 reversals. The psychoacoustic spectral ripple discrimination threshold was defined as the mean of the last eight reversals on the three-alternative forced-choice threshold tracking function [35]. All subjects completed at least five repetitions of the test to minimize any learning or attention effects. The final threshold was taken as the mean of all completed tests.

Evoked Potential Methods

Evoked Potential Stimuli. The stimuli used in the evoked potential paradigm were similar to those used in the psychoacoustic paradigm except that 4000 pure tones ranging from 100 to 8000 Hz were used to cover the full frequency range of the CI filter bank. The lower pure tone range in the psychoacoustic stimuli allowed for the stimuli to be generated and presented faster while still presenting some energy to the highest CI high-frequency band.

Standard and ripple phase-inverted stimuli with durations of either 300 or 500 ms and with 0.125, 0.25, 0.5, 1, 2, 4 and 8 ripples/octave were generated and stored. Examples of the stimuli characterization at one and four ripples/octave can be seen in Fig. 1. There was no significant difference for the use of 300 or 500 ms stimuli with respect to the CI artifact, therefore, data from both stimuli duration were pooled together for analysis. The same set of stored stimulus tokens were used for all presentations to all subjects. In Trinity College Dublin stimuli were presented via a standard PC soundcard (44.1 kHz sampling rate) and in University of California, Irvine stimuli were presented using a USB digital to analog converter (DAC, 44.1 kHz sampling rate) (NI-USB 6221, National Instruments, Austin, TX).

Evoked Potential Acquisition. Fig. 2 shows a wideband, high-sampling rate, acquisition system that uses single-channel artifact attenuation to record late auditory evoked potentials in response to the spectral ripple stimuli presented in an oddball paradigm. The setup, along with the artifact attenuation

Table 1. Psychoacoustic and neural discrimination thresholds.

Subject ID	Implant	Tested Ear	Years of CI Experience	Psychoacoustic Spectral Ripple Discrimination Threshold (RPO)	Neural Spectral Ripple Discrimination Threshold (RPO)		
					Positive Area	Negative Area	Total Area
UCI 01	Maestro	Left	2	0.574	0.420	0.398	0.434
UCI 02	Freedom	Right	5	1.403	1.008	0.900	0.989
UCI 03	Freedom	Left	9	2.210	3.202	6.335	5.974
UCI 03	Freedom	Right	1	1.542	2.085	1.188	2.407
UCI 04	Freedom	Right	4	2.595	1.252	0.659	1.045
TCD 01	Freedom	Left	3.5	1.158	1.793	0.665	0.763
TCD 02	Freedom	Left	4	0.381	0.193	0.337	0.225
TCD 03	Clarion 1.2	Right	12	0.948	0.909	0.589	0.953
TCD 04	Freedom	Left	7	0.618	0.248	0.221	0.237
TCD 05	Freedom	Left	5	2.172	2.957	2.861	2.987
TCD 06	Freedom	Right	1	0.658	*	*	*
TCD 07	Freedom	Right	1	0.778	*	0.161	0.150
TCD 08	CI512	Right	1	0.400	0.473	0.239	0.409
TCD 09	Freedom	Left	3.5	0.235	0.176	*	0.138
TCD 10	Freedom	Right	3.5	0.312	0.821	0.546	0.739
TCD 11	CI24RE	Right	9	1.113	0.489	0.833	0.782
TCD 12	Freedom	Right	4	0.931	1.618	1.497	1.597
TCD 13	CI24R	Left	8	0.463	*	0.461	0.482
TCD 14	CI24M	Right	12	1.503	1.717	1.870	1.827
TCD 15	Freedom	Left	5	0.240	*	*	*

RPO- Ripples per octave.

* Unable to estimate a neural spectral ripple discrimination threshold.

doi:10.1371/journal.pone.0090044.t001

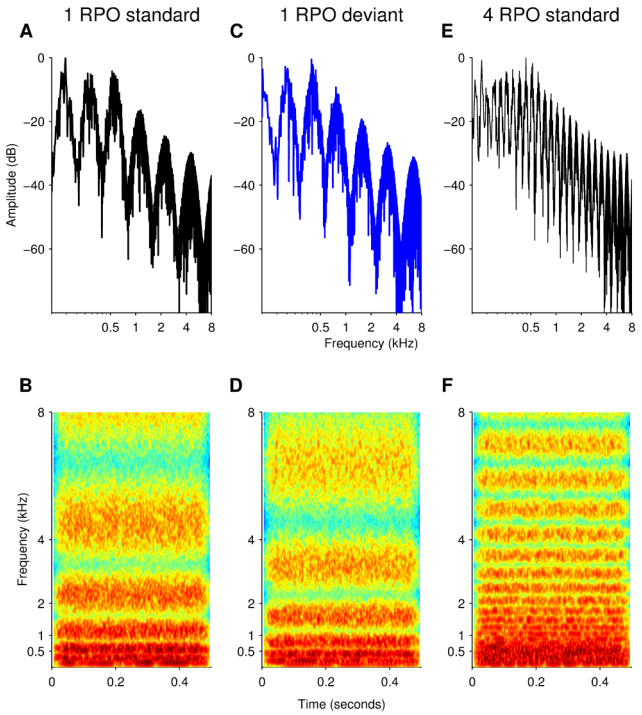

Figure 1. Stimuli characterization. (A) Frequency spectrum of a 500 ms standard stimulus with spectral peak density of one ripple per octave (RPO). Stimuli were composed of the sum of pure tones in a range of 0.25–5 kHz (psychoacoustic) or 0.1–8 kHz (electrophysiology). Spectral amplitudes were defined by a full-wave rectified sinusoidal envelope. One spectral peak can be clearly distinguished at the 0.5–1 kHz octave. Peak to valley amplitude of 30 dB as well as the high frequency attenuation of the speech-shaped filter can also be seen. (B) Spectrogram of the standard stimulus described, showing the frequency content of the stimulus along the 500 ms duration. Spectral peak density of one RPO can clearly be resolved in the 4–8 kHz octave. (C) Frequency spectrum of the corresponding phase-inverted, or deviant, stimulus employed along with the standard stimulus at one RPO in an oddball paradigm. The spectral envelope is shifted by $\pi/2$ with respect to the standard stimulus, as observed in the 0.5–1 kHz octave. (D) Spectrogram of the deviant stimulus, showing the inversed frequency content along the 500 ms duration with respect to the standard stimulus. (E) Frequency spectrum of a standard stimulus with spectral peak density of four RPO showing the increased spectral density with respect to the one RPO stimuli. (F) Spectrogram of the standard stimulus at four RPO. Spectral peak density of four RPO can clearly be resolved in the 4–8 kHz octave.
doi:10.1371/journal.pone.0090044.g001

procedure, is described in detail elsewhere [36]. Briefly, the sampling rate on the analog to digital converter (ADC) (NI-USB 6221, National Instruments, Austin, TX) was set to 125 kHz, the amplifier (SRS 560, Stanford Research Systems, Sunnyvale, CA) gain was set to 2000, the amplifier high-pass filter was set to 0.03 and the low-pass filter to 100 kHz. Standard gold cup surface electrodes were placed at Cz, on the mastoid and on the collarbone, these last two electrodes were placed contralateral to the CI location. The positive end of the amplifier was connected to Cz, the negative end to the mastoid and the ground to the collarbone. Electrode impedances were always below 5 kΩ and care was taken to ensure that impedances were matched to within 1 kΩ to minimize low frequency artifacts [36]. The output of the amplifier was connected to one channel on the ADC. A trigger pulse generated simultaneously with the stimulus, and presented on a separate channel, was connected to a second channel on the ADC and used to synchronize stimulus presentation and acquisition.

Evoked Potential Procedure. Standard and ripple phase-inverted stimuli with the same number of ripples/octave were presented in an unattended oddball paradigm. The deviant stimulus was the ripple phase-inverted stimulus, having an occurrence probability of 10%, and the standard stimulus was the non-inverted stimulus. The inter-onset interval for each stimulus presentation was one second. One run began with 20 presentations of the standard stimulus after which the deviant randomly occurred at least once in every 10 stimulus presentations, with the additional condition that a deviant was never to be followed by another deviant. The paradigm was repeated at least four times for every subject, each time using stimuli with a different number of ripples/octave. Subjects were instructed to ignore the stimulus and to minimize movement to avoid movement artifacts in the recordings. Each oddball paradigm lasted approximately 12–15 minutes. Subjects watched a silent captioned film and rest breaks were provided after each run or upon subject's request. EEG data collection lasted approximately one hour per subject. At Trinity Centre for Bioengineering the acquisition sessions took place in a dedicated EEG room, while at the University of California Irvine, the sessions took place in a sound booth.

Evoked Potential Epoching. Raw EEG data were segmented into long epochs of 1100 ms, 300 ms pre- to 800 ms post-stimulus onset to avoid filter edge affects. Shorter epochs of 100 ms pre- to 500 ms post-stimulus were used for plotting the data. A baseline correction of 150 ms pre-stimulus was applied in all filtered epochs. Epochs were classified as response to standard or deviant stimuli and averaged across presentations. Online averaging and artifact attenuation allow the real time display of the evoked potential response to both standard and deviant stimuli. To speed up data collection a run was terminated when collecting more deviant responses did not significantly change the shape of the averaged deviant waveform. This change was evaluated by measuring the sum of squared differences of the averaged deviant epochs every time a new epoch was included, when the sum of squared differences stabilized at a low value it was determined that no significant change would be produced with the addition of more epochs. This was typically once 60 or 70 deviant responses were acquired, with a minimum of 50 deviants per run always being collected. A difference (or mismatch) waveform was calculated by subtracting the response to the standard stimuli from the response to the deviant stimuli. The oddball paradigm was repeated using stimuli with different numbers of ripples/octave, yielding one difference waveform for each ripple/octave stimulus.

Evoked Potential Artifact Attenuation. Mc Laughlin et al. [36] showed that with the wideband, high sampling-rate acquisition system, the CI related artifact consists of two components: a high frequency component which is a direct representation of the stimulation pulses and a low frequency component which is related to the envelope of the stimulation pulses. A 2nd order Butterworth band-pass filter (2–20 Hz, 12 dB/octave slope) was applied to the averaged standard and deviant responses (Fig. 3A and B single responses before filtering, Fig. 3C and D averaged responses after filtering). The low-pass edge of this filter attenuated the high frequency artifact component and the high-pass edge removed drift. The filter was applied using a zero-phase forward and reverse digital filtering method (filtfilt command, MATLAB).

It was observed that, within a subject, the signal envelopes derived from the CI stimulation pulse sequence associated to the standard and deviant stimuli were similar (compare Fig. 3A and B). A cross-correlation of 112 sets of standard and deviant CI

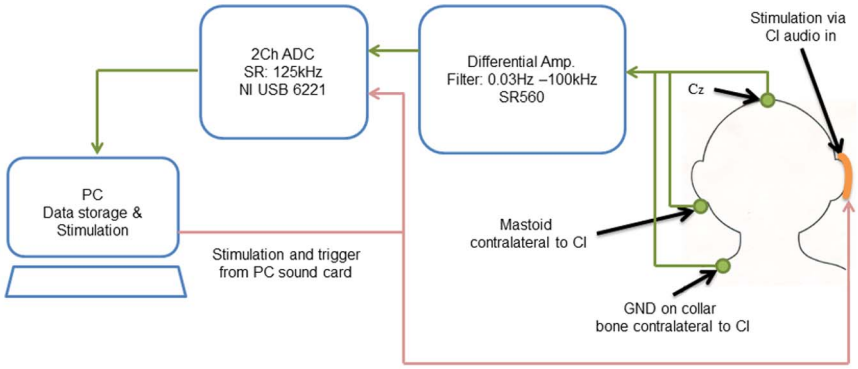

Figure 2. Single-channel acquisition set-up. Single-channel EEG acquisition system, featuring wideband and high-sampling rate recordings. EEG is recorded from electrode position Cz, referenced to the mastoid contralateral to the tested ear and grounded on the collar bone. The EEG signal is amplified with a biological differential pre-amplifier (SR560, Stanford Research System, Sunnyvale, CA) with filter settings at 0.03 Hz and 100 kHz. The signal is then digitized with an ADC (NI-USB 6221, National Instruments, Austin, TX) sampled at 125 kHz and recorded with a custom made software made in MATLAB (The MathWorks, Natick, MA). Stimulus and trigger presentation is done through the sound card of the computer. The trigger is fed to the ADC for event synchronization and the stimulus is presented via a personal audio cable to the auxiliary port of the subject's speech processor.
doi:10.1371/journal.pone.0090044.g002

stimulation pulse sequences supported this observation (mean normalized correlation = 0.8871, standard deviation = 0.1597). With the result that any low frequency artifact component was equally present in both the response to the standard and the response to the deviant (compare onset and offset artifacts in Fig. 3C and D), calculating the difference waveform adequately attenuated any low frequency artifact components, leaving a difference waveform dominated by neural response (Fig. 3E).

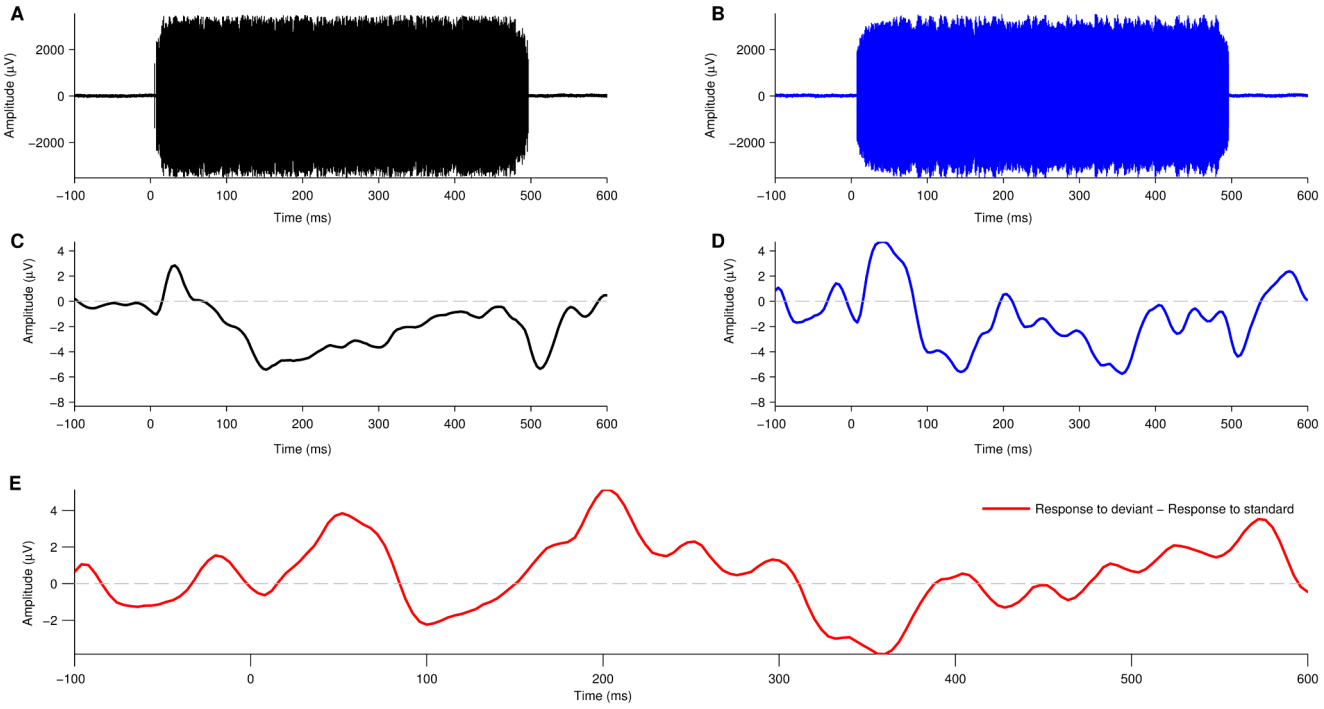

Figure 3. Artifact attenuation and evoked potential extraction. (A)–(B) Single EEG acquisition epoch of a 500 ms stimulus presented to a CI user. Data acquisition at a high-sampling rate (125 kHz) allows for the CI artifact to be clearly resolved from the recorded data as a high frequency and large amplitude component present during the 500 ms of stimulus duration (standard in black, deviant in blue). (C)–(D) Applying a 2nd order Butterworth band-pass filter (2–20 Hz) to the averaged epochs, recorded from an oddball paradigm, it is possible to attenuate the CI artifact and extract the evoked potential (EP) elicited to the each stimulus type (standard in black, deviant in blue). The N100, characteristic of auditory EPs can be identified in both standard (C) and deviant (D) stimuli types as a negative peak at around 100–150 ms. In some cases, after filtering, a low-frequency artifact is present at stimulus onset and offset with similar shape and amplitude in both standard and deviant responses. (E) A difference waveform is calculated by subtracting the neural response elicited to the standard stimuli from the neural response elicited to the deviant stimuli. This method allows further attenuation of residual low-frequency artifacts.
doi:10.1371/journal.pone.0090044.g003

Evoked Potentials: Spectral Ripple Discrimination Thresholds

Hypothesis and Methodological Overview. If a listener can acoustically perceive a difference between a standard and deviant stimulus, the evoked potential response to the deviant stimulus, when presented in an oddball paradigm, will differ in shape from that evoked by the standard stimulus [33,37]. This response is normally quantified by calculating a difference waveform, i.e. deviant response minus standard response and is often referred to as mismatch negativity. If the standard and deviant responses are the same, the difference waveform should be flat; while if they differ, the difference waveform will show oscillations. In practice the noise inherent in evoked potential recordings means that even if the underlying standard and deviant waveforms are identical the difference waveform will still show some oscillations. Therefore, to calculate a neural discrimination threshold it was necessary to first quantify the amount of noise in the difference waveform and then define what quantifies a significant difference waveform response.

Calculating the Difference Waveform Noise Floor. The noise present in one difference waveform was calculated by applying a bootstrap method to all the standard responses collected for that subject during that run. A randomly chosen sub-sample of 10% of all standard responses was chosen and averaged together to create a bootstrapped deviant response (Fig. 4A, blue line). The remaining 90% of the standard stimuli was then averaged together to create bootstrapped standard response (Fig. 4A, black line). The bootstrapped deviant was subtracted from the bootstrapped standard to give a bootstrapped difference waveform (Fig. 4B, red line). If no noise were to be present in the recording this bootstrapped difference waveform would be completely flat. Thus, oscillations present in the bootstrapped difference waveform quantify the noise present in the recording. The bootstrap procedure was repeated to generate 54 separate bootstrapped difference waveforms. The noise floor was defined as the standard deviation of all bootstrapped difference waveforms at each time point for positive and negative values (Fig. 4B, black lines).

Defining a Significant Difference Waveform Response. To quantify the difference waveform the area above the noise floor within a 90 to 450 ms time window was calculated. This time window allows for the expected evoked potential components such as N1, P2, N2, P3 or MMN to be included in the analysis. Given that the difference waveform is defined as microvolts in function of time in milliseconds, the area above the noise floor is defined as microvolts times milliseconds 'μVms'. A neural spectral ripple discrimination threshold was then defined as the point at which this area dropped below a predetermined significance level. As the aim of this study was to develop an objective evoked potential test to accurately predict the psychoacoustic spectral ripple discrimination threshold, the significance level was determined by calculating the neural threshold for a range of different significance levels and selecting the significance level which gave the best correlation with the psychoacoustic threshold across all subjects. The 'Defining a Significance Level' section presents details of how this procedure was applied together with results from a validation study where data from all 19 subjects were randomly partitioned into two groups. One group was used to estimate the significance level and the other group to test the accuracy of this significance level by predicting the psychoacoustic spectral ripple discrimination threshold.

Results

Psychoacoustic Spectral Discrimination Thresholds

Table 1 summarizes the individual spectral ripple discrimination thresholds for all ears tested. The range (0.235 to 2.595 ripples/octave) and mean (1.012 ripples/octave) are in general agreement with previously reported values for spectral ripple discrimination in CI listeners [13,14,38].

Evoked Potential Spectral Ripple Discrimination Thresholds

Evoked Potentials and Difference Waveform. Fig. 5A shows an example of evoked potential waveforms recorded using an oddball paradigm in response to a 0.25 ripples/octave stimuli. The black line shows the response to the standard (standard spectral ripple stimulus) and the blue line the response to the deviant (inverted spectral ripple stimulus). This user reported hearing a difference between the standard and the deviant stimulus (psychoacoustic spectral ripple discrimination threshold of 2.210 ripples/octave) and correspondingly there was a marked difference in the response to the deviant. The deviant response has larger amplitude P2 than the standard response. It also contains a N3 and P4 component which are not present in the standard response. Fig. 5B shows the difference waveform calculated by subtracting the standard from the deviant response. The P2, N3 and P4 differences are apparent in the difference waveform and, importantly, their peaks are above or below the noise-floor indicating that the neural response to the deviant is significantly different than the neural response to the standard.

To determine a neural spectral ripple discrimination threshold, responses to spectral ripple stimuli with an increasing number of ripples/octave were measured in all subjects. The standard and deviant responses for one subject to stimuli with 0.25, 0.5, 1 and 2 ripples/octave are shown in Fig. 6A. The large positivity, around 40 ms, present in all standard and deviant responses is probably an onset artifact. The standard responses to the 0.25, 0.5, 1 and 2 ripples/octave stimuli are similar. However, the deviant responses change as the number of ripples/octave is increased. The deviant response to the 0.25 ripples/octave stimulus shows a large increase in the N1 and P2 component when compared with the standard response. As the number of ripples/octave increases (and the stimuli begin to sound more alike) this N1-P2 difference becomes smaller and delayed, until at 2 ripples per octave the response to the deviant is essentially the same as the response to the standard. This subject had a psychoacoustic spectral ripple discrimination threshold of 1.503 ripples/octave. Fig. 6B shows the difference waveforms. Since the onset artifact (around 40 ms) was equally present in both standard and deviant responses it is significantly attenuated in the difference waveform. Calculating the area above and below the noise floor (shaded) within a 90–450 ms time window allows a quantification of the difference in the neural response to the standard and deviant stimuli. This area is large for 0.25 ripples/octave where the subject perceives a clear difference between the standard and deviant stimuli and is negligible at 2 ripples/octave where the subject reports that the standard and deviant stimuli sound the same.

Defining a Significance Level. In Fig. 7, the area above and below the noise floor, and the total area, are plotted as a function of ripples/octave for the same subject shown in Fig. 6. It is clear that as the number of ripples/octave increases, the area above and below the noise floor decreases, i.e., the standard and deviant responses become similar. To allow the objective estimation of neural spectral ripple discrimination thresholds, a significance level (i.e. an area in microvolt times millisecond 'μVms') was defined as

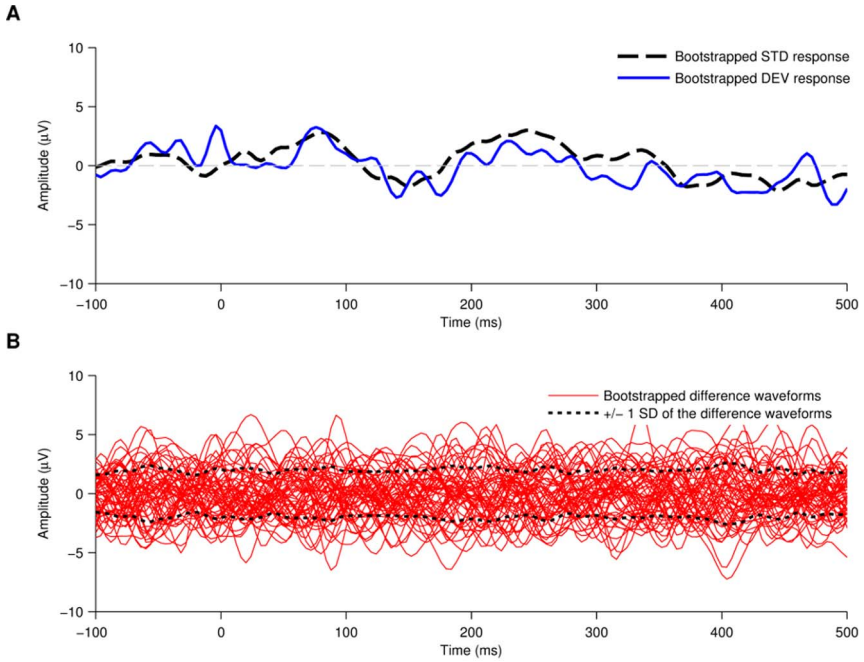

Figure 4. Noise floor calculation of the neural response. (A) The noise floor was calculated with a statistical bootstrap method. A random 10% sub-sample of epochs from the standard stimulus type was averaged to create a bootstrapped deviant response whilst the remaining epochs were averaged together to create a bootstrapped standard response. (B) A difference waveform was calculated by subtracting the bootstrapped standard response from the bootstrapped deviant response. This process was repeated 54 times, each time with a different randomly selected 10% sample of standard epochs. The noise floor of the signal was defined as +/− one standard deviation of the 54 resulting difference waveforms.
doi:10.1371/journal.pone.0090044.g004

the threshold below which area differences between the standard and deviant response can be considered perceptually negligible.

A bootstrap method was employed to define and validate this significance level for the three different area measurements. The approach, described in detail below and in a flow chart in Fig. 8A,

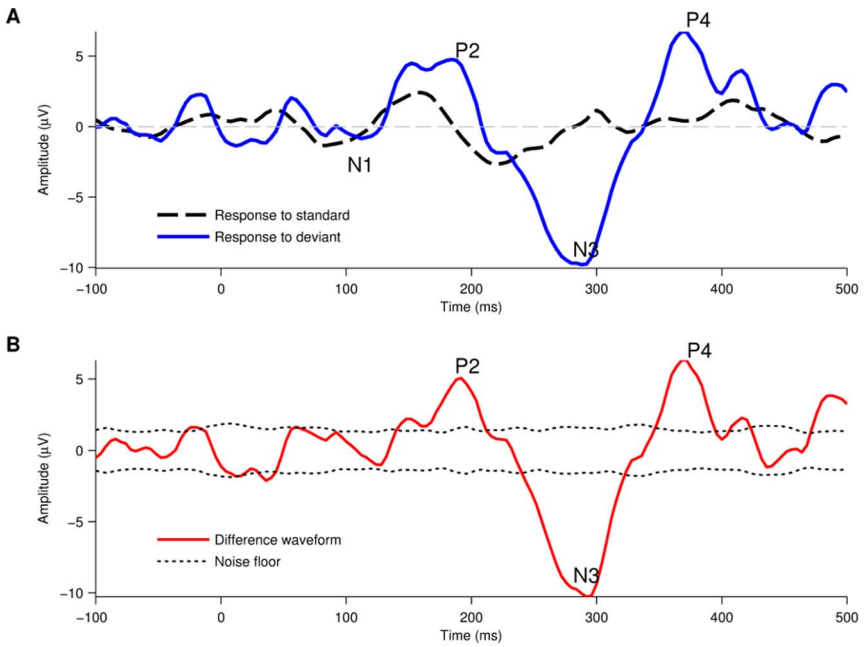

Figure 5. Example of the difference waveform elicited using the oddball paradigm. (A) Evoked potential responses elicited to 608 standard stimuli and 65 deviant stimuli at 0.25 RPO. When the standard and deviant stimuli are perceived as different sounds, the morphology of the neural response to the deviant stimuli (blue trace) is significantly different than the response to the standard stimuli (dashed, black trace). (B) The difference waveform represents the mismatch between the responses elicited to each stimulus type.
doi:10.1371/journal.pone.0090044.g005

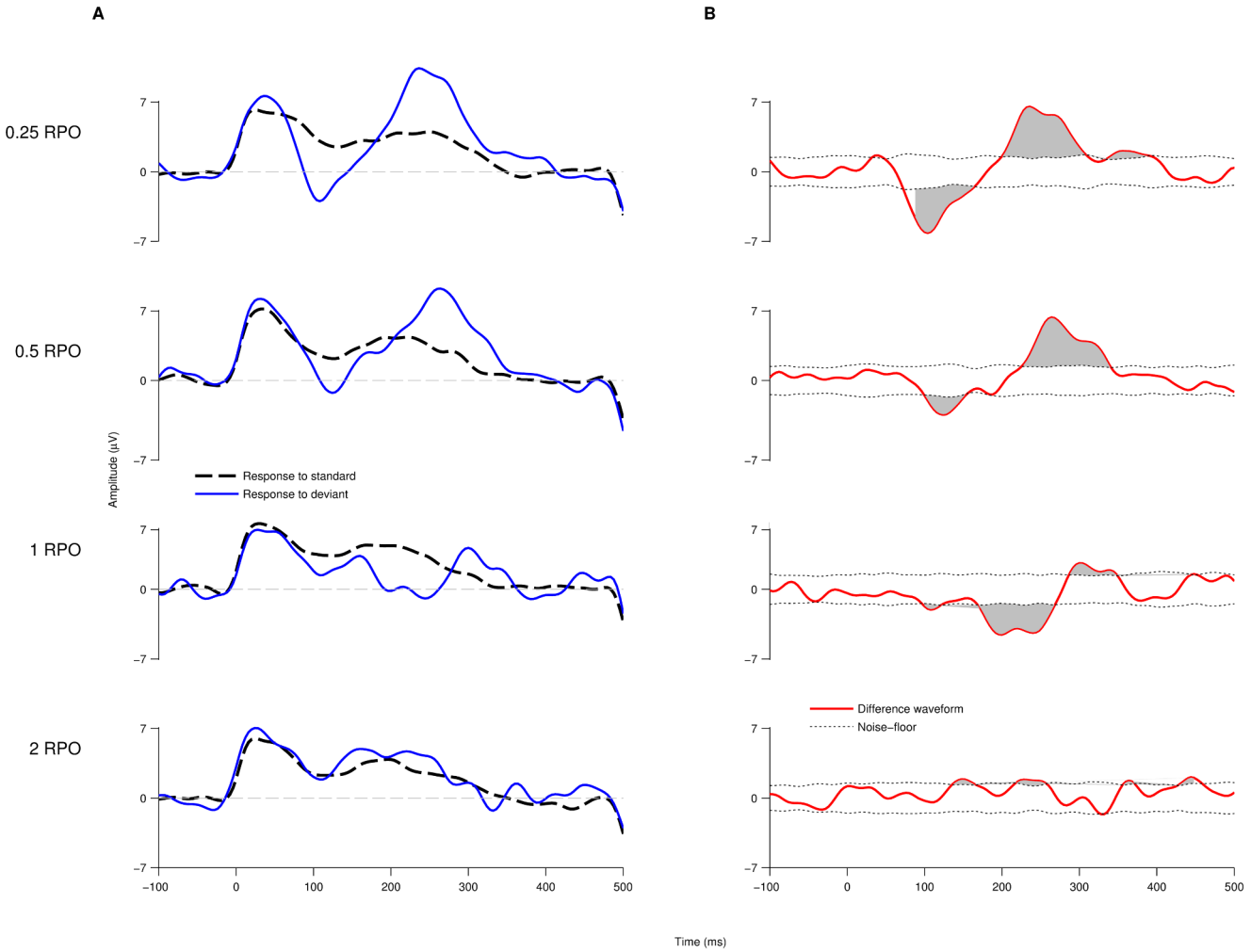

Figure 6. Sequential decrease of the difference waveform's area above the noise floor. (A) Evoked potential traces of standard and deviant stimuli elicited at 0.25, 0.5, 1 and 2 RPO. As the spectral density increases, the neural responses to the standard and deviant stimuli become more similar. (B) The difference waveform at each spectral density shows a sequential decrease of the mismatch between the responses elicited to each stimulus type. The area above the noise floor of the signal (shaded grey) is taken as an indicator of said mismatch decrease.
doi:10.1371/journal.pone.0090044.g006

operated by first dividing the data into two groups. The first group (a determination group) was employed to determine one significance level, for all members, which gave the best correlation with the known psychophysical thresholds. The second group (an estimation group) was then employed to test how well this significance level could estimate the known psychophysical threshold.

Data from the 20 tested ears were separated in two groups: a determination and an estimation group. The determination group contained 12 randomly selected datasets whilst the estimation group contained the remaining 8 datasets. This partition ratio was chosen so that the estimation group represented more than a third of the total sample. Each dataset contained at least four measurements presenting stimuli with different ripples/octave. For the determination group, the neural spectral ripple discrimination threshold was calculated and linearly regressed with the measured psychoacoustic threshold for each subject. If the area never went below the significance level the dataset was excluded. This regression was tested for a range of 19 different predetermined significance levels, ranging from 10 μVms to 100 μVms at 5 μVms increments, yielding 19 different (determination) R^2 and p-values (Fig. 8B). Significance levels, for which the regression yielded a p-value greater than 0.01 or which excluded more than two datasets, were discarded. From the remaining significance levels, the one that yielded the greatest regression R^2 was selected (Fig. 8B, red dot). The selected significance level was applied to the estimation group to determine the neural spectral ripple discrimination threshold and then quantify, using linear regression, how well this predicted the psychophysical threshold (Fig. 8C). If this (estimation) regression yielded a p-value less than 0.05 with no dataset exclusions then the significance level was accepted. Otherwise, the significance level was rejected. One point on Fig. 8C represents one of the accepted estimation R^2 and p-values. Fig. 8C shows the p-values as a function of the regression R^2 value for the estimation group's linear regression.

This process was repeated, each time using a different random partitioning of the datasets into determination and estimation groups, until 20 significance levels that satisfied the criteria were generated (Fig. 8D). This shows that the significance level chosen performs accurately when estimating the psychoacoustic thresholds measured for each subject. The final significance levels defined for this study (and employed in Section 3.4) was the

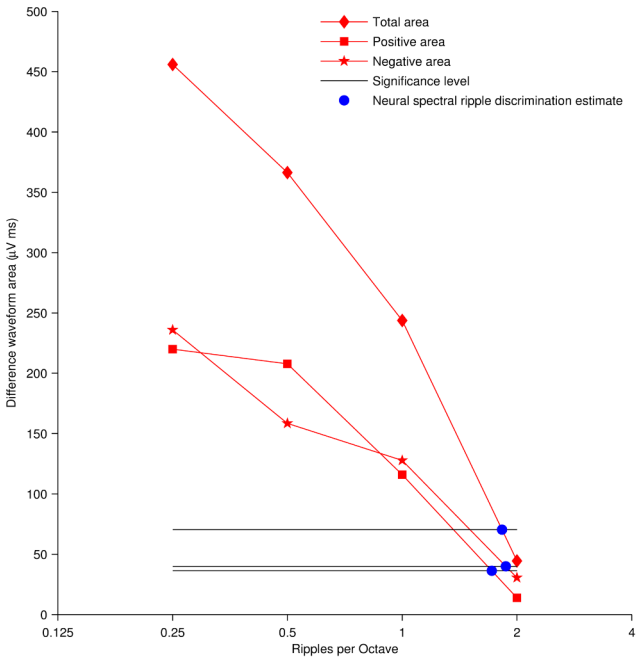

Figure 7. Estimation of the spectral ripple discrimination threshold based on neural responses. The neural spectral ripple discrimination threshold is estimated as the point where the mismatch between the neural responses dropped below a set significance level. Thresholds were estimated with three different area above the noise floor measurements: positive area, negative area and total area above the noise floor.
doi:10.1371/journal.pone.0090044.g007

average of the accepted significance levels. The entire process was repeated for the positive, negative and total area measurements.

For the total area the mean significance level was determined to be 70.4 μVms (17.7 standard deviation). Two tested ears did not yield a neural threshold (Fig. 9A). For one tested ear (TCD 06 in Table 1) the area above the noise floor for all recordings was below the significance level defined, and for the remaining exclusion (TCD15 in Table 1), the area above the noise floor did not drop below significance level. The mean neural threshold across 18 datasets was 1.230 ripples/octave (1.386 standard deviation).

For the positive area the mean significance level was determined to be 36.3 μVms (13.8 standard deviation). Four datasets did not yield a neural threshold using the positive area (Fig. 9B). The area above the noise floor from two tested ears (TCD 13 and TCD 15 in Table 1) did not drop below the significance level in any of the four recordings. Contrastingly, the area above the noise floor from the remaining two exclusions (TCD 06 and TCD07 in Table 1) was below the significance level in all four recordings. Hence, it was not possible to estimate the neural spectral ripple discrimination threshold. The mean neural threshold for the remaining 16 datasets was 1.121 ripples/octave (0.920 standard deviation).

For the negative area the mean significance level was determined to be 40 μVms (3.9 standard deviation). Three datasets did not yield a neural threshold (Fig. 9C). The area above the noise floor of three tested ears (TCD 06, TCD 09 and TCD15 in Table 1) was below the significance level in every recording, making it not possible to estimate a neural spectral ripple discrimination threshold with the defined significance level. The mean neural threshold across 17 datasets was 1.116 ripples/octave (1.458 standard deviation). The individual neural thresholds for the positive, negative and total area are reported in Table 1.

Correlation between Psychoacoustic and Neural Thresholds

Linear regression of the psychoacoustic spectral ripple discrimination thresholds with the neural spectral ripple discrimination thresholds produced a squared Pearson's correlation coefficient (R^2) of 0.60 and p-value$<$0.01 for total area (Fig. 9A), $R^2 = 0.65$ and p-value$<$0.01 for the positive area (Fig. 9B), and $R^2 = 0.50$ and a p-value$<$0.01 using the negative area (Fig. 9C).

Results from paired t-tests between psychoacoustic and neural thresholds, in all three area measurements, show no significant difference between the metrics: p-value = 0.75, t = 0.32 for positive area; p-value = 0.93, t = 0.09 for negative area; and p-value = 0.68, t = −0.41 for total area above the noise floor. A Steiger's Z test was employed to compare the correlations derived from the positive, negative and total area calculations. Results indicate that there is no significant difference between: the positive area and negative area correlations (Z = 1.51, p-value$>$0.05); the positive area and the total area correlations (Z = 1.14, p-value$>$0.05) and; the negative area and the total area correlation (Z = −1.34, p-value$>$0.05).

Discussion

The present study developed and validated a method to objectively assess spectral ripple discrimination in a population of CI listeners using an oddball EEG paradigm. Using a clinically applicable single channel set-up [36], it was possible to acquire evoked potential responses to standard and deviant stimuli in CI listeners. Analysis of the difference waveform showed a strong correlation with behavioral spectral ripple discrimination thresholds, validating the utility of this approach as a clinical assessment tool.

Artifact removal

It was possible to distinguish the expected N1-P2 complex from the evoked potential traces. The large positivity at around 40 ms and negativity at around 500 ms after stimulus onset found in some subjects (see Fig. 3C and Fig. 3D) are most likely on-set and off-set artifacts caused by high-pass filtering of the low frequency (or pedestal) artifact component identified by Mc Laughlin et al. [36] and others [39–42] related to the CI's response to the stimuli. The 40 ms delay in the on-set artifact is caused by a combination of the rise time of the stimuli (50 ms), the CI processor delay (~5 to 8 ms as observed in single stimulus presentations, see Fig. 3A and Fig. 3B) and the high-pass filter characteristics. When present, on-set and off-set artifacts where equally present in both standard and deviant responses. Thus, the subtraction operation, employed to obtain a difference waveform, attenuated these artifacts. The analysis time window (90 to 450 ms) also minimized any potential artifact influence on the area measurement used to determine the neural spectral ripple discrimination threshold.

Objective assessment of neural thresholds

Judging the presence or absence of a neural response in cortical evoked potentials (or in a difference waveform) is generally a subjective task. This study developed and validated an objective statistical approach to determine the point at which a response in the difference waveform became perceptually non-significant. Parts of this approach are similar to the integrated mismatch negativity metric developed by Ponton et al. [43]. Measuring the peak amplitude of specific components in the spectral ripple

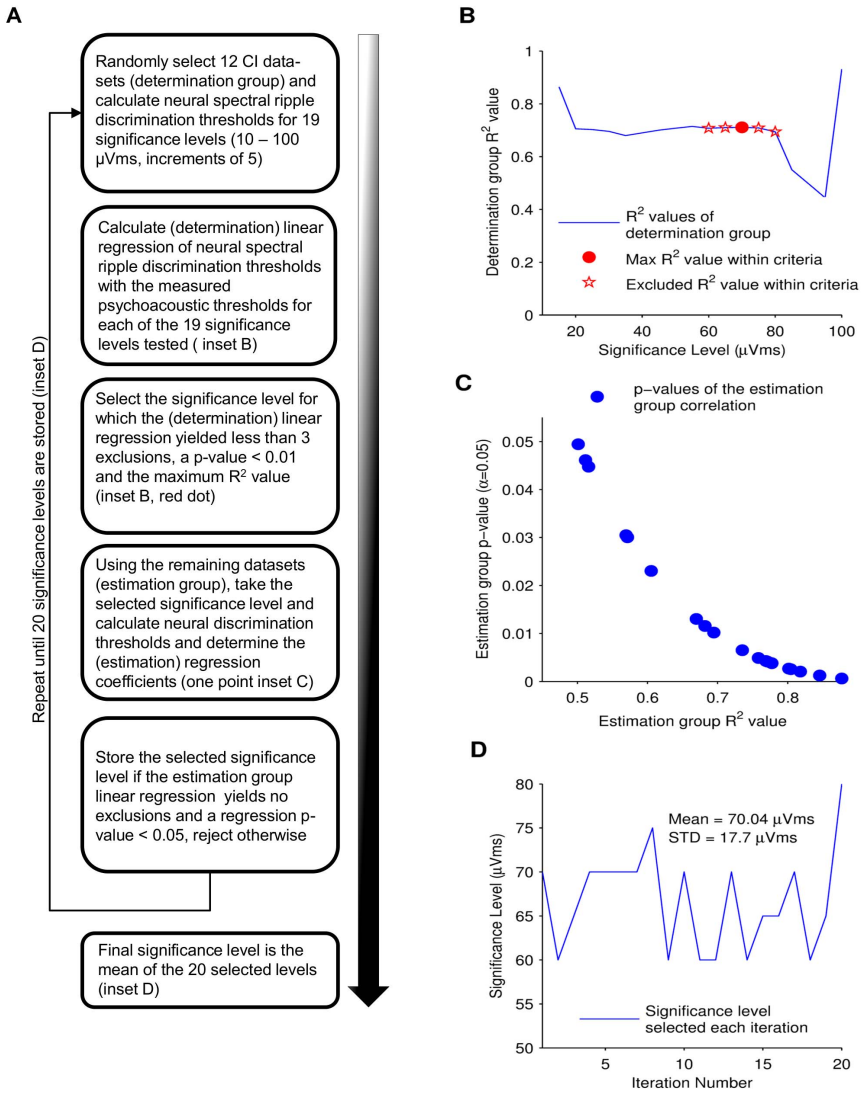

Figure 8. Bootstrapped determination of the significance level. (A) Describes the progression of the bootstrapping method employed to determine the level at which neural spectral ripple discrimination thresholds were estimated and regressed with the measured psychoacoustic thresholds. (B) The square of the Pearson's correlation factor (R^2) vs. the 19 significant levels tested on the determination group is plotted. The significance level that yields the maximum R^2 value within the selection criteria, identified as the red point in the plot, is selected to continue with the bootstrap method, the rest are excluded (hollow stars). (C) The selected significance level is evaluated with estimation group. The regression's p-value plotted vs. the regression's R^2 value resulting from the significance level evaluation on the estimation group for 20 bootstrap iterations. If the evaluation yields no exclusions and a p-value less than 0.05, the significance level is stored. (D) The bootstrap method is repeated to select 20 different significant levels. The mean of the selected values is employed as the final significance level.
doi:10.1371/journal.pone.0090044.g008

difference waveform is difficult because not all subject's responses exhibit a similar morphology (compare Figs. 5 and 6). The more general approach taken in this study, of measuring the area above or below a bootstrapped determined noise floor, avoids this difficulty. An area-, as opposed to peak-, based metric has the added advantage of reducing noise, an important consideration when using difference waveforms which are by definition noisier than the responses from which they are derived. To define a significance level, below which a difference waveform area would be considered perceptually insignificant, a second bootstrap method was applied. Fig. 8C shows that, for 20 different data partitions, the selected significance level reasonably predicts the psychophysical thresholds of the estimation group. Additionally, variations of the significance level between around 20 and 80 μVms do not tend to produce large variations in the R^2 values (Fig. 8B), and most partitions of the data produce an estimate of the significance level close to 70 μVms (Fig. 8D). This shows that the good correlation between neural and psychophysical thresholds (Fig. 9) is robust and is not simply dependent on subjectively selecting the appropriate significance level. The use of the positive, negative or total area between the noise floor and the difference waveform did not yield a significant difference when estimating spectral discrimination thresholds. However, using the total area, above the positive and negative noise floor, succeeded to estimate a spectral ripple discrimination threshold in the largest number of tested ears.

In cases where the cortical responses were too small compared to the noise floor, such as TCD06 and TCD15, it was difficult to estimate a neural spectral ripple discrimination threshold. While monitoring the impedance levels accordingly during the recording

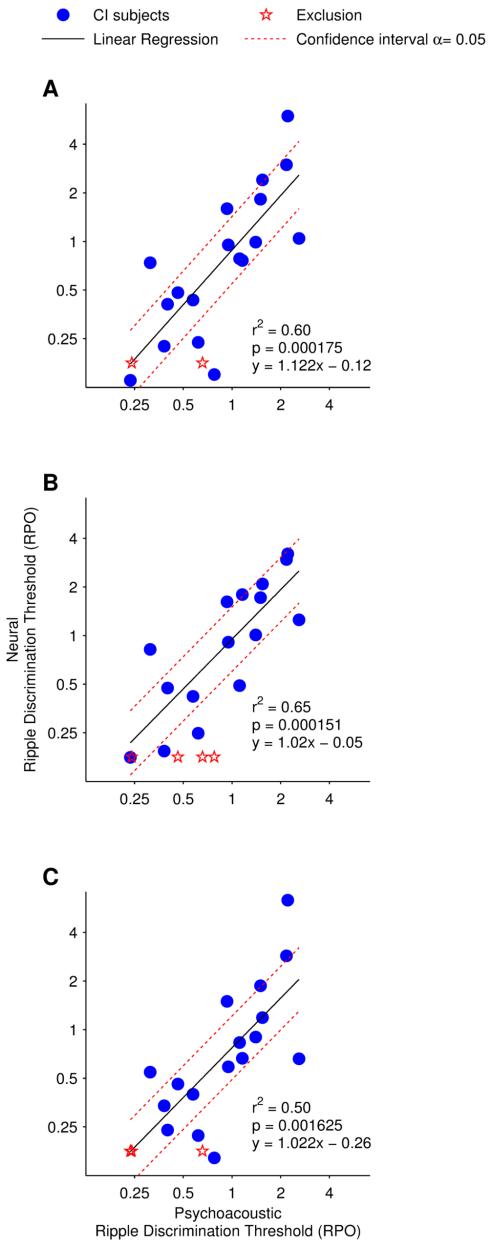

Figure 9. Correlation of neural and psychoacoustic spectral ripple discrimination thresholds. Linear regression of the psychoacoustic spectral ripple discrimination thresholds with the neural spectral ripple discrimination thresholds for each of the analyzed area above the noise floor measurements: (A) total area above the noise floor; (B) Positive area above the noise floor; and (C) negative area above the noise floor.
doi:10.1371/journal.pone.0090044.g009

may reduce noise and CI artifact, small or unreliable cortical evoked potential responses from some subjects is a limitation when estimating neural spectral ripple discrimination thresholds. Reducing the noise in the signal as much as possible by limiting subject motion and external interference and increasing the stimulus presentation level may help get a better response in these subjects.

Potential Clinical Applications

Previous work by our group [36] highlighted the elegance of single channel EEG acquisition and artifact attenuation in CI users. The simple, yet robust, approach makes it feasible for use within a clinical environment, with faster and more comfortable acquisition than with high density EEG set-ups. The results presented in this study suggest that the single channel EEG acquisition and artifact attenuation is a reliable method for measuring cortical responses to an oddball paradigm in CI users.

In addition to simply evaluating a CI subject's spectral resolution, it may also be possible to use the method to fine tune a subject's frequency map. Typically, a CI processor would be loaded with a standard frequency map, i.e. predefined frequency bands assigned to each electrode of the CI. An objective metric for spectral resolution, such as the one presented in this study, could allow the evaluation of customized frequency maps, in search of the map that allows the best spectral resolution. The time required to obtain spectral discrimination thresholds, approximately one hour, is a limiting factor for this potential application. However, being an objective metric, the possibility of an automated process may reduce the number of man-hours required for the task. Furthermore, the development of intra-cochlear recording methodologies that allow the recording of cortical evoked potentials without the additional EEG systems [44] may benefit from objective metrics as a building block for the development of automated frequency tuning processes.

Current efforts to enhance spectral resolution via different electrode stimulation modalities, i.e. partial bipolar stimulation (pBP), tripolar stimulation (TP) and partial tripolar stimulation (pTP), benefit from psychoacoustic evaluation of frequency resolution [45–47]. Objective assessment of spectral resolution using an oddball paradigm could be beneficial when evaluating different electrode stimulation modalities in CI populations where standard psychoacoustics cannot be performed such as young infants. The use of an oddball paradigm such as the mismatch negativity (MMN) has reported successful in normal hearing and cochlear implant infant populations [48–50]. Evidence in literature suggests that the pitch discrimination characteristics of the MMN in infants is developed between two and four months of age [49].

Clinical applications involving the use of cortical evoked potentials may be limited by the confounding factor of maturation changes during the longitudinal development of cortical potentials. The development of cortical auditory potentials can extend into adolescence [50] and even after prolonged acoustic deprivation, cortical auditory potentials can be re-developed over a period of time [30]. Changes in the morphology, latency and amplitude of potentials over time represents an impediment when performing a within subject cortical evoked potential assessment. Trainor et al. [51] identified changes in the EEG morphology of the MMN in young infants, with an age range of two, three, four and six months, suggesting that the difference at each age may be associated with layer-specific maturational processes in auditory cortex. However, the method developed in this study may overcome these limitations due to the robust nature of the oddball paradigm response and its applicability with different age populations as well as clinical conditions [33,49,50]. Despite maturational changes reflected by the EEG morphology of the MMN in young infants, the cognitive change detection mechanism associated with the MMN has been proposed to be developed between two and four months of age [49].

Provided that a spectral ripple discrimination threshold could be obtained with an oddball paradigm at any stage of the cortical auditory potential maturation process, a within subject assessment

can be conducted regardless of the developmental changes presented during the duration of the assessment. Nonetheless, determining the applicability of spectral rippled stimuli as well as the complexity of the paradigms and the presentation rate for younger populations requires further investigation.

Conclusions

In conclusion, the results presented in this study demonstrate that cortical responses to an oddball paradigm, utilizing complex stimuli, can be recorded with a single channel EEG acquisition set-up from a CI population. This cortical evoked potential based method can provide an estimated spectral ripple discrimination threshold in adult CI listeners. Further research is required to investigate the relationship of the objective assessment of spectral resolution with speech perception scores, as well as to investigate the applicability of the proposed objective method in a population of infant CI recipients.

Acknowledgments

The authors would like to acknowledge the 19 cochlear implant participants, for their dedication and willingness during the experimental sessions.

Author Contributions

Conceived and designed the experiments: ALV RBR MML FGZ LV JS PW. Performed the experiments: ALV MML. Analyzed the data: ALV MML RBR FGZ JS LV PW. Contributed reagents/materials/analysis tools: LV JS PW. Wrote the paper: ALV MML RBR FGZ JS LV PW. Critically revising the manuscript for important intellectual content; RBR FGZ LV PW JS ALV. Subject recruiting for research; LV JS PW ALV.

References

1. Zeng F-G (2004) Trends in cochlear implants. Trends in Amplification 8: 1–34.
2. Waltzman SB, Roland JT (2005) Cochlear implantation in children younger than 12 months. Pediatrics 116: e487–e493.
3. van Dijk JE, van Olphen AF, Langereis MC, Mens LH, Brokx JP, et al. (1999) Predictors of cochlear implant performance. Audiology 38: 109–116.
4. Blamey P, Arndt P, Bergeron F, Bredberg G, Brimacombe J, et al. (1996) Factors affecting auditory performance of postlinguistically deaf adults using cochlear implants. Audiology and Neurotology 1: 293–306.
5. Clark JH, Yeagle J, Arbaje AI, Lin FR, Niparko JK, et al. (2012) Cochlear implant rehabilitation in older adults: literature review and proposal of a conceptual framework. Journal of the American Geriatrics Society 60: 1936–1945.
6. Loizou PC (1999) Introduction to cochlear implants. IEEE Engineering in Medicine and Biology Magazine 18: 32–42.
7. Zeng F-G, Rebscher S, Harrison W, Sun X, Feng H (2008) Cochlear implants: system design, integration, and evaluation. IEEE Reviews in Biomedical Engineering 1: 115–142.
8. Pisoni DB, Cleary M, Geers AE, Tobey EA (1999) Individual differences in effectiveness of cochlear implants in children who are prelingually deaf: New process measures of performance. The Volta Review 101(3): 111–164.
9. Zeng F-G, Grant G, Niparko J, Galvin J, Shannon R, et al. (2002) Speech dynamic range and its effect on cochlear implant performance. The Journal of the Acoustical Society of America 111: 377–386.
10. Lazard DS, Bordure P, Lina-Granade G, Magnan J, Meller R, et al. (2010) Speech perception performance for 100 post-lingually deaf adults fitted with Neurelec cochlear implants: comparison between Digisonic® Convex and Digisonic® SP devices after a 1-year follow-up. Acta Oto-Laryngologica 130: 1267–1273.
11. Friesen LM, Shannon RV, Baskent D, Wang X (2001) Speech recognition in noise as a function of the number of spectral channels: Comparison of acoustic hearing and cochlear implants. Journal of the Acoustical Society of America 110: 1150–1163.
12. Fu QJ (2002) Temporal processing and speech recognition in cochlear implant users. Neuroreport 13: 1635–1639.
13. Henry BA, Turner CW, Behrens A (2005) Spectral peak resolution and speech recognition in quiet: normal hearing, hearing impaired, and cochlear implant listeners. Journal of the Acoustical Society of America 118: 1111–1121.
14. Won JH, Drennan WR, Rubinstein JT (2007) Spectral-ripple resolution correlates with speech reception in noise in cochlear implant users. Journal of the Association for Research in Otolaryngology 8: 384–392.
15. Supin A, Popov VV, Milekhina ON, Tarakanov MB (1997) Frequency-temporal resolution of hearing measured by rippled noise. Hearing Research 108: 17–27.
16. Litvak LM, Spahr AJ, Saoji AA, Fridman GY (2007) Relationship between perception of spectral ripple and speech recognition in cochlear implant and vocoder listeners. Journal of the Acoustical Society of America 122: 982–991.
17. Jones GL, Drennan WR, Rubinstein JT (2011) Relationship between channel interaction and spectral-ripple discrimination in cochlear implant users. Journal of the Acoustical Society of America 133: 425–433.
18. Horn D, Werner L, Rubinstein JT, Won JH (2013). Spectral Ripple Discrimination in Infants: Effect of Ripple Depth and Envelope Phase Randomization. 36th Association for Research in Otolaryngology Annual MidWinter Meeting 36:289–290.
19. Abbas PJ, Brown CJ (1988) Electrically evoked brainstem potentials in cochlear implant patients with multi-electrode stimulation. Hearing Research 36: 153–162.
20. Brown CJ, Hughes ML, Luk B, Abbas PJ, Wolaver A, et al. (2000) The relationship between EAP and EABR thresholds and levels used to program the Nucleus 24 speech processor: data from adults. Ear and Hearing 21: 151–163.
21. Franck KH, Norton SJ (2001) Estimation of psychophysical levels using the electrically evoked compound action potential measured with the neural response telemetry capabilities of Cochlear Corporation's CI24M device. Ear and Hearing 22: 289–299.
22. Hughes ML, Brown CJ, Abbas PJ, Wolaver AA, Gervais JP (2000) Comparison of EAP thresholds with MAP levels in the nucleus 24 cochlear implant: data from children. Ear and Hearing 21: 164–174.
23. Dimitrijevic A, John MS, Picton TW (2004) Auditory steady-state responses and word recognition scores in normal-hearing and hearing-impaired adults. Ear and Hearing 25: 68–84.
24. Firszt JB, Chambers RD, Kraus, Reeder RM (2002) Neurophysiology of cochlear implant users I: effects of stimulus current level and electrode site on the electrical ABR, MLR, and N1-P2 response. Ear and Hearing 23: 502–515.
25. Ponton CW, Don M, Eggermont JJ, Waring MD, Masuda A (1996) Maturation of human cortical auditory function: differences between normal-hearing children and children with cochlear implants. Ear and Hearing 17: 430–437.
26. Sharma A, Nash AA, Dorman M (2009) Cortical development, plasticity and re-organization in children with cochlear implants. Journal of Communication Disorders 42: 272–279.
27. Brown CJ, Etler C, He S, O'Brien S, Erenberg S, et al. (2008) The electrically evoked auditory change complex: preliminary results from nucleus cochlear implant users. Ear and Hearing 29: 704–717.
28. Gilley PM, Sharma A, Dorman MF (2008) Cortical reorganization in children with cochlear implants. Brain Research 1239: 56–65.
29. Hofmann M, Wouters J (2010) Electrically evoked auditory steady state responses in cochlear implant users. Journal of the Association for Research in Otolaryngology 11: 267–282.
30. Pantev C, Dinnesen A, Ross B, Wollbrink A, Knief A (2006) Dynamics of auditory plasticity after cochlear implantation: a longitudinal study. Cerebral Cortex 16: 31–36.
31. Torppa R, Salo E, Makkonen T, Loimo H, Pykalainen J, et al. (2012) Cortical processing of musical sounds in children with Cochlear Implants. Clinical Neurophysiology 123: 1966–1979.
32. Won JH, Clinard CG, Kwon S, Dasika VK, Nie K, et al. (2011) Relationship Between Behavioral and Physiological Spectral-Ripple Discrimination. Journal of the Association for Research in Otolaryngology 12: 375–393.
33. Naatanen R, Kujala T, Escera C, Baldeweg T, Kreegipuu K, et al. (2012) The mismatch negativity (MMN)–a unique window to disturbed central auditory processing in ageing and different clinical conditions. Clinical Neurophysiology 123: 424–458.
34. Byrne D, Dillon H, Tran K, Arlinger S, Wilbraham K, et al. (1994) An international comparison of long-term average speech spectra. Journal of the acoustical society of America 96: 2108.
35. Levitt H (1971) Transformed up-down methods in psychoacoustics. Journal of the Acoustical Society of America 49: Suppl 2:467+.
36. McLaughlin M, Lopez Valdes A, Reilly RB, Zeng FG (2013) Cochlear Implant Artifact Attenuation in Late Auditory Evoked Potentials: A Single Channel Approach. Hearing Research 302:84–95.
37. Picton TW, Alain C, Otten L, Ritter W, Achim A (2000) Mismatch negativity: different water in the same river. Audiology and Neuro-otology 5: 111–139.
38. Henry BA, Turner CW (2003) The resolution of complex spectral patterns by cochlear implant and normal-hearing listeners. Journal of the Acoustical Society of America 113: 2861–2873.
39. Wong DD, Gordon KA (2009) Beamformer suppression of cochlear implant artifacts in an electroencephalography dataset. IEEE Transactions on Biomedical Engineering 56: 2851–2857.
40. Viola FC, Thorne JD, Bleeck S, Eyles J, Debener S (2011) Uncovering auditory evoked potentials from cochlear implant users with independent component analysis. Psychophysiology 48: 1470–1480.
41. Gilley PM, Sharma A, Dorman M, Finley CC, Panch AS, et al. (2006) Minimization of cochlear implant stimulus artifact in cortical auditory evoked potentials. Clinical Neurophysiology 117: 1772–1782.

42. Friesen LM, Picton TW (2010) A method for removing cochlear implant artifact. Hearing Research 259: 95–106.
43. Ponton CW, Don M, Eggermont JJ, Kwong B (1997) Integrated mismatch negativity (MMNi): a noise-free representation of evoked responses allowing single-point distribution-free statistical tests. Evoked Potentials-Electroencephalography and Clinical Neurophysiology 104: 143–150.
44. Mc Laughlin M, Lu T, Dimitrijevic A, Zeng F-G (2012) Towards a Closed-Loop Cochlear Implant System: Application of Embedded Monitoring of Peripheral and Central Neural Activity. IEEE Transactions on Neural Systems and Rehabilitation Engineering 20: 443–454.
45. Landsberger DM, Srinivasan AG (2009) Virtual channel discrimination is improved by current focusing in cochlear implant recipients. Hearing Research 254: 34–41.
46. Wu C-C, Luo X (2013) Current Steering with Partial Tripolar Stimulation Mode in Cochlear Implants. Journal of the Association for Research in Otolaryngology 14: 213–231.
47. Zhu Z, Tang Q, Zeng F-G, Guan T, Ye D (2012) Cochlear-implant spatial selectivity with monopolar, bipolar and tripolar stimulation. Hearing Research 283: 45–58.
48. Cheour M, Alho K, Ceponiene R, Reinikainen K, Sainio K, et al. (1998) Maturation of mismatch negativity in infants. International Journal of Psychophysiology 29: 217–226.
49. He C, Hotson L, Trainor LJ (2009) Maturation of cortical mismatch responses to occasional pitch change in early infancy: Effects of presentation rate and magnitude of change. Neuropsychologia 47: 218–229.
50. Ponton CW, Eggermont JJ, Don M, Waring MD, Kwong B, et al. (2000) Maturation of the mismatch negativity: Effects of profound deafness and cochlear implant use. Audiology and Neuro-Otology 5: 167–185.
51. Trainor L, McFadden M, Hodgson L, Darragh L, Barlow J, et al. (2003) Changes in auditory cortex and the development of mismatch negativity between 2 and 6 months of age. International Journal of Psychophysiology 51: 5–15.

Appendix B Conference Papers

35th Annual International Conference of the IEEE EMBS
Osaka, Japan, 3 - 7 July, 2013

Auditory Mismatch Negativity in Cochlear Implant Users: A Window to Spectral Discrimination

Alejandro Lopez-Valdes, Myles Mc Laughlin, Laura Viani, Peter Walshe, Jaclyn Smith, Fang-Gang Zeng and Richard B. Reilly, *Senior Member, IEEE*

***Abstract*—A cochlear implant (CI) can partially restore hearing in patients with severe to profound sensorineural hearing loss. However, the large outcome variability in CI users prompts the need for more objective measures of speech perception performance. Electrophysiological metrics of CI performance may be an important tool for audiologists in the assessment of hearing rehabilitation. Utilizing electroencephalography (EEG), it may be possible to evaluate speech perception correlates such as spectral discrimination. The mismatch negativity (MMN) of 10 CI subjects was recorded for stimuli containing different spectral densities. The neural spectral discrimination threshold, estimated by the MMN responses, showed a significant correlation with the behavioral spectral discrimination threshold measured in each subject. Results suggest that the MMN can be potentially used to obtain an objective estimate of spectral discrimination abilities in CI users.**

I. Introduction

Hearing impairment (HI) is the most frequent sensory deficit in human populations, being present in over 250 million people globally [1]. Patients suffering from HI are subject to social isolation due to their reduced capability to communicate and interact with their surroundings. A cochlear implant (CI) partially restores hearing in patients suffering from severe to profound sensorineural HI by electrically stimulating the auditory nerve. According to the Food and Drug Administration (FDA), as of December of 2010, over 219,000 people around the globe have received a CI [2].

The large outcome variability in CI users, such as the variable speech perception performance among users, prompts the need for more objective measures of CI speech perception performance [3]. Firszt et al. reported a correlation between CI users' speech perception abilities and mid-latency cortical auditory evoked potentials (CAEP) elicited by simple stimuli [4]. The use of complex stimulation, such as spectrally rippled noise instead of pure tone stimulation, may be better at characterizing a CI user's neural processing abilities as suggested by psychoacoustic studies [5]. Previous research suggests that it may be possible to measure behavioral and physiological spectral discrimination in CI users by means of acoustic change complex (ACC) paradigms [6], [7].

The mismatch negativity (MMN) is a CAEP paradigm that allows the exploration of high order auditory processing in subjects with different clinical conditions and with minimal effort or engaged attention [8]. The present study explores the possibility to employ MMN, combined with complex stimuli, in a clinical set-up as an electrophysiological metric for spectral discrimination of CI users.

An electrophysiological metric of spectral discrimination may be a powerful tool for the audiologists when assessing speech rehabilitation progress in CI users. An objective metric may allow an improved evaluation of hard-to-test adult CI patients as well as enabling an objective examination of pediatric populations where behavioral testing is not possible.

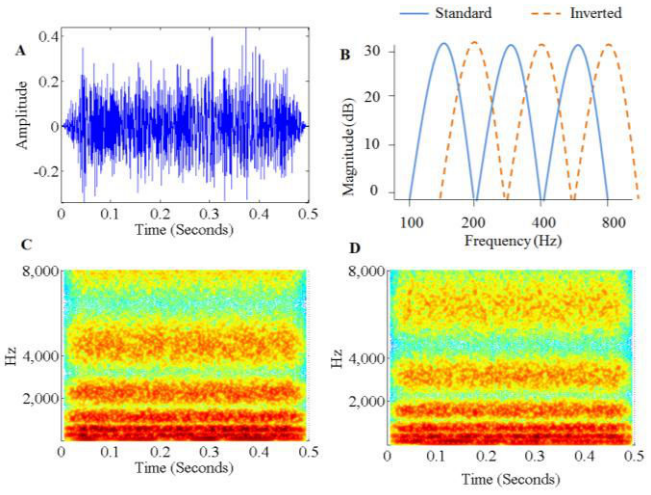

Figure 1: Description of one RPO stimuli A**:** Stimulus representation on the time domain. **B:** Sinusoidal spectral ripple envelope applied to create the standard and inverted stimuli with a ripple amplitude of 30dB peak to valley. **C:** Spectral content of the standard stimulus at one RPO. **D:** Spectral content of the inverted stimulus at one RPO.

This research was funded by a Common European Master's course in Biomedical Engineering (CEMACUBE) scholarship and the Graduate Research Education Programme in Engineering awarded by the Higher Education Authority to A. Lopez-Valdes and a Marie Curie Fellowship to M. McLaughlin.

Alejandro Lopez-Valdes*, Myles McLaughlin and Richard B. Reilly are with the Trinity Centre for Bioengineering, Trinity College Dublin, Dublin 2, Ireland (*corresponding author, e-mail: lopezvaa@tcd.ie, mclaugmy@tcd.ie, richard.reilly@tcd.ie; phone: +353-1-8964214; fax: +353-1-6772442)

Laura Viani, Peter Walshe and Jaclyn Smith are with the National Cochlear Implant Programme in Beaumont Hospital, Dublin 9, Ireland (e-mail: lauraviani@beaumont.ie, peterwalshe@beaumont.ie, jaclynsmith@beaumont.ie).

Fang-Gang Zeng is with the Hearing and Speech Lab (HESP) in the University of California at Irvine, USA (e-mail: fzeng@uci.edu).

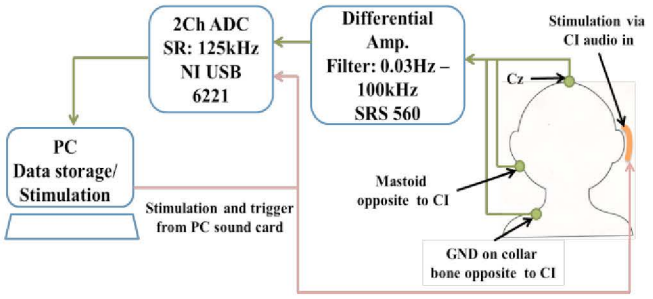

Figure 2: Schematic layout of the high sample rate and high bandwidth single channel EEG acquisition system.

II. Methods

A. Background

10 CI subjects were recruited from the National Cochlear Implant Programme at Beaumont Hospital in Dublin, Ireland. Inclusion criteria were: postlingually implanted subjects, age restricted from 18-75 years, absence of any additional linguistic or developmental problems and implant turn-on date no shorter than 6 months prior to the study.

The MMN was elicited by presenting a set of standard and deviant auditory stimuli, fed directly to the CI via the auxiliary input of the speech processor. The stimulus repetition rate was 1Hz and the occurrence of a deviant presentation was random with a probability of 10%. Five 10-minute MMN recordings were acquired from each subject. Recordings took place inside an electrically isolated room, with the subject sitting comfortably while viewing a silent film.

In addition to the electrophysiological measurement, spectral discrimination was assessed with psychoacoustic testing for each subject. A behavioral adaptive three-alternative forced-choice test was repeated five times by each subject to determine their mean behavioral spectral discrimination threshold.

B. Stimuli

The standard stimulus (90%) was spectrally rippled broadband noise; the deviant (10%) was the inverted version, having an equal number of ripples per octave (RPO). The broadband noise was created by a summation of 4000 pure tones with frequencies from 100Hz to 8,000 kHz. The spectral ripple was created with a full wave rectified sinusoidal envelope on a logarithmic amplitude scale and with maximum amplitude of 30 dB peak-to-valley as described by [5]. Fig. 1 illustrates the spacing of the spectral peaks, as well as the difference in frequency content of the standard and the deviant stimuli having both a spectral density of one RPO. Spectral peaks were equally distributed on a logarithmic frequency scale. The sinusoidal ripple envelope, for the inverted stimulus, had $\pi/2$ phase shift with respect of the one used for the standard stimulus. Stimuli were delivered electronically, through the auxiliary input of the CI's speech processor, as indicated in Fig. 2.

C. Electroencephalography (EEG) Recording System

Single channel EEG recordings were acquired using a customized high sampling rate and high bandwidth system.

Fig. 2 shows the layout of the above described system. Electrode positions were placed at the vertex (Cz) and the mastoid, contralateral with respect to the tested ear. The system ground was located at the collar bone. The EEG signal was pre-amplified via a Stanford Research Systems biological pre-amplifier (filter settings: 0.03Hz – 100kHz) and then digitized into a PC via a National Instruments analog to digital converter (sampling rate: 125kHz).

Sampling rate and filter settings exceed those typically employed in conventional EEG acquisition systems. Sampling rate and filter setting were chosen to clearly acquire and resolve the CI related artifact, caused by the CI stimulation pulses as shown in Fig. 3.

D. Signal Processing

After inspection of the recordings, it was identified that the recorded signal was composed of three elements: 1) the neural response over time NR(t); 2) high frequency artifact over time HFA(t), generated by the CI electrical stimulation; and 3) DC artifact assumed to be related to the stimulation pulse amplitude (PA) over time DCA(PA,t). Hence:

$$SIG(t) = NR(t) + HFA(t) + DCA(PA,t) \quad (1)$$

The acquisition system allows for clear acquisition of large amplitude and high frequency CI related artifact. Fig. 3 shows the full effect, captured with the customized acquisition system, of the CI electrical stimulation. The large amplitude (> 1000 μV) and the high frequency (>1000 Hz) generated by the CI during the stimulus presentation, compromises the acquisition of a CAEP.

Artifact attenuation was performed as described by Mc Laughlin et al. [9] and its briefly described below. Fig. 4 is a graphical representation of the steps involved in the attenuation process.

The signal described in (1) was band-pass filtered, with a 2nd order Butterworth filter digitally implemented, with cut-off frequencies of 2Hz – 30Hz in order to reduce the high frequency artifact, yielding:

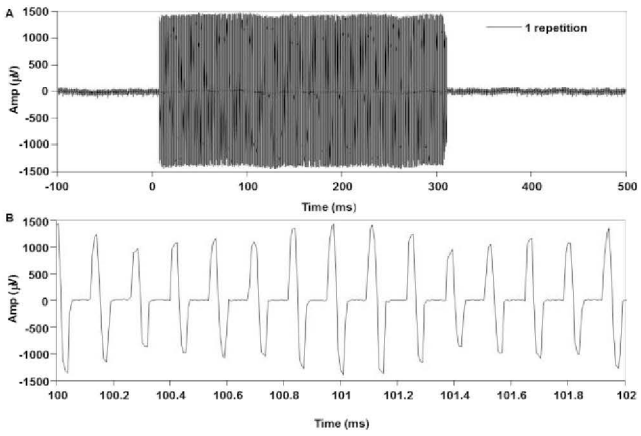

Figure 3: A) 600ms epoch of EEG recording of a CI subject during a 300ms stimulus presentation. B) 2ms zoom of the recorded EEG epoch showing the biphasic pulses of the CI stimulation.

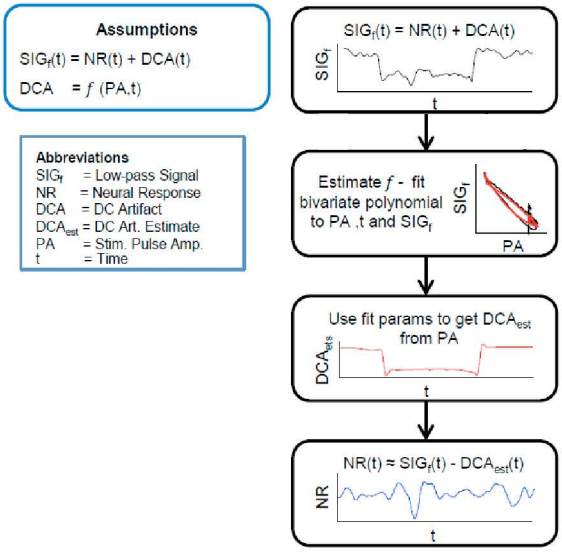

Figure 4: The desired neural response is recovered from the low-passed recorded signal by substracting a bivariate polynomial estimation of the DC artifact, assumed to be related to the stimulation pulse amplitude and time.

$$SIG_f(t) = NR(t) + DCA(PA,t) \quad (2)$$

Given our assumption that the DC artifact is a function of PA and time, an estimate of the DC artifact (DCAest(t)) was calculated with a bivariate polynomial fit of the stimulation pulse amplitudes as depicted in Fig. 4.

Neural responses were recovered by subtracting the DC artifact estimate from the filtered signal described in (2) in the form:

$$NR(t) \approx SIG_f(t) - DCA_{est}(t) \quad (3)$$

III. Results

The MMN was calculated by subtracting the neural response elicited by the standard stimulus from the neural response elicited by the deviant stimulus. To define a neural spectral discrimination threshold, the spectral density of the stimuli was increased (i.e. 0.25RPO, 0.5RPO, 2RPO) until the area under the curve between the MMN and the noise floor of the signal had dropped below a significance level. The noise floor of the signal was determined as +/- one standard deviation of the signal, using a boot-strap method to the standard responses.

Fig. 5 illustrates how a well-defined MMN response to a spectral density of 0.25 RPO (Fig. 5A) decreases as the spectral density increases to 0.5 RPO (Fig. 5B). The MMN response drops below the noise level as the spectral density increases to 2 RPO (Fig. 5C), thus losing the discrimination capability.

An adaptive three-alternative forced-choice test was performed to every subject to determine the behavioral spectral discrimination threshold for validation of the MMN metric.

A significant correlation (r^2=0.66, p=0.004175)) was found between the neural RPO detection threshold and the behavioral RPO detection threshold in CI subjects, as shown in Fig. 6.

IV. Discussion

The aim of this study was to investigate if an objective metric based on MMN estimates the spectral discrimination ability of CI users. Such a metric would have great potential as a tool for assessment of speech perception performance in CI users.

The results presented in this study indicated that the MMN can estimate the spectral processing abilities of CI users. Given the known correlation between speech perception and the behavioral spectral discrimination threshold [5], it is predicted that there is a correlation with neural spectral discrimination threshold and speech perception; however, this remains to be tested.

The findings show that the correlation between the MMN metric and the behavioral metric, in this study, is not one to one. This may be attributed to the difference on the cognitive load required between the three-alternative forced-choice test and the MMN paradigm. A matched, MMN-like task to determine the behavioral spectral discrimination thresholds may be used to explore this further.

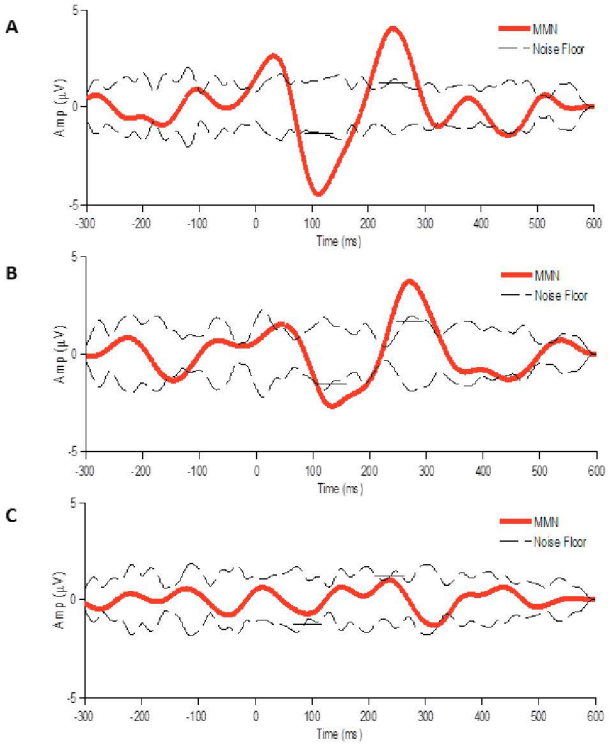

Figure 5: Sequencial fading of the MMN response as the simuli increases in spectral ripple density. **A:** MMN elicited to a stimuli containing 0.25 RPO. **B:** MMN elicited to a stimuli containing 0.5 RPO. **C:** MMN elicited to a stimuli containing 2 RPO.

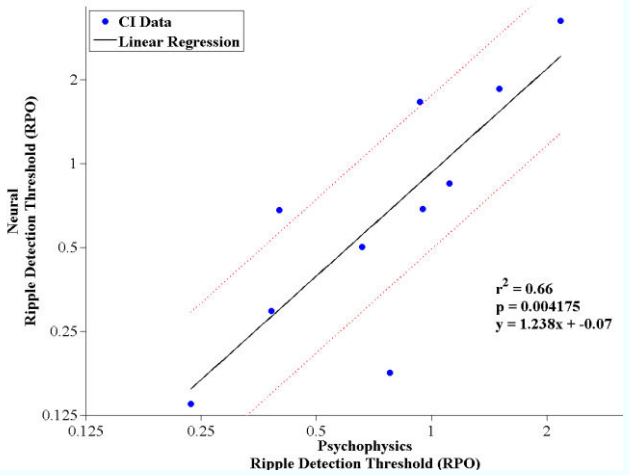

Figure 6: Correlation between the behavioral spectral ripple detection versus the neural spectral ripple detection of 10 CI subjects. (r^2=0.66, p=0.004175)

Previous studies have investigated the possibility of using EEG as an objective metric for spectral discrimination. Won et al. [6] developed a single interval ACC paradigm for estimation of behavioral and physiological spectral discrimination thresholds in CI users. Findings show that the cognitive load of the discrimination task is likely to influence the number of discriminable ripples per octave [6]. Stoody et al. [10] investigated the use of MMN for spectral modulation contrast detection in normal hearing subjects. Their findings show presence of the MMN at 10dB and 20dB of spectral modulation contrast; however, there was no indication of a threshold metric [10].

The neural spectral discrimination findings of this study are consistent with the behavioral spectral discrimination findings by Won et al. [5] with respect to CI users having lower spectral discrimination than normal hearing subjects.

This study aims to provide an objective metric to assess spectral discrimination of CI users during normal use of their device. For this reason, the inclusion of the signal conditioning stages by the speech processor may yield a better approach than bypassing the CI control and directly manipulating the stimulating electrodes as used by Won et al. [6] and Brown et al. [7].

V. Conclusions

This study developed an objective method to estimate the spectral discrimination abilities in CI users based on EEG recordings and a MMN paradigm.

MMN is a simple and straight-forward EEG paradigm that can be performed in a clinical environment. Using a single channel EEG recording system reduces the acquisition time for the clinician and represents a more comfortable scenario for the patient to be tested.

The literature suggests that with the use of other EEG paradigms such as the ACC may also be possible to estimate the spectral discrimination threshold in CI users [6], [7]. Nonetheless a comparison between the effectiveness of MMN and ACC as an estimate of spectral discrimination is yet to be performed.

Research towards a clinical objective metric for evaluation of CI performance may provide the audiologist with additional tools for an optimal tailoring of individual rehabilitation processes. This in turn will maximize the outcome of the CI and contribute to reduce the large outcome variability currently observed among the CI user community.

Acknowledgment

The authors would like to thank the Higher Education Authority (HEA), in Ireland, and the European Commission's Marie Curie Fellowship for supporting this research.

References

[1] World Health Organization (WHO), "Deafness and Hearing Impairment," *Journal*, [online], pp. 5, (Date 2012), Available http://www.who.int/mediacentre/factsheets/fs300/en/index.html.

[2] National Institute of Deafness and other Communication Disorders (NIDCD), "Cochlear Implants," [online], (Date 2011), Available http://www.nidcd.nih.gov/health/hearing/pages/coch.aspx/.

[3] F.G. Zeng, "Trends in cochlear implants," *Trends in amplification*, vol. 8, (no. 1), pp. 1-34, 2004.

[4] J.B. Firszt, R.D. Chambers, Kraus, and R.M. Reeder, "Neurophysiology of cochlear implant users I: effects of stimulus current level and electrode site on the electrical ABR, MLR, and N1-P2 response," *Ear and Hearing*, vol. 23, (no. 6), pp. 502-15, Dec 2002.

[5] J.H. Won, W.R. Drennan, and J.T. Rubinstein, "Spectral-ripple resolution correlates with speech reception in noise in cochlear implant users," *JARO Journal of the Association for Research in Otolaryngology*, vol. 8, (no. 3), pp. 384-92, Sep 2007.

[6] J.H. Won, C.G. Clinard, S. Kwon, V.K. Dasika, K. Nie, W.R. Drennan, K.L. Tremblay, and J.T. Rubinstein, "Relationship Between Behavioral and Physiological Spectral-Ripple Discrimination," *JARO-Journal of the Association for Research in Otolaryngology*, vol. 12, (no. 3), pp. 375-393, 2011.

[7] C.J. Brown, C. Etler, S. He, S. O'Brien, S. Erenberg, J.R. Kim, A.N. Dhuldhoya, and P.J. Abbas, "The electrically evoked auditory change complex: preliminary results from nucleus cochlear implant users," *Ear and Hearing*, vol. 29, (no. 5), pp. 704-17, Oct 2008.

[8] R. Naatanen, T. Kujala, C. Escera, T. Baldeweg, K. Kreegipuu, S. Carlson, and C. Ponton, "The mismatch negativity (MMN)--a unique window to disturbed central auditory processing in ageing and different clinical conditions," *Clinical neurophysiology : official journal of the International Federation of Clinical Neurophysiology*, vol. 123, (no. 3), pp. 424-58, Mar 2012.

[9] M. McLaughlin, A. Lopez Valdes, R.B. Reilly, and Z. Fang-Gang, "Cochlear Implant Artifact Attenuation in Late Auditory Evoked Potentials: A Single Channel Approach," *Hearing research*, In Review.

[10] T.M. Stoody, A.A. Saoji, and S.R. Atcherson, "Auditory Mismatch Negativity: Detecting Spectral Contrasts in a Modulated Noise1," *Perceptual and Motor Skills*, vol. 113, (no. 1), pp. 268-276, 2011.

7th Annual International IEEE EMBS Conference on Neural Engineering
Montpellier, France, 22 - 24 April, 2015

Electrophysiological Correlates of Spectral Discrimination for Cochlear Implant Users

Alejandro Lopez Valdes*, Myles Mc Laughlin, Laura Viani, Peter Walshe, Jaclyn Smith, Fan-Gang Zeng and Richard B. Reilly, *Senior Member, IEEE*

***Abstract*—A cochlear implant (CI) can partially restore hearing in patients with severe to profound sensorineural hearing loss. Proper programming and evaluation of the CIs are key aspects determining success in the restoration of hearing for patients. Recent evidence suggests that cortical auditory evoked potentials, elicited via an unattended oddball paradigm, can provide objective information on CI spectral discrimination abilities, which in turn may be useful for assessing speech perception performance. This study investigates the applicability of an acoustic change paradigm for objective evaluation of CI users' ability to resolve spectral content via single channel electroencephalography. Acoustic change complex (ACC) responses were obtained from 13 CI users and correlated with psychoacoustic spectral discrimination abilities. The applicability of the acoustic change paradigm was compared to that of the unattended oddball paradigm. The neural spectral discrimination threshold, estimated via the ACC responses, showed a non-significant correlation with the behavioral spectral discrimination threshold. In contrast, the neural spectral threshold estimated via an unattended oddball paradigm showed a significant correlation with the behavioral threshold. Results suggest that the unattended oddball paradigm is a more robust paradigm than the ACC to objectively evaluate CI users' ability to resolve spectral ripples. Nonetheless, the ACC can be used in some CI users and may be considered as an additional tool for objective evaluation of CI performance.**

I. Introduction

Hearing impairment is one of the most frequent sensory deficits in the human population [1], and cochlear implants (CI) have successfully restored partial hearing to over 300,000 people worldwide [2]. There is a critical need to provide clinicians and audiologists with the appropriate tools to ensure optimal rehabilitation for this rapidly growing population, particularly for pediatric CI users. Objective measures of CI performance have shown a promising future for the evaluation of hearing rehabilitation in adult and infant CI user populations.

This research was part funded by Cochlear Ltd., a scholarship from the Graduate Research Education Programme in Engineering awarded by the Higher Education Authority to A. Lopez-Valdes and a Marie Curie Fellowship to M. McLaughlin.

Alejandro Lopez-Valdes*, Myles Mc Laughlin and Richard B. Reilly are with the Trinity Centre for Bioengineering, Trinity College Dublin, Dublin 2, Ireland (*corresponding author, e-mail: lopezvaa@tcd.ie, richard.reilly@tcd.ie; phone: +353-1-8964214; fax: +353-1-6772442)

Laura Viani, Peter Walshe and Jaclyn Smith are with the National Cochlear Implant Programme in Beaumont Hospital, Dublin 9, Ireland (e-mail: lauraviani@beaumont.ie, peterwalshe@beaumont.ie, jaclynsmith@beaumont.ie).

Fan-Gang Zeng is with the Hearing and Speech Lab (HESP) in the University of California at Irvine, USA (e-mail: fzeng@uci.edu).

It has been suggested that cortical auditory evoked potentials (CAEP) can be used to evaluate speech perception performance in CI populations [3]. There are a number of electroencephalography (EEG) paradigms that can be used to elicit CAEPs. The unattended oddball paradigm (i.e. mismatch negativity) allows the exploration of higher order auditory processing in subjects with different clinical conditions and minimal effort of engaged attention [4]. In a previous study by our group, we developed an objective metric of CI spectral discrimination with an unattended oddball paradigm via single channel EEG [5]. Nonetheless, other CAEPs such as the acoustic change complex (ACC) have also been proposed to probe cortical discrimination abilities in normal hearing and CI populations [6-10]. Previous research suggests that it may be possible to measure behavioral and physiological spectral discrimination in CI users by means of acoustic change complex (ACC) paradigms [9, 10].

The study presented in [10] showed a correlation between electrophysiological and behavioral spectral ripple discrimination via single-interval change presentation (i.e. ACC for electrophysiological discrimination and yes/no for behavioral discrimination). Furthermore, it validated the relationship suggested in [11] between spectral ripple discrimination and speech perception performance in noise. The present study explored the possibility to employ an ACC paradigm, in combination with the CI artefact attenuation methodology described in [12], for evaluation of spectral ripple discrimination in CI users as an alternative method to the metric previously proposed in [5].

The possibility to employ different methods for evaluating spectral discrimination in CI users, without the need to modify a clinic-friendly set-up, may be an attractive option for clinicians and audiologists when assessing CI rehabilitation and performance.

II. Methods

A. *Participants*

13 CI participants volunteered for this study, 10 recruited from the National Cochlear Implant Programme at Beaumont Hospital in Dublin, Ireland and 3 recruited from the Hearing and Speech Lab at the University of California in Irvine, USA. Inclusion criteria were: postlingually implanted participants, age restricted from 18-75 years, absence of any additional linguistic or developmental problems and implant switch-on date no shorter than 6 months prior to the study. All participants provided informed consent and the procedures

were approved by the corresponding ethical authorities at each location.

B. *Electrophysiological and Behavioral Paradigms*

1) Acoustic Change Paradigm

Electrophysiological ACC was elicited to a successive presentation of 120 acoustic change stimuli. The stimulus presentation rate was 0.33 Hz with an inter-stimulus interval of one second. At least four 6-minute recordings were acquired from each participant with different stimuli. Recording took place inside an electrically isolated room and participants were instructed to ignore the stimulus presentation and direct their attention to a silent, captioned film.

Behavioral acoustic change discrimination was measured via a single-interval psychoacoustic test. Acoustic change stimuli and non-change stimuli were presented randomly with a total of 120 presentations each. Upon stimulus presentation, the participant was asked to press a button, on a graphical interface, indicating 1 if there was no change in the stimulus or 2 if an acoustic change was present. At least four psychoacoustic tests were performed with the same stimuli as in the ACC paradigm. A psychometric curve was fitted to the behavioral results to determine psychoacoustic discrimination thresholds as the point where correct identification of acoustic change dropped below 50%.

2) Unattended Oddball Paradigm

A mismatch waveform (MMW) was elicited by presenting a set of standard and deviant auditory stimuli in an unattended oddball paradigm. The stimulus repetition rate was 1Hz and the occurrence of a deviant presentation was random with a probability of 10%. At least four 15-minute recordings were acquired from each participant with different stimuli. These recordings also took place inside an electrically isolated room, with the participant sitting comfortably while attending to a silent, captioned film.

Due to the difference in the nature of the ACC and unattended oddball paradigms, an additional behavioral discrimination test was conducted. A psychoacoustic two-up, one-down, adaptive three-alternative forced-choice test was repeated five times by each participant to determine their mean behavioral spectral discrimination threshold. A sequence of three stimuli was presented in one run, two of which were standard and one of which was the deviant. The participant had to identify the deviant stimulus by pressing on a graphical interface. The test ran until 13 reversals occurred and the discrimination threshold was calculated as the mean of the last eight reversal values.

C. *Stimuli*

Spectrally rippled broadband noise stimuli were generated for both paradigms. The broadband noise was created via summation of 4000 pure tones with frequencies from 100 Hz to 8,000 kHz. The spectral ripple was created with a full wave rectified sinusoidal envelope on a logarithmic amplitude scale and with maximum amplitude of 30 dB peak-to-valley as described in [11]. Spectral peaks were equally distributed on a logarithmic frequency scale, and the number of spectral peaks per frequency octave defines the ripple density of the stimulus (RPO).

Acoustic change stimuli were 2000 ms in duration with a spectral inversion at the mid-point. Spectral inversion was a phase shift of the sinusoidal ripple envelope of $\pi/2$ with respect to the first 1000 ms of the stimulus. Standard and deviant stimuli generated for the unattended oddball paradigm were 500 ms in duration and the deviant stimulus was spectrally inverted with respect to the standard stimulus. Both stimuli had equal RPO density. Fig. 1 illustrates the spectrogram for standard (A, left), deviant (A, right) and acoustic change stimuli (B) generated at one RPO.

Stimuli were delivered electrically, through the auxiliary input of the CI's speech processor at a comfortable loudness level.

D. *Data Recording*

Single channel EEG recordings were acquired using a customized high sampling rate and high bandwidth system previously developed by the authors [5, 12]. Electrodes were placed at the vertex (Cz) and the mastoid, contralateral with respect to the tested ear. The system ground was located at the collar bone. The EEG signal was pre-amplified via a Stanford Research Systems biological pre-amplifier (filter settings: 0.03 Hz – 100 kHz) and then digitized into a PC via a National Instruments analog to digital converter (sampling rate: 125 kHz).

E. *Signal Processing*

1) Acoustic Change Paradigm

Raw EEG data were segmented into long epochs of 300 ms pre-stimulus to 2500 ms post-stimulus onset to avoid filter edge effects. The three stage CI artifact attenuation procedure developed in [12] was applied to the ACC responses. Baseline correction of 150 ms pre-stimulus was applied to the filtered epochs. Epochs were filtered with a pass-band (2-20 Hz) 2nd order Butterworth filter.

The ACC amplitudes were measured as a ratio of the change response amplitude, generated after the spectral inversion, over the amplitude of the stimulus onset response. The stimulus onset response is equivalent to the N1-P2 complex, characteristic of CAEPs. The change response is

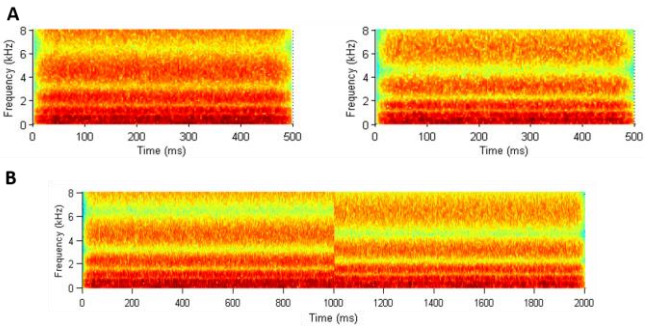

Figure 1: Description of a one RPO stimuli **A:** Stimuli spectrogram as separate standard (left) and deviant (right) presntation as employed in the unattended oddball paradigm. Standard and deviant presentations had equal number of RPOs but inverted spectral content. **B:** Stimulus spegtrogram of a fused spectral change presentation as employed in the acoustic change paradigm. Spectral inversion occurred at the midpoint of the simulus duration.

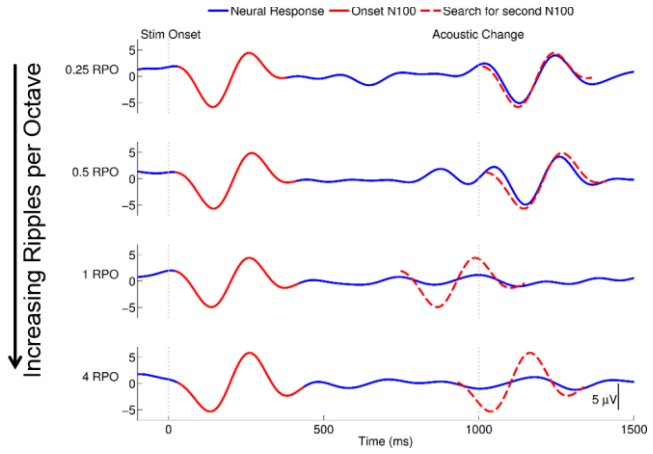

Figure 2: Template search of acoustic change responses based on the stimulus onset response. Identifiable ACC responses can be observed at 0.25 and 0.5 RPO densities while no ACC responses are evident at 1 and 4 RPO densities.

generated approximately 100 ms after the spectral inversion and it is similar in morphology to the N1-P2 response but smaller in amplitude. For each RPO density, the N1-P2 response was manually selected from a region of interest of 90 to 250 ms after stimulus onset. In order to identify the change response, a normalized version of the selected N1-P2 response was cross-correlated with the normalized region of interest of 1090 to 1250 ms after stimulus onset. The time stamp of maximum correlation was defined as the change response. Fig. 2 illustrates this template search mechanism. N1-P2 responses were manually selected at each RPO density and the corresponding template was located after the acoustic change (i.e. 1000 ms after stimulus onset). At RPO densities of 0.25 and 0.5 the change response was located using a template search based on the onset response whereas at RPO densities of 1 and 4 no change response was identified.

The neural spectral ripple discrimination threshold was defined as the RPO density where the ACC amplitude dropped below 11%. This value was selected based on the average noise floor of each participant's recording.

2) Unattended Oddball Paradigm

MMW were calculated with the methodology proposed in [5] and it will only be briefly described here. Raw EEG data were segmented into long epochs of 300 ms pre-stimulus to 800 ms post-stimulus onset. Epochs were separated into standard and deviant and averaged across each type. Averaged epochs were filtered with a pass-band (2-20 Hz) 2nd order Butterworth filter. Baseline correction of 150 ms pre-stimulus was applied to the filtered epochs. MMW were calculated as the difference waveform resulting from subtracting the standard response from the deviant response. The noise floor of the signal was calculated via a bootstrap difference waveform calculated from the standard epochs. The area under the curve of the MMW above and below (+/-) the noise floor was deemed as a significant response.

Fig. 3 illustrates how a clear MMW response to a spectral density of 0.25 RPO decreases as the spectral density increases to 0.5 RPO, 1 RPO and 2 RPO.

The neural spectral discrimination threshold was defined as the point when the MMW area under the curve dropped below a significant level which was statistically derived from the data.

III. Results

1) Behavioral Results

Psychoacoustic spectral ripple discrimination thresholds via the single interval forced choice task were in the range of 0.35 to 5.22 (mean= 1.74, standard deviation= 1.33) RPO. In two participants, the fitting of the psychometric function was not possible due to ceiling effects. Spectral discrimination thresholds for the same participants via the three-alternative forced-choice paradigm were in the range of 0.24 to 2.60 (mean= 1.05, standard deviation= 0.73).

2) Electrophysiological Results

Neural estimates of spectral discrimination via the ACC paradigm could only be derived in seven participants with a mean threshold of 1.01 (standard deviation= 0.72) RPO. Neural thresholds via the unattended oddball paradigm were successfully derived in 11 participants with a mean threshold of 1.21 (standard deviation= 0.89) RPO.

Fig. 4 shows the linear regression of the behavioral thresholds with the neural thresholds for both methods, ACC on the left and unattended oddball on the right. The ACC correlation of the seven neural thresholds with the single interval psychoacoustic thresholds was non-significant (r^2=0.55, p-value>0.05). The unattended oddball correlation of the 11 neural thresholds with the three-alternative forced-choice psychoacoustic threshold was significant (r^2= 0.37, p-value<0.05). Individual metric performance can be seen in Fig. 5.

IV. Discussion

The present study compared two different methods to objectively estimate spectral ripple discrimination in a population of CI patients. The ACC was evaluated as a

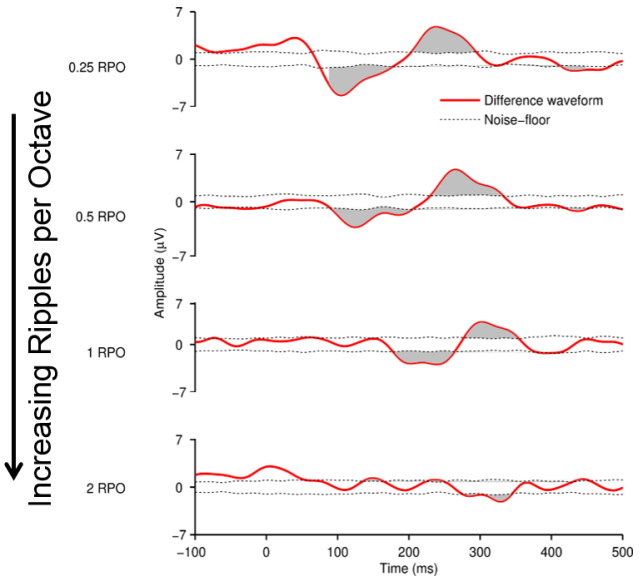

Figure 3: Exemplary data for one participant showing sequential fading of the MMW response as the spectral ripple density increases from 0.25 RPO to 2 RPO.

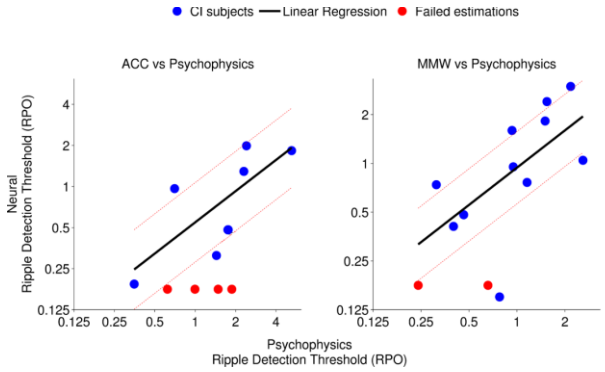

Figure 4: Correlation between the behavioral and neural spectral ripple discrimination. Red lines inidcate 95% confidence intervals. ACC paradigm on the left (correlation coefficient= 0.76, r^2=0.55, p>0.05), MMW on the right (correlation coefficient= 0.76 ,r^2=0.37, p<0.05).

potential CAEP for assessing spectral ripple discrimination and was compared to the unattended oddball method developed in [5]. This study confirms the robustness of the unattended oddball paradigm as an objective metric and presents the ACC as an additional objective metric.

A desirable advantage of the ACC paradigm over the unattended oddball paradigm is the shorter acquisition time, six minutes for the ACC vs 15 minutes for the unattended oddball paradigm. However, the representation of the spectral inversion in the ACC stimuli may generate additional temporal cues such as the switching on and off of stimulation electrodes allowing the CI patients to distinguish a change. An evidence of this effect may be the ceiling effect in two participants where they were able to discriminate changes in the sound at all RPO densities whereas their three-interval forced-choice tests indicated lower discrimination abilities.

It is conceivable that the lack of an ACC response, in some participants, is due to the high noise floor in the recording session rather than from the paradigm. Nonetheless, the unattended oddball paradigm, recorded during the same session yielded better results. The effect of stimulus delivery must be further investigated. It is possible that spectral ripple inversion may be clipped due to the 'fast attack' of the automatic gain control in the speech processors, preventing an ACC response. Electrodograms of the change stimuli could clarify this theory. This effect, in addition to a different signal processing approach, may explain why ACC were always present in [10], where the stimuli were delivered in free field, as opposed to this study.

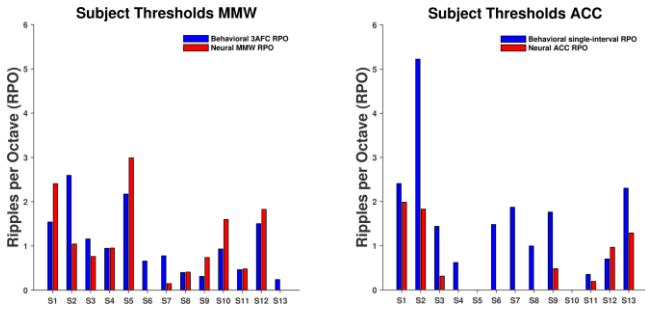

Figure 5: Individual subject perfomance shown in contrast with the corresponding behavioral trheshold. MMW estimantes compared to the three-alternative forced-choice (3AFC) psychoacoustic on the left. ACC estimates compared to the single-interval psychoacoustic on the right.

V. Conclusions

The present results suggest that it is possible to use the ACC in a single channel EEG acquisition system as an alternative to estimate spectral ripple discrimination in some CI patients. Despite its longer acquisition time, the unattended oddball paradigm is more robust than the ACC measure in estimating the behavioral spectral resolution for the described stimulation protocol.

Acknowledgment

The authors would like to thank Cochlear Ltd, the Higher Education Authority (HEA) in Ireland, and the European Commission's Marie Curie Fellowship for supporting this research.

References

[1] World Health Organization (WHO), "Deafness and Hearing Impairment," http://www.who.int/mediacentre/factsheets/fs300/en/index.html, [August 2012, 2012].

[2] National Institute of Deafness and other Communication Disorders (NIDCD), "Cochlear Implants," http://www.nidcd.nih.gov/health/hearing/pages/coch.aspx/, [August 2012, 2011].

[3] J. B. Firszt, R. D. Chambers, Kraus, and R. M. Reeder, "Neurophysiology of cochlear implant users I: effects of stimulus current level and electrode site on the electrical ABR, MLR, and N1-P2 response," *Ear Hear,* vol. 23, no. 6, pp. 502-15, Dec, 2002.

[4] R. Naatanen, T. Kujala, C. Escera, T. Baldeweg, K. Kreegipuu, S. Carlson, and C. Ponton, "The mismatch negativity (MMN)--a unique window to disturbed central auditory processing in ageing and different clinical conditions," *Clin Neurophysiol,* vol. 123, no. 3, pp. 424-58, Mar, 2012.

[5] A. L. Valdes, M. Mc Laughlin, L. Viani, P. Walshe, J. Smith, F.-G. Zeng, and R. B. Reilly, "Objective Assessment of Spectral Ripple Discrimination in Cochlear Implant Listeners Using Cortical Evoked Responses to an Oddball Paradigm," *PloS one,* vol. 9, no. 3, pp. e90044, 2014.

[6] B. A. Martin, "Can the acoustic change complex be recorded in an individual with a cochlear implant? Separating neural responses from cochlear implant artifact," *Journal of the American Academy of Audiology,* vol. 18, no. 2, pp. 126-140, 2007.

[7] B. A. Martin, and A. Boothroyd, "Cortical, auditory, evoked potentials in response to changes of spectrum and amplitude," *J Acoust Soc Am,* vol. 107, no. 4, pp. 2155-61, Apr, 2000.

[8] B. A. Martin, A. Boothroyd, D. Ali, and T. Leach-Berth, "Stimulus presentation strategies for eliciting the acoustic change complex: increasing efficiency," *Ear Hear,* vol. 31, no. 3, pp. 356-66, Jun, 2010.

[9] C. J. Brown, C. Etler, S. He, S. O'Brien, S. Erenberg, J. R. Kim, A. N. Dhuldhoya, and P. J. Abbas, "The electrically evoked auditory change complex: preliminary results from nucleus cochlear implant users," *Ear Hear,* vol. 29, no. 5, pp. 704-17, Oct, 2008.

[10] J. H. Won, C. G. Clinard, S. Kwon, V. K. Dasika, K. Nie, W. R. Drennan, K. L. Tremblay, and J. T. Rubinstein, "Relationship Between Behavioral and Physiological Spectral-Ripple Discrimination," *JARO-Journal of the Association for Research in Otolaryngology,* vol. 12, no. 3, pp. 375-393, Jun, 2011.

[11] J. H. Won, W. R. Drennan, and J. T. Rubinstein, "Spectral-ripple resolution correlates with speech reception in noise in cochlear implant users," *J Assoc Res Otolaryngol,* vol. 8, no. 3, pp. 384-92, Sep, 2007.

[12] M. Mc Laughlin, A. Lopez Valdes, R. B. Reilly, and F.-G. Zeng, "Cochlear implant artifact attenuation in late auditory evoked potentials: A single channel approach," *Hearing research,* vol. 302, pp. 84-95, 2013.

7th Annual International IEEE EMBS Conference on Neural Engineering
Montpellier, France, 22 - 24 April, 2015

An Approach to Develop an Objective Measure of Temporal Processing in Cochlear Implant Users Based on Schroeder-phase Harmonic Complexes

Anne M. Leijsen, Alejandro Lopez Valdes, Myles Mc Laughlin, Jaclyn Smith, Laura Viani, Peter Walshe, Richard B. Reilly, *Senior Member, IEEE*

Abstract— **Recent evidence suggests that cortical auditory evoked potentials recorded by EEG may be used to obtain an objective measure of spectral sound processing abilities in cochlear implant (CI) users. As speech perception depends on both spectral and temporal processing abilities, developing an objective measure of sound processing in the temporal domain is necessary for a complete evaluation of CI speech performance. This study explored the feasibility to objectively assess sound processing in the temporal domain employing a method based on EEG and complex temporal stimuli such as the Schroeder-phase harmonic complexes. Psychoacoustic discrimination abilities were measured employing a four-interval two-alternative forced choice paradigm. Neural discrimination abilities were measured by recording single-channel EEG during an unattended oddball paradigm. Psychoacoustic and neural discrimination abilities were analyzed for correlation. A strong, but non-significant, correlation was found in three out of six subjects. Schroeder-phase harmonic complexes may have utility as stimuli in the development of an objective measure of temporal processing in CI users. Furthermore, they provide new insights on temporal processing in CI users that may benefit the development of the CI.**

I. Introduction

Since the introduction of the cochlear implant (CI) in 1978, the device has developed into one of the most successful neural implants available to date. However, one of the remaining challenges to obtain optimal sound perception and speech performance is fine-tuning the implant's electrode map to the individual user. Current fine-tuning procedures are subjective and difficult to employ in certain user groups, such as infants and congenital deaf people. Therefore, the development an objective measure of sound perception and speech performance that offers clinical potential is of interest.

It has been suggested that sound perception may be objectively measured by the electrically evoked stapedius reflex threshold [1], the electrically evoked compound action potential [2] or the electrical auditory brainstem response [3]. However, these measures demonstrated only moderate correlation with threshold (T-) and/or comfort (C-) levels and are therefore not reliable to set a complete parameter map [3]-[6].

Speech performance, i.e. the ability to interpret speech provided through the CI, depends on both spectral and temporal processing abilities. Recent evidence suggests the potential of recording cortical auditory evoked potentials (CAEPs) as an objective measure of spectral processing in CI users [7]. Nevertheless, only limited research has been conducted on objective measures of temporal processing. He et al. investigated electrically evoked auditory event-related potentials in response to temporal gaps of various lengths in a train of stimuli [8]. The reported results demonstrated the potential of the method as an objective measure of gap detection abilities in CI users, but lacked a direct comparison with behavioral thresholds. Additionally, experimental evidence of the electrically evoked auditory steady state response, also known as the amplitude modulation following response, has demonstrated its potential as an objective measure of amplitude modulation detection ability in CI users [9], [10]. However, the current method requires the full attention of the subject and neural potential recordings with a minimum experimental setup of at least eight EEG electrodes. Both issues are limiting its clinical benefits.

Schroeder-phase harmonic complexes have recently been proposed as a potential behavioral measure of temporal discrimination abilities in CI users [11]. Schroeder-phase harmonic complexes are sound pairs based on an algorithm originally described by Schroeder et al. [12] and have equal frequency spectra, minimal amplitude modulations, but different temporal fine structures. An example of the differences in temporal fine structure is shown in Fig. 1, showing a Schroeder-phase harmonic complex with a fundamental frequency of 50Hz.

This study explored the feasibility to objectively assess temporal processing employing a method based on Schroeder-phase harmonic complexes in a single-channel EEG paradigm. An unattended objective assessment of temporal processing based on a neural imaging paradigm may be relevant in a clinical environment, specifically for pediatric user groups. Additionally, it may provide new insights on temporal processing that may benefit the development of the CI.

Research funded by the Trinity Centre of Bioengineering and a scholarship to AML from the Erasmus Mundus program CEMACUBE.

A.M. Leijsen is with the Trinity Centre of Bioengineering, Trinity College, University of Dublin, College Green, Dublin 2, Ireland and the faculty of Biomedical Engineering, Czech Technical University, Zikova 1903/4, 166 36 Prague 6, Czech Republic (corresponding author; phone: +353-1-8964212; e-mail: leijsena@tcd.ie).

A. Lopez Valdes, M. Mc Laughlin and R.B. Reilly are with the Trinity Centre for Bioengineering, Trinity College, University of Dublin, College Green, Dublin 2, Ireland.

J. Smith, L. Viani and P. Walshe are with the National Cochlear Implant Programme, Beaumont Hospital, Beaumont Road, Dublin 9, Ireland.

978-1-4673-6389-1/15/$31.00 ©2015 IEEE

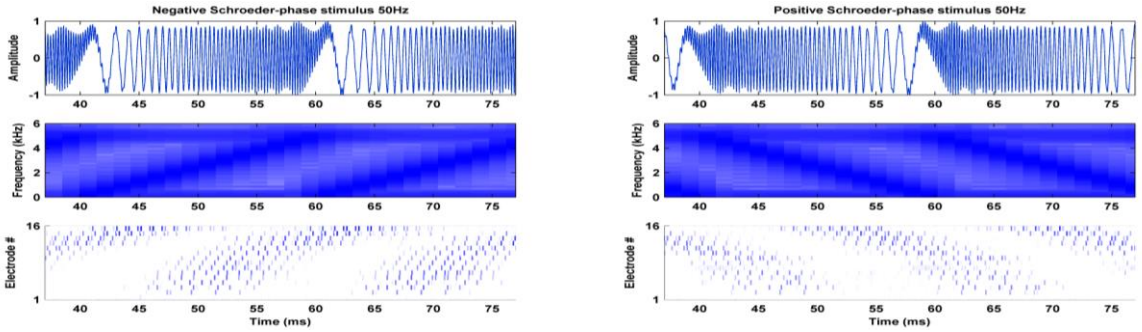

Fig 1. Time plots, spectrograms and electrodograms of negative (left column) and positive (right column) Schroeder-phase stimuli.

II. Methods

A. Subjects and Ethics Statement

Six CI users (four male) ranging in age between 27 and 74 (mean=55) years were recruited through the National Cochlear Implant Programme of Beaumont Hospital, Dublin, Ireland. All subjects were implanted unilaterally with a device manufactured by Cochlear Ltd and had at least 2.5 years of experience with their device. All subjects participated voluntarily and signed an informed consent form before participating in the experiment. Experimental procedures were approved by the Ethics Medical Research Committee at Beaumont Hospital and the Ethical Review Board at Trinity College Dublin. Demographics are provided in Table I.

B. Stimulus Generation and Presentation

Schroeder-phase harmonic complexes were generated digitally by a summation of equal-amplitude sinusoidal harmonics with predetermined fundamental frequencies of 50, 100, 200 and 400Hz, in which the harmonics' phases were determined by:

$$\theta_n = \pm \pi n (n+1) / N, \quad (1)$$

where θ_n is the phase of the nth harmonic, n is the nth harmonic, N is the total number of harmonics in the complex (5000/fundamental frequency) with the positive or negative sign indicating the construction of positive or negative Schroeder-phase stimuli, respectively. Higher fundamental frequencies result in a higher temporal complexity of the stimulus. All stimuli had a sample frequency of 44.1 kHz and duration of 500ms. A cosine squared ramp (i.e. a gradual slope starting at zero and ending at one) was applied to avoid clicks at the onset and offset of the stimulus.

TABLE I. Subject Demographics

Subject ID	Sex	Age (yrs.)	Ear of implant	CI experience (yrs.)	Implant type
SCI03	M	66	Right	13	Nucleus 5
SCI05	M	74	Left	10	Nucleus 5
SCI06	M	70	Right	2.5	Nucleus 5
SCI07	F	39	Left	7	Nucleus Freedom
SCI08	F	51	Left	7	Nucleus Freedom
SCI09	M	27	Left	11	Nucleus 5

The sound stimuli were presented to the subject via a digital to analogue converter to the accessory input of the CI processor. Stimulation levels were set for each subject to a self-reported volume that was loud but comfortable.

C. Psychoacoustic Measure

Psychoacoustic (PA) Schroeder-phase discrimination abilities were obtained by a four-interval two-alternative forced choice test. Four Schroeder-phase stimuli of the same fundamental frequency (three negative, one positive) were presented interleaved with 100ms of silence. The positive Schroeder-phase stimulus occurred randomly in either the second or the third interval. The listeners were asked to choose either the second or the third stimulus according to what they identified as different. Following each trial, visual feedback of the correct answer was provided. Each fundamental frequency was presented 24 times, resulting in test blocks of 96 trials. Each subject completed a total of four test blocks.

D. Cortical Auditory Evoked Potential Recordings

CAEPs were obtained via the high-sampling rate single-channel EEG system developed by Mc Laughlin et al. [13]. A schematic of this recording setup is given in Fig. 2. The reference and ground electrodes were respectively located at the mastoid and collar bone contralateral to the ear of stimulation. The active electrode was placed at Cz. Impedances were ensured to be at a maximum of 5 kΩ.

Positive and negative Schroeder-phase stimuli of the same fundamental frequency were presented in an unattended oddball paradigm with a target probability of ten percent. Stimuli were interleaved with 1s of silence. Subjects were instructed to attend to a captioned, silent film during the recording periods.

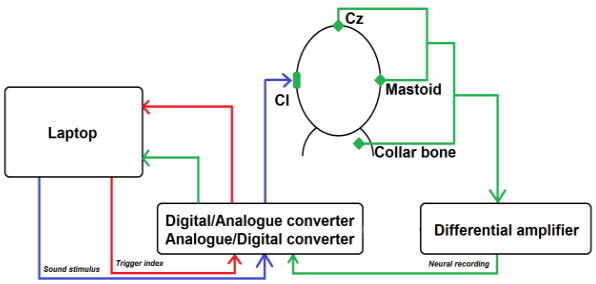

Fig 2. Schematic of the CAEP recording setup. Neural potentials are recorded at Cz and amplified by a single-channel differential amplifier. Sound stimuli are sent via a digital/analogue converter to the accesory input of the implant.

E. Data Analysis

Raw EEG data were epoched from 800ms pre-stimulus to 800ms post-stimulus onset and baseline corrected. CI artefact attenuation was performed as recommended by Mc Laughlin et al. and Lopez Valdes et al. [13; 7]. Epochs were filtered with a pass-band (2-10 Hz) 2nd order Butterworth filter and reduced to 250ms before stimulus onset to 300ms after stimulus offset for analysis.

Difference waveforms were calculated by subtracting the average response to the standard (negative) from the response to the deviant (positive) stimuli. To define significant peaks and troughs in the difference waveform, a noise floor was calculated using a bootstrap method, as previously described by Lopez Valdes et al. [7]. The area under the difference waveform that exceeded the noise floor level (referred to as the MMW area and measured in µVms) was considered as a significant difference.

Single subject and group mean MMW areas and psychoacoustic (PA) scores were analyzed for correlation employing a Spearman's rank-order correlation test.

III. Results

CI subjects generated average correct discrimination scores in the PA paradigm of 64±16.8, 67±18.1, 56±11.9 and 51±9.1% (mean±SD) for the 50, 100, 200 and 400Hz Schroeder-phase stimuli, respectively. Although temporal complexity of the stimuli was expected to increase with increasing fundamental frequencies of the Schroeder-phase harmonic complexes, no monotonic relationship was found between the individual PA scores and the fundamental frequencies. Instead, a repeated measure ANOVA with assumed sphericity (Mauchly's Test of Sphericity, $\chi^2(5)=5.578$, p=0.364) revealed no statistically significant difference between the average scores.

MMW areas of the group mean CAEP responses were calculated to be 9.8, 0, 0.006 and 0 µVms for the 50, 100, 200 and 400Hz Schroeder-phase stimuli, respectively (see Fig. 3). No significant correlation was revealed between the average MMW areas and the average PA scores (r_s=0.258, n=4, p=0.742).

Single subject analysis revealed a strong, but non-significant, correlation in three subjects (r_s=0.8, p=0.2, subjects SCI05, SCI06, SCI07) and a moderate correlation in one subject (r_s=0.4, p=0.6, SCI03). Two subjects showed a negative correlation (r_s=-0.8, p=0.2, SCI08 and SCI09). All correlations are also shown in Fig. 4.

IV. Discussion

The Schroeder-phase discrimination test employed in this study replicates the work of Drennan et al. [11]. However, the authors of that study reported average correct Schroeder-phase discrimination scores of 84, 80, 67 and 58%, respectively, which differs from the scores obtained in this study (respectively 64, 67, 56 and 51%). Several factors may account for this. Firstly, Drennan et al. employed the Schroeder-stimuli in open field, while this study stimulated

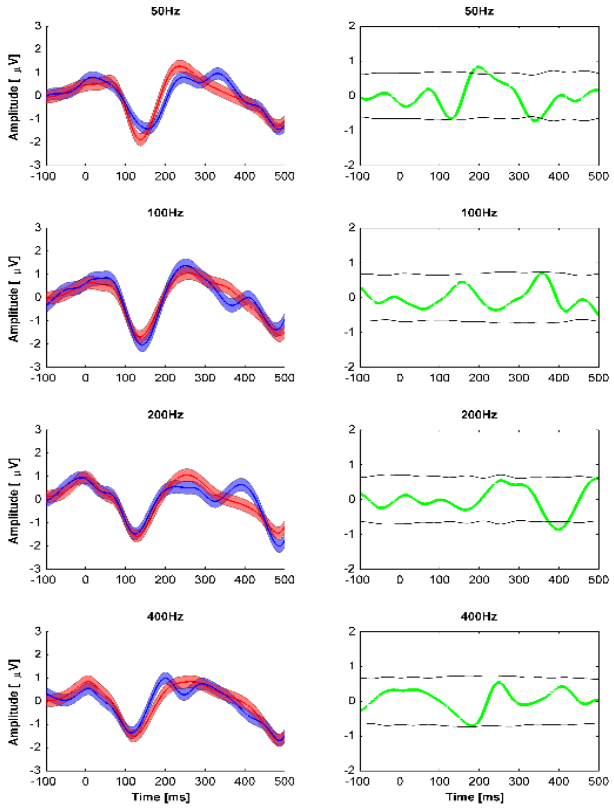

Fig 3. Group mean responses and their standard error to the standard (negative) (red, left column) and deviant (positive) (blue, left column) Schroeder-phase stimuli and their corresponding difference waveforms (green, right column). MMW areas were absent or minimal.

through the accessory input of the device. By-passing the microphone of the device decreases the amount of environmental noise, but may have resulted in a difference in processing of the implant due to the 'fast attack' action of the automatic gain control circuitry.

Secondly, the study of Drennan et al. [11] included users of Advanced Bionics and Cochlear Ltd devices, while in this study all the subjects had Cochlear Ltd devices implanted. The higher stimulation pulse rate on Advance Bionics devices in comparison the cochlear devices (i.e. 1800 Hz vs 1100 Hz) may have a critical impact on the temporal representation of positive and negative Schroeder-phase stimuli. An indication of this effect is suggested by the study presented in [14], where two Advance Bionics processing strategies with different stimulation pulse rates were evaluated, showing different results of behavioral Schroeder-phase discrimination.

Lastly, one need to include the possibility of chance due to the limited cohort recorded in the studies (24 in the study of Drennan et al. [11] vs six in the current study). Further research is necessary to investigate the performance of our cohort using stimuli presented in open field and more subjects have to be recruited in order to include subjects with all device types and to exclude performance variation by chance.

Grand average results did not show a correlation between MMW area (a measure of neural discrimination abilities)

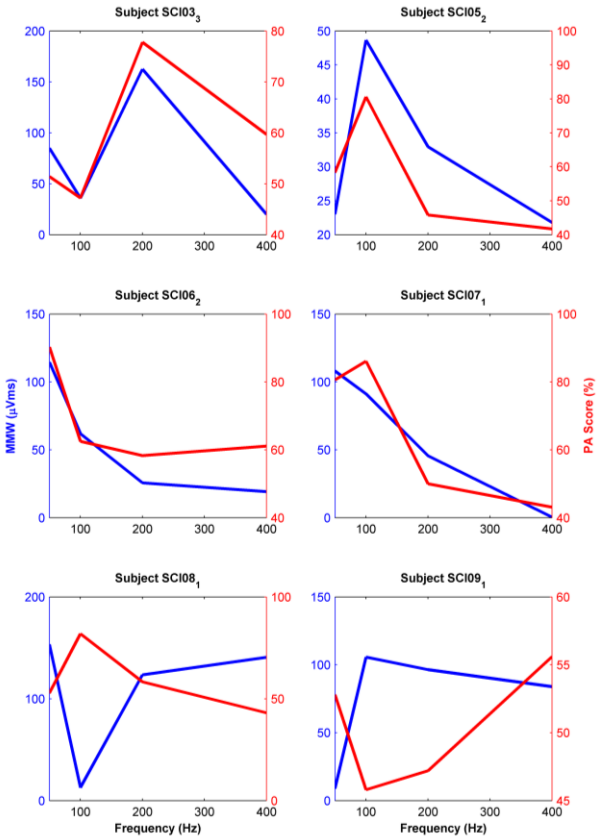

Fig. 4. MMW areas (blue) and PA scores (red) of individual subjects. A strong, but non-significant, correlation was found in subject SCI05, SCI06 and SCI07 (r_s=0.8, p=0.2).

and PA scores (a measure of behavioral discrimination abilities). It is suggested that this is an effect of the high inter-subject variability of the results. Variability in MMW area can be a result of variability in electrode impedance levels, stimulation volume, neural anatomy, implant series, and others.

Individual scores showed a high, but non-significant, correlation in three out of six subjects (r_s=0.8, p=0.2). It is proposed that higher correlation scores would be obtained if more data points (i.e. recordings from more different fundamental frequencies) were available. The negative correlation in subjects SCI08 and SCI09 may be explained by the specific characteristics of the data. SCI08 did not show clear CAEP responses to any of the four recorded frequencies. SCI09, on the other hand, did not show any Schroeder-phase discrimination ability in the PA test. Observed correlation values of those subjects may therefore not be reliable.

It should be noted that CAEP responses and PA scores are expected to be variable depending on the fatigue and the level of attention experienced by the subject. The correlation between the diurnal dependence of these two measures is unknown and may have influenced the outcomes of the study. The current study does not control for fatigue variance and recordings have taken place at any day of the week and both in the mornings and in the afternoons. It may be of interest to investigate the exact effects of day time on both the PA scores and the CAEP responses.

V. Conclusion

The main aim of this study was to explore the feasibility of the use of Schroeder-phase harmonic complexes as an objective measure of temporal processing abilities in CI users. A strong, but non-significant, correlation was found in three out of six subjects. Schroeder-phase harmonic complexes may have utility as stimuli in the development of an objective measure of temporal processing in CI users. Furthermore, they provide new insights on temporal processing in CI users that may benefit the development of the CI.

Acknowledgment

We would like to thank all subjects who participated in the experiments.

References

[1] K. Stephan, K. Welzl-Mueller, H. Stiglbrunner, "Stapedius reflex threshold in cochlear implant patients," *Audiology,* vol. 27, pp. 227-23, 1988.

[2] N. Dillier, W.K. Lai, B. Almqvist, C. Erohne, J. Müller-Deile, M. Stecker, E. von Wallenberg, "Measurement of the electrically evoked compound action potential via a neural response telemetry system," *Ann. Otol. Rhinol. Laryngol.,* vol. 111, pp. 407-14, 2002.

[3] C.J. Brown, M.L. Hughes, B. Luk, P.J. Abbas, A. Wolaver, J. Gervais, "The relationship between EAP and EABR thresholds and levels used to program the nucleus 24 speech processor: data from adults," *Ear Hear*, vol. 21, pp. 151-63, 2000.

[4] K.C.L. de Andrade, M.D.C. Leal, L.F. Muniz, P.D.L. Menezes, K.M.G. de Albuquerque, A.T.L. Carnaúba, "The importance of electrically evoked stapedial reflex in cochlear implant," *Braz. J. Otorhinolaryngol.,* vol. 80, pp. 68-77, 2014.

[5] D.C. Dees, E. Wallenberg, B. van Dijk, "Normative findings of electrically evoked compound action potential measurements using the neural response telemetry of the Nucleus CI24M cochlear implant system", *Audiol. Neurootol.,* vol. 10-2, pp. 105-16, Jan. 2005.

[6] M.L. Hughes, "Fundamentals of clinical ECAP measures in cochlear implants: part 1: use of the ECAP in speech processor programming [www document]

[7] A. Lopez Valdes, M. Mc Laughlin, L. Viani, P. Walshe, J. Smith, F.-G. Zeng, R.B. Reilly, "Objective assessment of spectral ripple discrimination in cochlear implant listeners using cortical evoked responses to an oddball paradigm," *PLoS One*, vol. 9, e90044, 2014.

[8] S. He, J.H. Grose, H.F.B. Teagle, J. Woodard, L.R. Park, D.R. Hatch, C. Buchman, "Gap detection measured with electrically evoked auditory event-related potentials and speech-perception abilities in children with auditory neuropathy spectrum disorder," *Ear Hear.*, vol. 34, pp. 733-44, 2013.

[9] M. Hofmann, J. Wouters, "Electrically evoked auditory steady state responses in cochlear implant users," *J. Assoc. Res. Otolaryngol.*, vol. 11-2, pp. 267-82, Jun. 2010.

[10] M. Hofmann, J. Wouters, "Improved electrically evoked auditory steady-state responses in cochlear implant users," *J. Assoc. Res. Otolaryngol.,* vol. 13-4, pp. 573-89, Aug. 2012.

[11] W.R. Drennan, J.K. Longnion, C. Ruffin, J.T. Rubinstein, "Discrimination of Schroeder-phase harmonic complexes by normal-hearing and cochlear-implant listeners," *J. Assoc. Res. Otolaryngol.,* vol. 9, pp. 138-49, Mar. 2008.

[12] M. Schroeder, "Synthesis of low-peak-factor signals and binary sequences with low autocorrelation," (Corresp.) *IEEE Trans. Inf. Theory*, vol. 16, pp. 85-89, 1970.

[13] M. Mc Laughlin, A. Lopez Valdes, R.B. Reilly, F.-G. Zeng, "Cochlear implant artefact attenuation in late auditory evoked potentials: a single channel approach," *Hear Res.,* vol. 302, pp. 84-95, 2013.

[14] W.R. Drennan, J.H. Won, K. Nie, E. Jameyson, J.T. Rubinstein, "Sensitivity of psychophysical measures to signal processor modifications in cochlear implant users," *Hear Res.*, vol. 262, pp. 1-8, 2010.